THE UNIVERSITY *of* EDINBURGH

Comparing Synthetic Aperture Radar and LiDAR for Above-Ground Biomass Estimation in Glen Affric, Scotland

Chue Poh Tan

Submitted for Doctor of Philosophy

The University of Edinburgh

December 2011

Declaration of Originality

I declare that the work contained in this thesis is my own, unless where due acknowledgement is made in the text. The thesis has been composed by myself and has not been previously accepted for a degree or professional qualification.

Signed:

CPTan

.....

Chue Poh Tan

15 December 2011

Abstract

Quantifying above-ground biomass (AGB) and carbon sequestration has been a significant focus of attention within the UNFCCC and Kyoto Protocol for improvement of national carbon accounting systems (IPCC, 2007; UNFCCC, 2011). A multitude of research has been carried out in relatively flat and homogeneous forests (Ranson & Sun, 1994; Beaudoin et al.,1994; Kurvonen et al., 1999; Austin et al., 2003; Dimitris et al., 2005), yet forests in the highlands, which generally form heterogeneous forest cover and sparse woodlands with mountainous terrain have been largely neglected in AGB studies (Cloude et al., 2001; 2008; Lumsdon et al., 2005; 2008; Erxue et al., 2009, Tan et al., 2010; 2011a; 2011b; 2011c; 2011d). Since mountain forests constitute approximately 28% of the total global forest area (Price and Butt, 2000), a better understanding of the slope effects is of primary importance in AGB estimation. The main objective of this research is to estimate AGB in the aforementioned forest in Glen Affric, Scotland using both SAR and LiDAR data.

Two types of Synthetic Aperture Radar (SAR) data were used in this research: TerraSAR-X, operating at X-band and ALOS PALSAR, operating at L-band, both are fully polarimetric. The former data was acquired on 13 April 2010 and of the latter, two scenes were acquired on 17 April 2007 and 08 June 2009. Airborne LiDAR data were acquired on 09 June 2007. Two field measurement campaigns were carried out, one of which was done from winter 2006 to spring 2007 where physical parameters of trees in 170 circular plots were measured by the Forestry Commission team. Another intensive fieldwork was organised by myself with the help of my fellow colleagues and it comprised of tree measurement in two transects of 200m x 50m at a relatively flat and dense plantation forest and 400m x 50m at hilly and sparse semi-natural forest. AGB is estimated for both the transects to investigate the effectiveness of the proposed method at plot-level.

This thesis evaluates the capability of polarimetric Synthetic Aperture Radar data for AGB estimation by investigating the relationship between the SAR backscattering coefficient and AGB and also the relationship between the decomposed scattering mechanisms and AGB. Due to the terrain and heterogeneous nature of the forests, the result from the backscatter-AGB analysis show that these forests present a challenge for simple AGB estimation. As an alternative, polarimetric techniques were applied to the problem by decomposing the backscattering information into scattering mechanisms based on the approach by Yamaguchi (2005; 2006), which are then regressed to the field measured AGB. Of the two data sets, ALOS PALSAR demonstrates a better estimation capacity for AGB estimation than TerraSAR-X. The AGB estimated results from SAR data are compared with AGB derived from LiDAR data. Since tree height is often correlated with AGB (Onge et al., 2008; Gang et al., 2010), the effectiveness of the tree height retrieval from LiDAR is evaluated as an indicator of AGB. Tree delineation was performed before AGB of individual trees were calculated allometrically. Results were validated by comparison to the fieldwork data. The amount of overestimation varies across the different canopy conditions. These results give some indication of when to use LiDAR or SAR to retrieve forest AGB. LiDAR is able to estimate AGB with good accuracy and the R^2 value obtained is 0.97 with RMSE of 14.81 ton/ha. The R^2 and RMSE obtained for TerraSAR-X are 0.41 and 28.5 ton/ha, respectively while for ALOS PALSAR data are 0.70 and 23.6 ton/ha, respectively. While airborne LiDAR data with very accurate height measurement and consequent three-dimensional (3D) stand profiles which allows investigation into the relationship between height, number density and AGB, it's limited to small coverage area, or large areas but at large cost. ALOS PALSAR, on the other hand, can cover big coverage area but it provide a lower resolution, hence, lower estimation accuracy.

Acknowledgements

First and foremost, I offer my sincerest gratitude to my supervisor, Iain Woodhouse, who has supported me throughout my PhD course with his patience and knowledge. He helped me to get on the road to the wonderful world of radar and provided an experienced ear for my doubts about writing a thesis. Without his constructive and helpful comments, this thesis would not have been completed or written. I am also very grateful to my co-supervisor, Genevieve Patenaude for much appreciated advice and guidance. She has always been very supportive and insightful.

Special thanks to all my fellow advisors, Shane Cloude, Juan Suarez and Neil Stuart for all your help, advice, lively discussions and encouragement. Shane Cloude was very kind to set aside time for informative discussions about my research results and pouring invaluable comments to improve my research work. Not only Juan Suarez has been a tremendous source of information on Glen Affric, but also he is generous in sharing his expertise on LiDAR data processing. Not to forget, Neil Stuart has also inadvertently, and without fail, provided something much greater in all the years I've known him: a friendly smile and a hello every time we met.

I would like to express my gratitude to the Commonwealth Commission for the full scholarship, without which this PhD would not have been possible. I would also like to thank the Forestry Commission and Forest Research Scotland for the access to field sites and particular thanks are due to those at the Northern Research Station, Roslin, Scotland, especially, Juan Suarez, Colin Edwards and Mike Perks for support and access to data.

I am also infinitely grateful for the help of Iain Cameron and Anthony Newton who have been extremely generous in sharing and demonstrating their knowledge about fieldwork surveying and post-processing of field data. A massive thank you to Iain Woodhouse, Armando Marino, Xing Ou and Antonio Delussu for their time and assistance during

fieldwork campaign. Thanks to all of you for working very hard, with very few breaks in freezing cold weather and wet condition.

Armando Marino, Karin Viergever, Matthew Brolly, Edward Mitchard and Gemma Cassells have fascinated me with their ability to conduct research work but have also given me detailed discussions on principles of SAR and some good laughs. In many ways I have learnt much from and because of all of them! Apart from that, Wolfgang Boerner, Hong Tat Ewe, Eric Pottier, Scott Hensley, Marc Simard, Kostas Papathanassiou, Keith Raney, Tony Freeman, Thuy Le Toan, Juan Sanchez Lopez and Shaun Quegan offered much advice and insight about polarimetry and biomass related topics throughout my research work. I'm very grateful to all my friends and colleagues who influenced my life and contributed, in different ways, to this thesis.

I would like to thank Peter Caccetta and Zheng Shu Zhou for providing funding support and an invaluable opportunity of a 6-week study visit at the CSIRO, Australia. Spending days at the CSIRO wouldn't have been so satiating and productive without sincere support, inspiration and friendship from Jeremy Wallace, Eric Lehmann, Suzanna Furby, Aloke Phatak, Mavis Dias and other fellow friends from the CSIRO that I overwhelmingly received.

Thanks to James Fraser, David and Avril Lyon, and Gordon McFarlane who not only continuously correct my English and teach me Scottish slang, but also make me feel at home in Edinburgh. In my daily work, I have been blessed with a group of cheerful fellow officemates, Luise Fisher, Tim Smith and Muriel Cote. I would like to extend a very sincere thank you to my family for their continuous support over the years. Last but not least, I owe the most extraordinary debt of thanks to Jason Lim, not only for showing genuine interest in my progress, but also a daily dose of care and enthusiastic motivation.

This thesis is dedicated to my late grandmother who passed away in the first few months of my PhD journey. No words are sufficient to describe her contribution to my life.

Table of Contents

Chapter 3: The Study Area: Glen Affric Conservation and Management Area, Scotland and Data Collection

Chapter 4: Above-Ground Biomass Estimation Using LiDAR

Chapter 5: Above-Ground Biomass Estimation Using ALOS PALSAR and TerraSAR-X

List of Figures

List of Tables

Chapter 1
Introduction

1.1 Problem Definition

Global climate change is one of the most urgent worldwide issues. According to the United Nations Framework Convention on Climate Change (UNFCCC), global warming is defined as "*a change of climate which is attributed directly or indirectly to human activity that alters the composition of the global atmosphere and which is in addition to natural climate variability observed over comparable time periods*" (UNFCCC, 1992, Article 1, Paragraph 2). Global efforts to mitigate this issue have been marked by the establishment of international agreements (IPCC, 2007; UNFCCC, 2011).

Forests make up around 31% of the world's land surface and their importance is widely recognised (Gibbs et al., 2007; Gullison et al., 2007; Ramankutty et al., 2007; Garg et al., 2011). One of the global efforts in combating global climate change is to reduce the carbon emission caused by human-induced deforestation and forest degradation (Stern, 2006). Reducing Emissions from Deforestation and Degradation (REDD) was formally introduced at The UNFCCC 13th Conference of the parties (COP13) in Bali in 2007 to create an international framework to halt deforestation and help to fight poverty while conserving biodiversity and sustaining vital ecosystem services (REDD, 2009). Due to the uncertainties of the current level of global carbon (IPCC, 2007; REDD, 2009; UNFCCC, 2011), there exists the need to accurately

estimate the biomass and carbon stocks to help improve our understanding of the global carbon cycle and to monitor the efficacy of global initiatives to combat climate change (Sierra et al., 2007).

1.2 Research Objectives

Estimation of above-ground biomass (AGB) in forest environments has gained much attention in recent years (Garcia-Martin et al., 2008; Caicoya et al., 2010; McNeil et al., 2010; Gang et al., 2010; Hall et al., 2010; Clewley et al., 2010; Lucas et al., 2010; Ying et al., 2011; Xie et al.,2011) because it determines the potential carbon emission that could be released to the atmosphere due to deforestation or forest land change. Earth Observation data offers great potential to remotely assess the AGB over large and/or remote areas. Although various methods for AGB estimation have been tested on relatively flat[2] areas where terrain effects were not significant (Ranson & Sun, 1994; Beaudoin et al.,1994; Kurvonen et al., 1999; Austin et al., 2003; Dimitris et al., 2005), research has only rarely been conducted in sparse and mountainous forests using Synthetic Aperture RADAR[3] (SAR) data (Cloude et al., 2001; 2008; Lumsdon et al., 2005; 2008; Erxue et al., 2009, Tan et al., 2010; 2011a; 2011b; 2011c; 2011d).

1. The aim of this research is to evaluate the capability of polarimetric SAR for estimating the forest AGB in Glen Affric, Scotland. The study area is chosen because it combines several difficult environments for remote sensing[4], including heterogeneous forest cover, sloped terrain and a broad distribution of tree heights. This can be done by

---

[1] Deforestation is generally defined as conversion of forests into non-forest land uses and forest degradation as quality deterioration of forest (i.e. the removal of carbon or carbon sequestering capacity from a forested area while remaining classed as a "forest").

[2] In this thesis, flat terrain is defined by assuming the topographic variation is less than half of the incidence angle within pixel slopes.

[3] RADAR is the acronym for RAdio Detection and Ranging and the term will be written as 'radar' throughout the thesis.

[4] Remote sensing can be defined as observing and analyzing a distant target using information from the electromagnetic spectrum (Jensen, 2007).

evaluating the capability of SAR (in this case, ALOS PALSAR and TerraSAR-X) data for AGB estimation by investigating the relationship between

a. observed SAR backscatter and field measured AGB

b. scattering mechanisms from a model-based polarimetric decomposition[5] and AGB

At the same time, the AGB estimation using LiDAR data is calculated allometrically after retrieving the tree height and delineating the individual tree crown. The results of AGB estimation using SAR and LiDAR are validated using fieldwork data. In the area where the fieldwork data is not available, the AGB derived from LiDAR data is used as a comparative data set to assess the capability of the proposed method using SAR in biomass estimation.

To achieve the aim, the following research questions are addressed:

1. How strong is the relationship between the SAR backscattering coefficient and AGB in Glen Affric?
2. How sensitive is the Yamaguchi decomposed ratio of volume-to-surface scattering in affecting the correlation with AGB?
3. How accurate is the AGB estimation at plot-level for ALOS PALSAR?
4. How is the comparison of AGB estimation between SAR and LiDAR in environments like Glen Affric?

[5] Model-based decomposition of polarimetric radar coherency matrix isolate specific scattering mechanisms for further quantitative analysis (van Zyl et al.,2011).

1.3 Context and relevance

Global climate change is anticipated to disrupt the Earth's climate system significantly by altering the exchange of water, carbon and other trace gases, among the oceans, atmosphere, and land (Stern, 2006). Although uncertainty exists in respect to the veracity, timing, and extent of climate change and its impacts, the vast body of scientific evidence now presents a compelling case that human activities have already changed the Earth's climate and, if current emission trends persist, the changes that are projected to occur over the course of this century are likely to be very dangerous.

Global temperatures have already risen by 0.76°C since 1850, and due to inertia in the climate system, a further 0.5–1.0°C of warming is expected over the next 50 years, even if atmospheric greenhouse gas (GHG) concentrations could be held at today's levels (Dawson & Spannagle, 2009). The average global surface temperature is likely to increase by a further 1.8-4.0°C this century and by up to 6.4°C in the worst case scenario (Adio et al., 2010). To date, emissions have already committed the Earth to a global mean temperature increase of approximately 1.5°C above preindustrial levels, and possibly 2.0°C. Global carbon dioxide (CO_2) has increased from c. 280μmol mol^{-1} at the start of the industrial revolution to 360 μmol mol^{-1}. It is anticipated to exceed 550 μmol mol^{-1} by around 2050 and may even reach 700 μmol mol^{-1} by 2100 (Hikosaka et al., 2010). Since carbon dioxide represents well over half of all GHG, curbing them is crucial in the mitigation efforts.

The Kyoto Protocol which is an international agreement linked to the United Nations Framework Convention on Climate Change (UNFCCC), set binding targets for 37 industrialized countries and the European community for reducing their collective emissions of GHG. These amount to an average of 5% against 1990 emission levels over the period of five years 2008-2012 (UNFCCC, 2011). The Climate Change Act 2008 introduced a binding reduction target requiring the UK to reduce its emissions by at least 80% by 2050 against 1990 levels (CCC, 2008). It also introduced a long-term

framework for monitoring emissions through a national carbon budgets system: caps on the total quantity of GHG permitted in the UK over a specified time. Each carbon budget covers a period of five years, with the first three carbon budgets running from 2008 to 2012, 2013-2017 and 2018-2022 (Figure 1) (EEA, 2011).

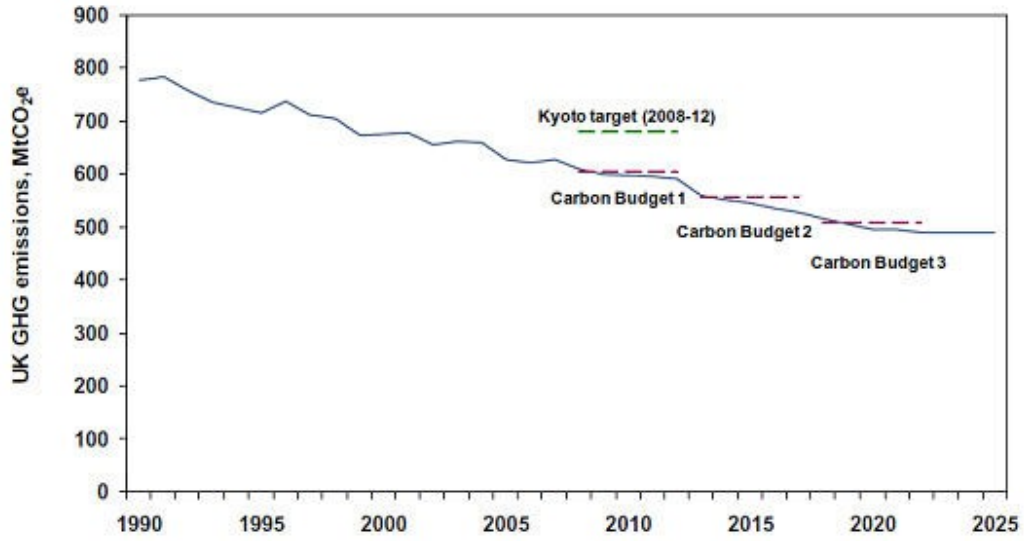

Figure 1. The projected UK emissions of greenhouse gases on net carbon account basis (including the purchase of allowances within the EU ETS) from 1990 to 2022.
Figure source: European Environment Agency website: http://www.eea.europa.eu/soer/countries/uk/soertopic_view?topic=climate%20change - published on 26 November 2010

The role played by forest in removing carbon dioxide from the atmosphere is recognised in the UK Government's Climate Change Programme (Defra, 2006). They store approximately 1200 gigatonnes of carbon which is considerably more than is present in the atmosphere (around 762 GtC) (IPCC, 2007). With the aid of remote sensing technology and forest inventory methods, it is important to be able to quantify both carbon stocks and rates of carbon exchange under the Kyoto Protocol in order to provide accurate estimates of net uptake and storage of carbon. This objective is notably

in, paragraph 71(c) of Decision 4/CP.15 (agreed at the Conference of the Parties in Copenhagen in 2009)

"…establishment of robust and transparent national forest monitoring systems and, if appropriate, subnational systems as part of national monitoring systems, that use a combination of remote sensing and ground-based forest carbon inventory approaches for estimating, as appropriate, anthropogenic forest-related GHG emissions by sources and removals by sinks, forest carbon stocks and forest area changes."

This thesis assesses the capability of ALOS PALSAR, TerraSAR-X and LiDAR for AGB estimation in Glen Affric, Scotland. The mountainous terrain and heterogenous canopy cover in the study area have made the biomass estimation challenging, but given that approximately 28% of the total global forest area lie in mountainous areas (Price and Butt, 2000), it is vital that we understand how SAR performs in these kinds of environments.

Owing to the advancement in polarimetric techniques in recent years, the azimuth slope compensation and decomposition procedure using the approach of Yamaguchi (Yamaguchi et al., 2005; 2006) should be capable of overcoming some of these challenges. After the azimuth slopes are compensated, the volume-to-surface scattering power is extracted to establish a relationship with the AGB. Cross validation with the fieldwork data has been conducted to evaluate the accuracy of the estimates. The results of this research are anticipated to have an impact on carbon accounting under the Kyoto Protocol, and further into the monitoring, reporting and verification of REDD, and will have implication for future Earth Observation satellites for the purpose of global AGB estimation.

1.4 Thesis Structure

Chapter 1 relates the AGB estimation in the context of international issues and outlines the objectives and research questions. The remote sensing approaches to estimate AGB are elaborated in Chapter 2. This is followed by the description of study area in which the location, characteristics and condition of the forests are discussed in Chapter 3. *In-situ* methods for the AGB estimation are also discussed as the fieldwork data are used to validate the result of AGB estimation derived by LiDAR and SAR. This chapter also outlines the specifications of the Earth Observation data used in this research. Chapter 4 defines the methodology of AGB estimation using LiDAR data and the results are discussed. Chapter 5 presents the AGB estimation approach using ALOS PALSAR and TerraSAR-X. The results validation is also given at the end of the chapter. Chapter 6 summarizes the research findings and answers the research questions addressed in Section 1.2. This chapter concludes the thesis with recommendations for future work.

Chapter 2

Forest Above-Ground Biomass Estimation Using *In-Situ* Observation and Remote Sensing Technologies

2.1 Introduction

This chapter emphasizes the current and future remote sensing technologies for measuring and monitoring forest. Remote sensing is defined as observing and analysing a target that is distant from the sensor, usually using information from electromagnetic signals (Jensen, 2007). These technologies have proven to meet the cutting-edge logistical challenge of forest observation in an accurate, repeatable and inexpensive manner over large areas (DeFries et al., 2002; Mayaux et al., 2005; Archard et al., 2007; Hansen et al., 2008; Kempeneers et al., 2011). The global significance and challenges of the AGB estimation are outlined in Section 2.2. A summary of the AGB estimation using various Earth Observation data including active and passive remote sensing are included in Section 2.3. This is followed by a look at the emerging technologies for AGB estimation that will become operational in the near future (Section 2.4). Note that this chapter focuses on giving an overview of current and near future Earth Observation that are specifically relevant to this thesis, rather than providing a comprehensive and exhaustive review. Section 2.5 concludes and summarises the chapter.

2.2 Global Significance and Challenges of AGB Estimation

Any effort to monitor the forests globally should begin with common definitions and measurements that may be applied worldwide. Defining a forest can be challenging due to the wide variation in forest ecosystem from one country to another, and the dynamic nature of forests at various stages of degradation or regrowth.

2.2.1 Defining Forest

The definition of forest versus non-forest has crucial importance for deforestation and degradation monitoring. FAO defined forest as a minimum canopy cover of 10%, height of 5 meters and area of 0.5ha (FAO, 2006). Australia, on the other hand, defines forest as a minimum tree crown cover of 20% and the potential to reach greater than 2 meters in height (Furby et al., 2007). The definition of forest in Ghana is a minimum area of 0.1 hectares with a minimum tree crown cover of 15% and minimum tree height of 2 meters. Under the Kyoto Protocol (UNFCCC, 2001), participating countries define forests within their borders by selecting one value of minimum area, tree height and crown cover from the following range:

- area: 0.05-1 hectare
- tree height: 2-5 meter
- crown cover: 10%-30%

An updated list of forest definitions by country can be found at http://cdm.unfccc.int/DNA/cdf/index.html and a summary of the national definition of forests for most of the countries are listed in Table AI.1.

2.2.2 Above-Ground Biomass

AGB is the total amount of biological material present above the soil surface over a specified area (Drake et al., 2003). FAO (2004) defined “biomass” as

"*organic material both above-ground and below-ground, and both living and dead, e.g., trees, crops, grasses, tree litter, roots, etc.*"

Above-ground biomass consists of all living biomass above the soil including stem, stumps, branches, bark, seeds, litter and foliage. Below-ground biomass comprises all living biomass of live roots, including small roots (2-10mm diameter) and large roots (>10mm diameter). Since fine roots are not able to be distinguished empirically from soil organic matter and the live biomass changes significantly seasonally, they are not taken into consideration as below-ground biomass (Samalca, 2007).

Much of the biomass assessment research has concentrated on above-ground biomass because it accounts for the majority of the total accumulated biomass in the forest ecosystem (Brown, 1997; Kraenzel et al., 2003; Laclau, 2003; Losi et al., 2003; Segura and Kanninen, 2005; Aboal et al., 2005). The below-ground biomass is rarely measured because it can only be assessed through *in-situ* measurements that are labour- and time-consuming. (GCOS, 2003). As carbon makes up approximately 50% of vegetative biomass, quantification of the biomass is important in forest ecosystem studies in order to estimate carbon pools at multiple scales (Montagnini and Porras, 1998; Losi et al., 2003; Nightingale et al., 2004; Montagu et al., 2005; Banskota et al., 2007; FAO, 2008).

2.2.3 Global Significance of AGB Estimation

Global climate change is occurring because of the dramatic increase of anthropogenic greenhouse gases that trap heat in the Earth's atmosphere. Of all greenhouse gases (other than water vapour), atmospheric carbon dioxide (CO_2) has the greatest warming potential (Middleton, 1999, DeFries et al., 2007) because of its relative abundance combined with its capacity to absorb effectively in the near IR. Global CO_2 has increased from 280μmol mol^{-1} at the start of the industrial revolution to 360 μmol

mol^{-1}. It is expected to exceed 550 μmol mol^{-1} by around 2050 and may even reach 700 μmol mol^{-1} by 2100 (Hikosaka et al., 2010).

Forests play an important role in locking up the excess CO_2 via photosynthesis, but the dynamic responses of carbon fluxes in terrestrial vegetation to CO_2 induced climate change is still poorly understood (Houghton & Ding, 2001; McCarthy et al., 2001; Metz et al., 2001; Treuhaft et al., 2004; Freer-Smith et al., 2008). Although forests only cover 31% of the Earth's terrestrial surface, they account for 13%-17% of global emissions, making it the third largest source of GHG emissions - larger than the entire global transport sector (Gibbs et al., 2007; Gullison et al., 2007; Ramankutty et al., 2007; Garg et al., 2011).

With an alarming rate of deforestation and forest degradation of around 13 million hectares of forest per year in the last decade (FAO, 2010), official national and international discussions were initiated on issues relating to reducing greenhouse gases emissions. The Stern Review on the Economics of Climate Change (Stern, 2006), commissioned by the UK government, specified the impact of forests in global climate change.

"*Action to preserve the remaining areas of natural forest is needed urgently*," it said, and called for "*large scale pilot schemes... to explore effective approaches to combining national action and international support*" (Nicholas Stern, 2006, 25).

The recent Conference of Parties (COP15) to the UNFCCC in 2009 adopted a decision on "*Methodological guidance for activities relating to reducing emissions from deforestation and forest degradation and the role of conservation, sustainable management of forests and enhancement of forest carbon stocks*" (MRV, 2011, 2). The latest COP16 in 2010, UNFCCC and REDD has been tasked with developing modalities for *"Measuring, reporting, and verifying anthropogenic forest-related emissions by sources and removals by sinks, forest carbon stocks and forest area changes resulting*

from the implementation of REDD+ activities, consistent with any guidance for MRV {Annex II [c])." (Goetz & Dubayah, 2011, 232).

For these reasons, the importance of remote sensing to estimate biomass at both national and international levels is increasing. Due to the limited capacity of methods for estimating the AGB, there still exists an uncertainty in knowledge of the exact level of carbon stored in forest biomass globally (Waring and Running, 1998; FAO, 2008; Garg et al., 2011; Maniatis et al., 2011). Improvements in large-area quantification of biomass using remote sensing techniques may help to reduce the uncertainty of AGB estimation in forested ecosystems and therefore improve our understanding of the role of forests in the global carbon cycle (Chen et al., 2004; Treuhaft et al., 2004; FAO, 2008; Kempeneers et al., 2011).

2.2.4 *In-situ* Approach for AGB Estimation

Ideally, global AGB forest can be mapped and the respective countries can resample the map to fit their forest definition and needs. In order to estimate AGB accurately, typically comparisons are made of AGB *in-situ* field data and remote sensing data derived using a chosen method. *In-situ* destructive measurement entails harvesting, drying and weighing trees. While it is the most direct and accurate method, this approach is impractical because it is laborious, time-consuming (and therefore costly) and destructive. Another approach is to use allometric equations or conversion factors to estimate AGB from specific measurements of such things as tree diameter, species-specific wood density and/or height and the correlations are extrapolated to the entire forest (Chave et al., 2005; Gibbs et al., 2007). These allometric equations have been developed through exhaustive measurement, usually destructive harvesting and weighing trees. However, there exists significant variation between AGB estimates using different allometric equations that, consequently, contributes bias or error in the estimates (Brown et al., 1995; 1997; Houghton et al., 2001; Chave et al., 2004; Maniatis et al., 2011).

2.3 Earth Observation Approach for AGB Estimation

Ground-based methods for the categorization and classification of forest inventories are costly in time, money and human resources. Remote sensing offers unique methods to observe Earth terrain or atmosphere from space using satellites (spaceborne), or from the air using aircraft (airborne).

Airborne and spaceborne images are becoming increasingly accessible due to the increasing number of companies and agencies operating sensors. Airborne sensors fly at a much lower altitude than satellite sensors, hence, producing a much smaller image coverage but higher quality data than satellite sensors. The advantage of airborne data acquisitions is that the user takes control on the mission in terms of time schedules, flight line arrangements, calibration measurements, and acceptable weather conditions. However, airborne sensors are relatively expensive due to fact that limited spatial coverage and multiple flight lines may be required to cover a study area. Spaceborne sensors can monitor a large area at a relatively cheaper cost, thus, are considered as the best way to monitor forest globally (Olander et al., 2008; Andersson et al., 2009; DeFries, 2008; Sanchez-Azofeifa et al., 2009). With the world's total forest area of over four billion hectares, any global effort to estimate the global AGB forest will have to rely heavily on spaceborne remote sensing (GCOS, 2003; TEMS; IGOS, 2004), with airborne data used as a supplement in areas where spaceborne data are lacking in quality, coverage or accuracy. Table 2.1 summarizes the advantages and disadvantages of airborne and spaceborne sensors while Table 2.2 lists the comparison of ground survey, airborne and spaceborne data for forest inventory in the United Kingdom.

Table 2.1. Advantages and disadvantages of airborne and spaceborne sensors

Airborne Sensors	Spaceborne Sensors
-Function at low altitude (5-11km) , hence, producing smaller image coverage	-Function at high altitude (200-36,000km) , hence, producing bigger image coverage
-Limited by fuel cost and range, crew logistics, weather and the need for permission to fly and take images	-Repeatedly around the entire globe and regardless of weather. No permission is required before taking satellite images of any country (UNOOSA, 2009).
-Relatively expensive due to limited coverage and multiple flight lines may be required to cover a study area	- Lower operational costs and cover larger areas for a fraction of the price of airborne missions (Patenaude et al., 2005; Swanson et al.,2009)
-Provide higher quality data	-Provide lower quality data
-More flexible in flight path	-Follow a fixed orbital path
-Easy to update new technology in the instruments, hence, often carry newer sensor technology	-Challenging to update new technology in the instruments
-Cheaper to launch	-Expensive to construct and launch into orbit

Table 2.2. Comparison of ground survey, airborne and spaceborne data for forest inventory in the United Kingdom (Patenaude et al., 2005).

	Monitoring from remote sensing	Forest area (km^2)	Approximate Costs[1]				
			Ground survey[2]	Optical[3]	Radar		LiDAR
				Satellite	Airborne	Satellite[3]	Airborne
				~£0.10/km^2	~£250/km^2	~£0.10/km^2	~£300/km^2
Above-ground carbon content loss from Article 3.3 Deforestation activities	Total UK forest area plus afforestation and reforestation since 1990	28k	~£3.5m	Less than ~£3k	~£7m	Less than ~£3k	~£8.4m
Above-ground carbon content gains from Article 3.3 Afforestation and Reforestation activities (forest growth only)	All UK forest area planted after December 1989	4.5k	~£307k	Less than ~£1k	~£615k	Less than ~£1k	~£738k
Above-ground carbon content gains from Article 3.4 Forest Management activities (forest growth only)[4]	All UK forest area planted after 1940[5]	19.25k	~£1.822 m	Less than ~£2k	~£3.644m	Less than ~£2k	~£4.373m

[1] Costs, rounded to the £1,000, provide guidance only and are for image acquisition without processing. Costs are for acquiring one dataset only (for forest to non-forest land cover change detection, at least two datasets are required).
[2] Medium resolution (15-50m)
[3] Data collection only, no processing. Estimates based on costs for generating the Country Side Survey 2000, http://www.countrysidesurvey.org.uk/archiveCS2000/ (Steve Smith, 2004, personal communication).
[4] Only if Forest Management elected by the United Kingdom
[5] Based on the assumption that all forests above 50 years of age have reached maturity and do not contribute significantly to the carbon sink (trees planted in 1970 has major contribution as sink for 30 years after 1990).

Airborne and spaceborne sensors can be divided into two categories (Figure 2.1):

- Passive sensors
- Active sensors

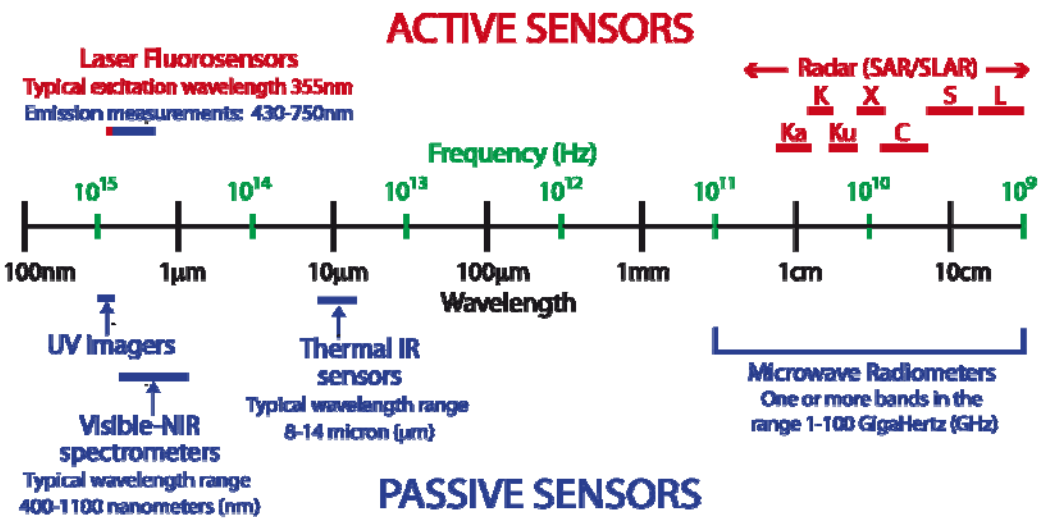

Figure 2.1. Electromagnetic spectrum used by passive and active sensors
Source: http://www.seos-project.eu/modules/marinepollution/marinepollution-c01-s02-p01.html

Wavelengths and frequencies of electromagnetic waves are used by the passive and active sensors to characterise the spectral range of light and radiation. In remote sensing, the electromagnetic radiation regions are near ultraviolet (UV) (0.3-0.4µm), visible light (400-1100nm), near shortwave, thermal infrared (8-14µm) for passive sensors and microwave (1mm - 1m) for active sensors. Figure 2.1 shows the wavelength regions for both active and passive sensors. The next sections start with a brief overview of the sensors and then explains the approach of the sensors in AGB estimation.

2.3.1 Passive sensors

Passive sensors detect the reflected or emitted electromagnetic radiation from natural sources. These include aerial photograph cameras and optical remote sensing sensors .

2.3.1.1 Aerial photography for AGB Estimation

The advent of aerial photography catered to the basic requirements of monitoring capabilities, and is one of the most widely used applications in remote sensing for governmental or commercial forest assessment, inventory and classification (Becker et al., 1995; Nakashizuka et al., 1995; Masst et al., 1997; Miller et al., 2000; Kohl & Hussendorfer, 2000; Katsch & Stocker, 2000; Haddow et al., 2000; Pitt et al., 2000; Cotton & Ettl, 2001). Cameras are utilized in aerial photography to capture images and can be of different types, namely, single-lens mapping, multiple-lens mapping, panoramic and digital. The cameras are commonly mounted on helicopters, aircraft and spacecraft. There are various types of photographic films available with respect to the types of emulsions used including panchromatic, infrared, normal colour and colour-infrared films. The scale of the photograph is crucial when aiming at forestry applications and ranges from 1:70,000 to 1:5,000 depending upon the goal of the study and terrain conditions. Aerial photography covers areas ranging from a few hundred to a few thousand hectares of forests, plantations and agro-forestry systems (Calle et al., 2007).

Google Earth has a huge collection of global high resolution imagery from various satellite and airborne sources with differing resolutions and dates of acquisition. Google Earth may not be useful for AGB estimation as yet, but the approach is important for land cover validation and visualisation (Olander et al., 2006; Bicheron et al., 2008; Helmer et al., 2009; IIASA, 2009).

Aerial photography offers some advantages over traditional ground-based mapping systems for biomass estimation. It covers a large area of the land at approximately the same scale, giving high resolution and better interpretation of features with stereoscopic vision (Calle et al., 2007). As with all remote sensing, it can be used for forests which are inaccessible at ground level. However, there are some disadvantages associated with aerial systems. The absence of georeferencing makes digitization difficult and it may have image distortion and errors, such as relief displacement and variable canopy shadowing, which may cause incorrect measurements, inaccurate positional location and scale from the photograph.

While aerial photography is more effective for monitoring larger areas compared to field surveys, it is costly for national inventories, especially where repetitive observations are required. Diameter at breast height (dbh) of trees is an essential indicator of biomass in allometric computation and it is impossible to obtain the measurement directly from aerial photographs. However, crown diameters can be estimated and regression models are used to estimate the diameter of the trees. Moreover, the problem of exactly aligning flight lines for temporal change detection studies and the costs associated with acquiring an airborne mission have constrained aerial forest inventory assessment and change detection studies.

2.3.1.2 Multi- and Hyper- spectral Sensors for AGB Estimation

Recent advances in remote sensing have led the way to the development of multi-spectral and hyper-spectral sensors (also referred to as imaging spectroscopy). In general, multi-spectral sensors measure reflectance of Earth's surface at relatively large bandwidths (70-400nm) and the data are usually composed of about 5 to 10 bands. In contrast, hyperspectral sensors combine imaging and spectroscopy in a single system to produce approximately 100 to 200 spectral bands of relatively narrow bandwidths (5-10nm) (Zheng et al., 2001). Most past and current hyperspectral sensors have been airborne (Table AI.2), with two recent exceptions: NASA’s Hyperion sensor on the EO-

1 satellite, and the U.S. Air Force Research Lab's FTHSI sensor on the MightySat II satellite.

Multi-spectral satellites are usually categorized into environmental satellites (Meteosat, GOES, NOAA), medium-resolution satellites (Landsat Multispectral Scanner (MSS), Indian Remote Sensing (IRS1), OPS-VNIR on Japanese Earth Resources Satellite -1 (JERS-1), Landsat Thematic Mapper (TM), Landsat Enhanced Thematic Mapper Plus (ETM+); and high resolution satellites (Satellite Pour l'Observation de la Terre (SPOT), IKONOS). Environmental satellites are best suited for frequent (daily or weekly) monitoring over relatively large areas, such as continents, subregions or countries. They are primarily used in meteorology and oceanography and, more recently, for monitoring vegetation conditions, principally of large pastures or forested areas, at scales from 1:10 million to 1:20 million. Medium-resolution satellites are generally represented by Landsat, MSS which has been in operation since 1972. They provide imagery at small to medium scale (1:1,000,000 to 1:200,000) for land use studies, and have particular application for forestry. High-resolution satellites are more recent and have principally been utilised since the mid-1980s. SPOT allows mapping at scales of up to 1:25,000. However, high resolution data are often offset by multifold increases in demand on computational power, analyst time and storage volumes.

The Landsat TM and ETM+ has 20 years of nearly continuous record of global land surface data since its inception. In Europe, there is the pan-European forest/non-forest map for the year 2000, based on Landsat ETM+ imagery (Pekkarinen et al., 2009) and the Corine Land Cover 2000 (CLC2000)[7] map (Bossard et al.,2000). The national land cover database is also based on both data types and it offers a full scale land cover map of the United States with 16 classes at a resolution of 30m (Homer et al., 2007;

[7] CLC2000 nomenclature covers 44 land cover classes which includes the agricultural as well as the urban and natural sector. The forest in the nomenclature of CLC2000 is defined as "areas ocupied by forest and woodlands with a vegetation pattern composed of native or exotic coniferous and/or deciduous trees and which can be used for production of timber or other forest products." (Bossard et al.,2000)

Xian et al., 2009). As of 2011, Landsat gobal mosaics are publicly free and global Landsat mosaics for 1975, 1990, 2000 and 2005 have been created (Lindquist et al., 2008; Hansen et al., 2008).

Much above-ground biomass work has been carried out using Landsat TM, NOAA AVHRR data, and other multi-spectral images. Most studies involve establishment of a relationship between a commonly used vegetation index such as NDVI (normalized difference vegetation index) with biomass or some biophysical parameter (Gibbs et al., 2007; Archard et al.,2007; Olander et al., 2008). Li et al. (2009) estimated the AGB for different forest types using six non-thermal Landsat TM bands and a variety of vegetation indices. Different forest types were demonstrated to have different relationship between the TM data and AGB. The results gave a good indication of the most appropriate TM bands in AGB estimation for different forest types; for hardwood forests these are TM7 and TM1, softwood forests are TM1 and TM5 and mixed forests are TM3 and TM5.

Several synergies of combined radar-optical approaches for forest mapping had been successfully conducted (Novo, 1995; Moghaddam et al., 2002; Wijaya et al.,2009; Lucas et al., 2010; Zhou et al., 2010). Moghaddam et al. (2002) showed that the estimation accuracy is significantly improved when radar and optical data are used in combination compared to estimating the same variable from a single data type alone. The optical classification corrected the SAR misclassification of vegetation due to surface roughness and soil moisture effects or similar backscatter responses from arboreal canopies (Hill et al., 2005). Multitemporal data of Moderate Resolution Imaging Spectroradiometer (MODIS) at 250m were fused with LISS-3 data at 25m spatial resolution, giving an accuracy of 88% (Kempeneers, 2011). However, this fusion is not considered in the thesis because in a cloud affected region like Glen Affric, optical data is not the most suitable choice.

Since multi-spectral sensors cover broad spectral bands, this reduces the ability to discriminate between two objects on the ground (Marmo, 1996). Therefore, they are not suitable for detailed mapping and identification of target, for which hyper-spectral sensors have been used. However, the volume of data collected from Hyperion is about 75 times larger than that for an equivalent area from six non-thermal Landsat ETM+ bands (Thenkabail et al., 2004). There are several studies that investigate the advantages of using discrete narrowband data from specific portions of the spectrum, rather than the broadband data, to obtain the most sensitive information on vegetation characteristics (Elvidge & Chen, 1995; Carter, 1998; Blackburn, 1999; Thenkabail et al., 2000).

Unlike multi-spectral sensors, hyperspectral sensors are capable of producing quantitative estimates of canopy biochemical properties such as leaf area index, chlorophyll, nitrogen, lignin and water content concentrations (Ustin et al., 2004; Goodenough et al., 2003; 2004; 2005a; 2005b; 2005c). Canopy models were developed not only to simulate hyperspectral top-of-canopy reflectance values for analysis of various biophysical and biochemical factors affecting canopy reflectance (Asner, 1998; Barnsley et al., 2000; Chen et al.,1999; Zarco-Tejada et al., 2004; Jacquemoud & Ustin, 2003; Riano et al., 2005; Li et al.,2005), but also to analyse biological invasion, biogeochemical change and nutrient availability in tropical ecosystems (Asner & Vitousek, 2005; Porder et al., 2005). Studies using hyper-spectral data to estimate biomass have been conducted under controlled laboratory conditions (Filella et al., 2004; Mutanga & Skidmore, 2004) and low spatial variability of biomass was found in the vegetation field such as wheat or corn (Hansen. 2003; Osborne et al., 2002; Xaxier et al., 2006) and mixed grassland (Mirik et al., 2005; Tarr et al., 2005; Geerken et al., 2005; He, 2006; Boschetti et al., 2007; Cho et al.,2007). Goodenough et al. (2008) demonstrated that biomass obtained from the airborne AVIRIS hyperspectral data correlated with biomass from ground measurement with R^2 of 0.90. The average classification accuracies was reported to exceed 89% in the forest species classification (Goodenough et al., 2003). While optical remote sensing data offers opportunities for mapping global forests, numerous challenges arise in analysing them. Unacceptable levels of cloud cover

persisted in about 25%-30% of the Landsat mosaic images in Ecuador and 16% in Congo basin (Olander, et al., 2008; Lindquist, et al., 2008). Optical remote sensing data is also not able to estimate three-dimensional structural forest components from a two-dimensional, horizontal image scene.

2.3.2 Active Sensors

Active sensors emit electromagnetic radiation, typically, microwave for Synthetic Aperture Radar (SAR) or visible and NIR for Light Detection And Ranging (LiDAR), and then receive the reflection of their emitted energy.

2.3.2.1 Synthetic Aperture Radar (SAR) for AGB Estimation

Synthetic Aperture Radar is an active sensor that builds an image through synthesizing a large antenna to improve spatial resolution (rather than using an impractically large physical antenna). Radar sensing has been developed on the basis of four technological principles (Olmsted, 1993):

- the ability of an antenna to emit a brief electromagnetic pulse in a precise direction
- the ability to detect the attenuated echo scattered from a target
- the ability to measure the time delay between emission and detection and thus the range to the target
- the ability to scan (by pointing or by linear motion) with the directional beam and examine an extended area for target

The wavelength of SAR determines the penetration depth of the signal and its interaction with soil moisture and water content of vegetation. Shorter wavelengths tend to be reflected by small tree structures such as twigs and thin branches at the top of the tree canopy whereas, the longer wavelengths tend to be reflected by the relatively larger structures such as the trunks and big branches. Good empirical relationship between SAR backscatter and biomass has been proven useful for AGB estimation (Kasischke et

al., 1995; Rignot et al., 1994; Imhoff, 1993; 1995; Kuplich et al., 2003; Jonforsen et al., 2007; Viergever et al., 2007; 2009; Mitchard et al., 2009; Ulander et al., 2011). However, depending on wavelength, polarisation, forest types and condition of the study area, the signal saturates at a certain level when the biomass is high (Le Toan et al., 2004). Studies over various forest types have proved the variation of saturation levels and that C-band commonly saturates at biomass densities of approximately 20-30 ton/ha, L-band at approximately 40-60 ton/ha and P band at approximately 100-120 ton/ha (Imhoff, 1995; Luckman et al., 1997; Hoekman and Quinones, 2000; Le Toan et al., 2004). Patenaude et al. (2005) reviewed 11 studies and reported that the accuracy for biomass estimation using SAR ranges between 50-96% across various forest types and bands. Several investigations reported that the radar backscatter is often correlated statistically with forest AGB before it reaches a certain saturation limit (Le Toan et al., 1992; Baker et al., 1994; Imhoff et al.,1995a; 1995b; Kellndorfer et al., 2003; Woodhouse, 2006; Takeshi et al., 2011). Since SAR backscatter is sensitive to topography, there is a need to correct the data radiometrically using high resolution DEM (Kellndorfer et al., 1998; Ticehurst et al., 2004). There are plenty of SAR data available, but the following discussion will focus on ALOS PALSAR and TerraSAR-X data as this research work uses both data for AGB estimation.

Rauste et al. (2007) reported that the estimation of growing stock volume is slightly more accurate with ALOS PALSAR radar images than with the earlier Japanese Earth Resources Satellite 1 (JERS-1), although both operated at L-band. Lucas et al. (2010) established a relationship between HH and HV backscatter from ALOS PALSAR, and above-ground biomass. More accurate above-ground biomass estimation was found when the surface moisture and rainfall are minimal. Combination of a forest growth model and a 3-dimensional forest backscattering coefficient model had been investigated to build a forest full polarization database (Guo et al., 2010). The inversion results derived from ALOS PALSAR Fine Beam Double Polarisation (FBD) data demonstrated that the distance threshold Look Up Table method was more desirable compared to the forest inventory data with mean absolute error less than 10 ton/ha (Guo et al., 2010).

McNeill et al. (2010) compared HH/HV and VV/HV dual polarization combinations from TerraSAR-X to estimate the pasture biomass in New Zealand. A linear regression using backscatter from the HH/HV combination was proven to be a better selection. While many other previous works (Lucas and Amston, 2007; Guo et al. 2008; 2010; Cassells et al. 2009; Mitchard et al., 2009; Lucas et al., 2010; Takeshi et al., 2011) showed the potential of ALOS PALSAR in biomass estimation, there has been very little work done on this in the UK (Cloude et al., 2001; 2008; 2010; 2011; Woodhouse et al., 2002; Tan, et al., 2010; 2011a; 2011b; 2011c; 2011d).

The advantages of radar data for AGB assessment are outlined in Table 2.3.

Table 2.3. Advantages and disadvantages of SAR data in AGB estimation

Advantages	Disadvantages
-All weather capability	-Interpretation requires knowledge of radar interaction with surfaces
-Day and night operation (independent of sun illumination)	-[8]Speckle and noise effects
-No effect of atmospheric constituents (multitemporal analysis)	-Saturation issue at certain level of biomass
-Forest canopy penetration possibility using longer wavelengths (L or P band)	-Challenging discrimination and mapping of tree species
-Complements visible/ infrared sensors (sensitive to terrain features and moisture)	-Topographic effects

[8] Speckle is the grainy salt-and-pepper pattern appearance in radar imagery caused by the interference from multiple scattering within the resolution cell.

-Good for discrimination the terrain structure (roughness) and drainage patterns -Images can be produced from different types of polarized energy (HH,HV,VH,VV) -Possibility for interferometric operation for 3-dimensional mapping	-Complicated processing and difficulty in understanding due to complex interactions

2.3.2.2 InSAR and POLInSAR systems for AGB Estimation

Polarimetry and interferometry have become promising emerging techniques for diverse range of classification applications by analysing the large amount of information it contains (Oliver & Quegan, 1998; Cloude & Papathanassiou, 1998; Papathanassiou & Cloude, 2001; Lee et al., 2003; Alberga, 2004; Famil et al., 2006; Sauer et al., 2007; Jager et al., 2007; Lee & Pottier, 2009; Hoekman et al., 2011; Ferro- Lopez-Sanchez et al., 2011). The use of SAR interferometry allows the derivation of forest height. Several studies estimated the canopy height from C-band Shuttle Radar Topography Mission (SRTM) digital surface model by subtracting a known ground elevation from surface elevation (Kellndorfer et al.,2004; Neeff et al., 2005; Walker et al.,2007). Sexton (2009) reviewed the accuracy of different InSAR measurement techniques and found that X-band and P-band wavelengths differencing was more accurate than SRTM-ground differencing but both InSAR methods were less accurate than LiDAR. In general, most of the InSAR measurements underestimate the forest height because they measure to the phase scattering centre, which is usually below crown level.

Polarimetric interferometric SAR (PolInSAR) utilizes polarimetric and interferometric information to model the vertical structure and height of forest from

SAR scattering models (Cloude & Papathanassiou, 1998; Papathannasiao & Cloude, 2001; Treuhaft et al., 2000; Le Toan et al.,2008). The basic concept of PolInSAR is to discriminate between the ground and the canopy response by using different polarization states and phase information. The FinSAR campaign was conducted to validate the PolInSAR tree height retrieval algorithm for boreal forest. Results showed that the tree height retrieved by Random Volume over Ground inversion model was comparable with the scatterometer measurements and forest stand wise inventory data (Praks et al., 2007). Cloud cover and biomass saturation suggest that a combination of low frequency SAR and interferometry, either PolInSAR or dual-band interferometric SAR (DBInSAR) can be a solution. Tropical forest biomass estimation using X-P DBInSAR and P-band backscattering cross section has been demonstrated from airborne GEOSAR (Williams et al., 2009; 2010).

In open forests with variable tree heights (referred to as heterogeneous stands) the behaviour of the height-extracting algorithm is unknown and height-biomass allometry cannot be easily applied. Mette et al. (2004) introduced an effective height derived from PolInSAR to estimate the biomass in this type of forest. Viergever et al. (2007; 2008; 2009) demonstrated that the retrieved canopy heights from both X- and C-band InSAR clear trend in vegetation patterns although they cannot give a good representation of biomass estimate due to the heterogeneity of the canopy.

ALOS-Indonesia PolInSAR Experiment (AIPEX) was tested to study the scattering and interferometric characteristics and to provide feedback to JAXA for future Earth Observation mission planning (2007). The recently launched TanDEM-X in June 2010 has shown potential for height estimation across a diversity of forest types and various POLInSAR-based height retrieval methods are still underway (Kugler et al., 2011; Papathanassiou, K. et al., 2011).

2.3.2.3 Light Detection And Ranging (LiDAR) systems for AGB Estimation

Another active sensor system, similar to radar is Light Detection And Ranging (LiDAR). LiDAR is a 'laser' (Light Amplification by Stimulated Emission of Radiation) system offering great potential for forest monitoring applications. This technology involves a scanning and ranging laser system that produces pinpoint accurate and high resolution maps. The sensor transmits coherent laser light at various visible or NIR (Near InfraRed) wavelengths, as a series of pulses to the target, from which some of the light reflects back to the sensor. It measures the time taken for a pulse of laser to travel between the sensor and the target. The pulse travels through the atmosphere and interacts with objects on the Earth's surface, and is then reflected back to the sensor. The time for the traverse is calculated, by assuming the speed of light through the atmosphere, and the intensity of the reflected radiation is measured. LiDAR digital elevation data can be generated at a variety of resolutions and obtain high resolution data.

The two most popularly used LiDAR systems are the laser profiler or altimeter and the reconnaissance or mapping LiDAR. The benefits of LiDAR in forestry applications is the acquisition of three-dimensional data of the forest structure, and data on canopy cover characteristics, leaf area index, crown cover and volume (Koetz et al., 2006, Dalponte et al., 2009; Huang et al., 2010; Chen et al., 2010; Allouis et al., 2010).

In the past several years, the use of airborne laser scanning (ALS) LiDAR to characterize forest structure and underlying terrain has proliferated (Means, J.E. et al., 2000; Lim, K. S. et al., 2003; Nelson, R. et al., 1984; Nelson, R. et al., 1988; Nelson, R. et al., 2004; Kraus, K., 1998). With LiDAR the ability to capture high-resolution images quickly and relatively independent of lighting conditions can be an advantage. Because of its ability to rapidly measure the Earth's surface at 20,000 to 75,000 records per second there are generally enough individual points to provide adequate coverage in the forested areas, even if only a small percentage of them reach the ground through the trees. It measures the return time for each beam to travel between the sensor and a target

using ultra-accurate clock (Renslow, 2000). The data point density depends on the number of pulses transmitted per unit time, the scan angle of the instrument, the elevation of the aircraft above-ground level, and the forward speed of the aircraft. The system is also capable of achieving high vertical accuracy with 15-20cm RMS and horizontal accuracy with 20-30cm RMS (Suarez et al., 2005).

Airborne LiDAR systems typically have a small measurement footprint in the range 0.3 to 3m while for large footprint LiDAR it is 10m to 25m, or as much as 70m for spaceborne systems. Large footprint LiDAR systems, usually referred to as surface LiDAR system, are based on waveform sampling techniques. Waveform distributions define the strength or energy of the laser return from a given footprint at different time or distance intervals, thereby recording the vertical distribution of the returned laser illumination from all canopy elements and the ground (Lefsky et al., 1999). Unlike the large footprint system, small footprint LiDAR is able to detect individual crowns and has finer ground spacing. It has great potential for estimating physical structure of trees such as height, crown diameter and canopy density. Small footprint systems are useful for discreet return systems in extracting both canopy and ground returns and they are represented by first and last returns. Vegetation canopy height is then defined by the difference between the last and first returns (Lefsky et al., 1999).

Large-footprint LiDAR, with its full waveform describing three-dimensional canopy structure has been used to estimate biomass in several types of forests (Means et al., 1999; Drake et al., 2002a; 2002b; 2003; Lefsky et al., 2002; Anderson et al., 2006; Sun et al., 2007; Boudreau et al., 2008). In tropical forests, the accuracies of biomass estimation are between R^2 of 0.66 and 0.93 (Drake et al., 2002a; 2002b; 2003). In temperate and boreal forests, predictive accuracies of biomass estimation is ranged between R^2 of 0.61 in the deciduous forests in northeast United States (Anderson et al., 2006) and R^2 of 0.95 in conifer forests in Pacific Northwest (Means et al., 1999). Lefsky et al. (2002) estimated above-ground biomass at three different forest types; temperate coniferous (fir species; Psedotsuga menziesii), temperate deciduous (yellow poplar

species; Liriodendron tulipifera) and boreal coniferous (black spruce species; Picea mariana) forests. An R^2 of 0.84 was obtained for all the three forest types. The authors concluded that the application of a single biomass model across three distinct forest types was successful.

Popescu et al. (2004) observed that the accuracies fall between R^2 of 0.32 and 0.81 in deciduous and pine forests while Patenaude et al. (2005) reviewed the accuracies of biomass estimation using small footprint and reported that the range is between R^2 of 0.45 and 0.91 in temperate forests. Nilsson (1996) utilised small footprint data to derive mean tree height for even-aged Scots pine stands and found that laser mean height is underestimated by 2.1 to 3.7 m. The underestimation is due to the fact that most LiDAR returns are from crown locations below the tree tops (Magnussen and Boudewyn, 1998). The results can be improved by further calibration using field data. Good correlations was found between laser measured and field measured canopy density (0.9) and height (0.95) for Loblolly pine stands by Young et al. (2000).

On the whole, LiDAR data offers unique features that could negate the need for extensive ground-based, small-scale field measurement of tree heights and other physical parameters as well as provide high positional accuracy.

2.4 Global Earth Observation Missions and Projects for Biomass Estimation

Various global Earth Observation missions have been considered to improve the understanding of forest dynamics globally. Carbon-3D was proposed to improve the knowledge about spatiotemporal patterns of major carbon fluxes and reduce the uncertainties about net effects of deforestation on CO_2 concentration. It combines the LiDAR system Vegetation Canopy LiDAR (VCL) with a Bidirectional Reflectance Distribution function (BRDF) . It aims to provide accurate global biomass map to serve the requirements of Integrated Observing Strategy Partnership (IGOS-P). Further international research related to the global carbon cycle is organised through the

European Space Agency Living Planet Programme, including the Earth Observation Envelope Programme (EOEP) and the Earth Watch Programme (EWP), the Orbiting Carbon Observatory (OCO) mission and the Global Monitoring of Environment and Security (GMES), a joint initiative of the European Commission and the ESA (Hese et al., 2005).

In connection with the Candidate Earth Explorer User Consultation meeting, six missions have been proposed within its Living Planet Programme to cover a range of environmental issues with the aim of furthering the understanding of the Earth system and changing climate (ESA Future Earth Explorer Missions, online, 2011):

- BIOMASS – to take global measurements of forest biomass.
- TRAQ (TRopospheric composition and Air Quality) - to monitor air quality and long-range transport of air pollutants.
- PREMIER (PRocess Exploration through Measurements of Infrared and millimetre-wave Emitted Radiation) – to understand processes that link trace gases, radiation, chemistry and climate in the atmosphere.
- FLEX (FLuorescence EXplorer) – to observe global photosynthesis through the measurement of fluorescence.
- A-SCOPE (Advanced Space Carbon and Climate Observation of Planet Earth) – to improve our understanding of the global carbon cycle and regional carbon dioxide fluxes.
- CoReH_2O (Cold Regions Hydrology High-resolution Observatory – to make detailed observations of key snow, ice and water cycle characteristics.

As a result, only three of the missions have been recommended for further investigation and the development is underway. They are BIOMASS, CoReH2O and PREMIER.

Among the three Earth Observation missions, only the BIOMASS mission is relevant to this thesis. The BIOMASS mission aims to provide continuous global

interferometric and polarimetric radar observations to determine the distribution and temporal changes of forest biomass at a global scale. Due to the sensitivity of longer wavelengths (P-band) to forest biomass combined with the advanced weather-independent capabilities of modern polarimetric and interferometric SAR instruments, the satellite is ideally suited for forest biomass mapping (Heliere et al., 2009). Data from the BIOMASS mission is aimed to reduce current uncertainties in the calculations of carbon stocks and fluxes associated with the terrestrial biosphere.

Another very important mission is the DESDynI (Deformation, Ecosystem Structure and Dynamics of Ice). The aim of the mission was to provide global estimates of above-ground biomass at a maximum spatial resolution of 500 m and an accuracy of 10Mg C ha^{-1} (up to 20% of the total) (Cook et al., 2009). This mission would have featured two sensors (an L-band Interferometric Synthetic Aperture Radar (InSAR) system with multiple polarization and a multiple beam LiDAR operating in the infrared (~ 1064 nm) with ~ 25 m spatial resolution and 1 m vertical accuracy) to provide observations for solid-Earth (surface deformation), ecosystems (terrestrial biomass structure) and climate (ice dynamics) (Kwoun et al., 2010). However, due to tight budget, the mission has been indefinitely deferred (Reference: http://www.spacenews.com/civil/110225-climate-missions-nasa-budget.html).

Although the ICESat-2 laser altimetry mission (anticipated to be launched in early 2016) is originally developed to quantify the amount of change in ice sheets and sea ice, it has some capability to map canopy heights in forests. Because of the vertical distribution of laser return from vegetation surfaces, ICESat-2 can be made to assess the forest biomass through the measurement of tree heights. Plans are also under way to scope a possible vegetation LiDAR mission using the international space station (Abdalati et al., 2010).

There is a prospective spaceborne mission concept using PolInSAR, the TanDEM-L. The satellite is designed for global forest height and biomass inventories,

large scale measurements of millimetric displacements due to tectonic shifts and systematic observations of glacier movements. It is based on co-flying two fully-polarimetric L-band SAR satellite and enables highly accurate interferometric measurements to derive contiguous 3-D structure profiles and their spatiotemporal evolution (Krieger et al., 2010).

A new venture by NASA JPL, the Orbiting Carbon Observatory-2 (OCO-2) mission is scheduled to be launched in February 2013. This mission will be NASA's first mission dedicated to collecting global measurement of carbon dioxide (CO_2). There are many other missions available and planned that hold great promise for forest mapping but they will not be discussed at length here. The list of available and expected missions is summarised in Table AI.1.

Global biomass estimation projects which are based on Earth Observation satellites are mainly driven by space agencies such as the European Space Agency (ESA) and the Japanese Aerospace Exploration Agency (JAXA). Biomass and carbon projects initiated under ESA are categorised into the Treaty Enforcement Services Using Earth Observation (TESEO) and Data User Element (DUE) programmes. Initiatives running under these flags are TESEO-Carbon, Kyoto Inventory, GlobCarbon and GlobColour. On the other hand, JAXA initiatives, Global Rain Forest and Global Boreal Forest Mapping project (GRFM/GBFM) and ALOS Kyoto & Carbon Initiative focus solely on JERS-1 and ALOS PALSAR.

The Integrated Global Carbon Observation (IGCO) initiative is linked with the Global Carbon Project (GCP) where GCP provides a framework for model development and intercomparison, advanced process studies and research-based observation; while IGCO plans strategy and implements plan for systematic, long-term observation of carbon fluxes, pools and process (Ciais et al., 2007). This partnership brings together the space agencies as represented by Committee on Earth Observation Satellites (CEOS),

the Global Observing Systems (GOOS), the Global Terrestrial Observing System (GTOS) and the Global Climate Observing System (GCOS).

Global Observations of Forest and Land Cover Dynamics (GOFC-GOLD) is an organisation that form the international coordination needed to ensure systematic long-term observations of land cover and forest change. The key roles of GOFC-GOLD in this goal is to increase international cooperation in the standardization, integration and use of data from multiple earth observation satellites, in conjunction with *in-situ* data, for mapping and monitoring the earth's forests, and to provide feedback to agencies responsible for space and *in situ* observations to enable them to improve the quality of observations. The summary of the global projects is listed in Table AII.1.

As a non-Earth Observation initiative, the Global Carbon Cycle aims to develop policy for climate mitigation, sustainable development and the provision of ecosystem services, both at national and international levels. It brings together carbon cycle resources, including information on national and regional carbon programmes and research agendas are listed in Table AII.2. These programmes offer carbon observations at scales ranging from local to global, enabling frequently updatable biomass estimation which represent the spatial heterogeneity of the forest more efficiently. The improved ability to monitor biomass stock and growth potential at inaccessible areas such as hilly and mountainous regions is important for carbon reporting under the Kyoto Protocol.

2.5 Chapter Summary

The recognition of AGB as one of the most important components in global carbon cycle has given rise to a number of global biomass studies. This chapter is intended to introduce remote sensing and give an overview of current and emerging remote sensing technologies for AGB estimation. Each sensor type has its advantages and disadvantages for AGB estimation. A major advantage of SAR images compared to optical images has been their ready availability under all weather conditions, hence,

making it an intriguing option in developing methods for operational inventory of forest monitoring and management applications. When comparing to airborne laser scanning or aerial photography, SAR is superior as it has both increased temporal and spatial coverage.

Coarse resolution sensors have the greatest capability for global coverage and temporal resolution, but their pixel resolution causes them to miss the majority of deforestation events (DeFries, et al., 2002; Rosenqvist, et al., 2003; Morton, et al., 2005; Archard, et al.,2007; Olander, et al.,2008; Azofeife et al.,2009). On the contrary, high resolution sensors allows fine measurement of individual tree and forest composition, but their small swaths limit their capability of wide coverage and repeatability acquisition (Anderson, et al., 2009).

In summary, airborne missions are relatively expensive to conduct and have much smaller image coverage or swath but are flexible and can provide high resolution data (Olander et al., 2008; Andersson et al., 2009). Spaceborne missions cover a large area less expensively and thus are viewed as the best way to measure global forests remotely (DeFries, 2008; Olander et al., 2008; Andersson et al.,2009; Sanchez-Azofeifa et al., 2009).

Chapter 3
The Study Area: Glen Affric Conservation and Management Area, Scotland

3.1 Introduction

The goal of this chapter is to give an overview of the study area, fieldwork data collection and Earth observation data acquisition. This chapter will do the following:

- to describe the geographical location, climate, topography, land use management and history of the study area (Section 3.2). This information gives an idea of how they are likely to affect the Earth Observation data. For instance, climate and rainfall affect the dielectric constant of the soil or vegetation. When moisture content of the soil or vegetation is high, the dielectric constant is high, consequently, the backscatter is high. The topography description conveys the information of the surface roughness of the study area which influence the values of the radar backscatter coefficient and scattering mechanisms. The rougher the surface, the higher the backscatter coefficient.

- to describe the field data collection, analysis and results (Section 3.3). Two campaigns of fieldwork data collection of the *in-situ* measurement were conducted by myself, a number of colleagues from The University of Edinburgh

and Forestry Commission staff. The fieldwork data was processed and the GPS observation files were converted to a format using the Ordnance Survey Great Britain '36 coordinate system. The analysis and interpretation of the fieldwork data concludes the section.

- to describe the specification and acquisition of Earth Observation data used for this thesis (Section 3.4). The data includes airborne LiDAR data and satellite radar images of ALOS PALSAR and TerraSAR-X. These data were geo-referenced to the same coordinate system (Ordnance Survey Great Britain '36) as the fieldwork data to allow further interpretation and analysis of the study area.

3.2 The Study Area : What is so special about Glen Affric?

The Glen Affric Caledonian[1] Pinewood Reserve is located in the northwest highlands of Scotland, at Ordnance Survey grid squares NH12 and NH22 (Forest Enterprise, 1997). It is chosen as the study area for this research because of

- its varied topography and range of forest cover types. They are mountainous and combines several crucial challenges for radar remote sensing, including heterogeneous forest cover, sloped terrain and a broad distribution of tree heights (Cloude et al., 2001). High hills of 470-700m surround the reserve entrance at the eastern end, whilst there are mountains of over 1000m to the west. Loch Affric and Beinn a Mheadhoin dominate the Glen and numerous smaller lochs and lochans are scattered over the glen. Figure 3.1 shows the location of Glen Affric.

[1] The Caledonian Forest takes its name from the Romans, who called Scotland 'Caledonia', meaning 'wooded heights' (Reference: http://www.treesforlife.org.uk/tfl.visi.html)

- the Caledonian forest conservation urge. In Scotland, the natural regeneration of the Caledonian forest over wide areas is seen as a major goal for Scottish conservation managers. Effective forest monitoring is required as European legislation now requires national conservation agencies, such as Scottish Natural Heritage, to monitor temporal change and report on the status of nationally and internationally important conservation areas (Cloude et al., 2001).

  Caledonian forest traditionally describes the ancient forest of Scots pine (Pinus Sylvestris) that was believed once to have covered a large proportion of the Scottish Highlands (McVean & Ratcliffe, 1962). During the Roman invasion in Britain, it is estimated that the Caledonian forest covered approximately 1.6 million ha of the Scottish Highlands. However, this area of genuinely native pinewood had declined to approximately 16,000 ha by the beginning of the 1990's (Aldhous, 1995; Featherstone, 1997; Annon, 2003).

  A decline in pinewoods in Scotland occurred as a result of regional climate change (increased rainfall, strong storms and colder winters) due to broad-scale features of global atmospheric circulation increasing precipitation levels and hence promoting the expansion of blanket bog and heath (Wolff & Tipping, 1999; Smout, 2003). Apart from the climatic conditions, it is also noted that anthropogenic activities such as deforestation and burning has contributed to the Caledonian forest decline (McKensie & Callander, 1995). Today, only remnants of the Caledonian forest are found in the Scottish Highlands and so are protected for conservation purposes.

- the availability of Earth Observation data for this area and the accessibility to the site for fieldwork campaigns. Airborne LiDAR data was thoroughly planned and acquired by The Environment Agency Science Enterprise Centre on behalf of Forest Research. Other remote sensing data such as ALOS PALSAR and TerraSAR-X data are also made available for the study area. Glen Affric is part

of the Upper Beauly Catchment Forest Design Plan (FDP) area (Forestry Commission, 2008) and contains the largest area of Caledonian forest owned by the Forestry Commission. Fieldwork campaigns were organised and carried out after obtaining permission to access the study area.

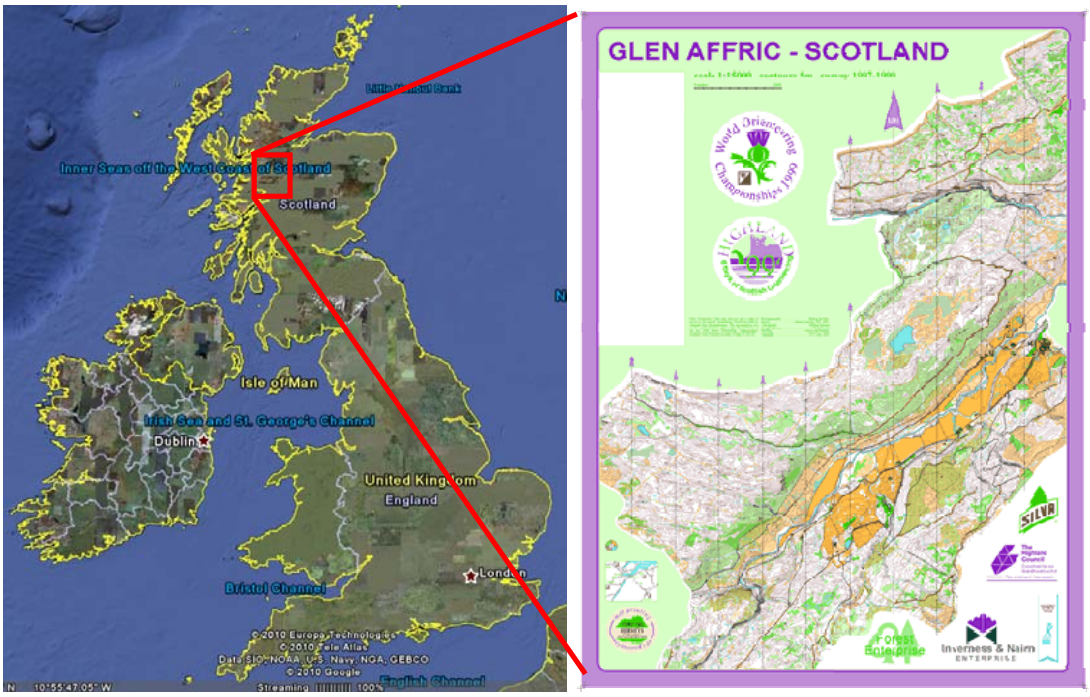

Figure 3.1. Location of Glen Affric. (Picture source: left - Google Earth Pro Trial Version 6.1 beta, right - Forestry Commission, 2008)

3.2.1 Climate

The climate of Glen Affric is temperate with frequent severe frosts and the duration of growing season is estimated at four to five months (Forest Enterprise, 1997). Based on the Ecological Site Classification (ESC), Glen Affric falls into the Cool Moist, Cool Wet, Sub-Alpine and Alpine zones (Pyatt, 1995; 2001). The annual rainfall varies from 1600mm east of Loch Beinn a Mheadhoin to 2800mm, west of Loch Affric. Steven

and Carlisle (1959) reported that the mean annual temperature in Glen Affric is 6.1°C where the mean temperature in January and July are 1.7°C and 12.2°C, respectively.

3.2.2 Geology and Topography

Glen Affric is underlain by metamorphic sedimentary rocks of the Moine series, including quartz-feldspar granulites, quartz-mica-schists, mica schist and gneisses (Steven & Carlisle, 1959; Forest Enterprise, 1997). Geomorphological evidence of glaciation is extensive, with glacial till deposits which creates a characteristic hummocky terrain. The nature of the soils varies locally with topography and aspect (Figure 3.2). The glen is dominated by brown earth soil with surface water gleys and deep peats occuring where drainage is poor at the eastern end (Ogilvy, 2004). Peat is extensive on upper slopes and to the west of Loch Beinn a Mheanhoin, including peaty podzols, peaty ironpad soils, peaty gleys, deep peat and rankers (Forest Enterprise, 1997).

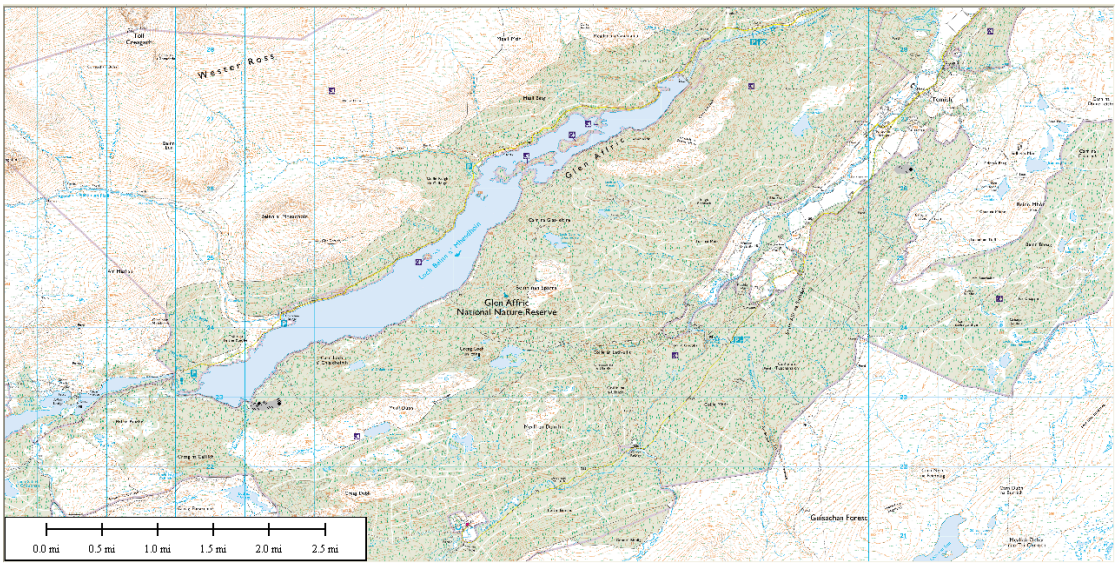

Figure 3.2. Glen Affric map to show the topography of the area. Crown Copyright Ordnance Survey. An EDINA Digimap/JISC supplied service.

3.2.3 Vegetation

Scots pine (*Pinus sylvestris*) dominates the canopy in the reserve (Rodwell,1991; Averis, 1994). This true cone bearing species can grow as high as 40 meters. Like other pines, the tree has 5-7cm long stiff waxy needles leaves which grow in pairs from the twigs. Originally, this species formed extensive forests over most of Britain. However, due to the anthropogenic activities in the last 2000 years and coupled with the gradual climate change 5000 years ago, it is something of an anomaly in that there are relatively few of the trees living today in northern Scotland (Forestry Commission, 2008).

The pinewoods towards the east have discrete patches of pine-birch (*Betula pubescens*) mixtures and patches of pine associated with a variety of other deciduous trees such as rowan (*Sorbus aucuparia*), goat willow (*Salix caprea*), alder (*Alnus glutinosa*) and aspen(*Populus tremula*) (Forest Enterprise, 1997). Interspersed with pinewoods, birch-oak woodlands types as well as one small ash wood are found in the far eastern pocket where brown earths predominate (Averis, 1994). Within woodland areas, ground vegetation includes *Calluna vulgaris, Deschampsia flexuosa, Empetrum nigrum, Erica spp., Vaccinium myrtillus, Vacccinioum vitis-idaea, Trichophorum cespitosum, Molinia caerulea, Sphagnum spp.* and *Hylocomium splendens* (Averis, 1994; Forest Enterprise, 1997).

The pine becomes more scattered towards the west and it occurs sparsely as small clumps or solitary trees on well-drained slopes and along river banks. The age distribution of Scots pine in Glen Affric is similar to other Scottish Highland pinewood remnants. Research has shown that trees are concentrated in the 143-202 year age-class with a lack of regeneration 60-120 years ago because of intensive grazing pressure (Arkle & Edwards, 1996). The lack of regeneration still characterises the native woodlands except where disturbance along roadsides has allowed seeding growth (Ogilvy, 2004). The biomass density in Glen Affric typically ranges from ~30 to

~150ton/ha (Cloude et al., 2008), although higher biomass density can be found in plantation managed forests. However, this assumption has not been adequately validated.

3.2.4 Land use and management history

Glen Affric forms part of the Upper Beauly Catchment Forest Design Plan (FDP) area and contains the largest area of Caledonian forest owned by the Forestry Commission as well as a range of other habitats of conservation importance. The name Affric comes from the Gaelic "Ath-Bhreach", meaning dappled ford. The forest in Glen Affric is thought to have existed for 8000 years since trees colonized the area after the last ice-age (MacRae, 1980; Forest Enterprise, 1997).

The estate of Glen Affric was originally owned by the small Chisholm clan from the 17th century AD. The Forestry Commission bought Glen Affric in 1951 and declared part of the glen as a 'Pine Reserve' (Wield, 2001) in 1960. Steps to restore and improve regeneration of the pinewood were taken. Deer fenced enclosures were put up to control the number of deers within the enclosure and to reduce grazing pressure. At the same time, young pines were planted to help the process of regeneration. Some years later it was observed that, with low deer numbers, natural seedlings were surviving in much greater numbers and a decision was made to cease planting in 1975 (Forest Enterprise, 1997).

As one of the most important native woodlands in Scotland, Glen Affric has been designated a 'Site of Scientific Interest' (Forest Enterprise, 1997; Wield, 2001) in 1975 and 'Caledonian Forest Reserve' in 1994. This means that its 10,645 ha will be managed for its heritage, environmental and conservation values. Since then, it has been proposed as a Special Area of Conservation (SAC) under the EU Habitats Directive and as a Special Protected Area under the EU Birds Directive. Funds from the EU LIFE programme and the Millenium Forest for Scotland project have also been acquired for

restoration activities. In April 2002, Glen Affric became a National Nature Reserve (NNR) (Ogilvy, 2004).

3.3 Fieldwork Data

3.3.1 Description of Fieldwork Measurement

Fieldwork measurement was carried out from 03 to 08 May 2009 in Glen Affric. The objective of the measurement campaign was to collect positional data as well as physical measurement data for the trees in Glen Affric in the semi-natural[2] and plantation forest areas. The physical parameter comprised of total tree height, height of first living branch, diameter at breast height (dbh) and density. Species identifications were made directly in the field. Ancillary data including the ground elevation data through spot height process and tree rings measurement were also conducted as value-added information to the research.

The field work data encompasses survey-grade positional data (comprising of x, y and z coordinates) within two transect areas of approximately 200m x 50m and 400m x 50m (Figure 3.3). A number of possible transect sites were identified during a desk-based study of the EO data before arrival at the field site. The candidate sites were visited during the first day of the fieldtrip. The first transect area consists of forest plantation while the second transect area covers the semi-natural forest along Loch Beinn a Mheadhoin. The data set consists of 531 mapped points for Scots pine (254), birch (53) and spruce (224). All trees with dbh more than 10cm occurring within 25 m to both sides of the main transect line were included in the data collection. Pre-planning involved discussion with the local officials and researchers from the Forestry Commission, AEL consultants and The University of Edinburgh. During the planning stages, it was envisaged that the transect should have a width of at least 25 m and a

[2] Semi-natural forest is defined as woodland site that has retained the native tree and shrub cover that has not been planted, although it may be managed by coppicing or felling and allowed to regenerate naturally.

length of approximately 400 m. The width dimension was based on the ALOS PALSAR pixel size of 12.5 m, so that a 25 m wide ground transect in the ALOS PALSAR range direction would include sufficient ground data to compare with the SAR data. It was anticipated that a transect length of approximately 400 m would be feasible for collecting sufficient data in a 5-day period. However, due to uncertainties on the time needed for data collection, the fieldwork was planned with flexibility in mind.

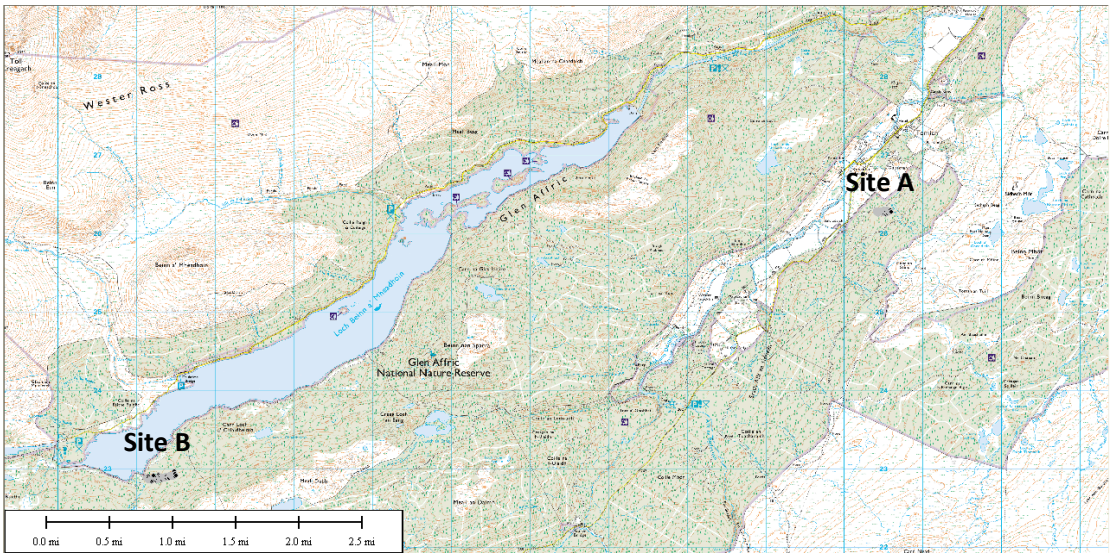

Figure 3.3. Location of Site A and Site B. Crown Copyright Ordnance Survey. An EDINA Digimap/JISC supplied service.

Site A is situated at approximately 500m South East of Guisachan with the centre coordinate of 826277.5N, 230452.2E. It is situated at approximately 500m South East of Guisachan. Figure 3.4 shows the location and the forest structure of the study site. The 2-D and 3-D projection of transect field data of Site A are shown in Figure 3.5 and Figure 3.6, respectively. The fieldwork measurement covers an area of 200m x 50m at this site.

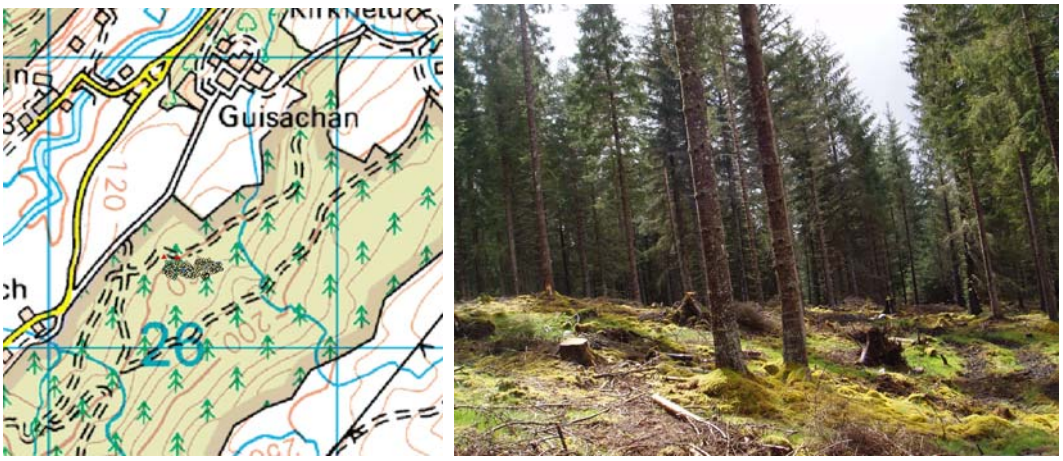

(a) (b)

Figure 3.4. (a) The geographical location of the transect at Site A on the Ordnance Survey Colour Raster in the scale 1: 50000, under the projection British Grid, WGS84, Crown Copyright Ordnance Survey. An EDINA Digimap/JISC supplied service (b) Photograph showing typical forest structure in Site A

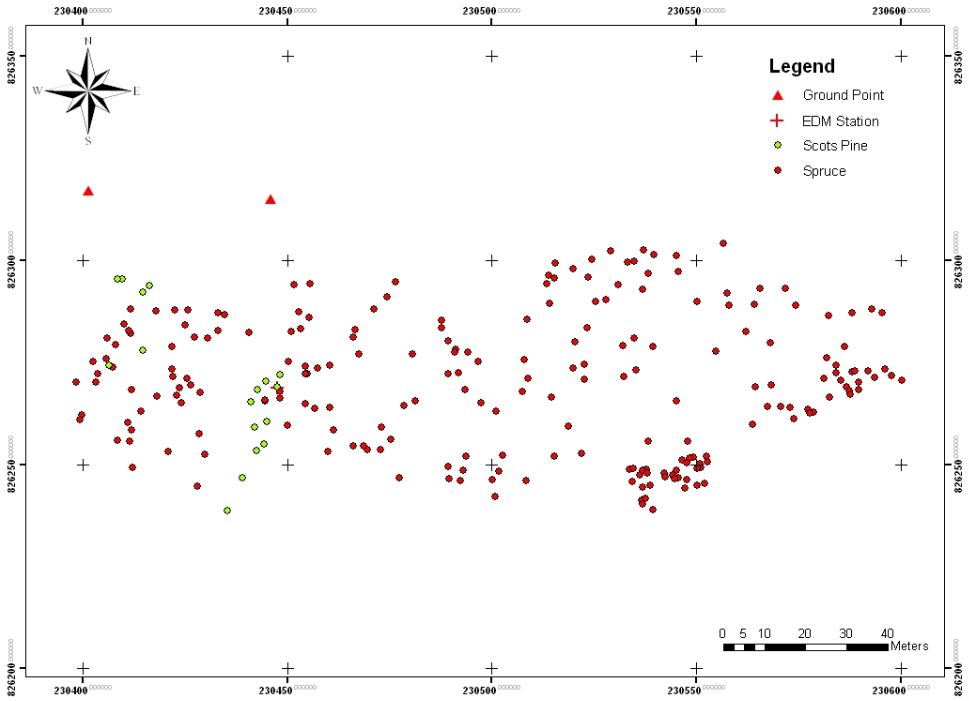

Figure 3.5. Location of trees measured in Site A. The circles in 'green' and 'red' indicate the location of the measured Scots pine and Spruce, respectively in the site.

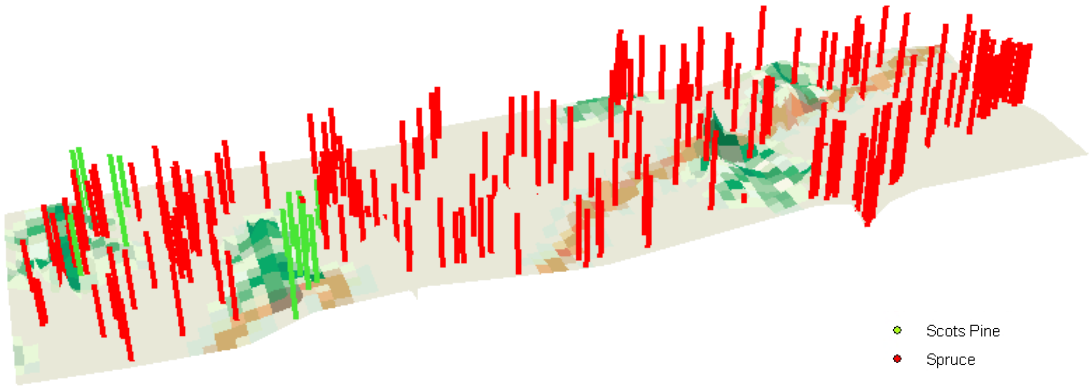

Figure 3.6. The 3-dimensional view of transect field at Site A that shows the distribution of the trees in plantation forest

On the other hand, Site B is located at approximately 15m South of Loch Beinn a' Mheadhoin and 1km South East of Loch a'Chlaidheimh (Figure 3.7). The centre coordinate of the field work transect is 822862.9N, 221279.3E with the measurement coverage of 400m x 50m along the transect. Figure 3.8 and 3.9 show the 2-D and 3-D projection of transect field data of Site B, respectively.

(a) (b)

Figure 3.7. (a) The geographical location of the transect at Site B on the Ordnance Survey Colour Raster in the scale 1: 50000, under the projection British Grid, WGS84, Crown Copyright Ordnance Survey. An EDINA Digimap/JISC supplied service (b) Photograph showing typical forest structure in Site B

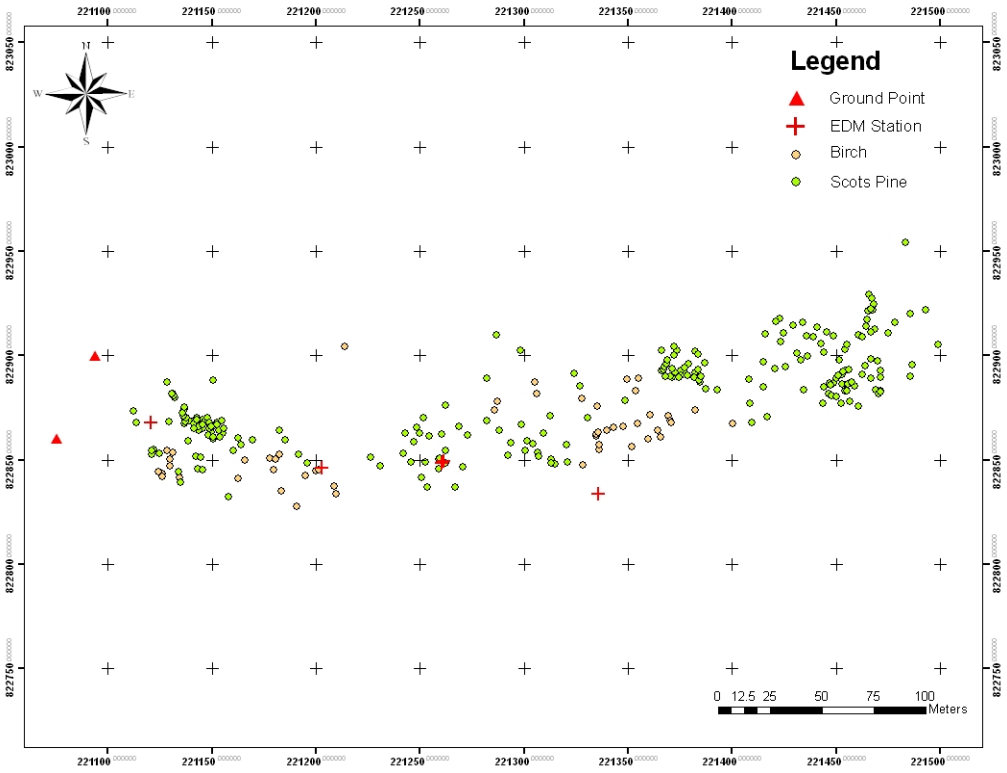

Figure 3.8. Location of trees measured in Site B. The circles in 'yellow' and 'green' indicate the location of the measured Birch and Scots pine, respectively in the site.

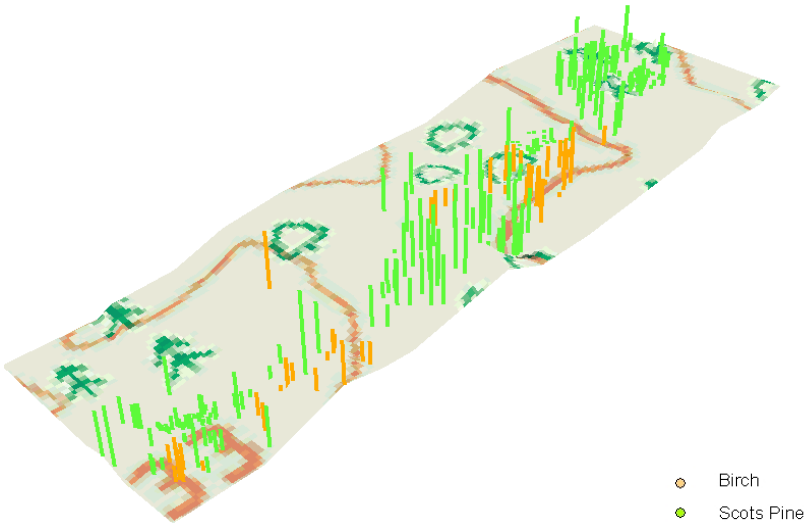

Figure 3.9. The 3-dimensional view of transect field at Site B that shows the distribution of the trees in semi-natural forest

Another intensive fieldwork was carried out for several months from winter 2006 to spring 2007 by the Forestry Commission. One hundred and seventy circular sample plots of 12.6 m radius were located in a sub-sample of the most abundant canopy structure forests. All plots were geo-referenced using a Garmin GPSMAP 60CSx, hand help GPS systems, with all data collected onto pre-forma excel spreadsheets on Toughbook CF18 portable data capture notebooks. Within each circular sample plot, the species was identified and physical parameters were measured. Figure 3.10 shows the location of the center coordinates of the sample plots. They are all scattered over the glen.

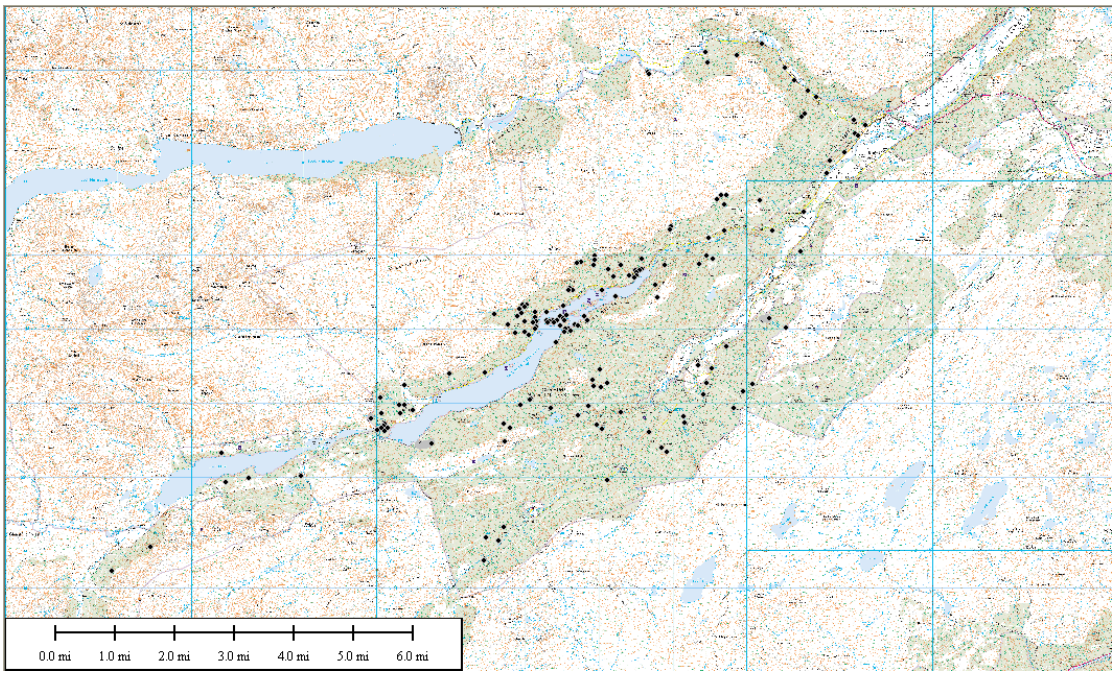

Figure 3.10. Location of all the center coordinates of the sample plots. Crown Copyright Ordnance Survey. An EDINA Digimap/JISC supplied service.

3.3.2 Description of Fieldwork Parameters

3.3.2.1 Diameter Breast Height (dbh)

The tree dbh is one of the important variables used in the estimation of tree and stand volume. Generally, it is defined as the outside bark diameter at breast height and the breast height is defined as 4.5 feet (1.37m) above the forest floor on the uphill side of the tree (Nix, 1997). In this fieldwork, a diameter tape is used for measuring tree diameter due to its convenient size and relative accuracy. Trees with special circumstances were measured according to standard procedures (Husch, et al., 2003). For leaning trees, the breast height were measured parallel to the lean on the high side of the tree and dbh were measured perpendicular to the longitudinal axis of the trunk. Trees that were crooked or had an abnormality at breast height such as limb and bulge, were measured just above the abnormality. Trees which consist of two or more boles forked at or above breast height were measured as one tree just below the enlargement caused by the fork; trees of which the bole forked below breast height were measured as separate boles, adding up the separate dbh values during processing of the data. The dbh distribution of trees in Site A and Site B are shown in Figure 3.11 and Figure 3.12, respectively.

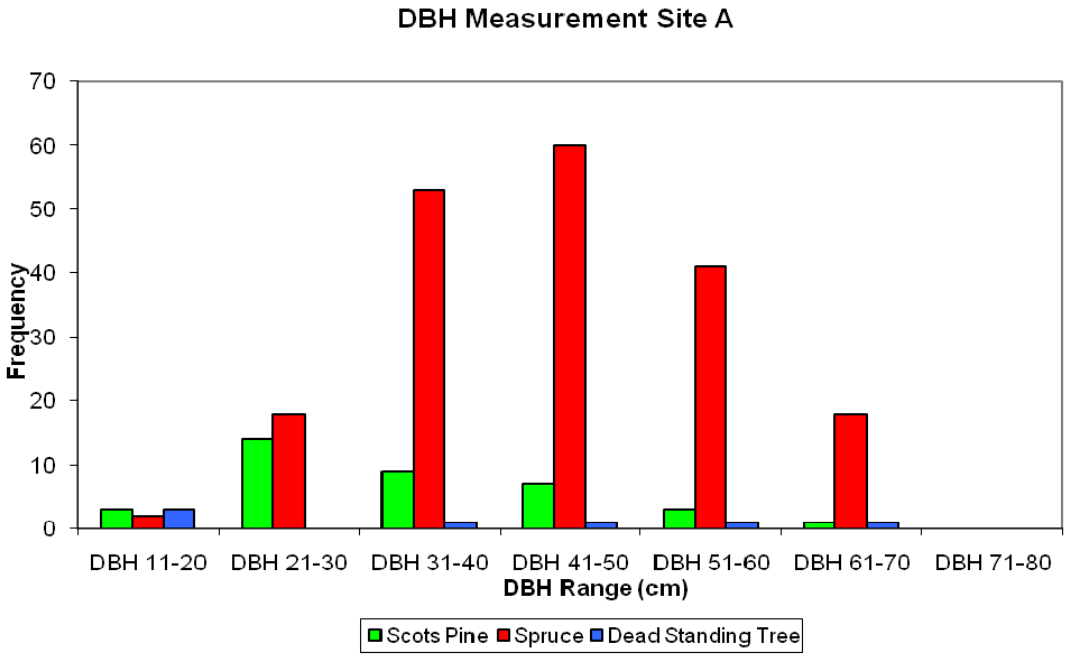

Figure 3.11. The dbh distribution of trees in Site A

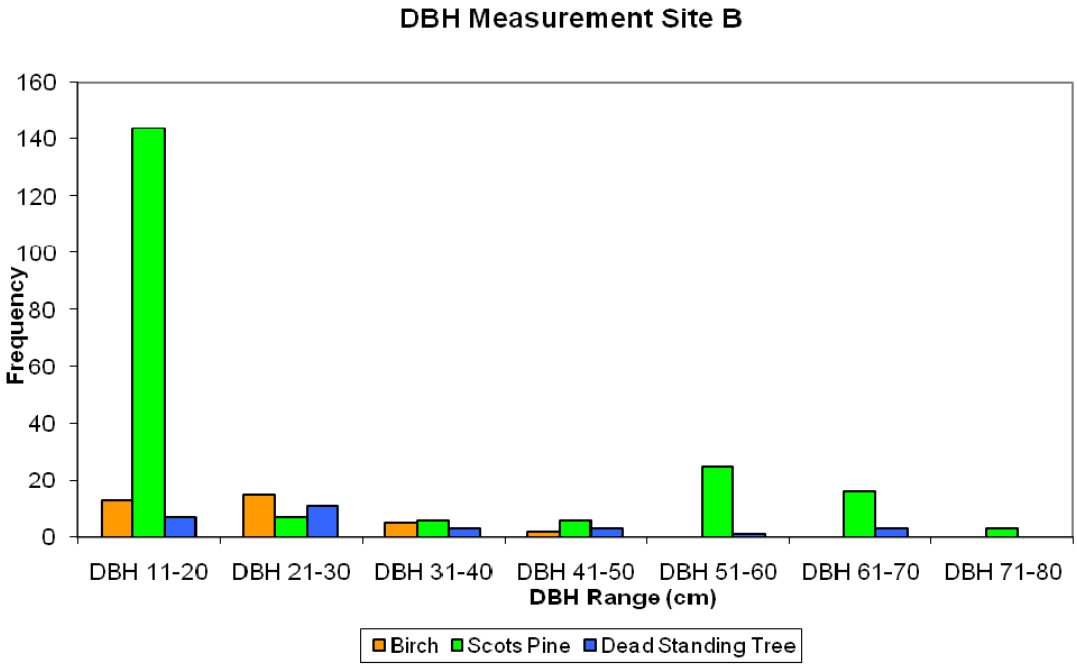

Figure 3.12. The dbh distribution of trees in Site B

3.3.2.2 Total Height and Bole Height

Total tree height is one of the most fundamental measurements in forest inventory and is an important variable in the quantitative assessment of forest biomass, carbon stocks, growth and site productivity. In the forestry context, total height is defined as the vertical distance between the ground level and tip of the tree (Husch et al., 1972) and bole height may be defined as the distance from the base of the tree to the base of the first living branch that forms a part of the tree crown (Brack, 1999). Unlike dbh, measurement of total height and bole height are difficult for tall trees, especially in a dense forest with trees close together and overlapping crowns. For this fieldwork, the total tree height and bole height are measured with the aid of Vertex hypsometer. The total tree height and bole height distribution of trees in Site A and Site B are shown in Figure 3.13, Figure 3.14, Figure 3.15 and Figure 3.16, respectively.

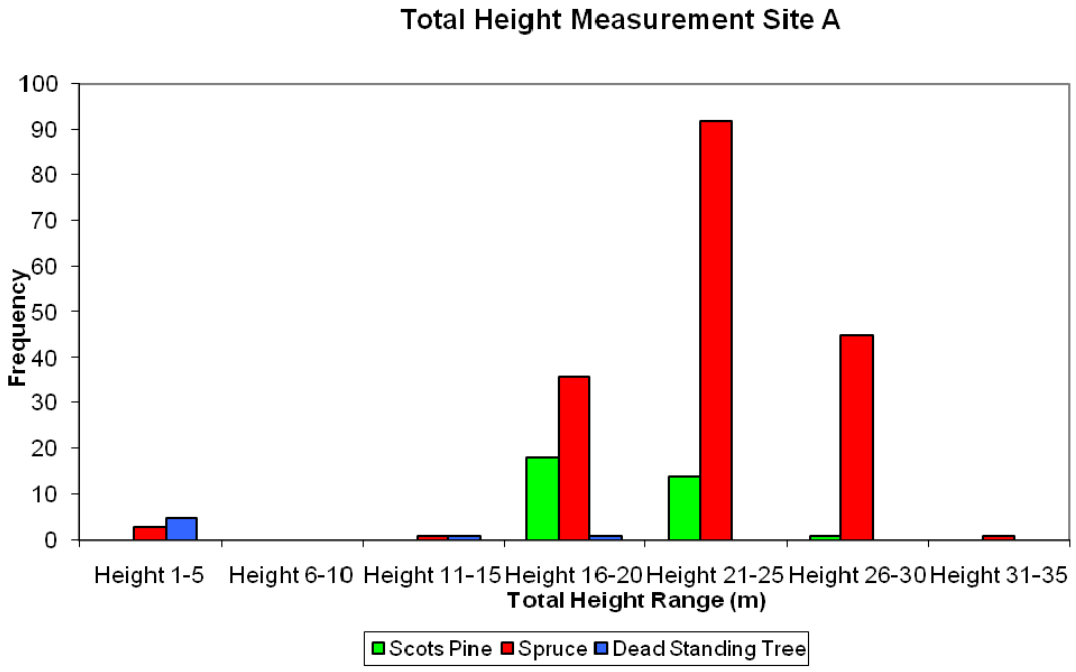

Figure 3.13. The total tree height distribution of trees in Site A

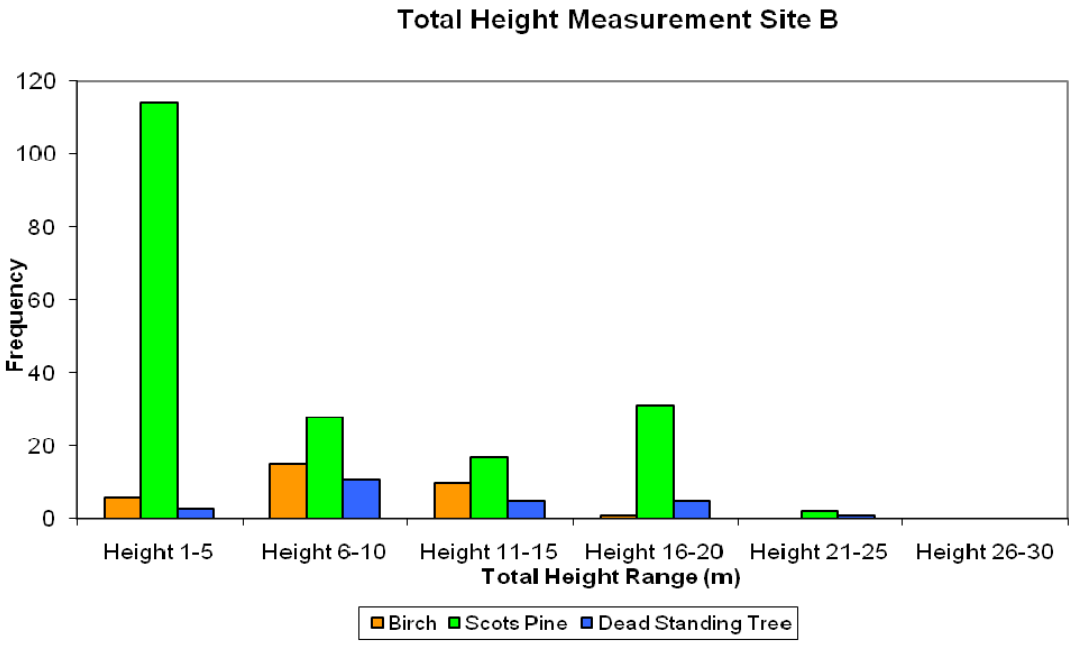

Figure 3.14. The total tree height distribution of trees in Site B

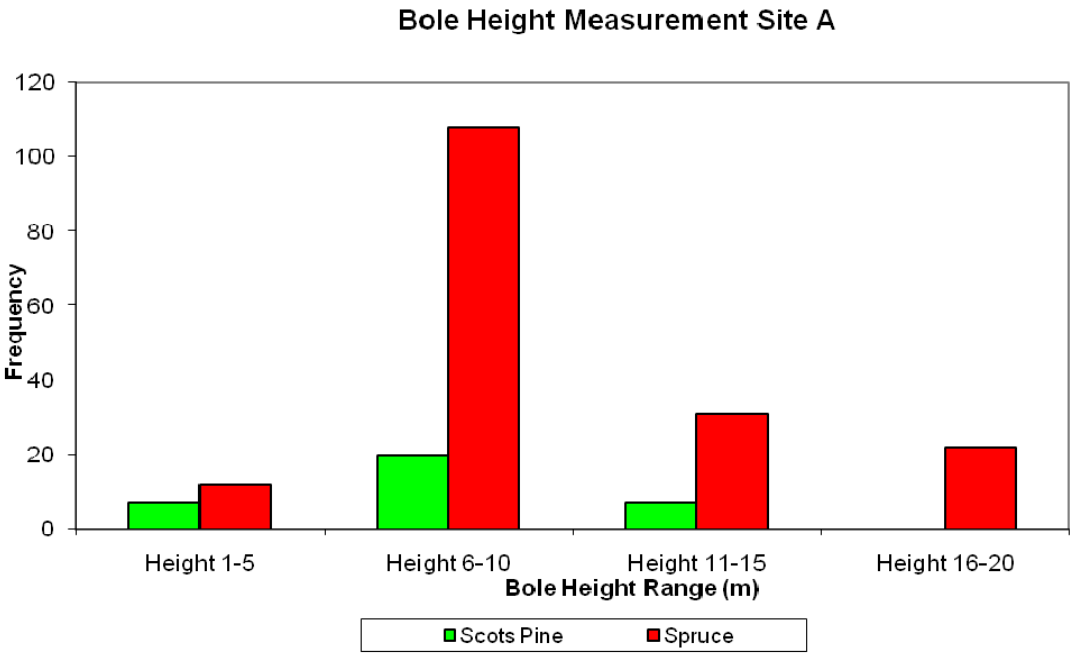

Figure 3.15. The bole height distribution of trees in Site A

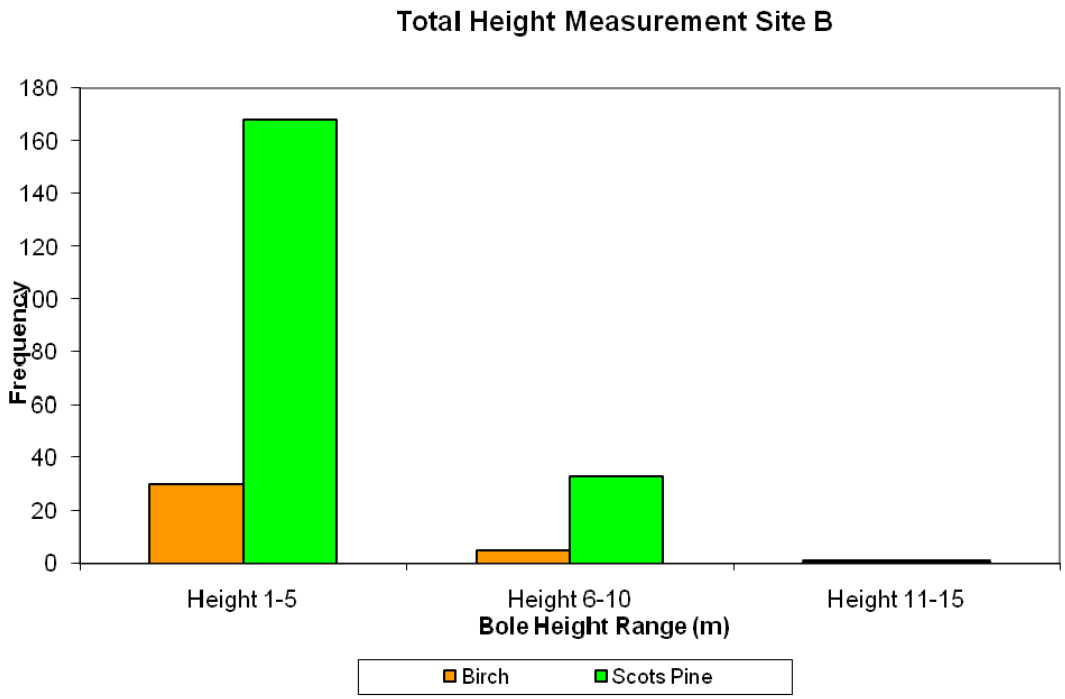

Figure 3.16. The bole height distribution of trees in Site B

An assessment has been made to examine the relationship between the forest structural parameters. As shown in Figure 3.17, the dbh and tree height are related in a power law function. The concomitant coefficient of determination is given for each species. It can therefore be deduced that biomass is also related to dbh and height of individual tree and the biomass for the field data was calculated using the allometric equation (Zianis et al., 2005) shown in Table 3.1. It is notable that the log-transformation equations were chosen because this type of equation generally solves the problem of heteroscedasticity, which represents the inconsistencies of error variance across the observations. Linear least-squares regression is then conducted on the transformed variables. This process is common because a linear function is easy to deal with and statistical theory is established (Smith, 1993). Complicated equations involving many parameters were not taken into consideration in this thesis since additional parameters do not significantly improve the fit of the model, but may create problem with the multicollinearity and reduce applicability of biomass equation (Overman, 1994).

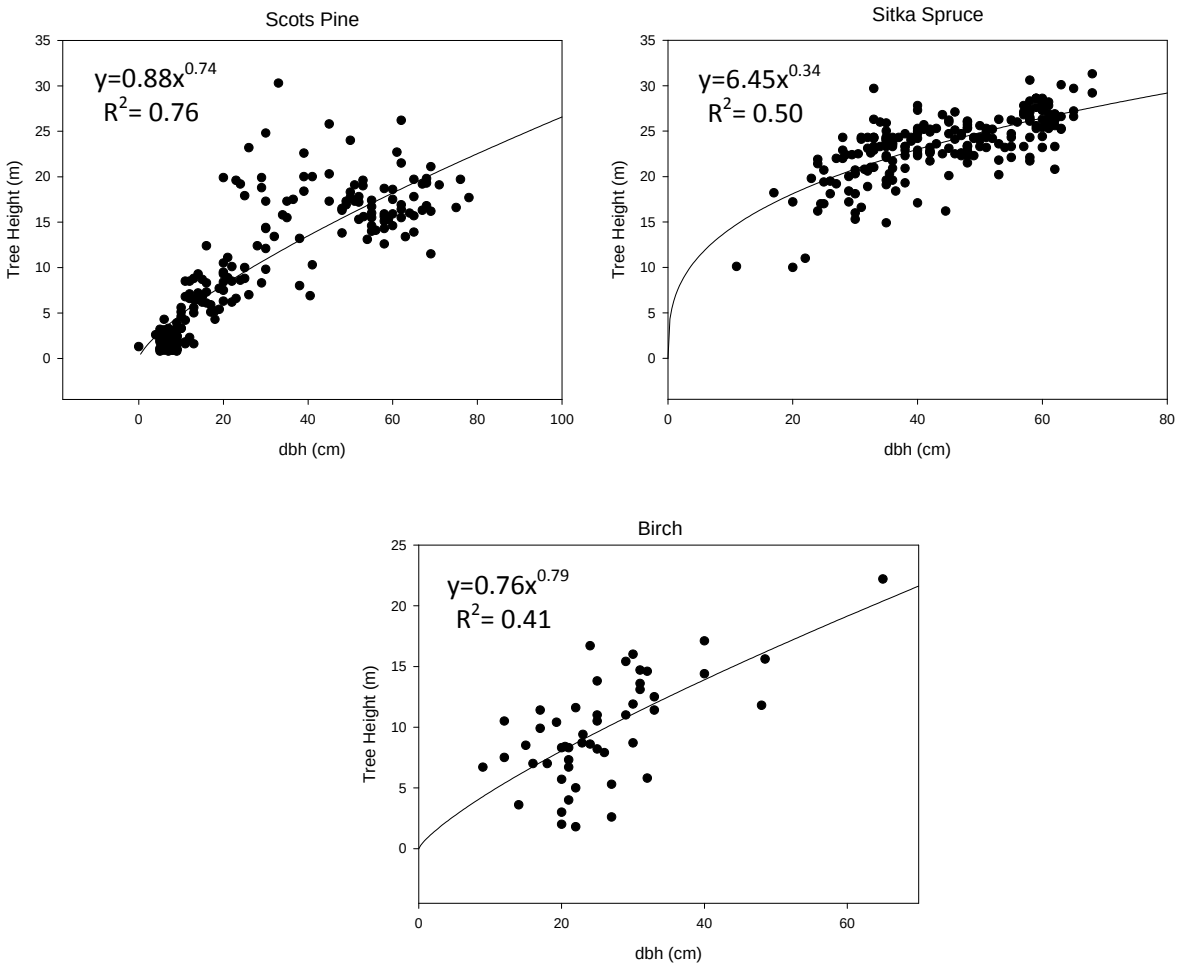

Figure 3.17. Scatterplots of tree height (in m) against dbh (in cm) as measured in the field for (a) Scots pine, (b) Sitka spruce and (c) Birch.

Table 3.1. Allometry equations to estimate above-ground biomass (Zianis et al., 2005)

Species	**Allometric Equations**	**y units**	**x units**	**R^2**
Scots Pine	$\log_{10}(y) = 0.981+2.289*\log_{10}(\pi*x)$	biomass, g	dbh, cm	0.996
Sitka Spruce	$\log_{10}(y)= -1.2908+\log_{10}(x_1.x_2^2).0.891$	biomass, kg	height,m dbh, cm	-
Birch	$\ln(y) = -2.4166+2.4227*\ln(x)$	biomass, kg	dbh, cm	0.985

3.3.2.3 Canopy Density

Forest canopy density is an essential parameter in the evaluation of forest status and is an important indicator of possible management interventions. Forest canopy density is defined as the proportion of the forest floor covered by the vertical projection of the tree crowns and it is measured using the spherical densiometer with the measurement interval of 5 m along the transect line in 4 directions: North, South, East and West. The percentage of the canopy cover is then calculated by averaging the four measurements data and multiplying it by 1.04. Figure 3.18 and Figure 3.19 show the result of the percentage canopy cover along transect in Site A and Site B, respectively. It is noted that the forest canopy density is higher in Site A compared to Site B which comprises of sparse and heterogeneous semi-natural forest.

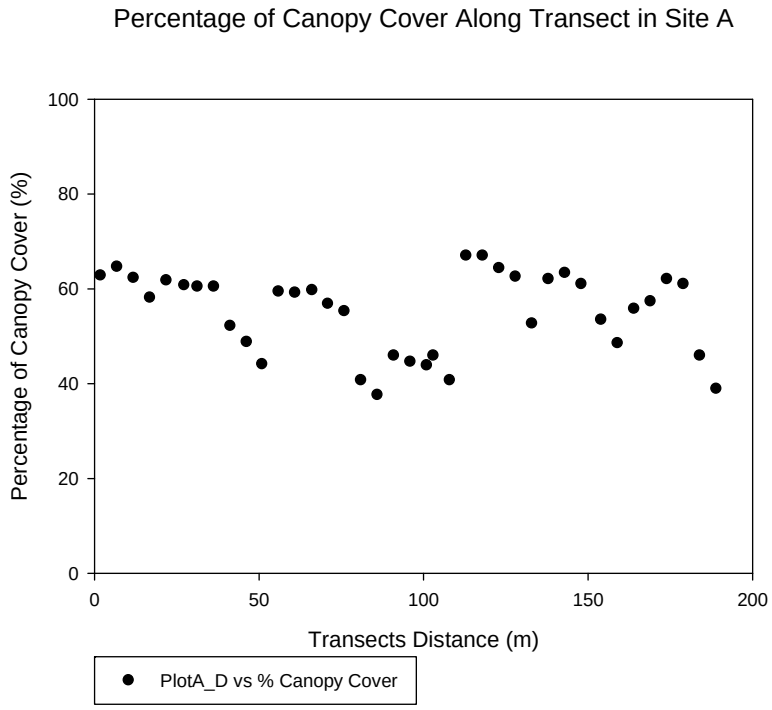

Figure 3.18. Percentage of canopy cover along transect in Site A

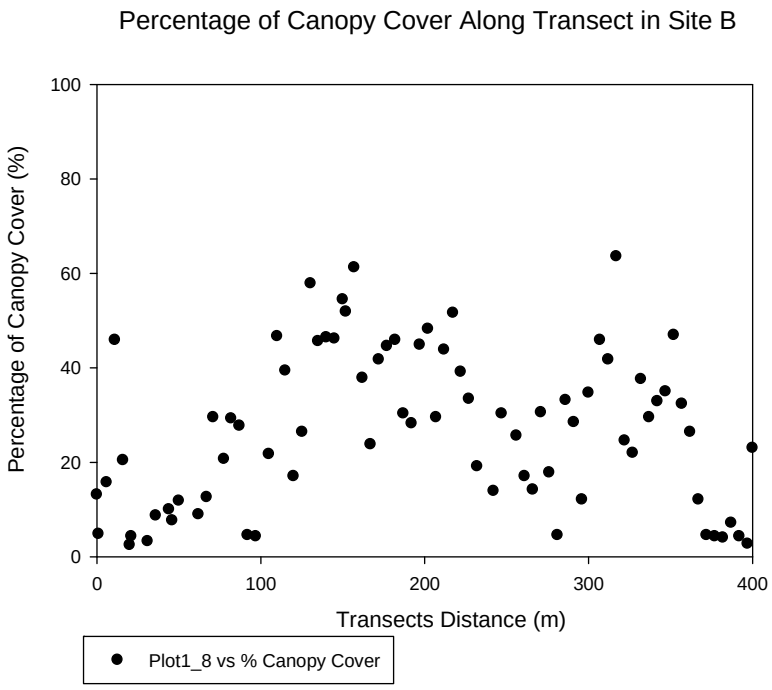

Figure 3.19. Percentage of canopy cover along transect in Site B

3.3.2.4 Tree Ring Measurement

As there were felling activities in Site A before the measurement, we took the opportunity to collect ancillary measurement data as added value information for the fieldwork. By random selection of felled trees, the number of tree rings was associated with the diameter of the stem (Figure 3.20). This measurement data is a good indicator of the tree growth and by investigating how dark and bright the rings are, the dry or wet season can be determined. The number of tree rings shows a linear relationship with the stem diameter as shown in Figure 3.21.

Figure 3.20. Tree ring and diameter of the stem measurement

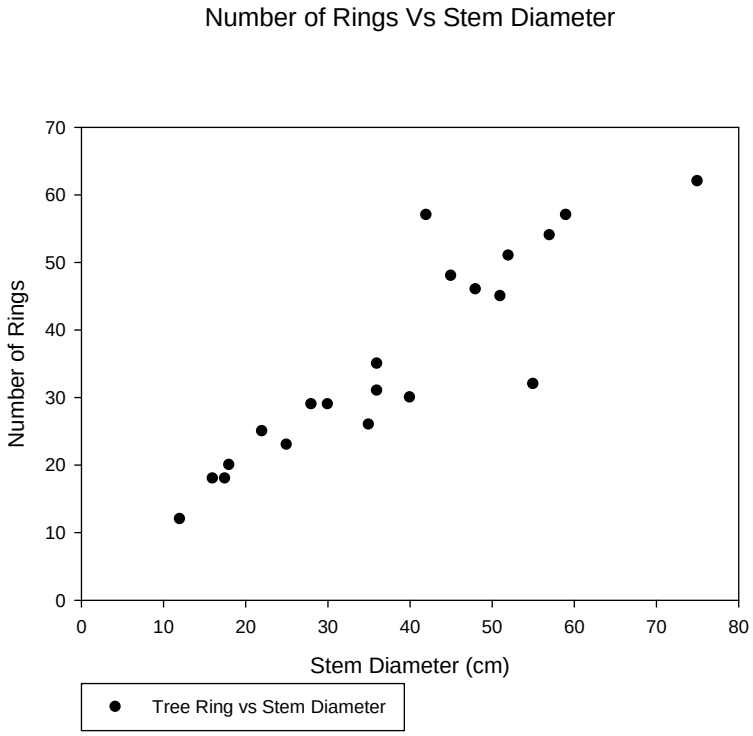

Figure 3.21. Relationship between tree ring measurement and stem diameter

3.3.2.5 Spot Elevation

Spot elevation measurement was done for Site A and Site B by getting the vertical angle in the total station observation. Figure 3.22 shows total station setup to acquire geographical location of trees and spot elevation. Prisms were placed randomly with at least 30 spots for each 50m x 50m in the field to obtain the elevation profile for the measurement sites. Figure 3.23 and Figure 3.24 show the 3-D spot elevation of Site A and Site B, respectively. The topography of the transect line is also plotted in Figure 3.25 to show the general elevation of the test sites.

Figure 3.22. Total station setup to acquire geographical location of trees and spot elevation

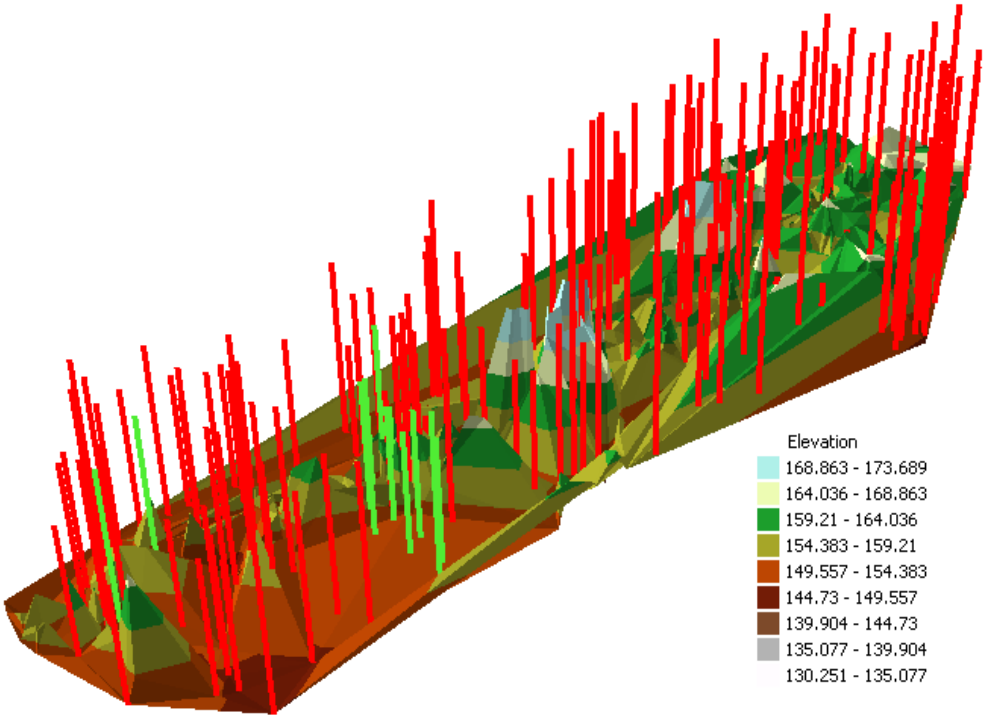

Figure 3.23. 3-D Spot elevation of Site A

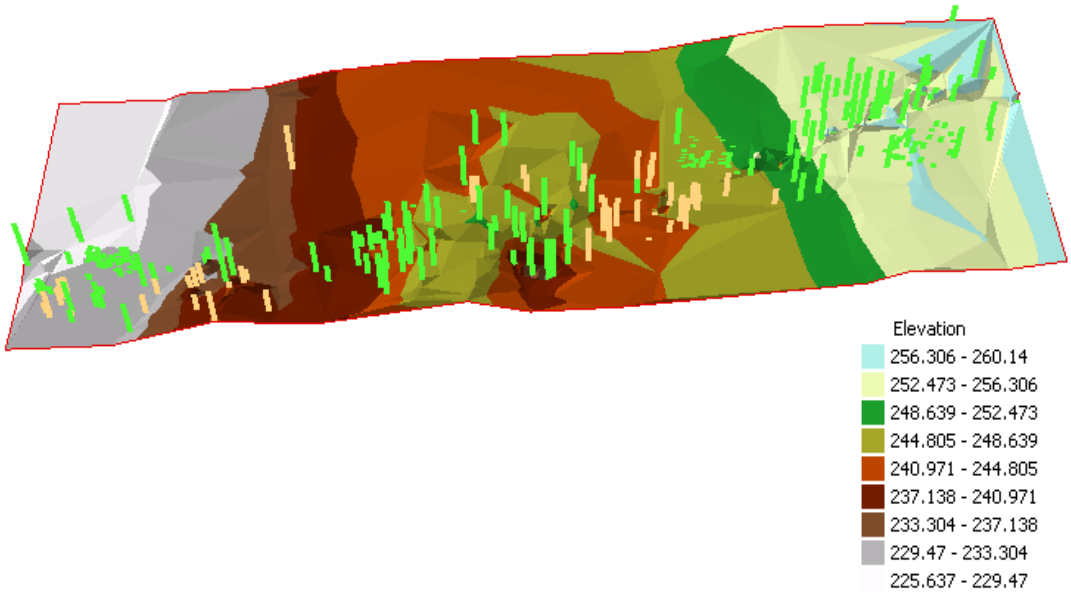

Figure 3.24. 3-D Spot elevation of Site B

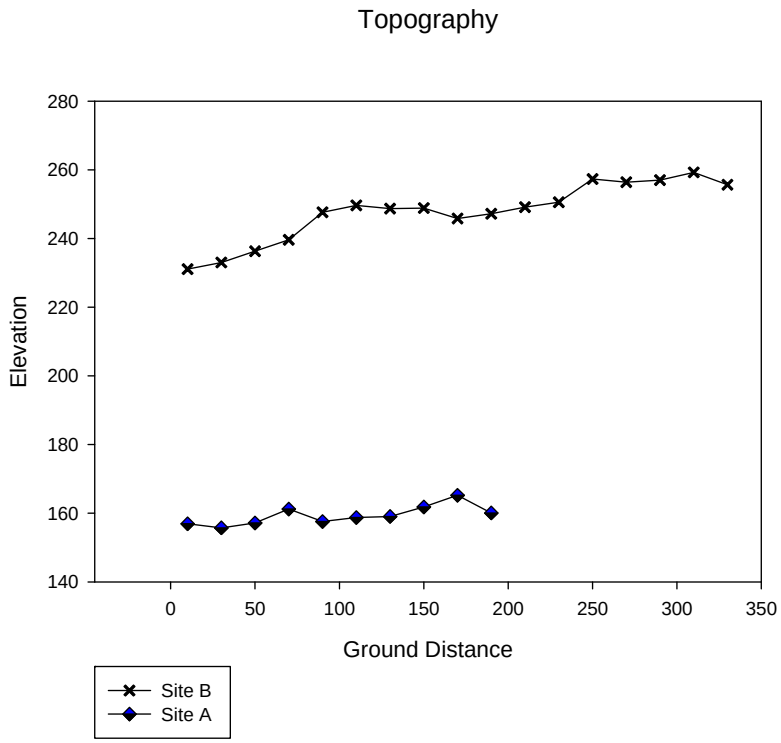

Figure 3.25. Topography along the transect line for Site A and Site B

3.4 Earth Observation Data

The data used in this research are full polarimetric ALOS PALSAR, TerraSAR-X and airborne LiDAR. The details of the data are discussed in the next section.

3.4.1 ALOS PALSAR

The ALOS Kyoto & Carbon Initiative forms the continuation of JAXA's JERS-1 SAR Global Rain Forest and Global Boreal Forest Mapping project (GRFM/GBFM) (Rosenqvist et al., 2007). It is led by the JAXA Earth Observation Research Center (EORC) and aims to assess ALOS PALSAR data to meet specific information requirements relating to the international environmental Conventions; Carbon Cycle scientists and Environmental Conservation program (CCC). ALOS PALSAR observations are spatially planned in units of geographical regions of semi continental

size, instead of individual scenes. To assure data acquisition temporally, the observation is implemented with a 46-day recurrence period (Rosenqvist et al., 2007). The technical facts of the sensor is shown in Table 3.2.

Table 3.2. Technical facts of ALOS PALSAR

ALOS PALSAR Technical Facts		
	Item	**Characteristics**
Launch	**Launch Vehicle**	H-IIA Launch Vehicle No.8
	Date	10:33 am on 24 January 2006 (JST)
	Launch Site	Tanegashima Space Center
Orbit	**Orbit**	Sun-Synchronous Sub-Recurrent
	Local Sun Time	10:30 AM
	Altitude	691.7 km on the equator
	Orbit Inclination	98.2 degrees
	Period	98.7 minutes
	Revolution	14+27/46 per day
	Recurrent Cycle	46 days
	Inter-orbit Distance	59.7 km on the Equator
	Repetition Accuracy	+/- 2.5km on the Equator

The PALSAR PLR mode data was requested to be processed at Level 1.1 and the specification is shown in Table 3.3. This level corresponds to Single Look Complex products and provided in slant range geometry. Two ALOS PALSAR fully polarimetric data were acquired on 17 April 2007 and 08 June 2009. Due to different spatial and high temporal baselines, these data are not suitable to perform interferometry data.

Table 3.3. ALOS PALSAR data characteristics (source: ALOS PALSAR data header)

PALSAR Acquisition Mode: Polarimetry (PLR)	
Central Frequency	1270MHz
PRF	2xFBS PRF
Range Sampling Frequency	16MHz

Chirp Bandwidth	14MHz
Polarisation	HH,HV,VV,VH
Off-Nadir Angle (Deg)	21.5
Incidence Angle (Deg)	23.9
Flight Direction	Ascending
Data Rate(Mbps)	240
Slant Range Resolution	9.5m
Azimuth Resolution	4.5m
Range Pixel Spacing	9.4m
Azimuth/Line Pixel Spacing	3.6m
Product Size	766Mbyte

The image was multilooked and geo-referenced to Ordnance Survey British Grid using Sarscape Modules version 4.2 (ITT, 2009) and the detailed information about the procedure is discussed in Section 5.2. In the geo-referenced procedure, the backscatter values were converted to beta nought. Beta nought which is commonly referred as radar brightness, represents the radar reflectivity per unit area in slant range. The beta nought is then converted to dB using the equation as below:

$$\beta^0{}_{dB} = 10 \bullet \log_{10}\left(\beta^0\right) \tag{3.1}$$

Figure 3.26 shows the ALOS PALSAR image in RGB representation where red represents VV represents backscatter, green represents HV backscatter and blue represents HH backscatter

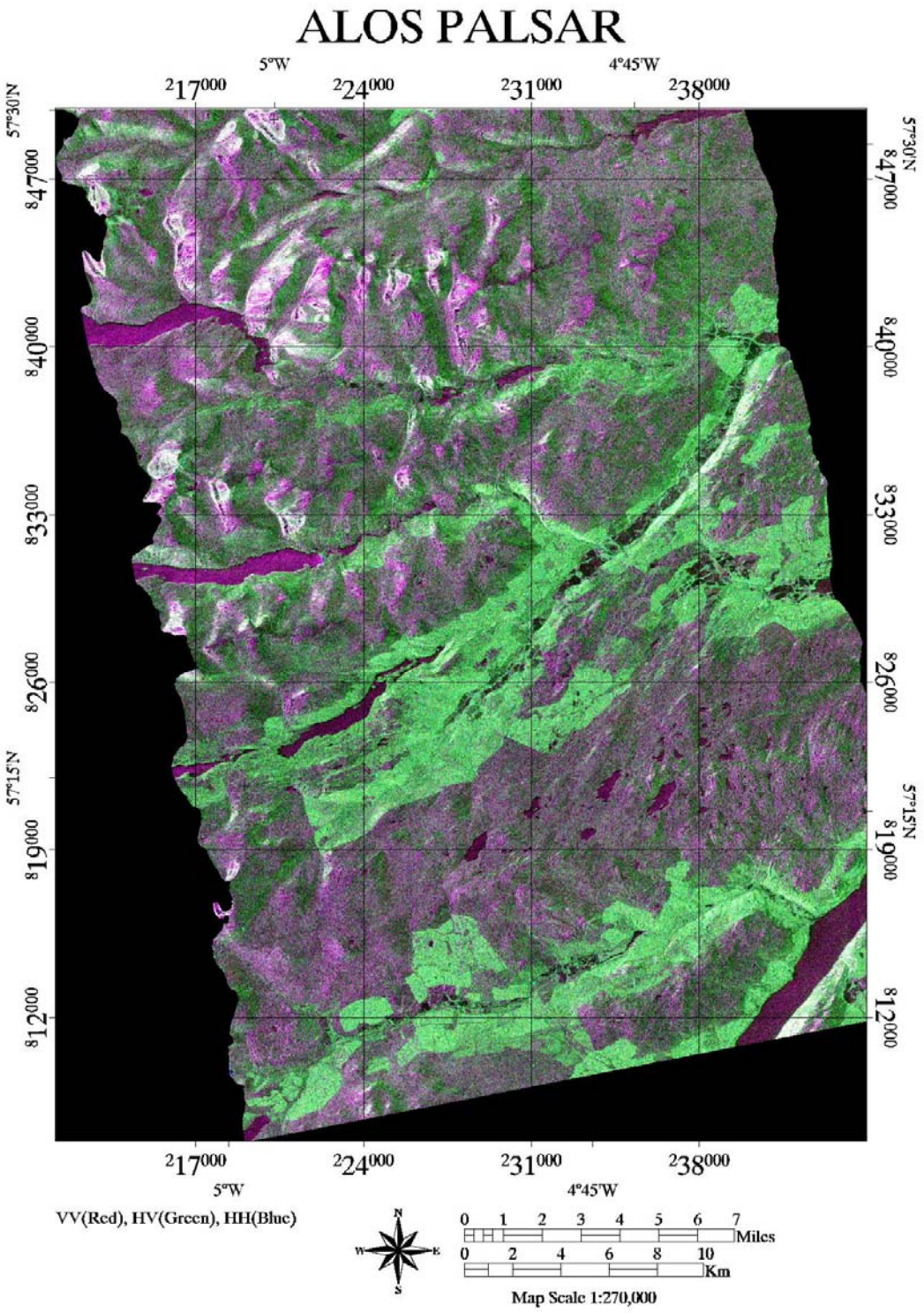

Figure 3.26. ALOS PALSAR in RGB representation where red represents VV backscatter, green represents HV backscatter and blue represents HH backscatter

3.4.2 TerraSAR-X

TerraSAR-X was successfully launched on 15 June 2007 and it has been fully operational since early 2008. It is the first German radar satellite to be implemented within a Public-Private Partnership (PPP) between the German Aerospace Center (DLR) and Europe's leading satellite specialist Astrium (Infoterra, 2011). The spacecraft has an active phased array X-band SAR mounted on it whilst circling the Earth in a polar orbit at 514km altitude. It is designed to provide high-quality X band radar images with a resolution of up to 1m. The technical facts of the sensor is shown in Table 3.4.

Table 3.4. Technical facts of TerraSAR-X

TerraSAR-X Technical Facts	
Operating life	5 years
Orbit	Sun-synchronous repeat orbit
Repeat Period	11 days
Equatorial Crossing Time (GMT)	18:00h ascending pass
	06:00h descending pass
Inclination	97.44 degrees
Altitude at the equator	514km
Antenna Type	Active Phases Array Antenna, electronically separable
Antenna Size	4.8m x 0.7m
Center Frequency	9.7 GHz (X-band)
Chirp Bandwidth	150 MHz/300 MHz
Nominal Acquisition Direction	Right side
Polarization	Single, dual-depending on imaging mode, quadruple is available as advanced polarization mode

In this research, the TerraSAR-X acquisitions are full polarimetric and they were carried out on 13 April 2010. The details of the data are listed in Table 3.5. It is a stripmap quadruple polarisation data which has full scattering matrix and allows derivation of further polarimetry analysis. The ground swath is illuminated with

continuous sequence of pulses while the antenna beam is fixed in elevation and azimuth (Infroterra,2009). Stripmap mode images have a coarser spatial resolution than Spotlight mode images, however, they allow imaging of larger areas. Since it is a Single Look Slant Range Complex data, each image pixel is processed to zero Doppler coordinates in range direction and the format data is in the DLR-defined binary COSAR format.

Table 3.5. TerraSAR-X data characteristics (source: TerraSAR-X data header)

TerraSAR-X Acquisition	
Central Frequency	9.65GHz (X-band)
Chirp Bandwidth	300MHz
Polarisation	HH,HV,VV,VH
Incidence Angle	43.9^0
Flight Direction	Ascending
Slant Range Resolution	1.7m
Azimuth Resolution	6.6m
Range Pixel Spacing	2.5m
Azimuth/Line Pixel Spacing	2.4m
Product Size	4.5Gbye

The raw data was processed using POLSARpro version 4.1.5 to minimise the differences in the image radiometry and to make the image readily comparable to other remote sensing images. It is multilooked and filtered before it is converted to coherency matrix format data using the equation as follows:

$$[T] = \frac{1}{2}\begin{bmatrix} \left\langle \left|S_{HH} + S_{VV}\right|^2 \right\rangle & \left\langle (S_{HH} + S_{VV})(S_{HH} - S_{VV})^* \right\rangle & 2\left\langle (S_{HH} + S_{VV})S_{HV}^* \right\rangle \\ \left\langle (S_{HH} - S_{VV})(S_{HH} + S_{VV})^* \right\rangle & \left\langle \left|S_{HH} - S_{VV}\right|^2 \right\rangle & 2\left\langle (S_{HH} - S_{VV})S_{HV}^* \right\rangle \\ 2\left\langle S_{HV}(S_{HH} + S_{VV})^* \right\rangle & 2\left\langle S_{HV}(S_{HH} - S_{VV})^* \right\rangle & 4\left\langle \left|S_{HV}\right|^2 \right\rangle \end{bmatrix} \quad (3.2)$$

Figure 3.27 shows the TerraSAR-X image in RGB representation where red represents VV backscatter, green represents HV backscatter and blue represents HH backscatter

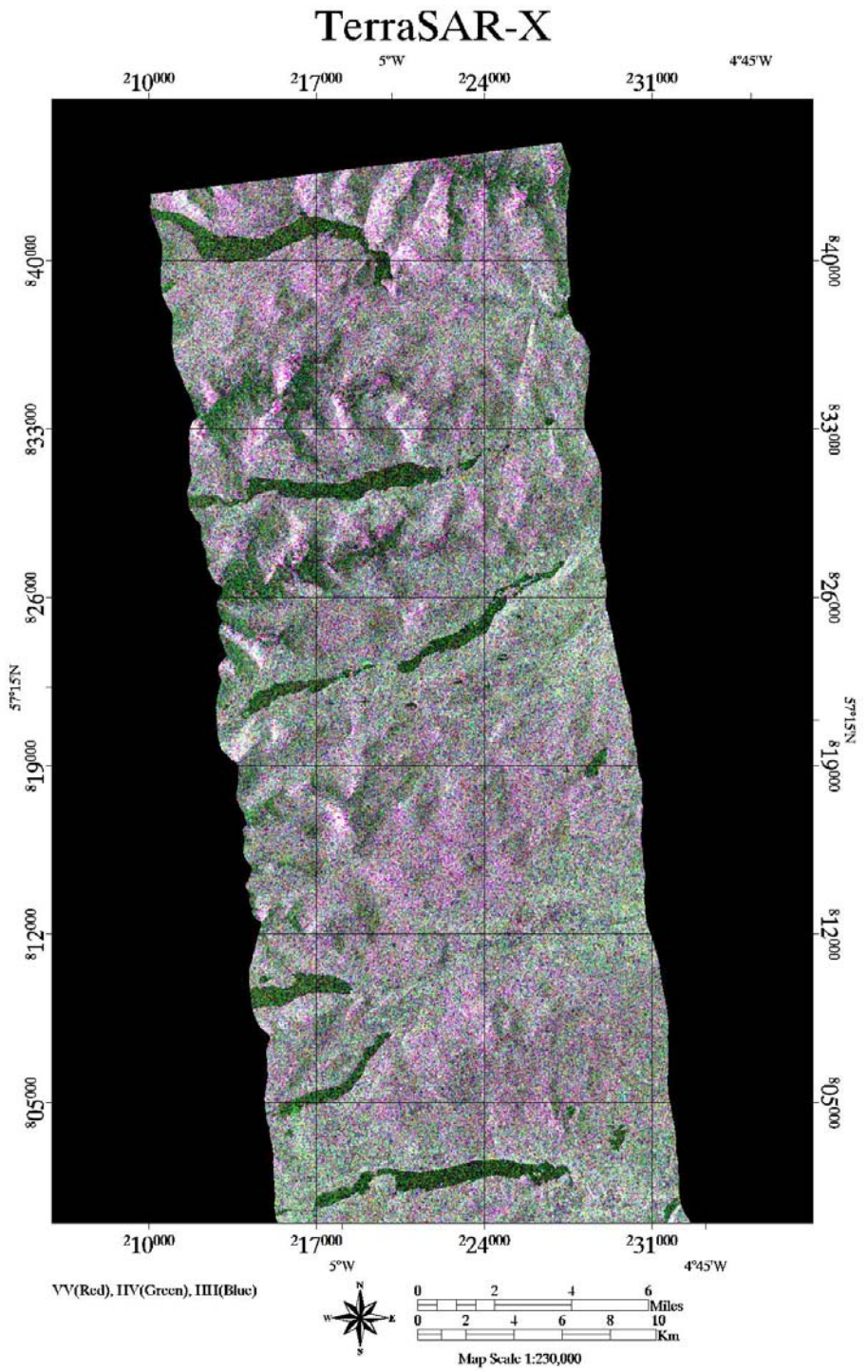

Figure 3.27. TerraSAR-X in RGB representation where red represents VV backscatter, green represents HV backscatter and blue represents HH backscatter

3.4.3 LiDAR

Airborne LiDAR data were acquired on 9th ,11th and 13th June 2007 by The Environment Agency Science Enterprise Centre on behalf of Forest Research. The Optech ALTM 3100 LiDAR system was used to record up to four return echoes per laser shot at approximately 0.25m resolution for an area of 58 km^2. As the result, an average pre-processed point density of approximately 12-16 points/m^2 producing good energy penetration throughout the canopy. Table 3.6 shows the specification of LiDAR system used for the data collection while Figure 3.28 illustrates the distribution of LiDAR data acquisition in Glen Affric.

Table 3.6. Optech Airborne Laser Terrain Mapper 3100 system specification

Optech Airborne Laser Terrain Mapper 3100	
Platform and acquisition agency:	Environment Agency aircraft (on behalf of Forestry Commission)
Sensor type:	Airborne laser scanner (LiDAR)
Pulses recorded:	1st, 2nd, 3rd and last pulses (and intensity)
Scan repetition rate:	100 kHz
Scan frequency:	68 Hz
Scan angle:	12^0 off-nadir, 24^0 total look
Data format:	Binary LiDAR exchange format (LAS)

The LiDAR data was georeferenced to Ordnance Survey British Grid using ENVI commercial software. An Ordnance Survey 1:10 000 Digital Terrain Model was utilized to compare the accuracy of the results. Further processing is discussed in detailed in Chapter 4.

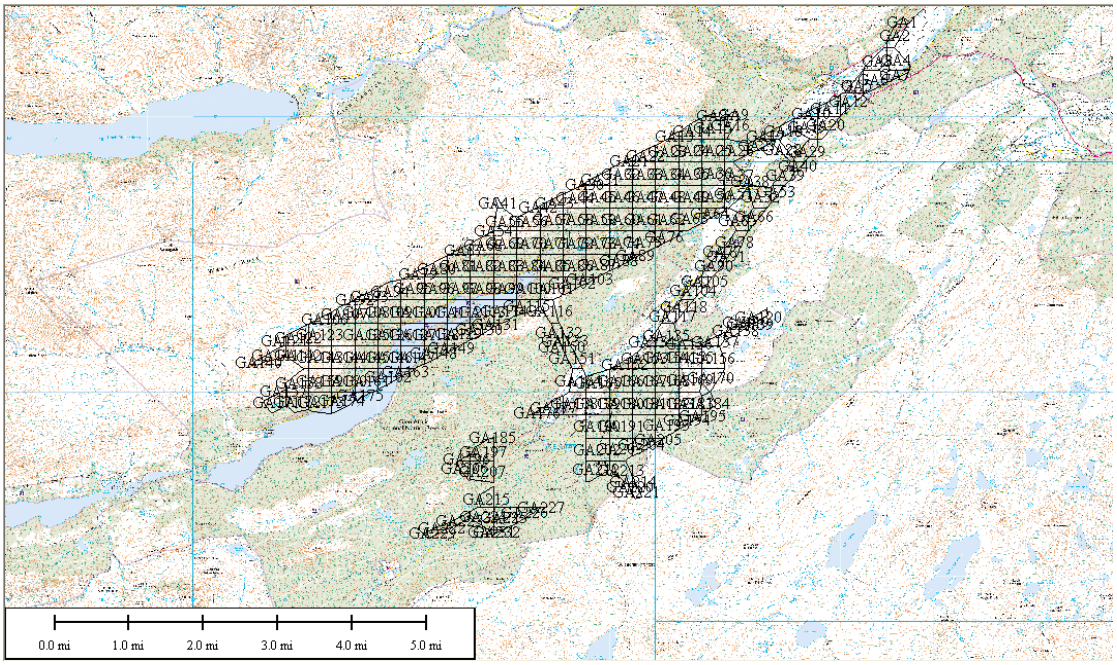

Figure 3.28. Distribution of LiDAR data in Glen Affric. Crown Copyright Ordnance Survey. An EDINA Digimap/JISC supplied service.

3.5 Chapter Summary

This chapter provided an overview of the study area and various data sources used, including Earth Observation and fieldwork measurement data. The study area, Glen Affric is one of the largest ancient Caledonian forests in Scotland as well as moorland, lochs and mountains. These landscapes offer great challenges for remote sensing. The Earth Observation data used in this research are spaceborne ALOS PALSAR, TerraSAR-X and airborne LiDAR data. Preprocessing of the Earth Observation data was done as a preparation for the main data processing and analysis as discussed in Chapter 4 and Chapter 5.

The year of data acquisition ranges from 2007 to 2010 and the fieldwork measurement campaigns were planned and conducted during the period so that results

can be compared and validated. Two transect areas of approximately 200m x 50m and 400m x 50m were mapped and measured. As a result, 3-dimensional models were constructed to show the physical structure of the two transects. Another fieldwork was conducted by the Forestry Commission staffs where one hundred and seventy circular plots of field data were collected. Tree species, diameter at breast height (dbh) and tree height were recorded. These data were used to compute the AGB allometrically and compared with the AGB derived from Earth Observation data.

Chapter 4

Above-Ground Biomass Estimation Using LiDAR

4.1 Introduction

This chapter presents the method and results of the biomass estimation using airborne laser scanning (ALS). In Section 4.2, a flow of the methodology is discussed. The data collection and the specification of the LiDAR data are elaborated. The data was processed to construct the Canopy Surface Model (CSM) and bare Earth model before the canopy height can be modelled. Using the canopy height information, an algorithm was designed to delineate the trees. The biomass of individual trees was computed allometrically by assuming all the trees are of Scots pine species, which is the dominant species in Glen Affric. The result was then validated with fieldwork data. A tree growth classification was demonstrated in Section 4.3. This is followed by the biomass estimation error factor. Section 4.5 summarizes the chapter.

4.2 Methodology

The utilization of airborne LiDAR technology to characterise the forest structure has made the estimation of the foliage cover and height possible over large areas. It has

become a prominent tool to collect not only accurate high-resolution three-dimensional data, but is also able to demonstrate detailed forest profiles. It is popularly used to estimate forest stand structure such as tree density, stand density, basal area, leaf area index and forest biomass (Andersen et al., 2006; Morsdorf et. al., 2004; Kini and Popescu, 2004; Dubayah and Drake, 2000, Naesset, 2002; Lim et al., 2003, 2004; Holmgren & Persson, 2004; Vazirabad & Karslioglu, 2010; Yu et al., 2011). The difference between the CSM from the first LiDAR returns and the digital terrain model (DTM) from the last return, represents the canopy height model (CHM). The penetration rate through the forest canopy depends on the density of trees and this is what offers sensitivity to properties such as leaf area index.

The two main approaches in deriving forest information from airborne LiDAR data have been those based on vertical points distribution and individual tree delineation. The overview of the proposed steps involved in the estimation of above-ground biomass using LiDAR is listed below:

1. Determine a sampling strategy, selection of plots (size and number), collection of forest inventory data (species), measurement of variables like tree dbh, height and other physical parameters.
2. Estimating above-ground biomass by creating regression model between field measurement data and biomass or allometric equations.
3. Acquisition of LiDAR data and pre-processing
4. Development of Canopy Height Model (CHM): A key parameter for establishing relationship with biomass. An algorithm is developed for tree delineation to locate trees and identify the total number of trees.
5. Derivation of relationship between CHM and biomass: biomass estimation using existing allometric equation.
6. Biomass estimate validation: the calculated biomass estimates is compared with inventory data to check for accuracy estimation.

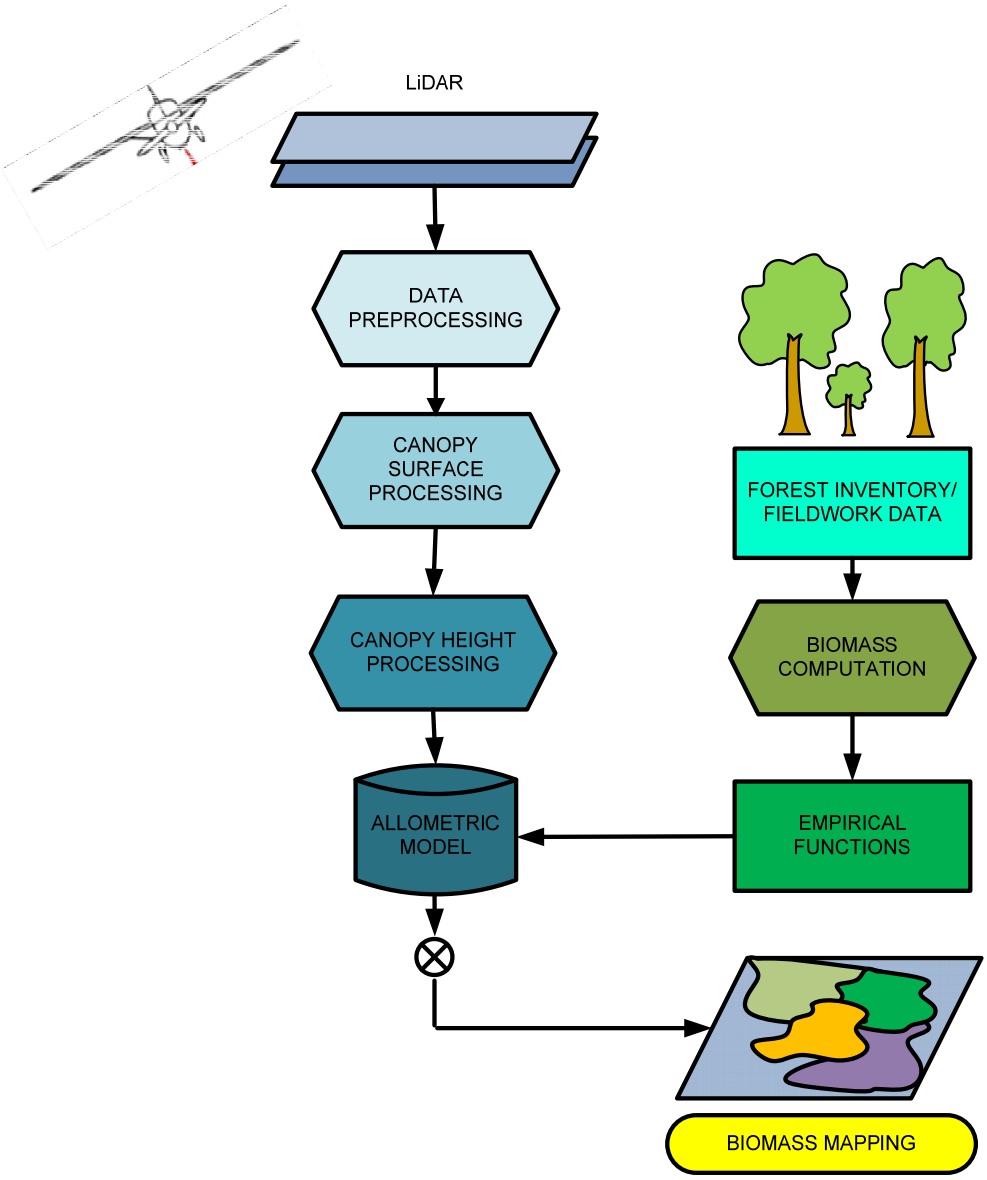

Figure 4.1. Flow chart of AGB biomass estimation using LiDAR

4.2.1 Data Collection

Airborne LiDAR data were acquired on 9th ,11th and 13th June 2007 by The Environment Agency Science Enterprise Centre on behalf of Forest Research. The Optech ALTM 3100 LiDAR system was used to record up to four return echoes per

laser shot at approximately 0.25m resolution for an area of 58 km^2. As the result, an average pre-processed point density of approximately 12-16 points/m^2 producing good energy penetration throughout the canopy. Each point has X, Y and Z coordinates in the British National Grid represented as 6 + 2 digits that gives theoretical positioning precision of 0.01m. For example 530871.00 (X), 189359.00 (Y), 23.51(Z). Two subsets of the airborne LiDAR data were used to demonstrate the difference between sparse and dense forest in Glen Affric. The dimension of both subsets are 500m x 500m (Figure 1) and the 3-D of the 2 forests are shown in Figure 4.2. The study area consists of Scots pine (*Pinus sylvestris*), Birch (*Betula spp.*), European larch (*Larix decidua*), Douglas fir (*Pseudotsuga menziesii*), miced conifers, Sitka spruce (*Picea sitchensis*), Norway spruce (*Picea anies*) and Lodgepole pine (*Pinus contorta*) in order of occurrence.

Table 4.1 The specification of Optech Airborne Laser Terrain Mapper 3100

Optech Airborne Laser Terrain Mapper 3100	
Platform and acquisition agency:	Environment Agency aircraft (on behalf of Forestry Commission)
Sensor type:	Airborne laser scanner (LiDAR)
Pulses recorded:	1st, 2nd, 3rd and last pulses (and intensity)
Scan repetition rate:	100 kHz
Scan frequency:	68 Hz
Scan angle:	12^0 off-nadir, 24^0 total look
Data format:	Binary LiDAR exchange format (LAS)

4.2.2 Data Processing

The data processing was done using FUSION software. It is a freeware developed by the USDA Forest Service Pacific Northwest Research Station and distributed by the USDA Forest Service Remote Sensing Applications Centre (McGaughey, R. J. & Carson, W.W., 2003). This software package was chosen as the data preparation tool due to its public availability and access. Apart from that, it is based on non-proprietary algorithms that allow for user adjustment and the processes that are used are documented in publicly available literature. FUSION uses the bare earth model and raw LiDAR points to generate the height and density cover.

The raw data of the LiDAR was filtered to identify the returns that lie on the bare earth surface at 0.5m resolution. The filtering algorithm is based on linear prediction (Kraus, K. & Pfeifer, N., 1998; Kraus, K. et al., 1972) and it is meant to discard noise. In the first step, a surface is computed with equal weights for all LiDAR points. The iterative algorithm includes an adaptive process to find the optimized parameter. After the filtering procedure is completed, a gridded surface model is created using a collection of data points. The surface model is stored in Preliminary Logging Analysis System (PLANS) DTM format (Twito et al., 1987). Individual cell elevations are calculated using the average elevation of all points within the cell. CSM is then created using a LiDAR point cloud as shown in Figure 4.3. CSM is a topographic model of the earth's surface that includes natural terrain features.

4.2.3 Construction of Canopy Height Model (CHM)

The Canopy Height Model (CHM) is a product of the CSM and the bare earth surface. The algorithm used by canopy model assigns the elevation of the highest return within each grid cell to the grid cell centre to provide a geometrically correct base map.

In order to construct the Canopy Height Model (CHM) as shown in Figure 4.4, the model subtracts the ground elevations (last return echoes) from the canopy return elevations (first returns). CHM is a topographic model of the difference between the bare earth and the CSM so that canopy height variations can be seen. It allows the comparison of tree heights without the effect of elevation. Canopy closure is also estimated by computing the number of returns over a specified height threshold. The proportion of the pulses that fall within the height ranges is calculated to help assess canopy penetration by the airborne sensor and estimate the vegetation density.

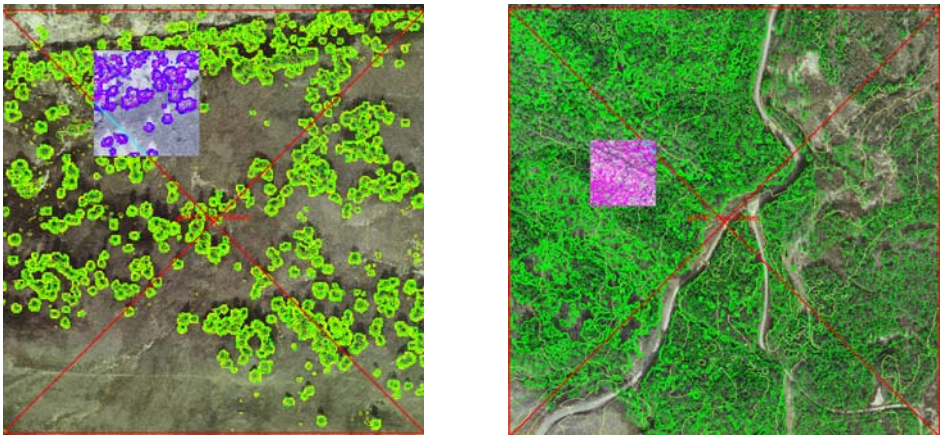

(a) (b)

Figure 4.2. Two subsets of the airborne LiDAR data (a) sparse semi-natural woodland, (b) dense plantation forest

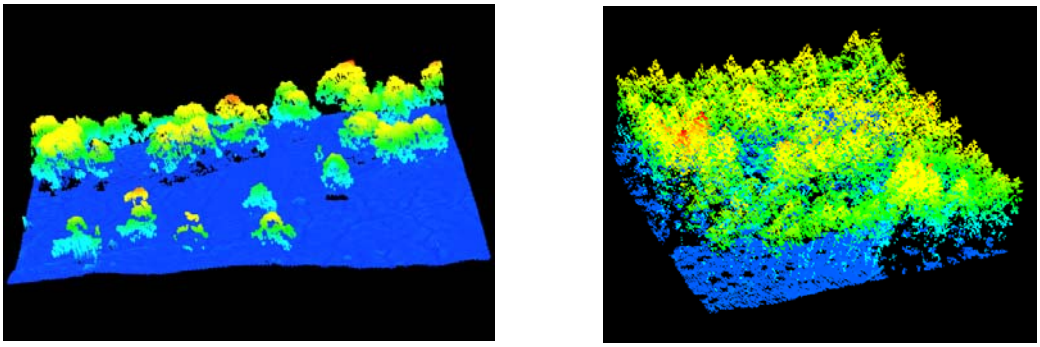

(a) (b)

Figure 4.3. 3-dimensional data representation for (a) sparse semi-natural woodland, (b) dense plantation forest

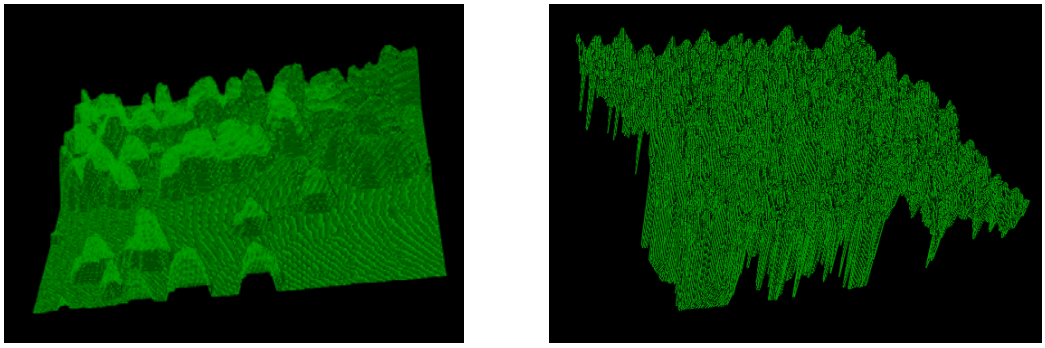

(a) (b)

Figure 4.4. Canopy Height Model for (a) sparse semi-natural woodland, (b) dense plantation forest

4.2.4 Tree Crown Delineation and Biomass Estimation

An algorithm was designed to delineate individual tree canopies solely from the LiDAR-derived 0.5m resolution canopy height model. Firstly, the CHM was smoothed with a kernel of 3x3 to obtain the best representation of the study area and to reduce the effects of spatial biases in geometric location (Wallentin, G., 2008). Based on the CHM, local maxima were located and classified as tree tops while local minima were classified as the lowest point of the tree crowns. The assumption that the higher the tree, the bigger the tree crown is made. In order to improve the accuracy of tree crown delineation, a post-processing step was done to eliminate trees that are initially classified as two separate trees, but in actual fact, are the same tree. An iterative tree delineation process was performed using a moving window size of 2.5m to avoid overestimation of number of trees. The moving window also keeps track of the x,y, and z information of each tree. In this algorithm, an assumption is made that there is no existence of overlapping trees, for instance, the occurrence of small trees under big trees. Additionally, the following stopping criteria are implemented in the algorithm. Firstly, only trees taller than 2m are considered in the tree delineation. This limitation is necessary to avoid points from understorey vegetation being assigned as the local maxima and considered as trees. Secondly, trees that lie in the regions consisting of equal or less than 5 pixels are

assumed not to be separate trees, but part of an adjacent tree. These regions are merged with the adjacent tree. The delineated crowns are visually compared with aerial photography. Figure 4.5 shows the position of the tree tops of the delineated tree crown on the aerial photograph and it is shown that they are comparable.

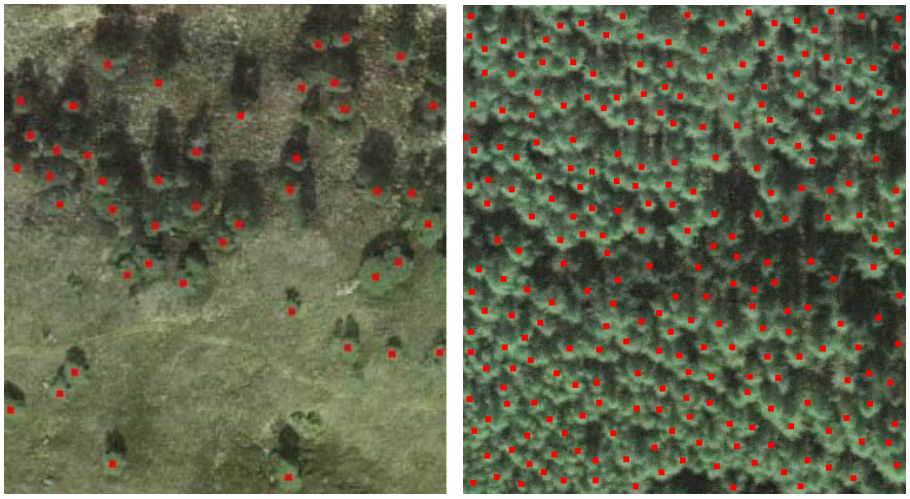

(a) (b)

Figure 4.5. Tree tops generated from the tree delineation procedure, superimposed on the aerial photograph to visually compare the effectiveness of the procedure in zoomed-in area of (a) sparse and (b) dense forests

With the assumption that all trees are of Scots pine species, individual tree biomass was computed using the allometric equation of Scots pine from previous literature (Zianis et al., 2005) for each delineated tree as shown in Figure 4.6. The biomass for the sparse semi-natural forest and dense plantation forest are estimated to be 45.7 ton/ha and 259.6 ton/ha, respectively.

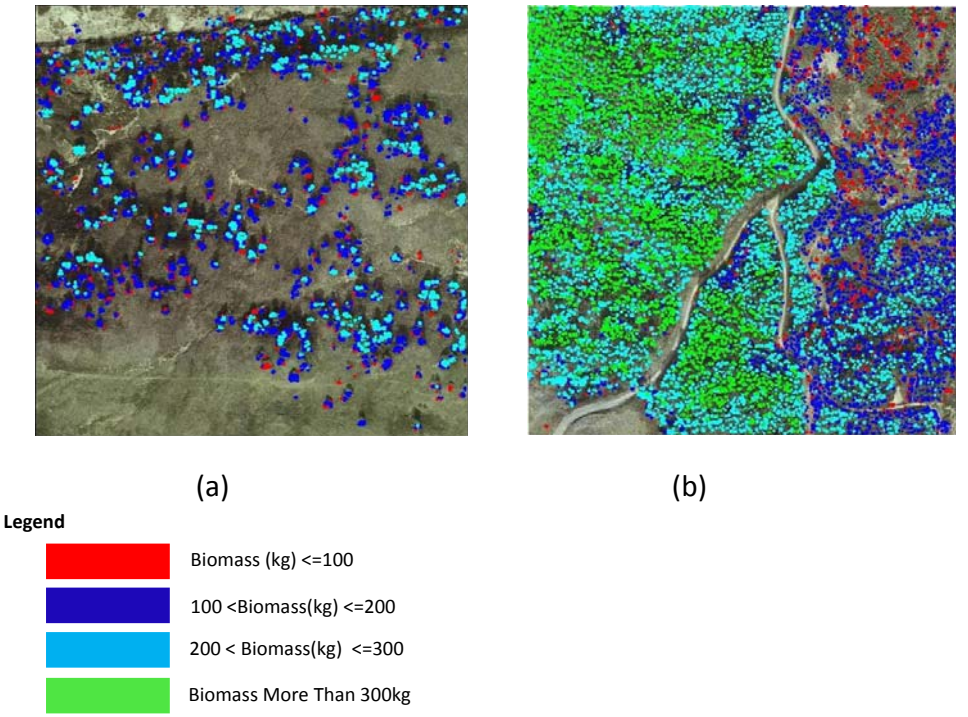

Figure 4.6. Biomass estimation of individual trees for (a) sparse semi-natural woodland, (b) dense plantation forest

4.2.5 Results Validation with Fieldwork Data

Biomass estimation is done over field test sites in Glen Affric using the CHM derived from LiDAR. The results are validated with the fieldwork data and the distribution of data is illustrated in Figure 4.7. Out of 170 field test sites, only 116 sites coincide with LiDAR data coverage. A number of statistical metrics is computed to provide the insight into the resulting evaluation (Table 4.2). The slope of the best-fit line between the biomass derived from LiDAR and biomass from fieldwork is desired to be as close as possible to unity. Slope values exceeding one indicate overestimation and vice versa. The coefficient of determination (R^2) is the ratio of variation to the total variation and it can be written as:

$$R^2 = \left[\frac{\sum (Y_m - \overline{Y}_m)(Y_c - \overline{Y}_c)}{\sqrt{\sum (Y_m - \overline{Y}_m)^2 (Y_c - \overline{Y}_c)^2}} \right]^2 \quad (4.1)$$

where Y_c is the estimated biomass, $\overline{Y}_c$ is the average of the estimated biomass, Y_m is the fieldwork biomass and $\overline{Y}_m$ is the average of the fieldwork biomass.

The root mean squared error (RMSE) is a measure of absolute deviation that highlights the readability and repeatability of the biomass. The equation can be derived as :

$$RMSE = \sqrt{\left[\frac{\sum (Y_c - Y_m)^2}{n} \right]} \quad (4.2)$$

where n is the number of study sites.

Some other statistical parameters such as mean absolute deviation (MAD), mean bias error (MBE), non-dimensional mean bias error (NDMBE), non-dimensional mean absolute deviation (NDMAD) and non-dimensional root mean squared error (NDRMSE) provide information of the correlation relationship. The equations are as follows:

$$MBE = \frac{\sum (Y_c - Y_m)}{n} \quad (4.3)$$

$$MAD = \frac{\sum |Y_c - Y_m|}{n} \quad (4.4)$$

$$NDMBE = \frac{\sum [(Y_c - Y_m)/Y_m]}{n} \quad (4.5)$$

$$NDMAD = \frac{\sum |[(Y_c - Y_m)/Y_m]|}{n} \quad (4.6)$$

$$NDRMSE = \frac{\sum [(Y_c - Y_m)/Y_m]^2}{n} \quad (4.7)$$

Further information about the statistical analysis can be found in Draper and Smith (1998), Montgomery and Peck (1992) and Caliskan et al. (2011).

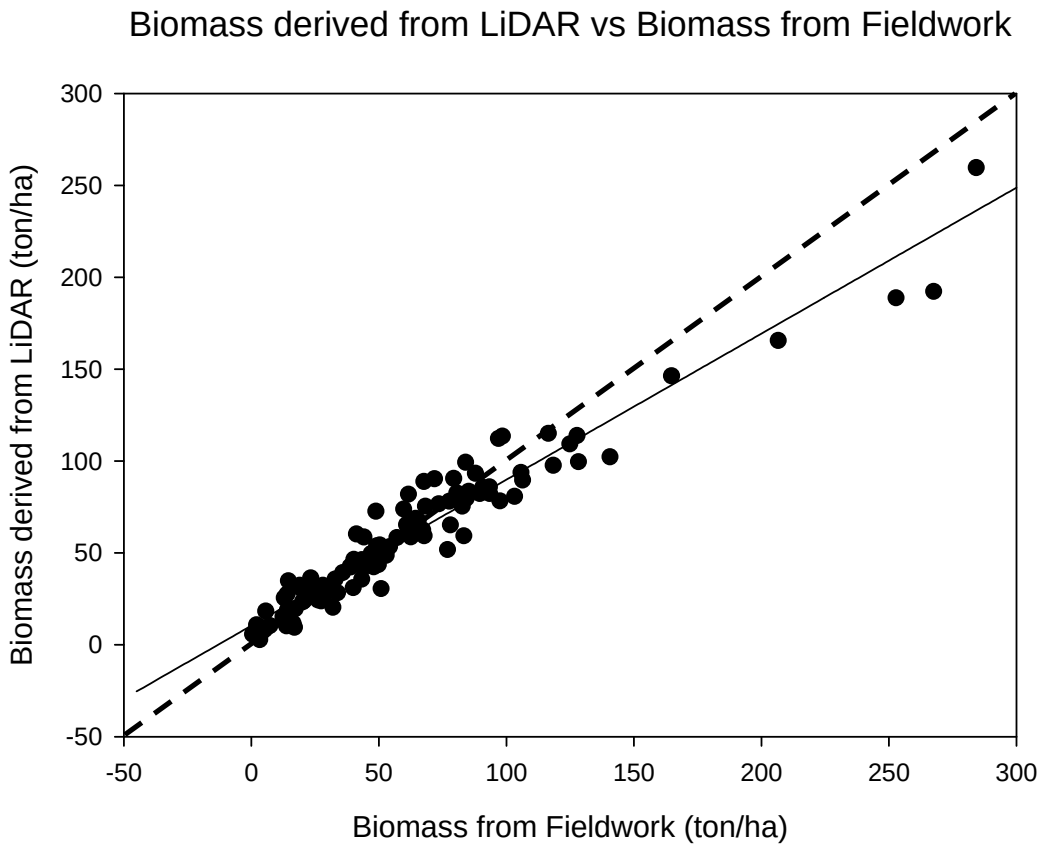

Figure 4.7. Regression graph for biomass derived LiDAR and biomass fieldwork

Table 4.2. Statistical metrics for result evaluation for LiDAR and fieldwork data

Data points	MAD	NDMAD	MBE	NDMBE	RMSE	NDRMSE	Slope	R^2
116	9.66	0.40	-1.64	0.27	14.81	1.21	0.80	0.97

In this work, the R^2 value obtained is 0.97 with RMSE of 14.81 ton/ha. In the case where the biomass measured from fieldwork is less than 100 ton/ha, the biomass is slightly overestimated by LiDAR while the biomass is underestimated in high density

forest. The number of first return ground hits, as a ratio of total first returns helps to define forest structure as an indicator of canopy cover. Stands with closer canopy cover result in a lower first return ground hit ratio, thus, underestimate the biomass. The variability of the height range gives rise to a higher deviation which relates to higher error in the estimation.

4.3 Tree Growth Classification

Canopy closure was estimated by dividing the number of returns by the total number of returns within each grid. The output ranges from 0% (very sparse forest with low canopy closure) to 100% (very dense forest with high canopy closure). The trees are then categorized into various classes, namely old dense growth, medium dense growth, young dense growth, old sparse growth, medium sparse growth and young sparse growth forests (Figure 4.8). The growth stages were determined by the tree height where tree height more than 20m was considered old growth, between 10m to 20m was considered medium growth and between 2m to 10m was considered the young growth. On the other hand, the density of the forest was determined by the canopy closure where canopy closure of more than 50% was categorized as dense forest and less than 50% as sparse forest.

From the forest growth analysis, it is found that there is 15.4% medium dense growth, 18.6% young dense growth, 20.4% medium sparse growth and 45.6% young sparse growth in the semi-natural forest and 24.6% of old dense growth, 29.0% medium dense growth, 18.9% young dense growth, 4.7% old sparse growth, 12.2% medium sparse growth and 10.6% young sparse growth in the plantation forest. The tree heights in semi-natural forest are less than 20m, therefore, no area has been classified as old growth. However, it is worth noting that due to the limitation of LiDAR which only provides pointwise sampling and not full area coverage like the optical systems, the laser data must be interpolated in order to convert the same coverage as an image. The

gridding process may introduce slight error when interpolating the data into the canopy height model.

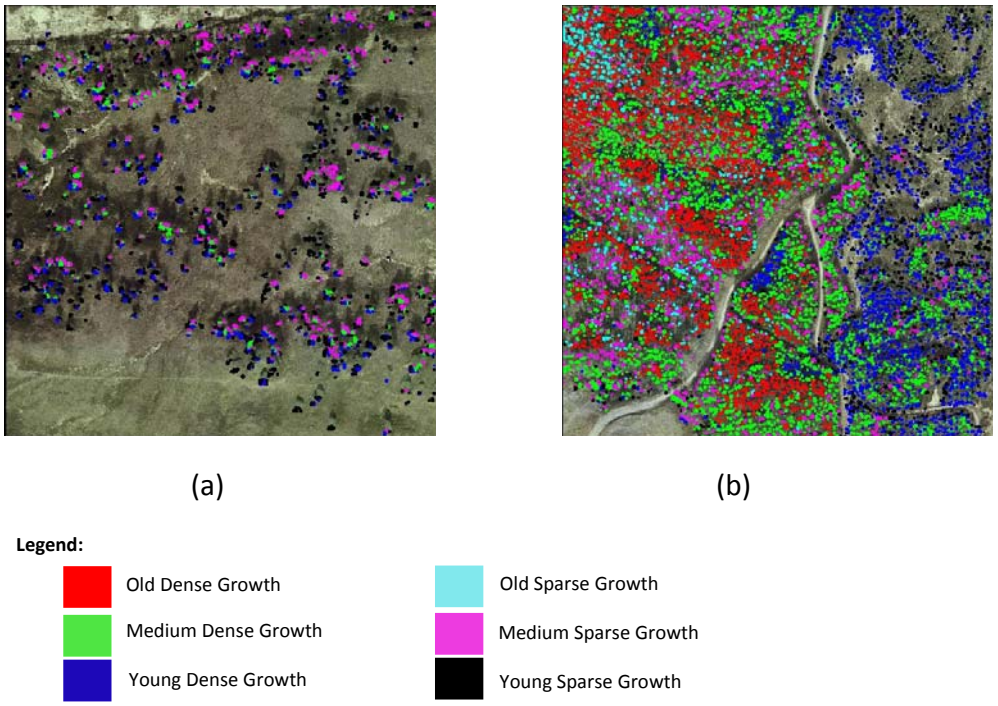

Figure 4.8. Tree Growth Classification for (a) sparse semi-natural woodland, (b) dense plantation forest. The forest in the semi-natural woodland is dominated by young sparse growth trees while the forest in the plantation forest is dominated by the old and medium dense growth.

4.4 Uncertainties of AGB Estimation Using LiDAR

In general, height derived from CHM constitutes a bias and standard error. The quality of the CHM is influenced by errors in both bare earth surface and CSM, with the first being either too high and the latter being too low, hence, manifesting a potential underestimation of CHM and above-ground biomass (Hyyppä et al., 2001; Gaveau and Hill, 2003). When comparing LiDAR derived bare Earth surface and OSDEM, the difference of error is less than 1.5m (Figure 4.9 shows the difference between the two

Earth surfaces with two profiles to demonstrate the line of sight profiles as shown in Figure 4.10 and Figure 4.11).

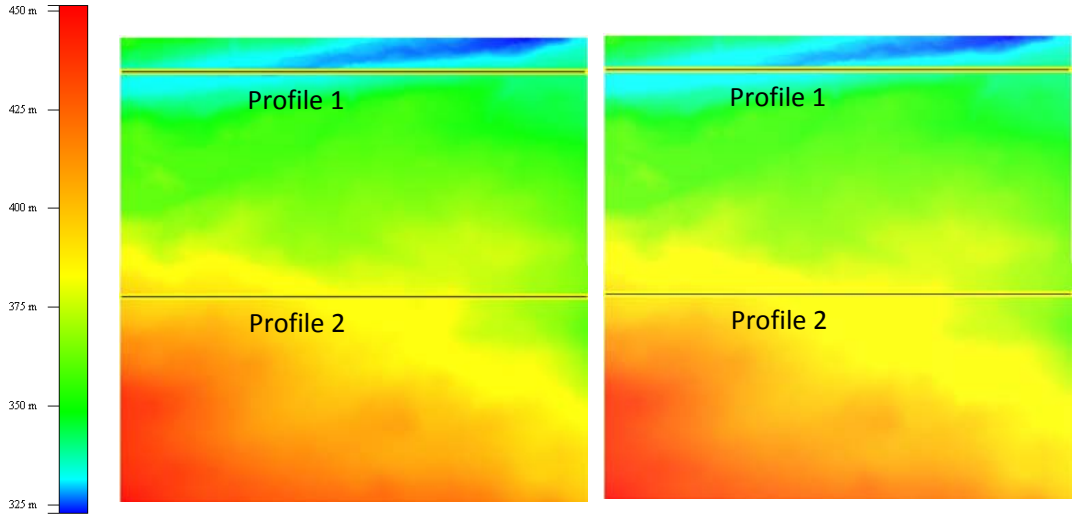

(a) (b)

Figure 4.9. Location of two profiles on the (a) LiDAR derived Bare Earth Surface (b) OSDEM data

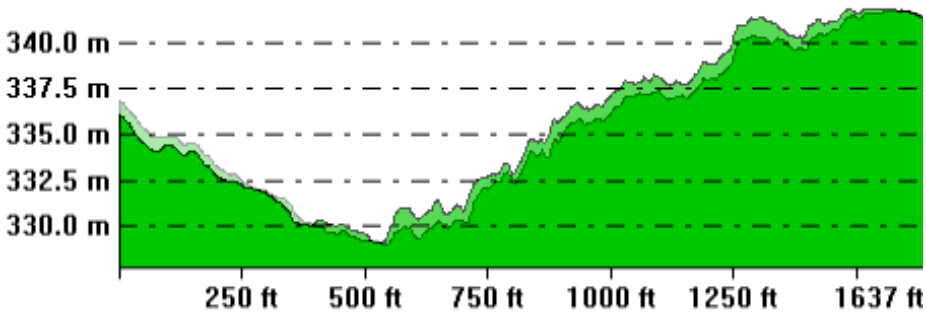

Figure 4.10. Overlay of line of sight profile 1 on the LiDAR derived Bare Earth Surface (dark line) and OSDEM data (light line)

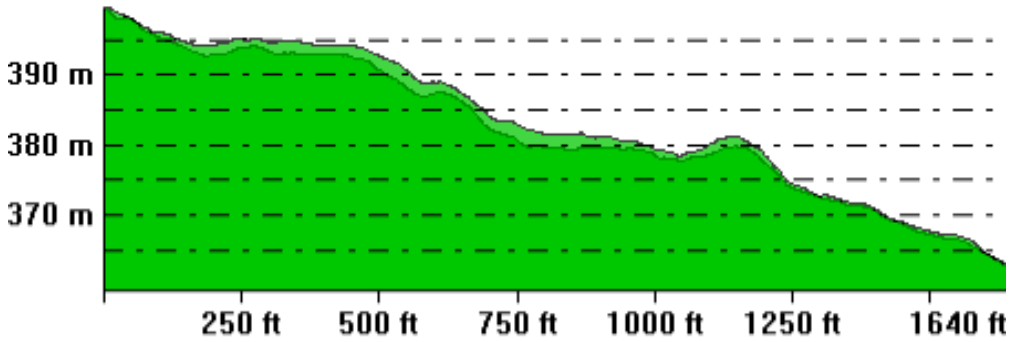

Figure 4.11. Overlay of line of sight profile 2 on the LiDAR derived Bare Earth Surface (dark line) and OSDEM data (light line)

Bias that might be induced by complexity of target such as slope and terrain roughness may further affect the accuracy of the estimation. Studies have shown that LiDAR scanning data includes low points under the ground level. These may be real returns or falsely interpreted elevation value from strong multiple scattering (Hyyppä, 1993). CHM error may occur in the area where slope is more than 45^{o} (Morsdorf, F., 2006). Apart from the errors caused by the bias and applied methodology, the quality of CHM derived from the scanning is also influenced by data characteristics such as first and last pulse, flight height, scan angle and point density.

Test flights (TopoSys, 1996) have demonstrated that in scanning angles of more than 10 degrees off-nadir, the amount of shadowed areas heavily increases, the number of measured ground hits decreases and the gaps in the CHM occur more frequently. Raber et al. (2002a) and Hodgson et al. (2003) discovered that land cover types contribute a significant factor that influences the accuracy of laser CHM. In the presence of land cover information, filtering procedure can be done to improve the accuracy of CHM. Results from previous literature (Kraus and Pfeifer, 1998, Hyyppä et al., 2000, Hyyppä et al., 2001, Ahokas et al., 2002, Reutebuch et al., 2003, Ahokas et al., 2002, Takeda, 2004) show that the accuracy deteriorates with the increase of density of the vegetation. This is due to the fact that the canopy cover and understory vegetation

prevents a large proportion of laser pulses from hitting the underlying surface, therefore, affecting the accuracy of CHM in dense forested areas.

On the other hand, if ground elevation or the uppermost portion of a forest canopy is not detected, then the canopy height will be underestimated. Basically, the underestimation of CHM is influenced by the density and canopy coverage of laser pulses, the algorithm used to obtain the CHM, the amount and height of under foliage and the sensitivity of system (Hyyppä and Inkinen, 1999, Persson et al. 2002, Gaveau and Hill, 2003, Leckie et al., 2003, Yu et al., 2004, Maltamo et al., 2004a).

Error may also arise from the random errors in the field measurement. As only 0.05ha of field measurement was conducted for 170 study sites, this area may not give a sufficient representation to determine the accuracy of the biomass estimation. It should be noted that the technique is unlikely to work as well in deciduous trees, since the tree delineation algorithm relies on the fact that the trees have only one well defined local maxima, which might not always be true for deciduous trees species.

The effect of scanning angle can also contribute to height and canopy cover estimation. Tree height, however, is less affected by scanning angle, while canopy cover are affected to a larger extend. The canopies seem to be denser when the scan angle is bigger because the probability of hitting the canopy element is higher. In our case, the height and canopy cover estimations are not significantly influenced by the scanning angle since the degradation of estimation only occur when the scanning angle is larger than 15^{o} (Ahokas et al., 2005).

4.5 Chapter Summary

The development of LiDAR technology has provided a means of obtaining detailed information on forest structure in the Glen Affric test site. In this chapter, the

potential of LiDAR data for tree growth classification and biomass estimation was assessed. The main conclusions are:

- In the sparse forests, accurate biomass estimation can be achieved. In this case, the ground elevation and the tree crowns are easily detected. Thus, CHM and biomass can be estimated with the RMSE=14.81 and R^2= 0.97. Note that in the dense forests, the biomass is underestimated. This is due to the fact that the canopy cover and understorey vegetation prevents a large proportion of laser pulses from hitting the underlying surface, therefore, affecting the accuracy of CHM in dense forested areas.
- Where the canopy closure and canopy height are available, the tree growth classification can be done. This information is important to facilitate a multifaceted analysis and study of forests in Glen Affric.

The results obtained from the analysis of LiDAR are encouraging and it can be incorporated to the existing mensuration models to estimate the biomass and to compare it with other remote sensing data. The high precision of estimates remains the principal challenge. Extension of LiDAR based forest biomass estimation to operational application is dependent on this factor, as well as the cost associated with large-scale LiDAR data acquisition. Future work in this area should compare the biomass estimation using other remote sensing and fieldwork data. The presence and location of the high biomass forests in Glen Affric will ultimately provide crucial information about the quality of the forest stands and lead to improvement in forestry management.

For the study at hand, the results of this chapter demonstrate that the LiDAR derived biomass data can be used as a valid estimate of AGB for evaluating the ALOS PALSAR data in the following chapter. This allows a more extensive (geographic) evaluation of the SAR data without the recourse to costly, time intensive field measurements.

Chapter 5
Above-Ground Biomass Estimation Using ALOS PALSAR and TerraSAR-X

5.1 Introduction

Due to the fact that SAR has higher temporal repeatability under all imaging conditions in comparison to optical satellite, radar imaging has become a compelling option in developing methods for operational inventory of forest resources from satellite. This chapter discusses the methodology of determining AGB using ALOS PALSAR and TerraSAR-X data. A flow chart is presented in Section 5.2 to give a general idea of the method with some remarks for each procedures. The detailed description for data preprocessing is explained in Section 5.3 and backscatter-biomass analysis in Section 5.4. Since the study area is mountainous, some discussion centres on the slope compensation (Section 5.5). The range slope correction is included in the data registration, whereas the azimuth slope effects are eliminated using the circular polarisation method. This is necessary to apply the Yamaguchi decomposition to retrieve the scattering mechanisms (Section 5.6). A sigmoid model is used to establish relationship between the volume-to-surface scattering and AGB (Section 5.7). Section 5.8 focuses on the results comparison where two sets of results are validated; ALOS PALSAR against LiDAR and ALOS PALSAR against TerraSAR-X. AGB estimation is also conducted at plot-level using ALOS PALSAR and the results is explained in

Section 5.9. Section 5.10 outlines the uncertainty of the research with concluding remarks in Section 5.11.

5.2 Methodology

The methodology of the AGB estimation using SAR data is described in Figure 5.1. Image preprocessing such as multilooking, geocoding and radiometric correction were performed before the backscatter analysis was done. Yamaguchi's model was used to decompose the total scattered power to volume, double bounce, helix and surface scattering mechanisms. In order to establish a relationship between the scattering mechanisms and AGB, regression analysis was conducted, thus, AGB was mapped using the regression equation. The overview of the proposed methodology is listed below:

1. Determine a sampling strategy, selection of plots (size and number), collection of forest inventory data (species), measurement of variables like tree dbh, height, etc.
2. Estimating AGB using field data and existing allometric equations.
3. Acquisition of ALOS PALSAR and TerraSAR-X data and pre-processing: procurement of appropriate ALOS PALSAR and TerraSAR-X data and preprocessing data such as multilooking and range slope correction.
4. Azimuth slope removal for ALOS PALSAR data: remove slope effects to account for the effective scattering pixel area.
5. Decomposition of scattering mechanism from full polarimetric data: Yamaguchi decomposition for extraction of scattering mechanisms.
6. Establishment of relationship between ratio of volume-to-surface scattering and AGB: calculation of correlation coefficients and regression equations. Estimation of AGB through modeling in GIS or application of equation.
7. AGB estimate testing and model validation: the calculated AGB estimates is compared with inventory data to check for accuracy estimation.

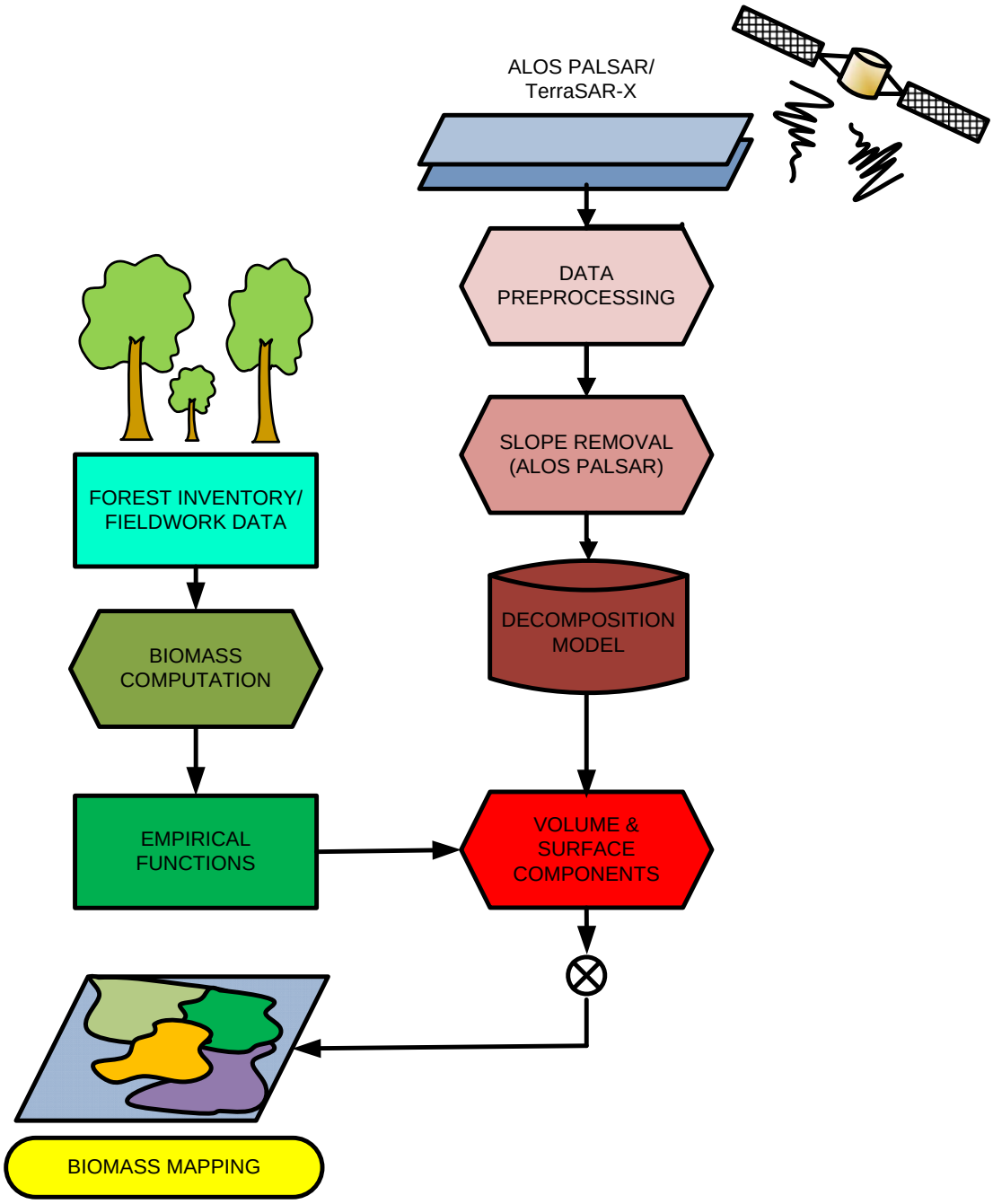

Figure 5.1. Flow chart of the research methodology for AGB estimation using ALOS PALSAR and TerraSAR-X

5.2.1 Data Preprocessing

Because the return signal bounces off from targets on the ground nearer to the satellite faster than those further away, it creates slight delay in return which affects the strength of the return beam and generates unevenness in the energy measurements. Hence, data preprocessing is essential not only to reduce speckle but also to correct distortion.

In general, a SAR signal processor aims to produce the highest possible resolution with amplitude and phase information. This type of data is also referred to as Single-Look Complex (SLC) data. Visually, such data appears very "speckled" and combined with the irregular pixel geometry, visual interpretation is challenging. Therefore, multilooking is done to improve the radiometric resolution. While true multilooking is done at an earlier stage in the processing, an effective multilook image can be generated by averaging the data over range or azimuth resolution cells. Since over-sampling is associated with the degradation in spatial resolution, the multilooking procedure should generate images with an optimal balance between number of looks and resolution.

The goal is to obtain in the multi-looked image approximately square pixels of the ground range and azimuth resolutions. Figure 5.2 (a) and (b) show the preprocessed images of ALOS PALSAR and TerraSAR-X in Pauli representation, respectively. In order to avoid over- or under-sampling effects, the data is multi-looked to approximate the same spatial resolution foreseen for the geocoded data. The ground resolution in range is defined as:

$$ground\ range\ resolution = \frac{slant\ range\ resolution}{\sin(incidence\ angle)} \tag{5.1}$$

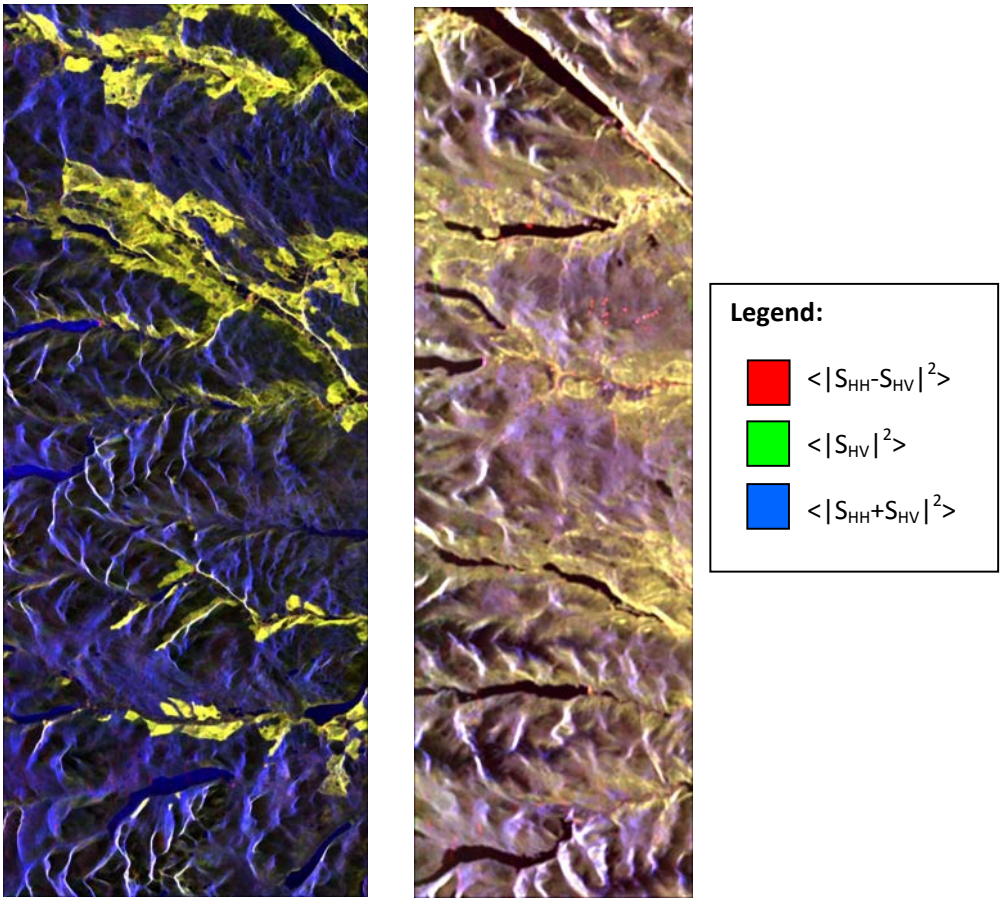

(a) (b)

Figure 5.2. The pre-processed images of (a) ALOS PALSAR and (b)TerraSAR-X in Pauli representation

5.2.2 Backscatter -AGB Analysis

AGB estimation has been successfully done using backscatter-AGB relationship in localised field sites (Hussin et al., 1994; Kasischke, et al., 1990, 1994; Dobson, 1992; Le Toan, et al., 1992; Kellndorfer et al., 2003; Woodhouse, 2006; Frank Rosillo-Catlle et al., 2007; Mitchard et al., 2009). Beaudoin et al. (1994) concluded from linear regression analysis between backscatter of forest stands and biophysical forest parameters such as stand height, basal area and dbh that higher correlation resulted at HV, followed by HH and VV. There is also evidence to demonstrate that a higher

correlation can be obtained when the radar backscatter at a longer wavelength is used because of its capability to penetrate deeper into the canopy (Leckie and Ranson, 1998). Because HV is originated mainly from the canopy volume scattering and trunk scattering (Le Toan, T et al., 1992), and is less affected by the surface scattering (Ranson and Sun, 1994, Frank Rosillo-Catlle et al., 2007), cross-polarization of L and P bands yielded the best sensitivities to AGB than the co-polarization. Theoretical models (Ulaby et al., 1990, Sun G., 1990) have also been developed to predict the radar backscatter as a function of the geometry and size of the forest canopies and radar system parameters. Wang et al. (1995) demonstrated that C-HH, C-HV, C-VV, L-VV and P-VV backscatter signal are less sensitive to AGB change while L-HH and P-HH or L-HV and P-HV backscatter signal are more suitable to be used to develop algorithms to retrieve forest AGB (Wang et al. 1995).

While these results are encouraging, most of these studies were conducted on monospecific stands in plantation settings or have involved only even aged stands of structurally similar species in the same genus (Imhoff, M. L., 1995). Furthermore, the issues of radar backscatter saturation when the AGB increases and the impact on backscatter variation in mountainous terrain have made the assessment of forest AGB more challenging. In the section, the backscatter-AGB analysis was tested on the geocoded HV signal of ALOS PALSAR data (Figure 5.3). Geocoding, radiometric and range slope correction were performed using SARscape Modules version 4.2 (ITT, 2009). A rigorous range-Doppler approach was applied to remove geometric distortions. The reconstruction of the imaging and processing geometry also takes range slope effects into consideration as well as the influence of Earth rotation and terrain height on the Doppler frequency shift and azimuth geometry (ITT, 2009). They are developed by SARMAP SA of Switzerland and integrated with ENVI for radar data processing and analysis. An Ordnance Survey DEM 1:10,000 downloaded from the Edina Digimap online service was used to correct the terrain of the study area. In order to ease validation at a later stage, all the data including the Ordnance Survey DEM data are

geocoded to Ordnance Survey Great Britain 1936 at Global Cartesian coordinate system WGS-84.

When applying a simple regression analysis on the study area, a very low correlation has been obtained. Figure 5.3 shows the regression graph between the HV and AGB and the regression equation can be written as:

$$HV = -14.2151+1.8251 *(1-\exp(-0.0488*AGB)),\ R^2 = 0.36 \quad (5.2)$$

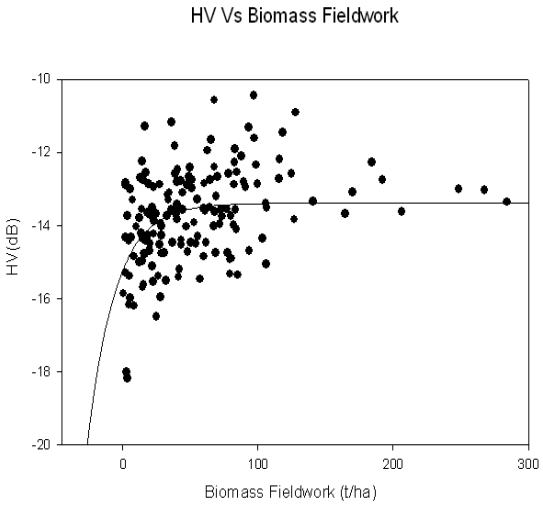

Figure 5.3. Regression Analysis between HV backscatter and AGB in Glen Afric using ALOS PALSAR data

With an R^2 of 0.36, the correlation is very low. The HV backscatter values are demonstrated to be higher than it should be and hence, overestimate the AGB. To resolve this issue, polarimetry techniques and the possibility of using longer wavelength radar and smaller incidence angles can be used. Longer wavelength data are less sensitive to azimuth slope variations due to the fact that the electromagnetic waves with small wavelength are less penetrative and more sensitive to small scatterers (Lee et al., 2000). Rougher surfaces also produce weaker returns at small incidence angles (Ulaby et

al., 1986). So, this is when polarimetry becomes useful because not only can it be used to decompose the coherency matrix[1] to different scattering mechanisms but also it can be used to remove the azimuth slopes induced by the orientation angle.

Radar polarimetry is the science of capturing, processing and analysing the polarisation state of an electromagnetic field (Lee & Pottier, 2009). The etymological meaning of the word polarimetry is :- 1) prefix 'polar' means polarisation and 2) suffix 'metry' means measure. It is a technique which allows the identification and separation of scattering mechanisms in the polarisation signature for natural scatterers characterisation and parameter estimation. Because it is sensitive to the orientation and physical information of the target, polarimetry offers several descriptive radar target detection parameters and lead to the advancement of decomposition theorems. Polarimetric data which operates at long wavelength such as L and P bands is able to penetrate into forest cover, hence, it is inherently sensitive to volume effects and provides vertical structure information for biomass mapping (Mette et al., 2002; Caicoya et al., 2010; Sauer et al., 2010; Zhang et al., 2011; Xu et al., 2011).

Polarimetry takes advantage of the fact that objects of different orientation influence the polarisation of the backscattered echo. For the case at hand, random volumes such as a forest canopy will noticeably depolarize the radar signal, whereas surface scattering polarizes the echo. Since the azimuth slope (the slope across the view direction) will also introduce a polarized signal, it is necessary to first account for variations in azimuth slope.

---

[1] Coherency matrix is represented in the context of vector-valued stationary stochastic processes with orthogonal increments (Barakat, 1963). It accounts for local variations in the scattering matrix and is the lowest order operator suitable to retrieve polarimetric parameters for distributed scatterers in the presence of speckle (Lee & Pottier, 2009).

5.2.3 Azimuth Slope Compensation

Azimuth slope compensation has been conducted to eliminate the effects of slope in the study area (Lee et al., 2000). When a polarimetric radar captures a horizontal surface, the horizontal polarization electric field is parallel to the surface. On the other hand, for a tilted surface, the horizontal vector is not parallel to the surface, hence, all the polarization components (HH, VV, HV and VH) are affected by the tilted slope. The amount of the slope-induced shift in the polarization orientation angle can be illustrated as the rotation of the vertical-horizontal basis vector about the line-of-sight (Lee et al., 2009). The basic concept of the procedure is to rotate the data about the line-of-sight by the negative of the polarization orientation angle induced by the topographical slopes (Lee et al., 2002; Schuler et al., 1996; Pottier et al., 1999) to make the horizontal component parallel to the sloping terrain surface. Each element of the polarimetric covariance matrices is compensated based on its polarization state.

The orientation angle shift causes rotation of both the scattering matrix and the circular covariance matrix about the line of sight. A few methods (Lee et al., 2000; 2002; 2009; Schuler et al., 1996; Pottier et al., 1999; Kasilingam et al., 2000) have been developed to estimate the azimuth slope-induced orientation angles. In this thesis, the circular polarization method is used because it is based on a theoretical derivation and proven to be simpler and more effective than other methods (Lee et al., 2009).

In the horizontal-vertical basis, the 2 x 2 complex backscattering S matrix can be expressed as (Boerner, 1990; Boerner et al., 1998; Kostinski & Boerner, 1986):

$$S = \begin{bmatrix} S_{HH} & S_{HV} \\ S_{VH} & S_{VV} \end{bmatrix} \tag{5.3}$$

where S_{HH} and S_{VV} produce the power return in the co-polarized channels and the elements S_{HV} and S_{VH} produce the power return in the cross-polarized channels.

The circular polarization components can be easily derived from the scattering matrix and they are shown below:

$$S_{RR} = \left(S_{HH} - S_{VV} + i2S_{HV}\right)/2 \tag{5.4}$$

$$S_{LL} = \left(S_{VV} - S_{HH} + i2S_{HV}\right)/2 \tag{5.5}$$

$$S_{RL} = i\left(S_{HH} + S_{VV}\right)/2 \tag{5.6}$$

By applying the rotation of a scattering matrix, the rotation by an orientation angle can be written as

$$\widetilde{S}_{RR} = S_{RR}\, e^{i2\theta} \tag{5.7}$$

$$\widetilde{S}_{LL} = S_{LL}\, e^{i2\theta} \tag{5.8}$$

$$\widetilde{S}_{RL} = S_{RL} \tag{5.9}$$

The rotated circular polarization covariance matrix G is then defined as

$$G = \left\langle \widetilde{c}\ \widetilde{c}^{*T} \right\rangle \tag{5.10}$$

$$G = \begin{bmatrix} \left\langle \left|S_{RR}\right|^2 \right\rangle & \sqrt{2}\left\langle \left(S_{RR}S_{RL}^{*}\right)e^{i2\theta} \right\rangle & \left\langle \left(S_{RR}S_{LL}^{*}\right)e^{i4\theta} \right\rangle \\ \sqrt{2}\left\langle \left(S_{RL}S_{RR}^{*}\right)e^{i2\theta} \right\rangle & 2\left\langle \left|S_{RL}\right|^2 \right\rangle & \sqrt{2}\left\langle \left(S_{RL}S_{LL}^{*}\right)e^{i2\theta} \right\rangle \\ \left\langle \left(S_{LL}S_{RR}^{*}\right)e^{i4\theta} \right\rangle & \sqrt{2}\left\langle \left(S_{LL}S_{RL}^{*}\right)e^{i2\theta} \right\rangle & \left\langle \left|S_{LL}\right|^2 \right\rangle \end{bmatrix} \tag{5.11}$$

$$\text{where } \widetilde{c} = \begin{bmatrix} \widetilde{S}_{RR} \\ \sqrt{2}\widetilde{S}_{RL} \\ \widetilde{S}_{LL} \end{bmatrix} \text{(Lee et al., 2009).} \tag{5.12}$$

The diagonal terms are rotation invariant and only the off-diagonal terms are affected with any change in the orientation angle. Therefore, these terms could be used for orientation angle derivation. It is worth noting that for a horizontal reflection symmetrical media, the $\widetilde{G}_{12}$ and $\widetilde{G}_{23}$ may have non-zero phase value and this affects the

estimate after the orientation rotation. To resolve this issue, $\widetilde{G}_{13}$ is utilized to determine the orientation angle (Lee et al., 2002).

By substituting

$$S_{RR} = \left(S_{HH} - S_{VV} + i2S_{HV}\right)/2 \tag{5.13}$$

$$S_{LL} = \left(S_{VV} - S_{HH} + i2S_{HV}\right)/2 \tag{5.14}$$

$$S_{RL} = i\left(S_{HH} + S_{VV}\right)/2 \tag{5.15}$$

into $\widetilde{G}_{13}$, we have

$$\left\langle S_{RR}S_{LL}^{*}\right\rangle e^{i4\theta} = \frac{1}{4}\left\{\left\langle -\left|\widetilde{S}_{HH} - \widetilde{S}_{VV}\right|^{2} + 4\left|\widetilde{S}_{HV}\right|^{2}\right\rangle - i4\,\mathrm{Re}\left(\left\langle\left(\widetilde{S}_{HH} - \widetilde{S}_{VV}\right)\widetilde{S}_{HV}^{*}\right\rangle\right)\right\} \tag{5.16}$$

and

$$-4\theta = Arg\left(\left\langle S_{RR}S_{LL}^{*}\right\rangle e^{i4\theta}\right) = \tan^{-1}\left(\frac{-4\,\mathrm{Re}\left(\left\langle\left(\widetilde{S}_{HH} - \widetilde{S}_{VV}\right)\widetilde{S}_{HV}^{*}\right\rangle\right)}{-\left\langle\left|\widetilde{S}_{HH} - \widetilde{S}_{VV}\right|^{2} + 4\left|\widetilde{S}_{HV}\right|^{2}\right\rangle}\right) \tag{5.17}$$

Since arctangent is calculated in the range of $[-\pi, \pi]$, the factor of 4θ limits the range of θ to $[-\pi/4, \pi/4]$(Lee et al., 2009).

In most cases of azimuthal symmetry , $\left(\left|\widetilde{S}_{HH} - \widetilde{S}_{VV}\right|^{2}\right)$ is greater than $4\left\langle\left|\widetilde{S}_{HV}\right|^{2}\right\rangle$, hence introducing a negative denominator. When the numerator is near zero, the arctangent is near $\pm\pi$, resulting in the orientation angle being equal to $\pm\pi/4$, instead of near zero as it should be. In order to compensate the error corresponding to the azimuth slope angle, the bias needs to be removed by adding π (Lee et al., 2002) .

Orientation angle, θ was calculated using the circular polarization method:

$$\theta = \frac{1}{4}\left[\tan^{-1}\left(\frac{-4\,\mathrm{Re}\left(\langle S_{HH} - S_{VV}\rangle S_{HV}^{*}\right)}{-\left\langle\left|S_{HH} - S_{VV}\right|^{2}\right\rangle + 4\left\langle\left|S_{HV}\right|^{2}\right\rangle}\right) + \pi\right] \tag{5.18}$$

$$\text{For } \theta > \frac{\pi}{4},\ \ \theta = \theta - \frac{\pi}{2}$$

where θ is the orientation angle shift and the subscript H denotes horizontal polarisation and V denotes vertical polarisation (Lee et al., 2009).

After obtaining the orientation angle, θ and the corresponding [T] the slope compensation can be done by

$$[T^{new}] = [U][T][U^{T}] \tag{5.19}$$

where the rotation matrix *U* can be expressed as

$$[U] = \begin{bmatrix} 1 & 0 & 0 \\ 0 & \cos 2\theta & \sin 2\theta \\ 0 & -\sin 2\theta & \cos 2\theta \end{bmatrix}. \tag{5.20}$$

Three transects were chosen to demonstrate the azimuth slope compensation effect in Glen Affric. Figure 5.4 shows the location of the chosen transects while Figure 5.5, Figure 5.6 and Figure 5.7 illustrate all the coherency matrix components and orientation angle along each transect. Theoretically, in an area where the orientation angle is completely induced by the azimuth slope, the compensation should make the averaged coherency matrix reflection symmetric (Cloude & Pottier, 1996). However, in practical, this is not possible because only the orientation angle is taken in consideration in the compensation procedure. The orientation angles span from -45^0 to $+45^0$. The coherency matrix can also be expressed as :

$$[T^{new}] = \frac{1}{2}\begin{bmatrix} \left\langle |S_{HH}+S_{VV}|^2 \right\rangle & \left\langle (S_{HH}+S_{VV})(S_{HH}-S_{VV})^* \right\rangle & 2\left\langle (S_{HH}+S_{VV})S_{HV}^* \right\rangle \\ \left\langle (S_{HH}-S_{VV})(S_{HH}+S_{VV})^* \right\rangle & \left\langle |S_{HH}-S_{VV}|^2 \right\rangle & 2\left\langle (S_{HH}-S_{VV})S_{HV}^* \right\rangle \\ 2\left\langle S_{HV}(S_{HH}+S_{VV})^* \right\rangle & 2\left\langle S_{HV}(S_{HH}-S_{VV})^* \right\rangle & 4\left\langle |S_{HV}|^2 \right\rangle \end{bmatrix} \quad (5.21)$$

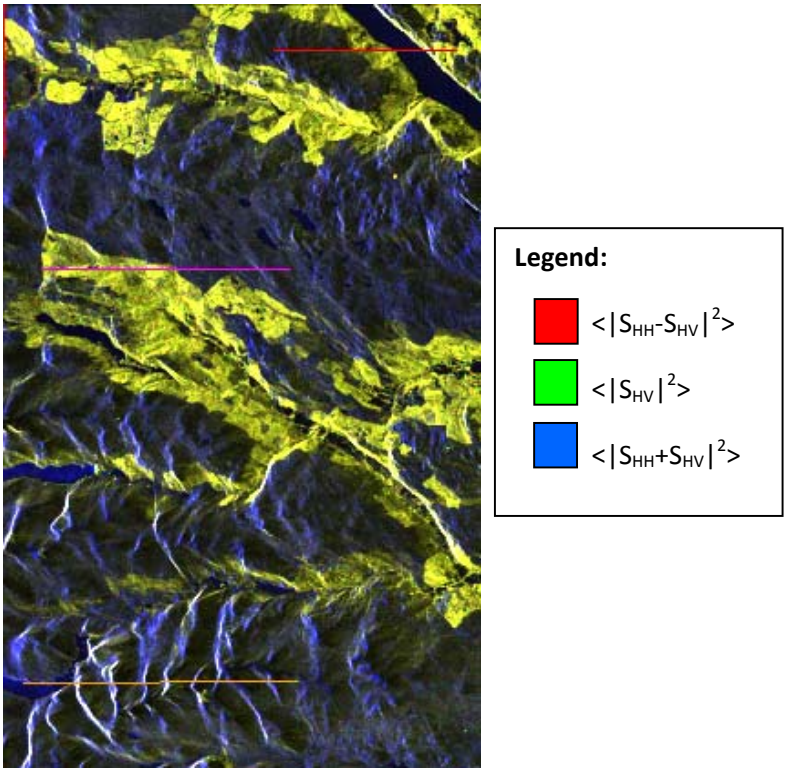

Figure 5.4. Location of three transects in Glen Affric to demonstrate the azimuth slope compensation effect. The transects are chosen at different terrain types; Profile 1 is located near the valley, Profile 2 has the combination of forested and non forested areas and Profile 3 is in a hilly area.

The $\langle (S_{HH}-S_{VV})S_{HV}^* \rangle$ term is shown to have the greatest effect with average reduction of -2.9 dB for the whole image while $\langle (S_{HH}+S_{VV})^2 \rangle$ term is rotation invariant and remains unchanged. The slope effect on $\langle (S_{HH}-S_{VV})^2 \rangle$ and $\langle (S_{HH}+S_{VV})(S_{HH}-S_{VV})^* \rangle$ shows slight increase in values. A large reduction can be observed in the term $\langle |S_{HV}|^2 \rangle$ with an average value of -2.5dB. Since Glen Affric is surrounded by mountainous moorland with isolated Scots pines, this area is dominated by Bragg scattering. In this

case, $<|S_{HH}|^2>$ is low and $<|S_{VV}|^2>$ is high and they are in phase. With the slope compensation, $<|S_{VV}|^2>$ and $<|S_{HH}|^2>$ are rotated along the line of sight , thus, $<|S_{HH} - S_{VV}|^2>$ is smaller than the original value.

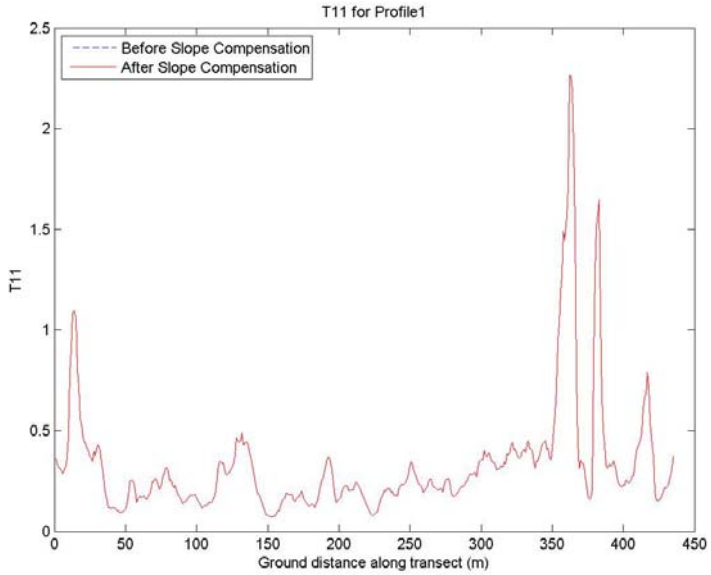

(a)

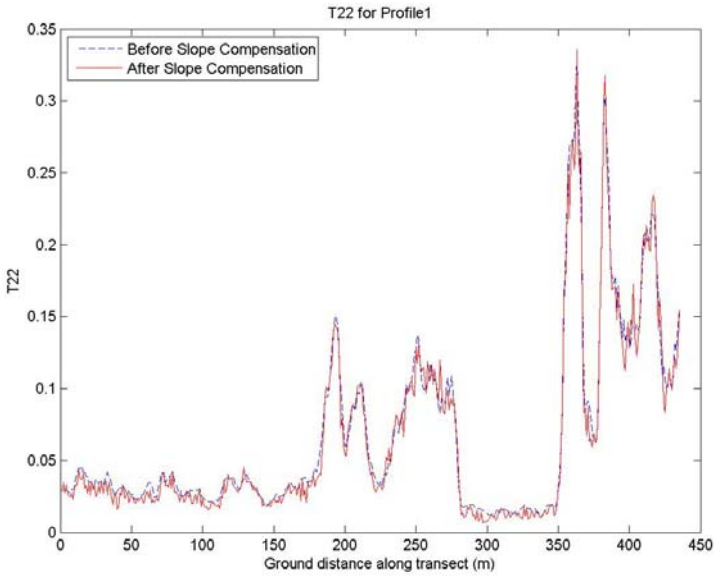

(b)

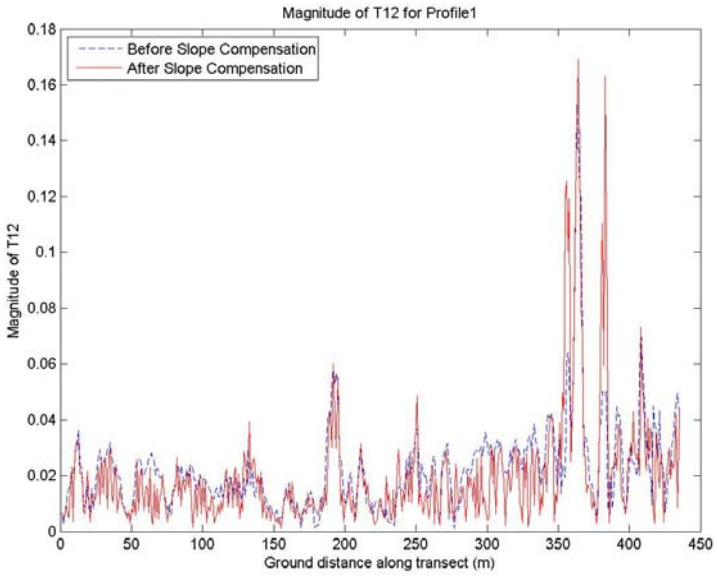
Magnitude of T12 for Profile1
Before Slope Compensation
After Slope Compensation
Magnitude of T12
Ground distance along transect (m)
0.18
0.16
0.14
0.12
0.1
0.08
0.06
0.04
0.02
0
0
50
100
150
200
250
300
350
400
450

(c)

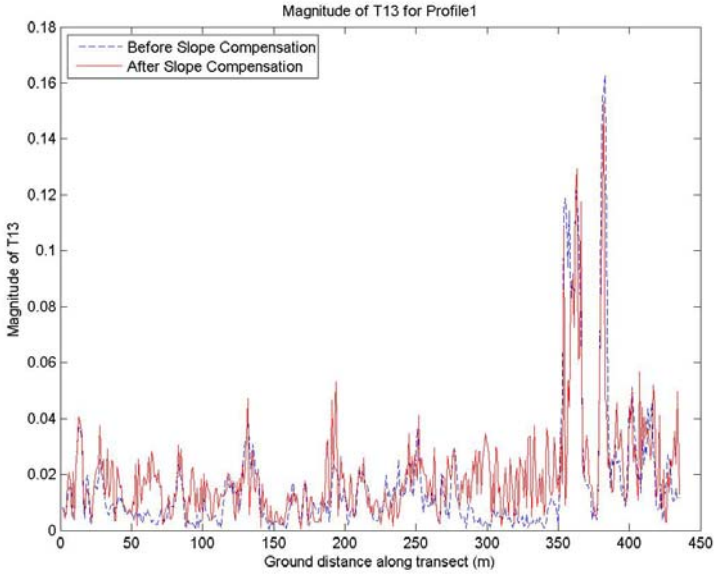
Magnitude of T13 for Profile1
Before Slope Compensation
After Slope Compensation
Magnitude of T13
Ground distance along transect (m)
0.18
0.16
0.14
0.12
0.1
0.08
0.06
0.04
0.02
0
0
50
100
150
200
250
300
350
400
450

(d)

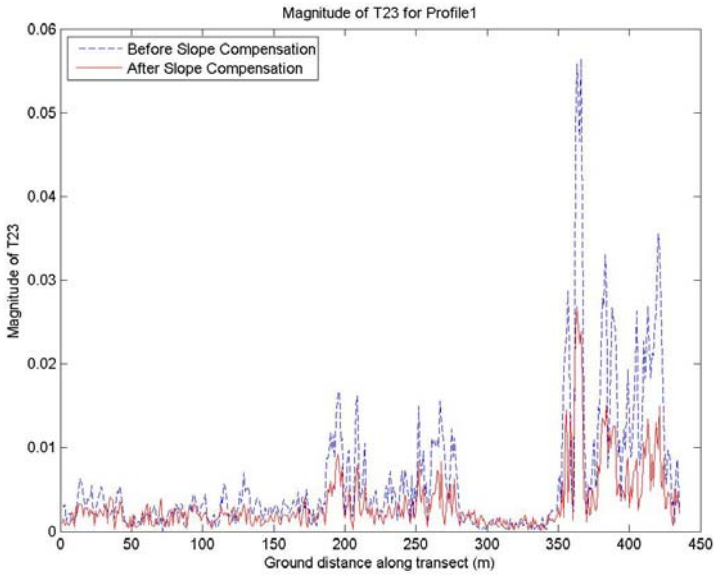
Magnitude of T23 for Profile1
Before Slope Compensation
After Slope Compensation
Magnitude of T23
Ground distance along transect (m)
0.06
0.05
0.04
0.03
0.02
0.01
0
0
50
100
150
200
250
300
350
400
450

(e)

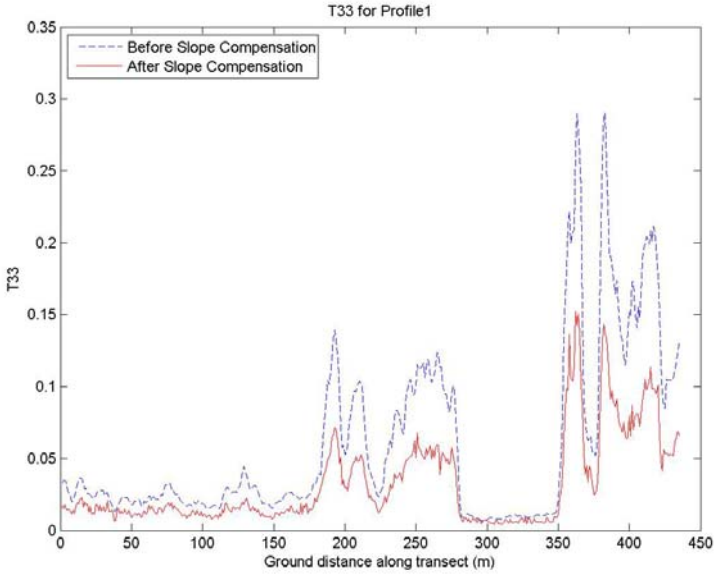
T33 for Profile1
Before Slope Compensation
After Slope Compensation
T33
Ground distance along transect (m)
0.35
0.3
0.25
0.2
0.15
0.1
0.05
0
0
50
100
150
200
250
300
350
400
450

(f)

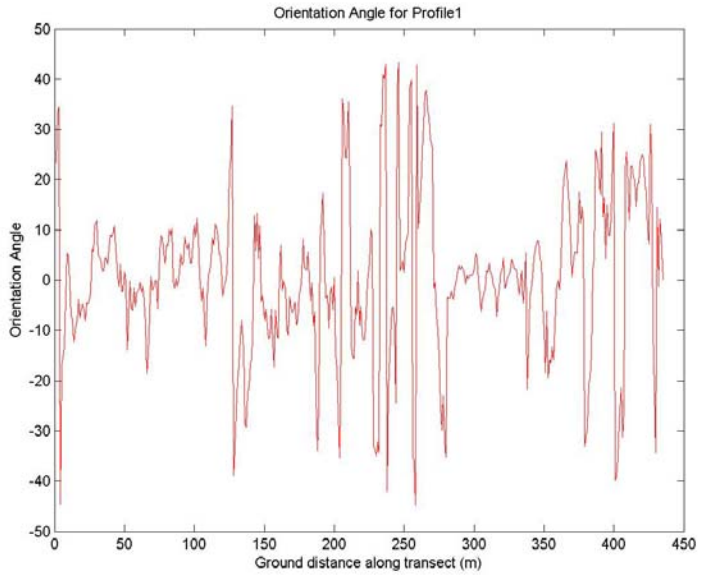

(g)

Figure 5.5. Effects of azimuth slope compensation for Profile 1 (a) T11, (b) T22 (c) Magnitude T12, (d) Magnitude T13, (e) Magnitude T23, (f) T33, (g) Orientation Angle. In the area where there is river, the orientation angle is almost zero, hence, the compensation effect for all the components is the least in the area.

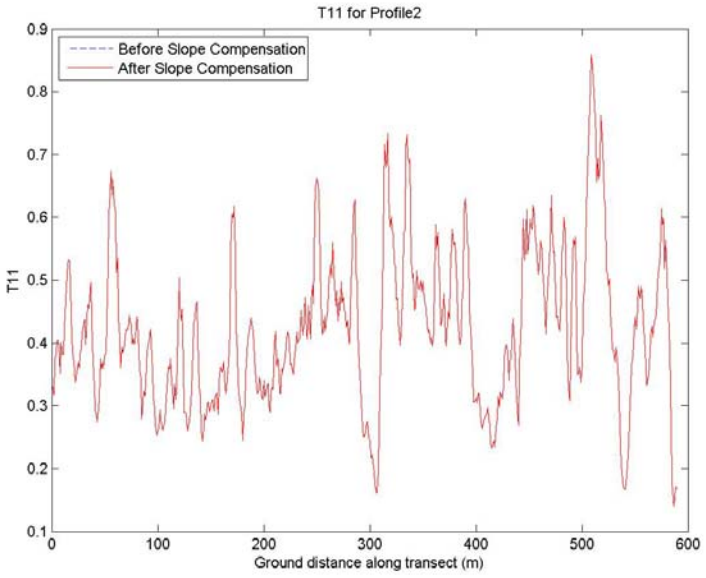

(a)

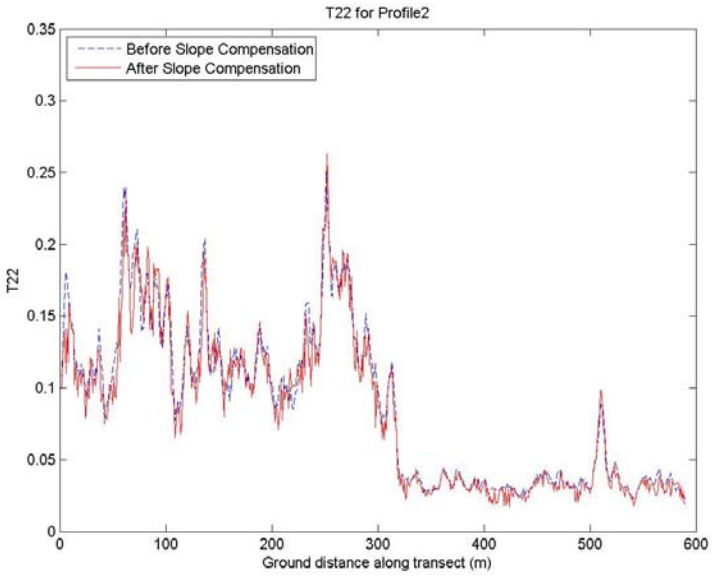
T22 for Profile2
Before Slope Compensation
After Slope Compensation
T22
Ground distance along transect (m)
0.35
0.3
0.25
0.2
0.15
0.1
0.05
0
0
100
200
300
400
500
600

(b)

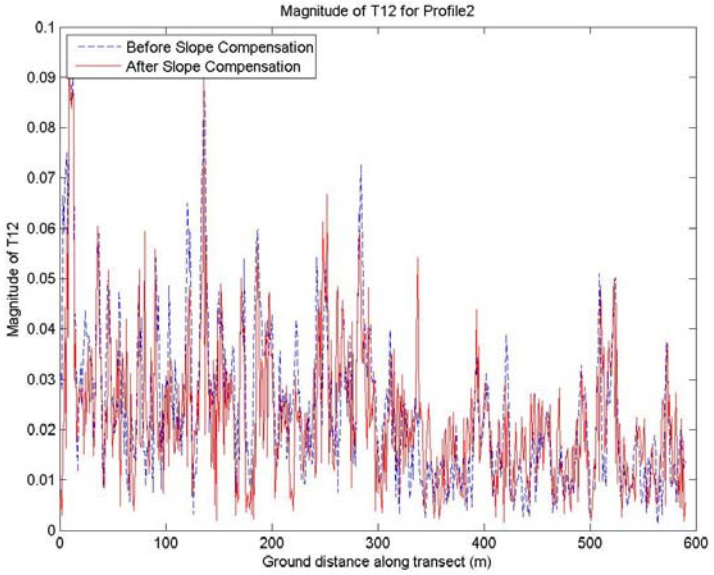
Magnitude of T12 for Profile2
Before Slope Compensation
After Slope Compensation
Magnitude of T12
Ground distance along transect (m)
0.1
0.09
0.08
0.07
0.06
0.05
0.04
0.03
0.02
0.01
0
0
100
200
300
400
500
600

(c)

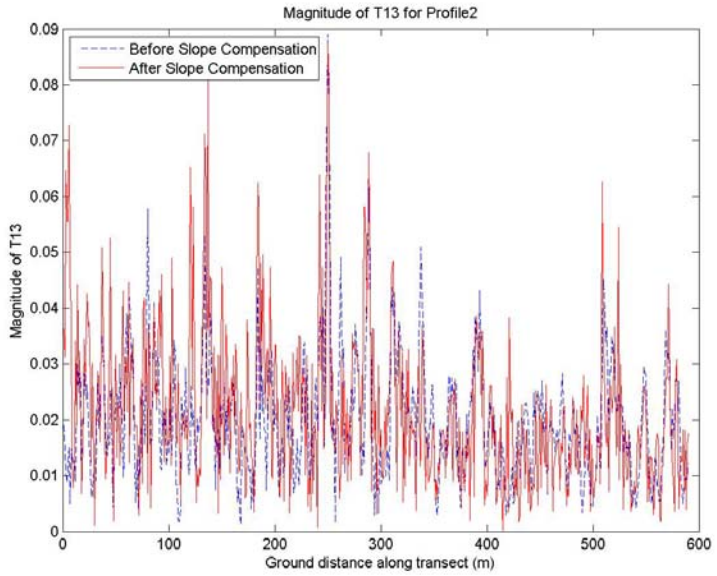
Magnitude of T13 for Profile2
Before Slope Compensation
After Slope Compensation
Magnitude of T13
Ground distance along transect (m)
0.09
0.08
0.07
0.06
0.05
0.04
0.03
0.02
0.01
0
0
100
200
300
400
500
600

(d)

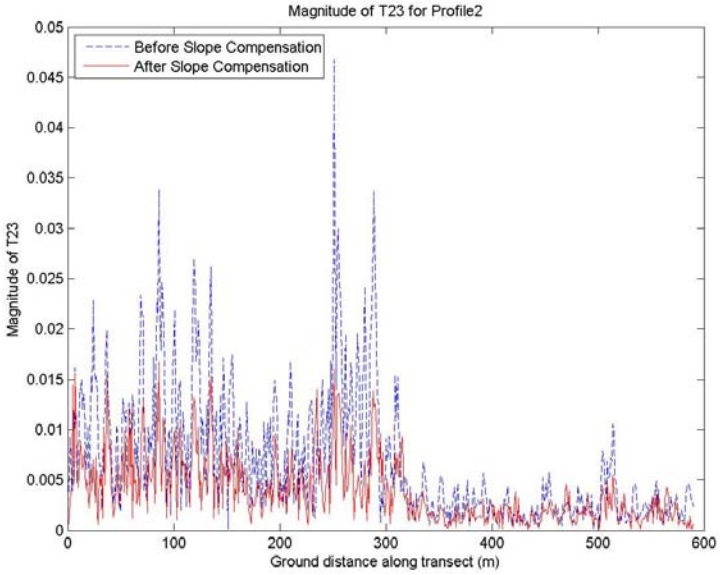
Magnitude of T23 for Profile2
Before Slope Compensation
After Slope Compensation
Magnitude of T23
Ground distance along transect (m)
0.05
0.045
0.04
0.035
0.03
0.025
0.02
0.015
0.01
0.005
0
0
100
200
300
400
500
600

(e)

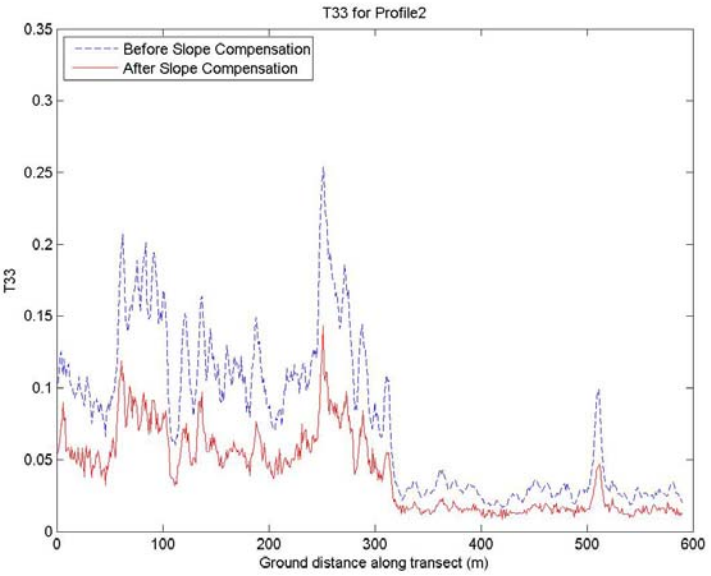

(f)

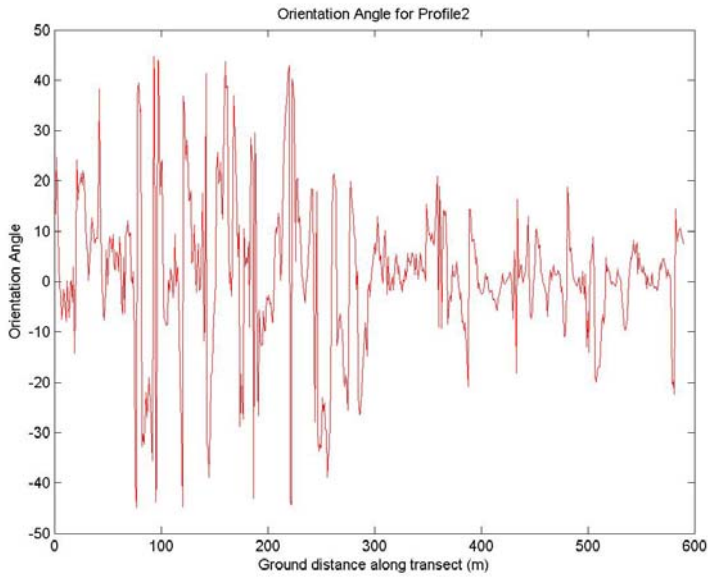

(g)

Figure 5.6. Effects of azimuth slope compensation for Profile 2 (a) T11, (b) T22 (c) Magnitude T12, (d) Magnitude T13, (e) Magnitude T23, (f) T33, (g) Orientation Angle. A great reduction can be observed in the vegetation area compared to non-vegetation area where the variation of orientation angle in the former area is higher than the latter.

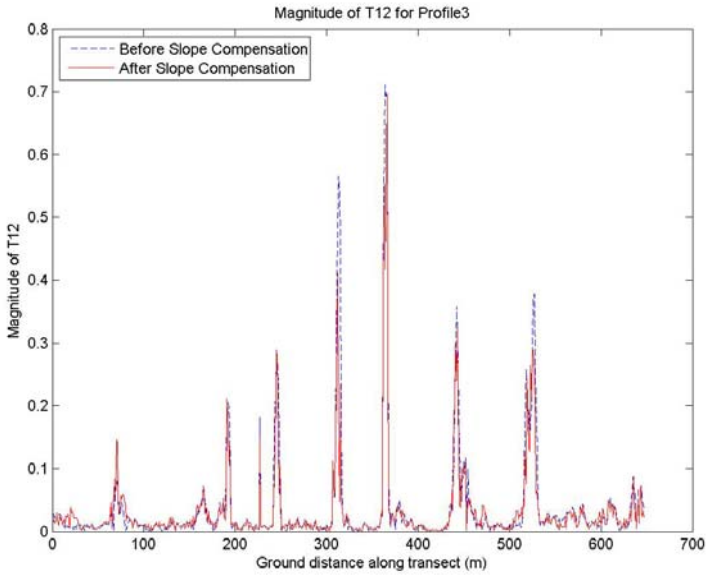
Magnitude of T12 for Profile3
Before Slope Compensation
After Slope Compensation
Magnitude of T12
Ground distance along transect (m)
0
0.1
0.2
0.3
0.4
0.5
0.6
0.7
0.8
0
100
200
300
400
500
600
700

(a)

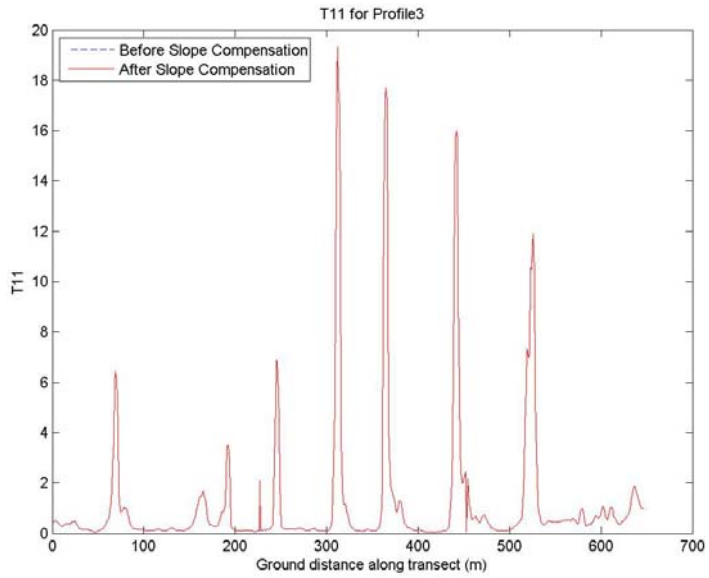
T11 for Profile3
Before Slope Compensation
After Slope Compensation
T11
Ground distance along transect (m)
0
2
4
6
8
10
12
14
16
18
20
0
100
200
300
400
500
600
700

(b)

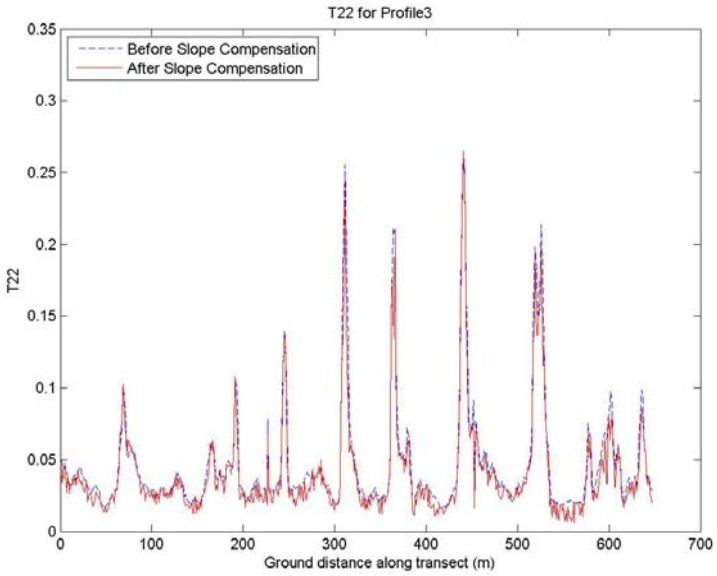
T22 for Profile3
Before Slope Compensation
After Slope Compensation
T22
Ground distance along transect (m)
0.35
0.3
0.25
0.2
0.15
0.1
0.05
0
0
100
200
300
400
500
600
700

(c)

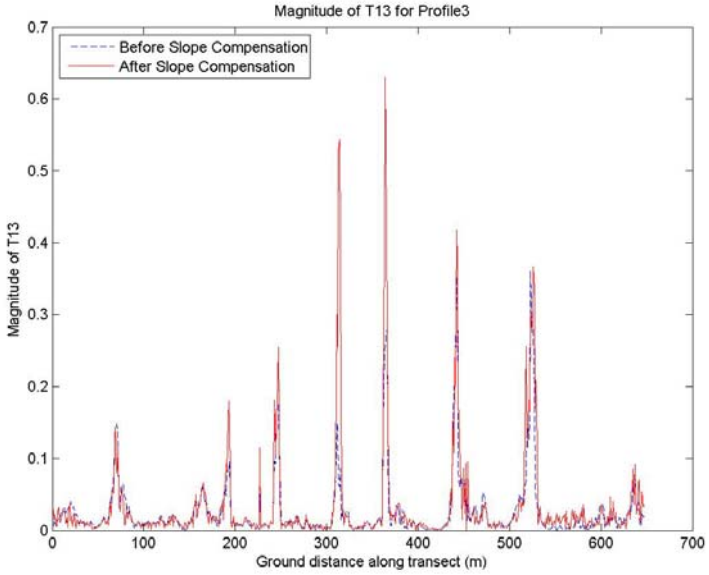
Magnitude of T13 for Profile3
Before Slope Compensation
After Slope Compensation
Magnitude of T13
Ground distance along transect (m)
0.7
0.6
0.5
0.4
0.3
0.2
0.1
0
0
100
200
300
400
500
600
700

(d)

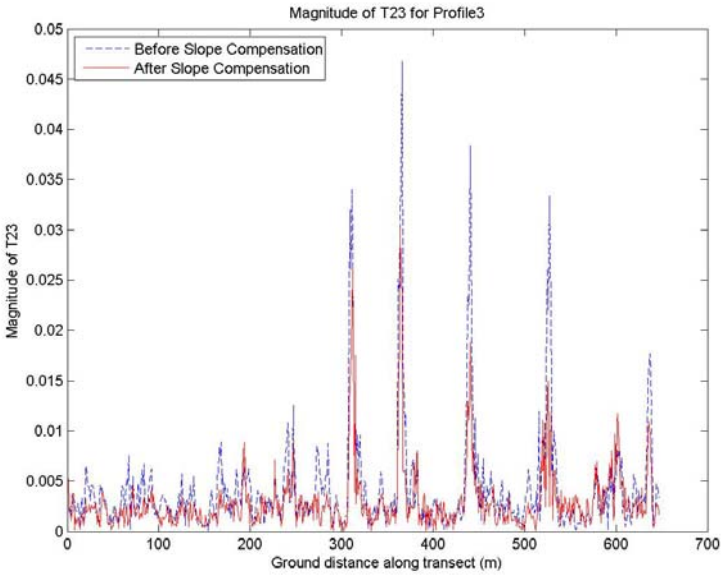
Magnitude of T23 for Profile3
Before Slope Compensation
After Slope Compensation
Magnitude of T23
Ground distance along transect (m)
0.05
0.045
0.04
0.035
0.03
0.025
0.02
0.015
0.01
0.005
0
0
100
200
300
400
500
600
700

(e)

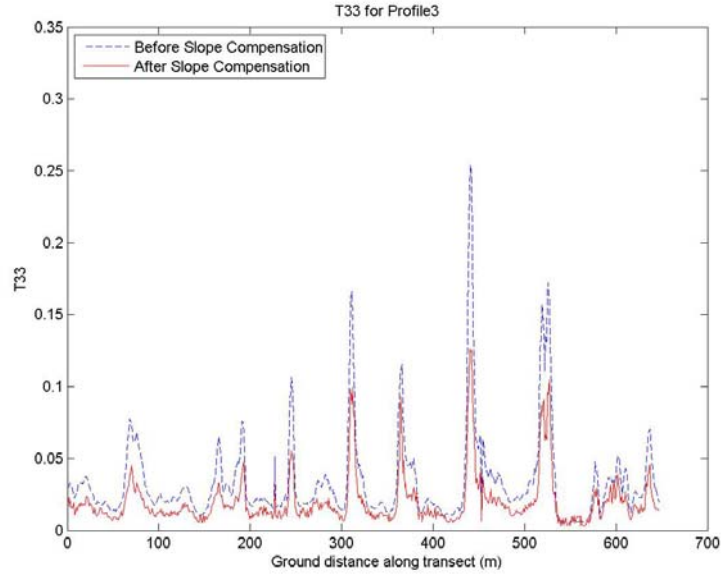
T33 for Profile3
Before Slope Compensation
After Slope Compensation
T33
Ground distance along transect (m)
0.35
0.3
0.25
0.2
0.15
0.1
0.05
0
0
100
200
300
400
500
600
700

(f)

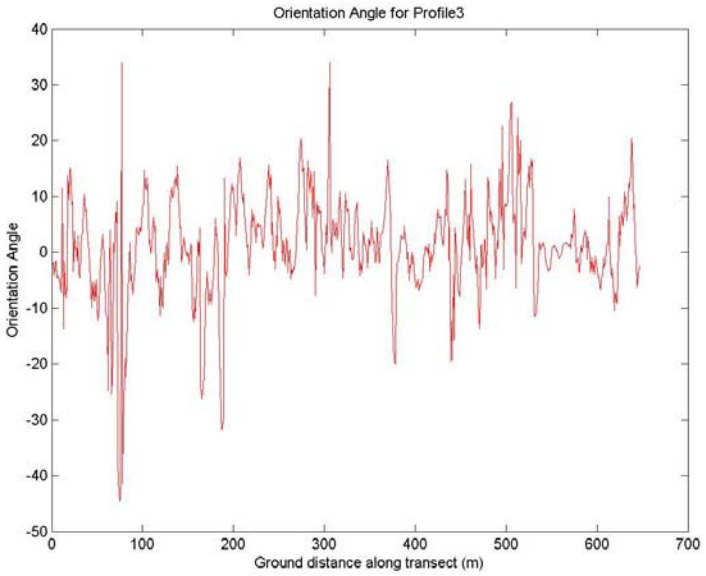

(g)

Figure 5.7. Effects of azimuth slope compensation for Profile 3 (a) T11, (b) T22 (c) Magnitude T12, (d) Magnitude T13, (e) Magnitude T23, (f) T33, (g) Orientation Angle. High variations occur when there are slopes along the profile and they are reduced after the azimuth compensation procedure.

5.2.4 Decomposition Theorems

The scattering signal in radar remote sensing is influenced by combination of speckle noise and random vector scattering effects from surface and volume scatterers. A multivariate statistical description is required to generate the concept of dominant scattering mechanism for land cover classification, target recognition or model inversion of scattering data. It involves an averaging process which leads to the concept of the distributed target. Unlike other conventional methods, decomposition theorems explore both amplitude and phase information and they are aimed at performing data interpretation based on sensible physical parameters such as the average target being invariant to changes in wave polarization basis.

There are two types of decomposition: coherent and incoherent. A disadvantage of coherent decompositions is that they do not consider the speckle noise effect which can distort the physical interpretation of coherent data. The coherent target decompositions are useful when only one dominant target component is expected and the other components are provided in support for constructing a suitable basis for the whole space of targets (Lee & Pottier, 2009). On the other hand, incoherent decomposition raises the issue of orthogonal spaces and considers the addition of coherency matrices, which implies the addition of power and no phase coherence between the elements. The orthogonal mechanisms can be separated as eigenvectors of the coherency matrix to solve the depolarisation problems (Cloude, 2009). Another method to exploit the eigenvalues and eigenvectors information is to consider the model-based decompositions such as the Freeman-Durden and Yamaguchi decompositions. The advantage of the model-based decomposition is that it is able to retrieve different scattering mechanisms without utilizing any ground truth measurements (Freeman et al., 1992; 1998; Yamaguchi et al., 2005; 2006). Yamaguchi decomposition is an improved version of the Freeman-Durden decomposition (Yamaguchi et al., 2005; 2006; Lee & Pottier, 2009) as it works under both reflection symmetry and non-reflection symmetry conditions. The details of the decomposition are discussed in the next section.

5.2.5 Yamaguchi Decomposition Model

One important alternative approach to incoherent decomposition is to fit physical models of scattering depolarisations to the polarimetric SAR observation to obtain the number and parameterization of each component (vanZyl, 1989; Freeman et al., 1998; Dong et al., 1998; Yamaguchi et al., 2005; 2006). The scattering model is used to describe the polarimetric backscatter from naturally occurring scatterers. The model in its simplest form involves a generic two-layer approach with a volume layer of particles above a non-penetrable surface. The total average backscatter is then determined from a 3 x3 coherency matrix composed of three main elements, without utilizing any ground truth measurements. The mechanisms in the Freeman-Durden decomposition model are

a canopy scatter from a cloud of randomly oriented dipoles, double-bounce scatter from a pair of orthogonal surfaces with different dielectric constants and Bragg scatter from a relatively smooth surface, in which the cross-polarized component is negligible (Yamaguchi et al., 2005). The scattering matrix S for Bragg surface is

$$S = \begin{bmatrix} \dfrac{\cos\theta - \sqrt{\varepsilon_r - \sin^2\theta}}{\cos\theta + \sqrt{\varepsilon_r - \sin^2\theta}} & 0 \\ 0 & \dfrac{(\varepsilon_r - 1)\{\sin^2\theta - \varepsilon_r(1 + \sin^2\theta)\}}{\left(\varepsilon_r \cos\theta + \sqrt{\varepsilon_r - \sin^2\theta}\right)^2} \end{bmatrix} \tag{5.22}$$

where θ is the local incidence angle and ε_r is the relative dielectric constant of the surface (Yamaguchi et al., 2005).

Although the three-component Freeman-Durden scattering power model can decompose SAR observations, there are two important assumptions that limit its applicability. The first assumption is that the application is restricted to a class of scattering problems and becomes invalid when we consider surface scattering with entropy different from zero (Lee & Pottier, 2009). The second assumption is that it only works under the reflection symmetry condition where $\langle S_{HH} S_{HV}^* \rangle = \langle S_{HV} S_{VV}^* \rangle = 0$. There is a possibility that the reflection symmetry condition does not hold (Yamaguchi et al., 2006). In order to accommodate the decomposition scheme for the more general scattering case encountered in complicated geometric scattering structures, Yamaguchi et al. introduced an additional term corresponding to non-reflection symmetric cases $\langle S_{HH} S_{HV}^* \rangle \neq 0$ and $\langle S_{HV} S_{VV}^* \rangle \neq 0$ (Lee & Pottier, 2009).

Yamaguchi (2006) also modified the volume scattering matrix in the decomposition according to the relative backscattering magnitudes of $\langle |S_{HH}|^2 \rangle$ versus $\langle |S_{VV}|^2 \rangle$. A cloud of randomly oriented dipoles is applied with a uniform probability

function for the orientation angles in the theoretical modelling of volume scattering. For vegetated areas where vertical structure appears to be rather dominant, the scattering from tree trunks and branches shows a nonuniform angle distribution. The proposed new probability distribution is given by

$$p(\theta)=\begin{cases}\frac{1}{2}\cos\theta, & for\ |\theta|<\frac{\pi}{2}\\ 0, & for\ |\theta|>\frac{\pi}{2}\end{cases} \tag{5.23}$$

where θ is the horizontal axis seen from the radar (Lee & Pottier, 2009).

Yamaguchi's four-component decomposition model (Cloude & Pottier, 1996; Yamaguchi et al., 2006) is used to decompose the coherency matrix, $[T]$ to proportions of volume, double bounce, surface and helix scattering mechanisms.

$$[T]=f_s\begin{bmatrix}1 & \beta^* & 0\\ \beta & |\beta|^2 & 0\\ 0 & 0 & 0\end{bmatrix}+f_d\begin{bmatrix}|\alpha|^2 & \alpha & 0\\ \alpha^* & 1 & 0\\ 0 & 0 & 0\end{bmatrix}+\frac{f_v}{4}\begin{bmatrix}2 & 0 & 0\\ 0 & 1 & 0\\ 0 & 0 & 1\end{bmatrix}+\frac{f_c}{2}\begin{bmatrix}0 & 0 & 0\\ 0 & 1 & \pm j\\ 0 & \pm j & 1\end{bmatrix} \tag{5.24}$$

where f_s, f_d, f_v and f_c are the expansion coefficients of surface, double, volume and helix scattering mechanisms, respectively (Yamaguchi et al., 2006). Detailed derivation of β and α can be found in the Yamaguchi et al. (2005; 2006). In this case, the coherency matrix and the construction is formed based on the mathematically orthogonal Pauli matrices to evaluate the second -order statistics of scattering matrix, S (Cloude & Pottier, 1996). The subscript H denotes horizontal polarisation and V denotes vertical polarisation.

After some derivations, the coefficients can be written as

$$f_v = 8\left\langle \left|S_{HV}\right|^2 \right\rangle - 4\,\mathrm{Im}\left\langle S_{HV}^{*}\left(S_{HH} - S_{VV}\right)\right\rangle \tag{5.25}$$

$$f_s = B \tag{5.26}$$

$$f_d = A - \frac{\left|C\right|^2}{B} \tag{5.27}$$

where

$$A = \frac{1}{2}\left\langle \left|S_{HH} - S_{VV}\right|^2 \right\rangle - 2\left\langle \left|S_{HV}\right|^2 \right\rangle \tag{5.28}$$

$$B = \frac{1}{2}\left\langle \left|S_{HH} + S_{VV}\right|^2 \right\rangle - 4\left\langle \left|S_{HV}\right|^2 \right\rangle + 2\left|\mathrm{Im}\left\langle S_{HV}^{*}\left(S_{HH} - S_{VV}\right)\right\rangle\right| \tag{5.29}$$

$$C = \frac{1}{2}\left\langle \left(S_{HH} + S_{VV}\right)\left(S_{HH} - S_{VV}\right)^{*} \right\rangle \tag{5.30}$$

Finally, the scattering powers P_s, P_d, P_v and P_c are determined by

$$P_s = f_s\left(1 + \left|\beta\right|^2\right) \tag{5.31}$$

$$P_d = f_d\left(1 + \left|\alpha\right|^2\right) \tag{5.32}$$

$$P_v = f_v \tag{5.33}$$

$$P_c = f_c \tag{5.34}$$

These components can then be used to examine the proportional contributions of different types of scattering and mapped across the observed scene. Even though the Yamaguchi decomposition is intended to apply to non-reflection symmetry case, the scheme automatically includes the reflection symmetry condition, thus proposing a decomposition scheme for the more general scattering case encountered in complicated geometric scattering structures (Lee & Pottier, 2009).

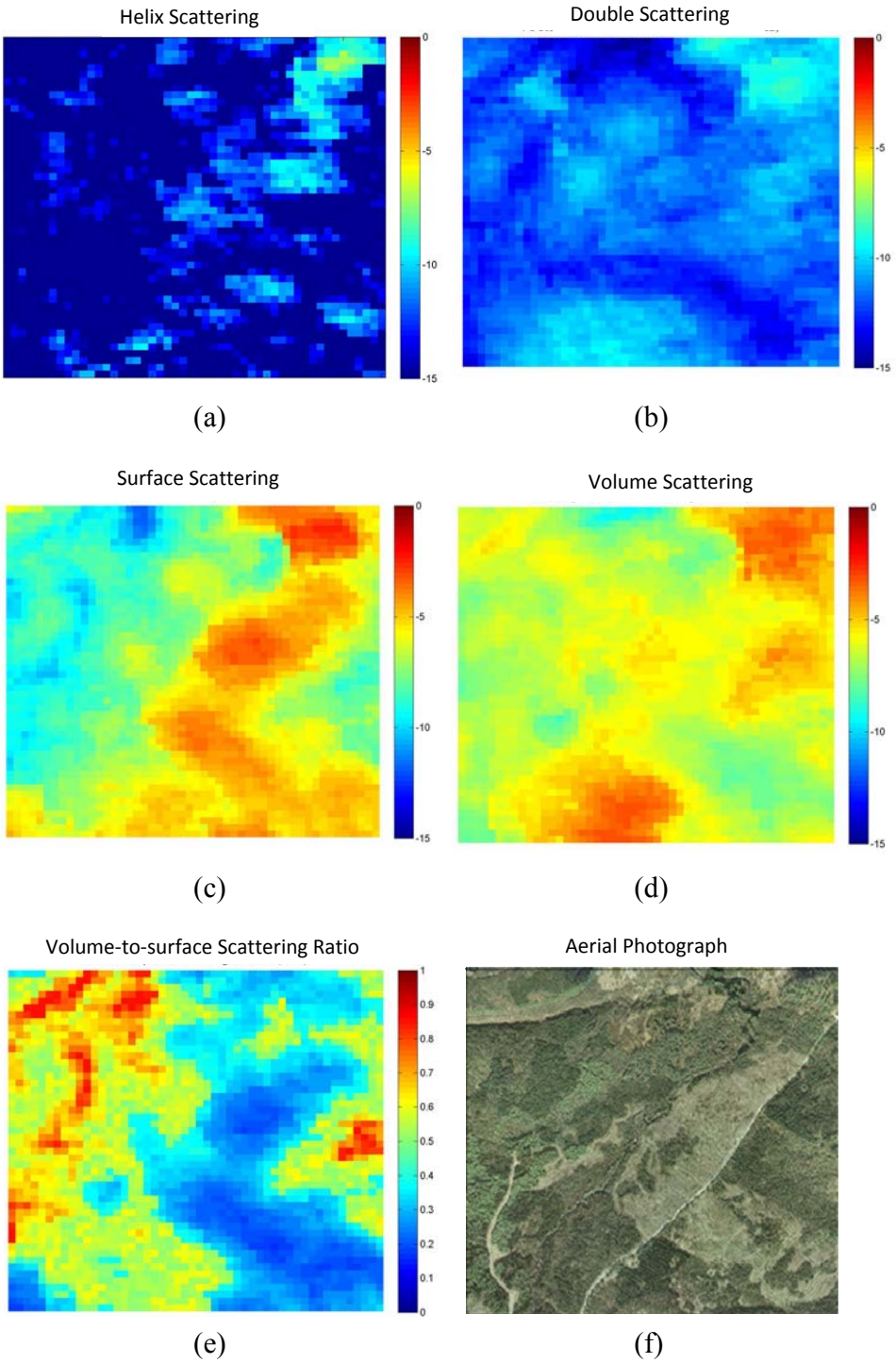

Figure 5.8. Scattering mechanisms decomposed using Yamaguchi model on ALOS PALSAR data with 1.5km for width and height (a) Helix scattering power (b) Double

bounce scattering power (c) Surface scattering power (d) Volume scattering power (e) Volume-to-surface scattering ratio(f) Aerial photograph of matching area

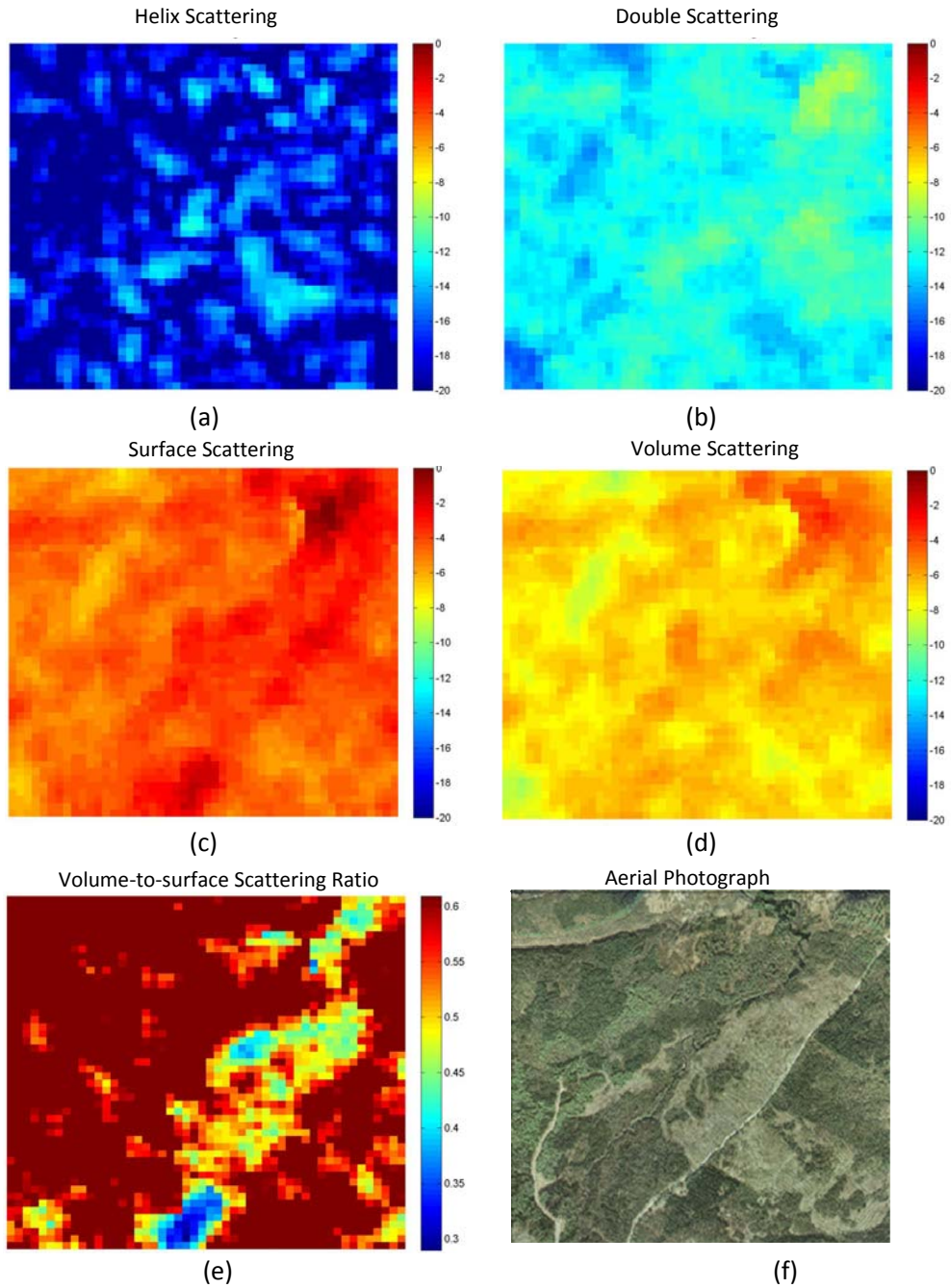

Figure 5.9. Scattering mechanisms decomposed using Yamaguchi model on TerraSAR-X data with 1.5km for width and height (a) Helix scattering power (b) Double bounce

scattering power (c) Surface scattering power (d) Volume scattering power (e) Volume-to-surface scattering ratio(f) Aerial photograph of matching area

Figure 5.8 and 5.9 show the four scattering mechanisms; helix, double bounce, surface, volume and volume-to-surface scattering power over the study area for ALOS PALSAR and TerraSAR-X data, respectively. It is shown that the helix scattering appears in the heterogeneous and sparse forest (Figure 5.8(a) and Figure 5.9(a)). These areas corresponds to the nonreflection symmetric case where $\left\langle S_{HH} S_{HV}^{*} \right\rangle \neq 0$ and $\left\langle S_{HV} S_{VV}^{*} \right\rangle \neq 0$. As depicted Figure 5.8 (b) and Figure 5.9(b), the double bounce scattering is believed to be relatively low compared to the volume and surface scattering values due to the nature of the landscape having varied topography, unlike forests on flat terrain which provide strong corner reflectors between vertical stems and horizontal ground. The expectation is that in areas of full cover forest, the volume scattering dominates over a surface scattering giving high ratio values. In sparse forest, the surface scattering dominates. The use of the ratio rather than the absolute amplitude term offers a more robust indicator of the physical structure as it removes the structural dependence in scattering from random media and variations in moisture content (Hellmann & Cloude, 2007; Neumann et al., 2010).

5.2.6 Regression Analysis

Regression analysis quantifies the relationship between dependent variable and one or more independent variables. Regression implies a cause and effect relationship in which a change in the value of an independent variable will result in an expected average change in the dependent variable. The quantitative relationship is expressed by an equation while the coefficient of determination (R^2) indicates the variation between the dependent and independent variables (Husch et al. 2003).

By making use of the two-layer approach of the volume-to-surface scattering, a relationship between the ratio and AGB obtained from over 170 fieldwork test sites is established. The strongest relationship was found between the ratio of volume to surface power scattering and AGB, using a sigmoid model, as this best fitted the backscatter data, accurately representing the loss of sensitivity at approximately 150 - 200 ton ha^{-1} (Figure 5.10).

The similar fitted model was used in the simple Water Cloud model (Attema & Ulaby, 1978), but the equation was chosen because it fitted the data better than any other relationship that was tested, rather than for theoretical reasons.

$$Vol / Surface = a + b\left[1 - e^{-c.AGB}\right] \tag{5.35}$$

In order to be used to create a AGB map as shown in Figure 5.12 , Equation 1 was rearranged to :

$$AGB = \frac{1}{c} \times -\ln\left[1 - \frac{Vol / Surface - a}{b}\right] \tag{5.36}$$

where a=0.36, b=0.54, and c=-0.01 with R^2=0.74 for ALOS PALSAR and a=0.45, b=0.26, and c=-0.02 with R^2=0.56 for TerraSAR-X.

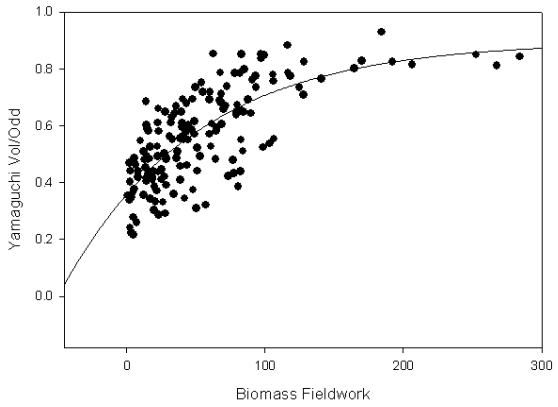

(a)

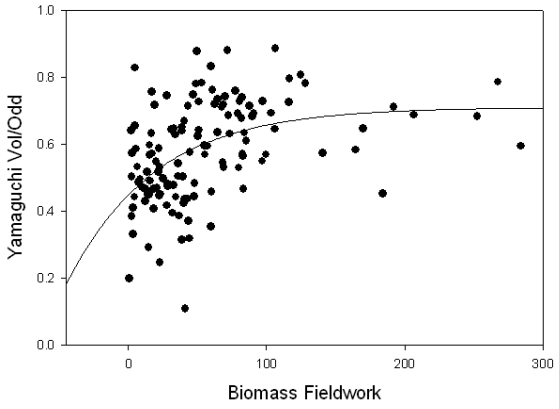

(b)

Figure 5.10. Regression relationship between the ratio of the volume and surface scattering powers and the field observed biomass, using data from (a) ALOS PALSAR, and (b) TerraSAR-X.

5.2.7 Result Validation

Airborne LiDAR data were acquired on 09 June 2007 while ALOS PALSAR fully polarimetric data were acquired on 17 April 2007 and 08 June 2009. The TerraSAR-X acquisitions are full polarimetric and they were carried out on 13 April 2010. The result of ALOS PALSAR acquired in 2007 was validated with airborne LiDAR data acquired on 09 June 2007 while ALOS PALSAR acquired in 2009 was compared with TerraSAR-X data acquired in 2010.

5.2.7.1 AGB Estimation Result Comparison: LiDAR and ALOS PALSAR

Biomass estimation using ALOS PALSAR and LiDAR are conducted in Glen Affric. The results are as shown in Figure 5.11. At the upper left corner of the image, the biomass is overestimated by ALOS PALSAR. This is possibly caused by tree stumps and dead trees, which are very common in the semi-natural forests like Glen Affric. Figure 5.12 show the examples of tree stumps appear in some areas of Glen Affric.

Aerial Photograph

(a)

Digital Elevation Model

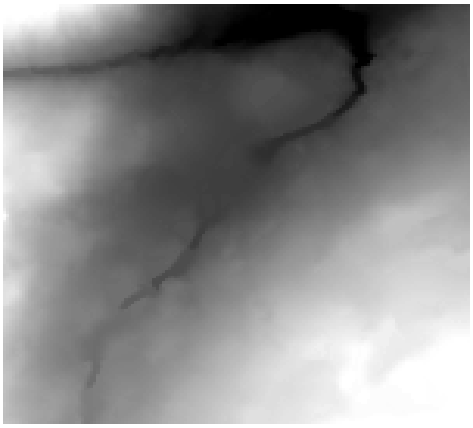

(b)

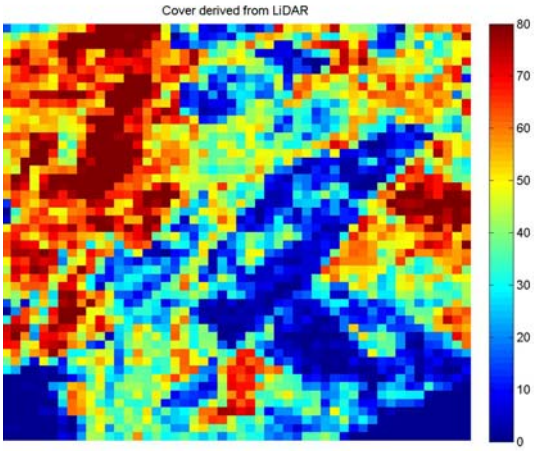

(c)

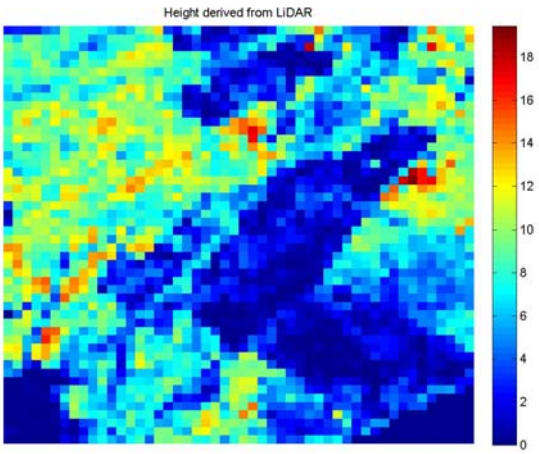

(d)

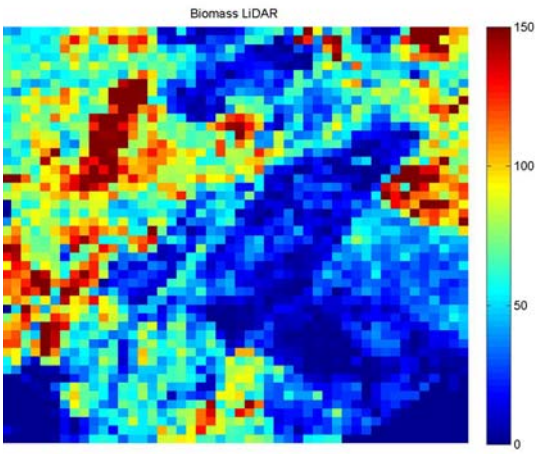

(e)

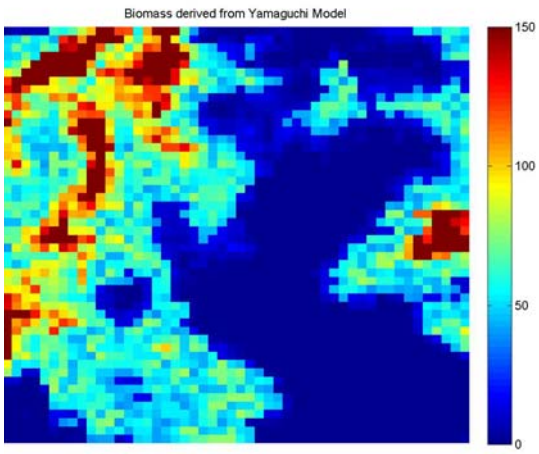

(f)

Figure 5.11 (a) Aerial photograph (b) Digital Elevation Model Model from Ordnance Survey DEM in the scale 1: 10000, under the projection British Grid, WGS84, Crown Copyright Ordnance Survey. An EDINA Digimap/JISC supplied service (c) Canopy cover (d) Height retrieved from CHM (e) AGB estimated using LiDAR acquired on 9 June 2007 (f) AGB estimation using ALOS PALSAR acquired on 17 April 2007

(a) (b)

(c) (d)

Figure 5.12. (a) Scots pine seedling beside a big pine stump in Glen Affric.
(b) Old tree stumps in bog woodland[2] in Glen Affric.
(c) The erosion of peat exposes the preserved stumps of ancient Scots pines.
(d) A healthy young Scots pine growing beside an old stump, as part forest regrowth to restore the Caledonian Forest in Glen Affric.
(Photos reference: http://www.treesforlife.org.uk/ilovepine/didyouknow_more.html)

In sparse forest, the above-ground biomass is underestimated by ALOS PALSAR. This is primarily due to the more open nature of individual crown structure and the heterogeneous open canopies environment. While we consider trees which are more than 2m high, the regression contributes some bias due to the volume scattering contributed by trees or vegetation with height less than 2m. The discrepancy in biomass estimates at

[2] Bog woodland is an area of peatland on which the high water table and shortage of nutrients restrict tree growth (Reference: http://www.treesforlife.org.uk/forest/ecological/bogwoodland.html).

the top right corner of the study area are likely due to shadow effects. The amount of missing coverage is dependent on the range of distribution of relief within the study area (Figure 5.11(b)).

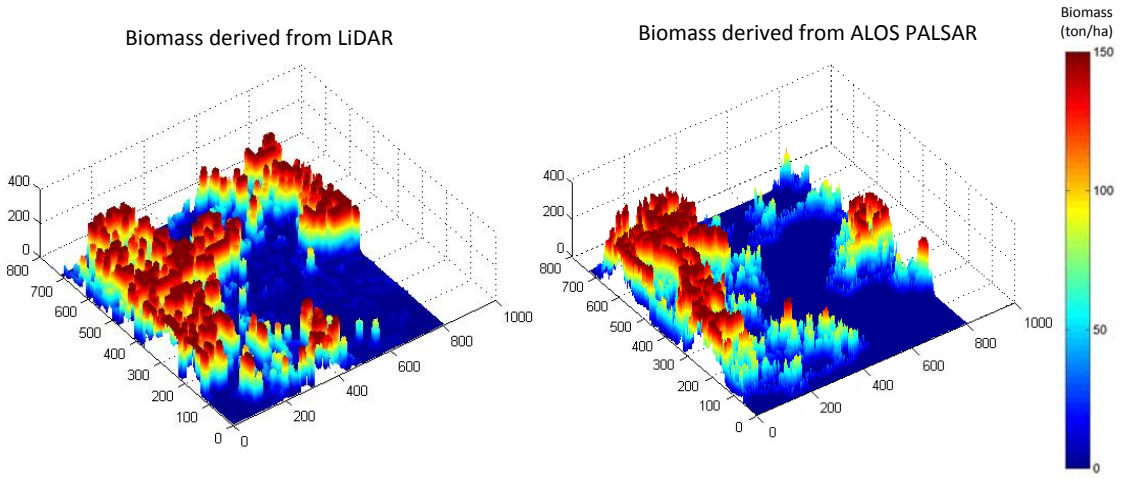

(a) (b)

Figure 5.13. 3-dimensional view of AGB estimated from (a) LiDAR and (b) ALOS PALSAR, (where the vertical dimension indicates the biomass estimate, not the height)

Figure 5.13 shows the 3-dimensional view of the AGB estimated using LiDAR and ALOS PALSAR. The total AGB derived from LiDAR and ALOS PALSAR over the test sites are 11,025 and 9,450 tonnes, respectively in the study area. Given the independent nature of the two approaches, it is an extremely encouraging result that the two results of total biomass for the area are within about 15%.

5.2.7.2 AGB Estimation Result Comparison: TerraSAR-X and ALOS PALSAR

Although TerraSAR-X data is less sensitive to azimuth slope variations because of its short wavelength, it is sensitive to small scatterers, hence produces smaller range of biomass compared to ALOS PALSAR data. Figure 5.14 shows the AGB estimated using TerraSAR-X and ALOS PALSAR.

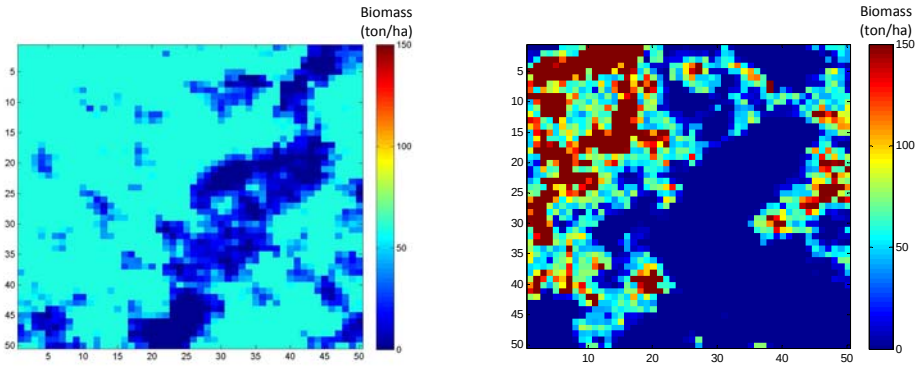

(a) (b)

Figure 5.14. AGB estimated using the proposed method for (a) TerraSAR-X (acquired on 13 April 2010) and (b) ALOS PALSAR (acquired on 08 June 2009)

It is clearly shown that the X band data is able to detect short vegetation in sparse forest region where they are less obvious in the L-band data. Due to the early AGB saturation, the AGB estimation using TerraSAR-X in the forest areas is underestimated.

The research is extended to map the biomass for the whole Glen Affric using TerrraSAR-X and ALOS PALSAR. Figure 5.15 and Figure 5.16 illustrates the biomass estimation using TerraSAR-X and ALOS PALSAR, respectively. Judging from the result, there is an obvious discrimination between the forest and non-forest areas where most of the forested areas achieved biomass values of 60 ton/ha. Biomass map using ALOS PALSAR, however, is able to separate between sparse and dense forest but with a saturation level at 150ton/ha. When compared with the fieldwork data, the R^2 and RMSE obtained for TerraSAR-X are 0.41 and 28.5 ton/ha, respectively while for ALOS PALSAR data are 0.70 and 23.6 ton/ha, respectively.

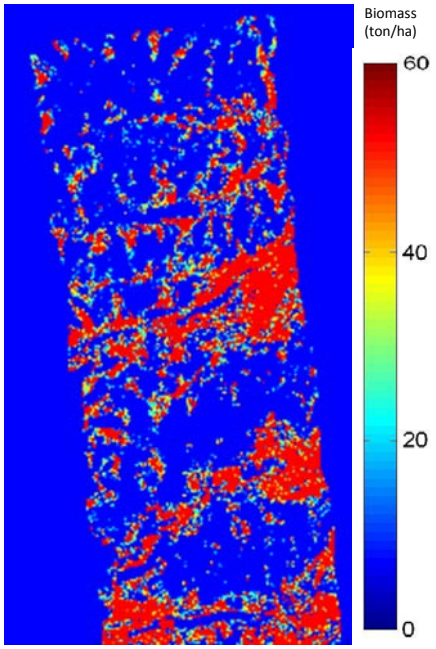

Figure 5.15. AGB estimated using TerraSAR-X (acquired on 13 April 2010)

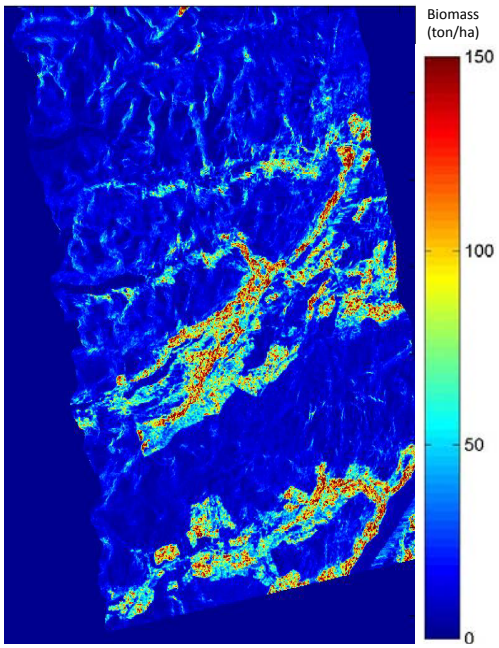

Figure 5.16. Biomass estimated using ALOS PALSAR (acquired on 08 June 2009)

5.2.8 Plot-Level Results Validation

A field transect was taken in dense and sparse forests during the fieldwork measurement. Each transect was divided into several 10m width sub-transects. Since the field transects contain similar lengths of field data and are located adjacent to each other, two sub-transects are used for both dense and sparse forests throughout the chapter. Furthermore, plot-level estimation is computationally heavier compared to area-based approach. As the profiles were taken in the range direction of ALOS PALSAR data, the effects of layover and shadowing will be apparent within the sub-transect. Not only were the tree profile drawn to demonstrate the woodland physical characteristics, but also volume-to-surface scattering ratio were investigated in ground distance along the transects for dense (Figure 5.17 and Figure 5.18) and sparse (Figure 5.19 and Figure 5.20) forests. Moving averages of biomass carbon were calculated using a window size of 20m in length for each 10m width sub-transect and a step size of 1m. The window is continuously moved 1m along the sub-transect and the average biomass carbon value is plotted against the centre position of the moving window. Note that biomass carbon makes up around half of the total biomass and all the figures show carbon content.

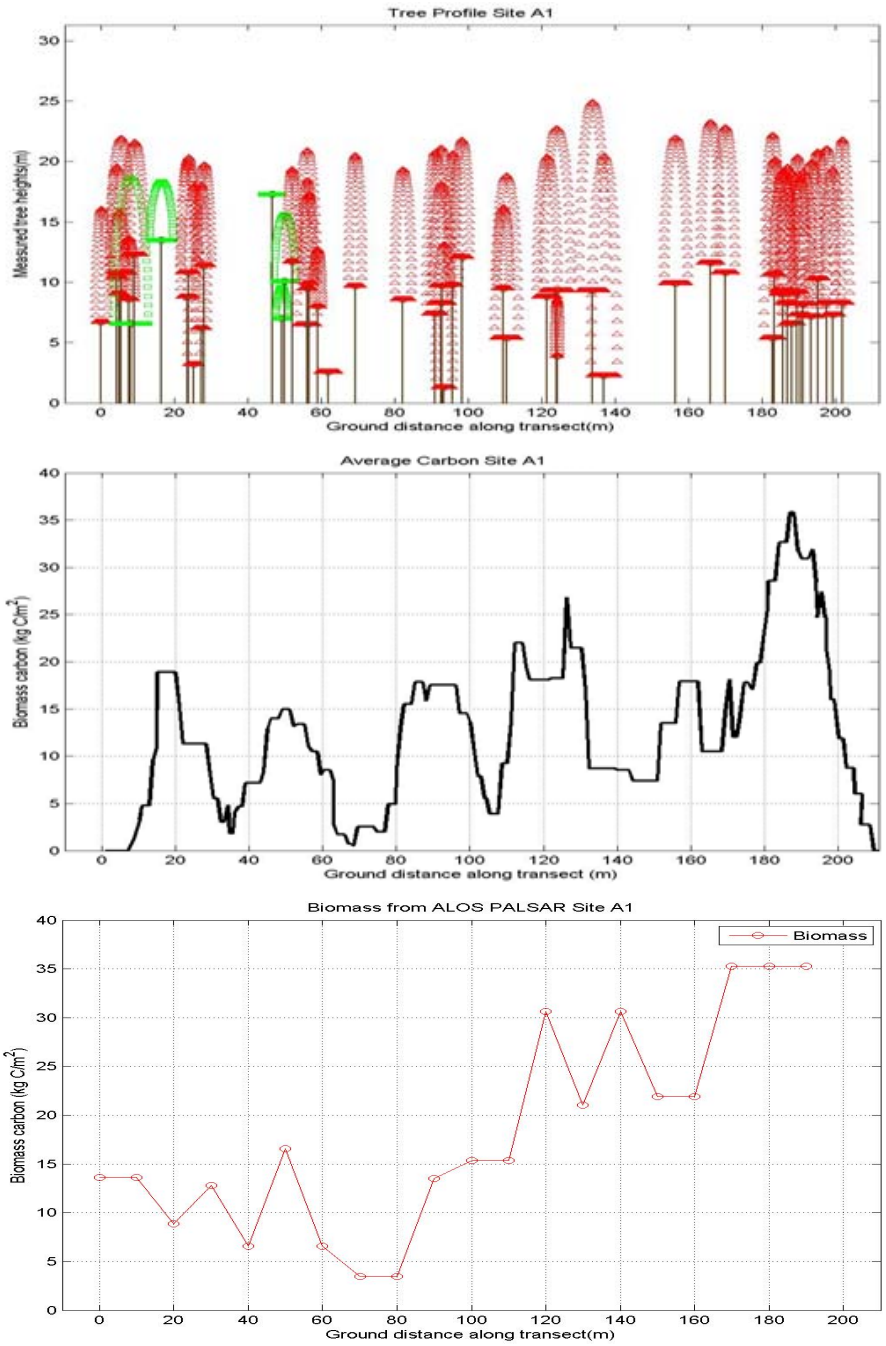

Figure 5.17. Profiles of Dense Forest (top) Tree profile for Profile 1, where the green trees represent the Scots pine species and red trees represent the Sitka spruce species (middle) Average field carbon for Profile 1, (bottom) Average estimated carbon for Profile 1

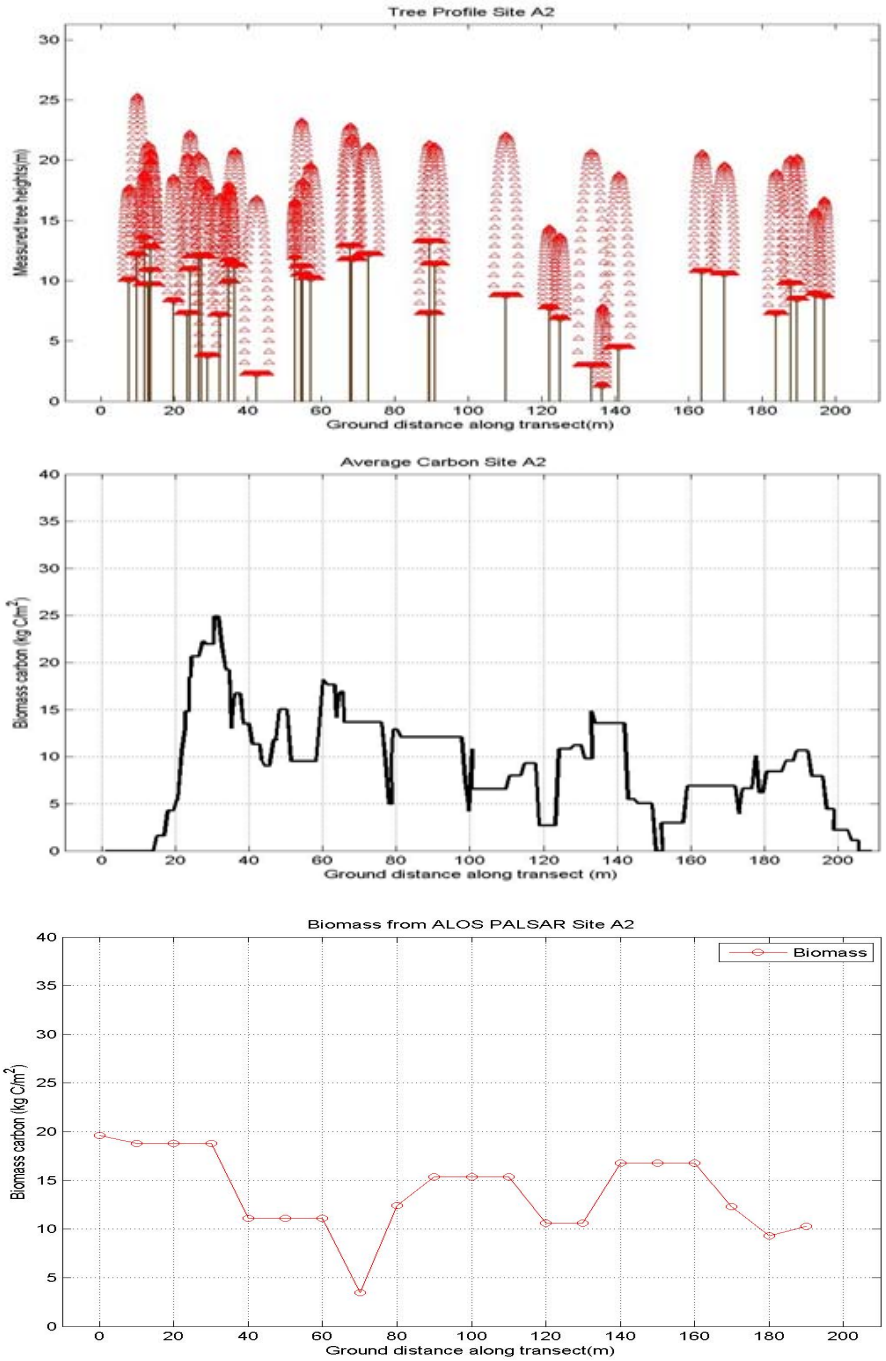

Figure 5.18. Profiles of Dense Forest (top) Tree profile for Profile 2, where the green trees represent the Scots pine species and red trees represent the Sitka spruce species (middle) Average field carbon for Profile 2, (bottom) Average estimated carbon for Profile 2

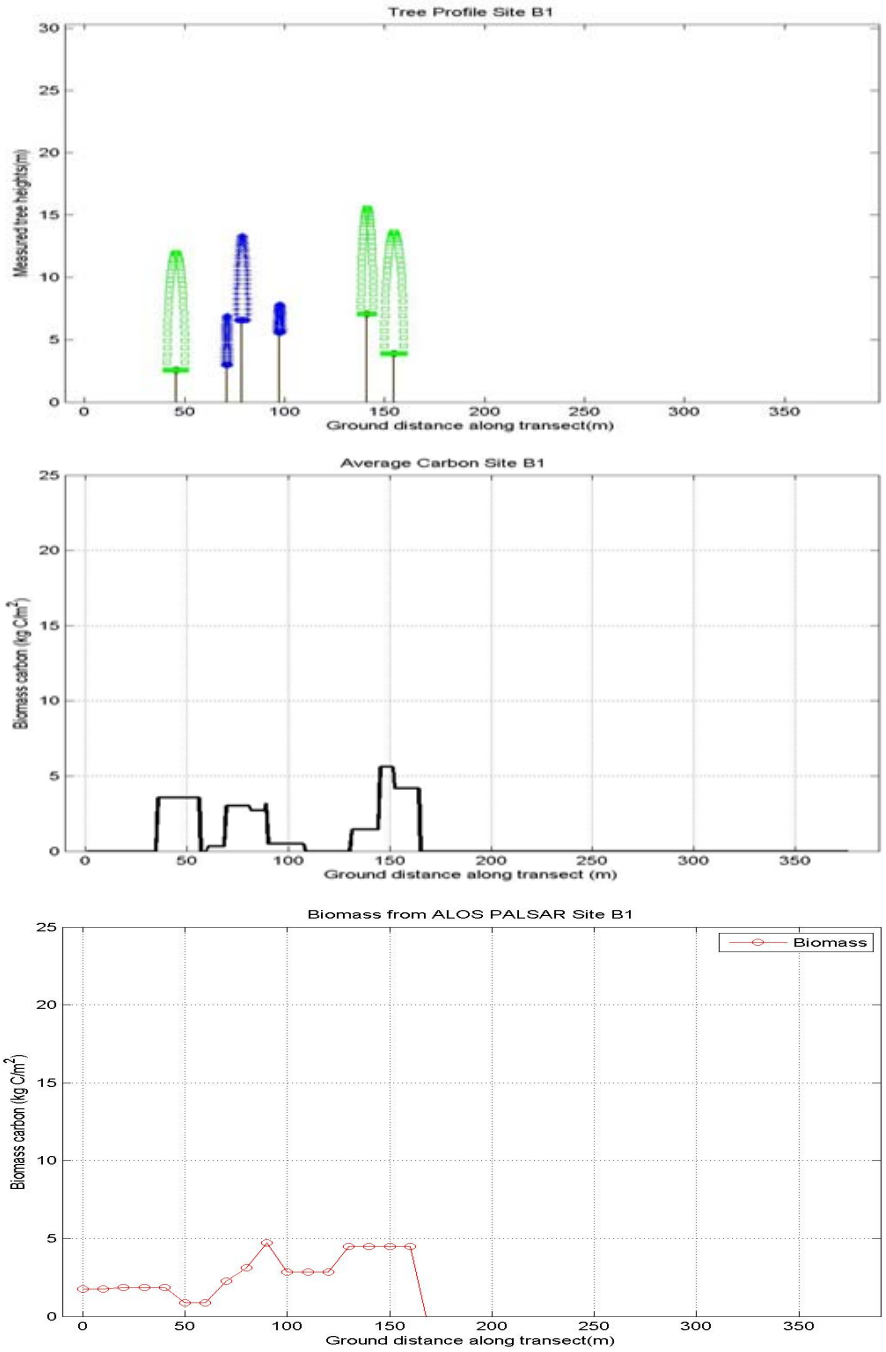

Figure 5.19. Profiles of Sparse Forest (top) Tree profile for Profile 1 where the green trees represent the Scots pine species and blue trees represent the Birch species, (middle) Average field carbon for Profile 1, (bottom) Average estimated carbon for Profile 1

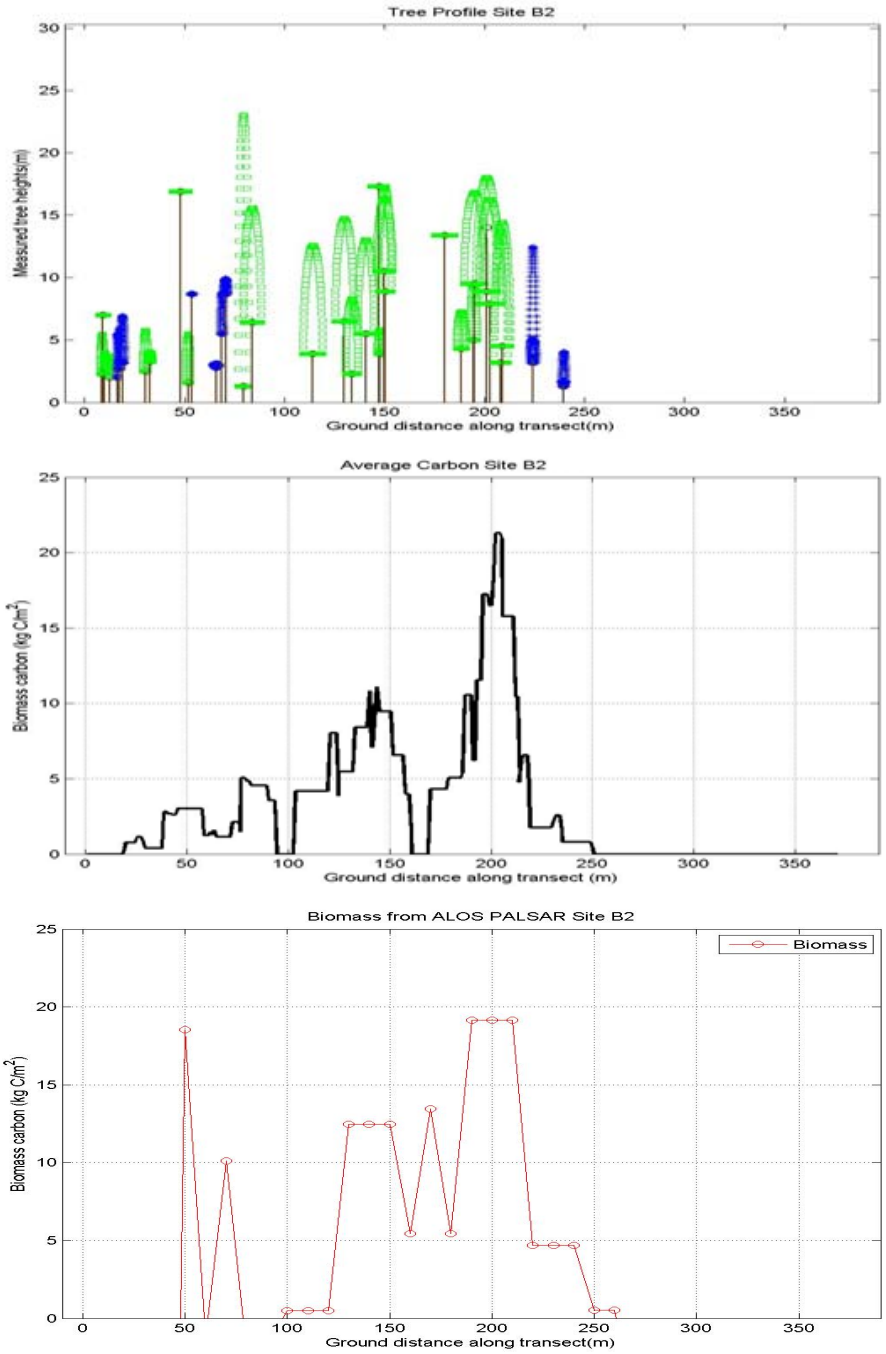

Figure 5.20. Profiles of Sparse Forest (top) Tree profile for Profile 2 where the green trees represent the Scots pine species and blue trees represent the Birch species, (middle) Average field carbon for Profile 2, (bottom) Average estimated carbon for Profile 2

Due to the saturation limitation of backscatter, the increase of AGB does not necessarily show an increase of backscatter. Interestingly, the volume-to-surface scattering was found to correlate well to AGB at plot-level. Using the regression equation, we estimated the AGB for both the dense and sparse forests. Biomass was computed for the field data as biomass carbon (in kg C/m^2) using allometric equations discussed. Overall, the biomass carbon is comparable with the fieldwork biomass in both forests.

5.3 Uncertainties of AGB Estimation Using SAR

Despite the large number of studies of biomass estimation, the levels of uncertainty[3] in the estimation using SAR have not been thoroughly investigated empirically. Most studies used the standard error of the regression equation as a measure of uncertainty, which yields errors in the order of 10 to 20 ton/ha. Harrell et al. (1997) and Ustin et al. (2004) demonstrated that the uncertainty can be in the range of 50 to 80 ton/ha. In the forest ecosystem where there are multiple tree species at various height and density, the uncertainties are greater in landscape (Kasischke et al. 1997). On this basis, data calibration is essential to quantify the pattern of biomass distribution using a fieldwork sampling approach. A generalised equation may not adequately represent the whole forest. Therefore, more fieldwork needs to be conducted at smaller scale to improve the accuracy of biomass estimation.

The saturation of SAR backscatter to forest biomass is a distinct limitation of radar as a tool for forest biomass mapping. The sensitivity of the radar response deteriorates as the biomass increases and this poses a problem in full forest where the biomass exceeds 150-200 ton/ha in ALOS PALSAR data.

---

[3] Uncertainty is defined as "lack of knowledge of the true value of a variable that can be described as a probability density function" (IPCC,2006).

Previous research (Brown et al., 1995, 1997, Houghton et al., 2001, Chave et al.,2004) investigated the source of error and concluded that the factors include tree level error, allometric model, plot positioning, fieldwork measurement and geocoding error. Estimation error introduced in choosing a suitable allometric model can be reduced by using average wood density as a site specific-parameter and should be calibrated (Ketterings et al., 2001).

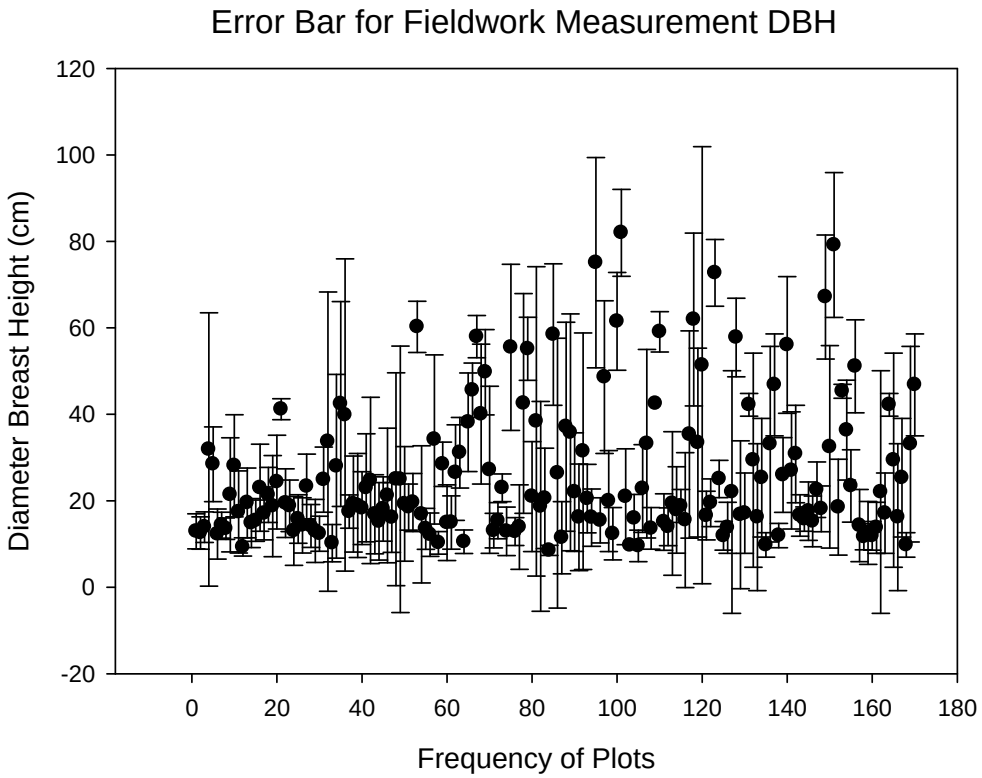

Figure 5.21. Error bars for diameter breast height measurement over 170 plots. It shows the mean and standard deviation of the plots and the overall RMSE is calculated by averaging the standard deviations of all the plots.

The selection of fieldwork plots and trees within plots also constitute uncertainty in the AGB estimate. The size of the sampling error is influenced by the sampling scheme, size, estimation methodology and inherent variability of the variable of interest (Cunia, 1986a, Cunia, 1986b). Measurement errors can be due to various factors such as

instrument error, recording error, inconsistent measurement technique and error due to the nature of the object. Since only the average tree dbh values and the total number of trees occurring in each plot were collected in the fieldwork measurement, it is not unlikely that the actual biomass at fine scale will differ from the averaged value and in this case, the overall RMSE obtained from the fieldwork measurement over 170 plots is 11.36cm, giving rise of 34.3 kg/tree. (Figure 5.21).

The choice of allometric model that describes the relationship of AGB and tree variables can also introduce a significant source of error in the AGB estimation. Several allometric equations of different tree species can be found in the literature (Aboal, 2005; Araujo, 1999; Arevalo, 2007; Brown, 1997; Cole and Ewel, 2006; de Gier, 1989, 1999, 2003; Ketterings et al., 2001; Overman et al., 1994; Zianis et al., 2005; Cunia, 1986b; Jenkins, 2003; Chave et al., 2004). One would obtain different results when different allometric models are used for the same dataset.

Considering other species exist in the study area such as shown in Table 3.1, the extreme case of error in the biomass estimation turns out to be 16.8%. Each biomass was computed allometrically by assuming all the trees are of one specific species. The average biomass for all the plots was compared among the species. Birch species turned out to be the extreme case of error and this is possibly due to the stiff hardwood as opposed to softwood Scots pine. Since Scots pine is the dominant species in Glen Affric, the possibility of the case to occur is even less likely. Scaling up from plot-level AGB estimates to regional AGB estimates often has low accuracy due to local variability in forest cover and density (Houghton et al., 2001; 2005).

5.4 Chapter Summary

In this chapter, the potential of ALOS PALSAR and TerraSAR-X was assessed to estimate biomass. Most commonly, the SAR backscatter coefficient is exploited in the above-ground biomass estimation (Hussin et al., 1991; Dobson et al., 1992; Le Toan et

al., 1992; Kasischke, 1992, 1994; Ranson and Sun, 1994; Wang et. al., 1995; Leckie and Ranson, 1998; Frank Rosillo-Catlle et al., 2007). However, due to the mountainous terrain in Glen Affric, azimuth slope compensation was carried out and the results showed significant reduction in T23 and T33 components.

The volume-to-surface scattering ratio was found to be best regressed with the AGB where the increase of the ratio was found to correspond to the increase of AGB in both dense and sparse forests. The magnitude of the full polarimetric total backscattered signal was not necessarily a descriptive and unique observation, but rather it was the contributions from multiple scattering mechanisms that provided more insight into the specific physical scattering process (Moghaddam & Saatchi, 1995). The increase of volume-to-surface scattering ratio was also found to correspond to the increase of AGB. Polarimetric decomposition approaches to biomass estimation are advantageous because they are less sensitive to variations in overall site conditions that can influence the total backscatter contributions (Hajnsek et al.,2000; Freeman, 2007).

When comparing TerraSAR-X accuracy to the ALOS PALSAR accuracy, biomass estimation was better with ALOS PALSAR, as expected. The sensitivity of the ALOS PALSAR and TerraSAR-X backscatter signals towards the biomass are also limited to less than 150ton/ha and 60ton/ha, respectively. While airborne LiDAR data allows detailed investigation into the relationship between height, number density and above-ground biomass, it's constrained to small coverage area. ALOS PALSAR, on the other hand, can cover big coverage area but it provides a lower resolution, hence, lower estimation accuracy. These results give some indication of when to use LiDAR or SAR to retrieve forest AGB. In general, biomass estimates are broadly comparable, but variations due to ground topography and spatial resolution are apparent at the sub-site scale.

Chapter 6

Conclusions and Recommendations

6.1 Introduction

The main goal of this thesis is to evaluate and compare the estimation of above-ground biomass (AGB) in Glen Affric using LiDAR and SAR data. The emphasis was on understanding the value of satellite SAR data for AGB using airborne LiDAR as a high-resolution comparative dataset. Correlation analysis was used to assess the relationship between field measured AGB and radar backscatter extracted from ALOS PALSAR and TerraSAR-X. Establishment of relationship between the AGB and the Yamaguchi decomposed parameters of radar backscatter was conducted to estimate the AGB. Through these approaches of AGB estimation, the research questions defined in Section 1.2 were properly answered. They are reproduced in the Section 6.2 as a point of reference for discussion of the research. This is followed by future work and recommendation (Section 6.3).

6.2 Research Questions

How strong is the relationship between the SAR backscattering coefficient and AGB in Glen Affric?

The SAR backscatter coefficient is exploited for the AGB estimation (Hussin et al., 1991; Dobson et al., 1992; Le Toan et al., 1992; Kasischke, 1992, 1994; Ranson and Sun, 1994; Wang et. al., 1995; Leckie and Ranson, 1998; Frank Rosillo-Catlle et al., 2007). Cross-polarization information of L and P bands have yielded good indicators to AGB distribution and they are proven to be determined by woodland characteristics, including tree height, canopy cover, basal area and stem density (LeToan et al., 1992; Ranson and Sun, 1994; Ferrazzoli and Guerriero, 1995; Imhoff, 1995, Kasischke et al., 1997; Kellndorfer et al., 2003; Woodhouse, 2006). However, analysis of backscatter-biomass relationship demonstrates that the backscatter do not have strong correlation with AGB in Glen Affric. The most significant correlation with AGB is the cross-polarization backscatter at L-band and this can be ascribed to the R^2 of 0.36. This low correlation is attributed to the fact that mountainous terrain influences the backscatter and radar backscatter saturates when the biomass increases. This makes the assessment of forest biomass in areas of mixed forest and varied topography much more challenging. The variations in the saturation level is determined by the experimental conditions and the forest characteristics such as dominant species, stem number density and canopy structure (Le Toan et al., 2004; Woodhouse, 2006). The result of the analysis show that in mountainous, heterogeneous forest areas like Glen Affric the assessment of AGB estimation is not straightforward by making use of the radar backscatter alone.

How correlated is the decomposed ratio of volume and surface scattering mechanisms with AGB?

The Yamaguchi decomposition method was applied on both ALOS PALSAR and TerraSAR-X data. Comparing the results with fieldwork data, the AGB estimated using the proposed method had a linear R^2 value of 0.70 and 0.41 for ALOS PALSAR and TerraSAR-X data, respectively. In parts of the image, the biomass is overestimated by ALOS PALSAR. This is possibly caused by tree stumps and dead trees which are very common in the semi-natural forest like Glen Affric. In sparse forest, the above-ground biomass is underestimated by ALOS PALSAR. This is primarily due to the more open

nature of individual crown structure and the heterogeneous open canopies environment. While we consider trees which are more than 2m high, the regression contributes some bias due to the volume scattering contributed by trees or vegetation with height less than 2m. The discrepancy in biomass estimates at the top right corner of the study area are likely due to topographic effects since even with slope correction, the larger the slope, the greater the likelihood of error in the SAR estimation. While X-band is less sensitive to azimuth slope variations because of its short wavelength, it is more sensitive to small scatterers, hence produces smaller range of volume-to-surface ratio compared to L-band. Due to the early AGB saturation, the AGB estimation using TerraSAR-X in the forest areas is underestimated. TerraSAR-X data is nevertheless useful in detecting short vegetation in sparse forest region where they are less obvious in the ALOS PALSAR data. Bearing in mind the sparse and heterogeneous nature of woodlands in Glen Affric, this correlations showed good improvement in the AGB estimation.

How is the AGB estimation at plot-level for ALOS PALSAR?

The ratio of volume and surface scattering indicated good correlation with field AGB. The results showed that the ratio provide an overview of the spatial distribution of woody AGB at plot-level. Overall, the biomass carbon is comparable with the fieldwork AGB in both sparse and dense forests.

How is the comparison of AGB estimation between SAR and LiDAR in environments like Glen Affric?

In this thesis, the accuracy of AGB estimation using ALOS PALSAR is 70% with RMSE of 23.6 ton/ha while accuracy using TerraSAR-X is 41% with RMSE of 28.5 ton/ha. The saturation limits of ALOS PALSAR and TerraSAR-X are 150 ton/ha and 60 ton/ha. Due to the early saturation. TerraSAR-X suffers more underestimation compared to ALOS PALSAR.

Overall, LiDAR is able to estimate AGB with good accuracy and the R^2 value obtained is 0.97 with RMSE of 14.81 ton/ha. In the case where the AGB measured from fieldwork is less than 100 ton/ha, the AGB is slightly overestimated by LiDAR while the AGB is underestimated in high-density forest. The high RMSE deviation can be interpreted to be indicative of the heterogeneity of the forest. The variability of the height range gives rise to a higher deviation which relates to higher error in the estimation.

Finding an optimum data for AGB estimation to achieve high accuracy but low operational cost is a big challenge for the remote sensing community. When comparing TerraSAR-X accuracy to the ALOS PALSAR accuracy, ALOS PALSAR showed a superior result. While airborne LiDAR data has very accurate height measurement and provides three-dimensional (3D) stand profiles which allows investigation into the relationship between height, number density and AGB, it is limited to small area coverage, or large areas but at large cost. ALOS PALSAR, on the other hand, can cover large areas but it provide a lower resolution, hence, lower estimation accuracy. These results give some indication of when to use LiDAR or SAR to retrieve forest AGB. However, it is noted that no single sensor is expected to provide consistently infallible AGB estimation under any circumstances of forests.

6.3 Future Work and Recommendations

Based on the findings of this research, there still exist some potential work deserving further research to improve the proposed method for AGB estimation. Due to the underlying topography relief and side-looking viewing geometry, the remote sensing data collected suffer geometric distortions such as layover and shadow. Scattering signals from these distortions are considered as missing coverage as they do not contain information about the terrain. Fusion of the SAR data with ascending and descending configuration is recommended for future work to retrieve terrain information from the opposite viewing geometry.

The exploitation of SAR images is still challenging due to the tricky data processing and imaging geometries. Having said that, owing to the high temporal repeatability under all weather condition, high-resolution satellite SAR data may play a key role in regional forest mapping. One promising alternative may be the use of SAR images for monitoring forest inventories performed with help of low-pulse ALS data. TerraSAR-X/TanDEM-X Single-pass SAR interferometery seems to be a very encouraging mission to provide useful information of the stand height with wide area coverage (Holopainen et al., 2010). This could provide a step towards mapping AGB regionally. The combination of polarimetric and interferometric information is anticipated to improve the accuracy of AGB estimation when compared to the use of SAR backscatter intensity only.

Ultimately, the scientific community is looking for ways to use remote sensing data to estimate forest AGB and to prove if such approach is even possible. The fact that these results show good relationships between volume-to-surface scattering ratio and AGB, tends to be very encouraging. However, due to saturation limit, the direct measures of AGB are not possible above the saturation level. The saturation issue may not apply to all forests, especially in savannas, most of the boreal forests and a large part of the temperate forests (GCOS, 2003; IGOS, 2004). Some relative information about crown structure and height may be derived to aid the AGB mapping. The possibility of using longer wavelength such as P-band and smaller incidence angles should also be explored to improve the saturation level. Another very promising technique is the combination use of GeoSAR observation with PALSAR data and natural sequestration modelling (Wiliams et al., 2009).

It should be noted that the technique is unlikely to work as well in deciduous trees, since the tree delineation algorithm relies on the fact that the trees have only one well-defined local maxima, which might not always be true for deciduous trees species. Further work is needed to develop a robust tree delineation technique that suits other forest types.

Large footprint LiDAR can also be considered as future work to map biomass over large geographic areas. Due to the cost incurred in small footprint LiDAR acquisition missions and the availability of spaceborne large footprint LiDAR, investigation to sample strategies to statistically represent different ecozones should be considered.

For a more comprehensive picture of the total biomass in a stand, below ground biomass should be also considered. This is because the amount and patterns of vertical variability of below-ground AGB are still much less known. While below-ground biomass stores a large portion of total carbon stocks (at least about 20%)(Sarmiento et al., 2005), it is rarely measured because it can only be assessed through *in-situ* measurements that is labor- and time-consuming. (GCOS, 2003).

Owing to the fact that the national inventories differ in standards and quality for many countries and because the detailed information available at national level is normally unavailable internationally, there are uncertainties in quantifying the biomass. The lack of a global standard definition for forest cover makes it challenging to create global forest maps. Further development and integration of SAR and optical data should be pursued seriously to define validated standards and standard biomass data products for mapping over wide geographic areas. Current different methodologies for data collection, analysis of forest biomass inventories and uncertainty assessment should be harmonized.

In this thesis, the biomass distribution has been mapped in Glen Affric. However, the need to comprehend not only the patterns of biomass distribution, but also changes in biomass over time is crucial (Houghton et al., 2001). All of the results compared in this study treat biomass as a static, rather than a dynamic property of ecosystems. In fact, biomass is continually changing as a result of natural or human-induced disturbances

and recovery. A more accurate biomass conception is to consider its dynamic nature by conducting multi-temporal studies of biomass.

This thesis evaluates the capability of Earth Observation data such as ALOS PALSAR, TerraSAR-X and LiDAR to estimate the AGB of heterogeneous and hilly forest in Glen Affric. Because there is a considerable amount of global forest located on hilly and mountainous region, the results of this research are expected to have an impact on carbon accounting under Kyoto Protocol and possible future forest monitoring under REDD. It is also anticipated to have implications for future Earth Observation sensors (see Table AI.1 outlined in Appendix I) for the purpose of global AGB estimation.

Appendix I

Available and Future Forest Mapping Sensors

Table AI.1. Available and Expected Sensors Relevant to Forest Mapping (Fagan & DeFries, 2009)

Sensor	Launch Date	Source	Spectrum	Resolution, Return Interval	Image Width
WorldView-2	2009	Comm. (USA)	VNIR, 9 bands	1.8m (1.5m pan), 1-4 days	16.4km
ARGO (RapidEye-6)	2009	Taiwan/ Germany	VNIR, 5 bands	5m daily	78km
RazakSat	2009	Malaysia	VNIR, 5 bands	5m (2.5pan)	20km
DubaiSat	2009	UAE	VNIR, 5 bands	5m (2.5pan)	20km
ALSAT-2A, 2B	2009	Algeria	VNIR, 5 bands	10m (2.5pan)	17km
EROS-C	2009	Israel	VNIR	2.8m (0.7pan)	11km
TanDEM-X	2009	Comm. (Germany)	SAR-X band, quad-polar	1-18m x 1-18m, 2-5-11days	10-100km x 5-150km

Resorcesat-2 (ISRO)	2009	India	VSWIR, 4 bands	23.5m, 24 days	141km x 141km
RASAT (Tubitak)	2009	Turkey	visible, 4 bands	15m (7.5m pan)	30km x 30km
NigeriaSat-2 (NASRDA)	2009	Nigeria	VNIR, 4 & 5 bands	5m (2.5 pan) & 32m	20km & 300km
COSMO-SkyMed 4 (ASI/MiD)	2009	Italy	SAR-X band, quad-polar	3-30m	10-200km x 100-200km
Meteor-M N1 (Roshydromet/Roscosmos)	2009	Russia	1) SAR, X-band, VV polarised. 2)VTIR, 6 bands. 3)VNIR, 3-6 bands	1) 400-1000m 2) 1000m 3) 60-120m	1) 450-1000m 2) 1000m 3) 60-120m
Meteor-M N2 (Roshydromet/Roscosmos)	2009	Russia	1) SAR, X-band, VV polarised. 2)VTIR, 6 bands. 3)VNIR, 3-6 bands	1) 400-1000m 2) 1000m 3) 60-120m	1) 450-1000m 2) 1000m 3) 60-120m
Kanopus-V N1 (Roshydromet/Roscosmos)	2009	Russia	VNIR	10.5-26m (2.1 pan) TBD	250km
Sich-2	2009	Ukraine	VNIR, 4 bands	7.8m	46.6km
RISAT-1	2009	India	SAR, C-band, quad-polar	3-40m	30-240km
HJ-1C(S-band SAR)	2009	China	SAR, S-band	20m	100km
Svea	2010	Sweden	TBD, passive high resolution	1.2-1.5m	8-12km
Pleiades 1 (CNES)	2010	France	VNIR, 5 bands	0.7m	20km x 20km
TES-HYS (ISRO)	2010	India	VSWIR, 200 bands	15m	30km x 30km
GISAT (ISRO)	2010	India	VTIR, 3, 4 & 150 bands	1.5km, 50m & 192-320m	

SARE-1 (CONAE)	2010	Argentina	SAR		
SAC-D (CONAE/NASA)	2010	Argentina/USA	TIR, 3 bands	350m	182-1000km
HY-1C (NSOAS/CAST)	2010	China	VTIR, 4 & 10 bands	250m & 1.1km	500km & 3083km
NPP (NASA/NOAA/DoD)	2010	USA	VTIR, 22 bands	400m - 1.6km	3000km
VENµS (CNES/ISA)	2010	Israel/France	VNIR, 12 bands	5.3m	27km
CBERS-3 (CRESDA/NPE)	2010	Brazil/China	1) NIR, 4 bands 2) NIR, 4 bands 3) VTIR, 4 bands 4) VSWIR, 4 bands	1) 20m 2) 10m (5 pan), 3-26 days 3) 40-80m, 26 days 4) 73m, 5 days	1) 120m, 2) 60km, 3)120km, 4)866km
HY-1D (NSOAS/CAST)	2010	China	visible, 4 bands	250m	500km
FY-3D (NRSCC/CMA)	2010	China	VSWIR, 20 bands; VTIR, 10 bands	250m & 1km & 1.1km	2800km
Elektro-L N2 (Roshydromet/Roscosmos)	2010	Russia	VTIR, 10 bands	1km visible 4 km 1R, daily	Full Earth disc imaged
Meteor-M N3 (Roshydromet/Roscosmos)	2010	Russia	1) SAR, X-band 2)Visible, 1 band	1)200-1000m 2)700-1400m	1) 450-600km 2) 2-2600km
SSOT	2010	Chile	VNIR, 5 bands	5.8m (1.45 pan)	
Kompsat-3	2010	South Korea	VNIR, 5 bands	2.8m (0.7m pan)	
Kompsat-5	2011	South Korea	SAR, X-band		
GeoEye-2	2011	Comm. (USA)	VNIR	1.65m, (0.25 pan)	
SAOCOM 1A (CONAE/ASI)	2011	Argentina/Italy	SAR, L-band	10-100m	40-320km
ASNARO	2011	Japan	passive high resolution	1m	
CARTOSAT-3 (ISRO)	2011	India	visible, 1 band (pan)	0.3m	6km
MetOp-B (EUMETSAT)	2011	EU	VTIR, 6 bands	1.1km, twice daily	3000km

Pleiades 2 (CNES)	2011	France	VNIR, 5 bands	0.7m	20km
DMSAR (ISRO)	2011	India	SAR, C/X-band		
Resourcesat-3 (ISRO)	2011	India	VSWIR, 4 bands	23m, 26 days	700km
Prisma (ASI)	2011	Italy	VSWIR, 200 bands	30m (2.5 pan)	30km
LDCM	2011	USA	VSWIR, 9 bands	30m (15 pan), 16 days	185km
Sentinel-1A (ESA/EC)	2011	EU	SAR, C-band, quad-polar	5-100m	8-400km
AMAZONIA-1 (INPE)	2011	Brazil	VNIR, 4 bands	40m & 12m, 5 days	800km & 110km
SAOCOM 1B (CONAE/ASI)	2012	Argentina/Italy	SAR, L-band	10-100m	40-320km
Astroterra (SPPOT-6)	2012	Comm. (France)	VNIR, 5 bands	8m (2pan), 1-5 days	60km
SAC-E/SABIA/mar (CONAE/NPE)	2012	Argentina/Brazil	VTIR, 15 bands		
Ingenio (SEOSAT) (CDTI/ESA)	2012	2012, Spain/EU	VNIR, 5 bands	10m (2-5 pan)	60km
EnMAP (DLR)	2012	Germany	VNIR	30m	30km
HY-3A (NSOAS/CAST)	2012	EU	SAR, X-band	1-10m	40-150km
SABRINA (ASI)	2012	Italy	SAR, X-band, quad-polar		
Sentinel-2A (ESA/EC)	2012	EU	VSWIR, 13 bands	10m (VNIR) and 20-60m (higher)	290km
Sentinel-1B (ESA/EC)	2012	EU	SAR, C-band, quad-polar	5-20m (extra wide 25x100m)	80-400km
Sentinel-3A (ESA/EC)	2012	EU	VSWIR, 21 bands	300m	750-1675km
ALOS-2	2012	Japan	SAR, L-band, quad-polar		

FY-3E (NRSCC/CMA)	2012	China	VSWIR, 20 bands & VTIR, 10 bands	250m-1km & 1.1km	2800km
FY-4 O/A (NRSCC/CMA)	2012	China	VTIR, 12 bands	1km visible, 2km IR, 4km TIR, daily	Full Earth disc imaged
TerraSAR-X2 (DLR)	2013	Comm. (Germany)	SAR, X-band, quad-polar	1-18m, 2.5-11 days	10-100km x 5-150km
NPOESS-1 (NOAA)	2013	USA	VTIR, 22 bands	400m-1.6km	3000km
CBERS-4 (CRESDA/NPE)	2013	Brazil/China	1) NIR, 4 bands 2) NIR, 4 bands 3) VTIR, 4 bands 4) VSWIR, 4 bands	1) 20m 2) 10m (5pan), 3-26 days 3) 40-80m, 26days 4) 73m, 5 days	1) 120m 2) 60km 3) 120km 4) 866km
MAPSAR (INPE/DLR)	2013	Brazil/Germany	SAR, L-band, quad-polar	3-20m, weekly revisit	30-55km
RADARSAT CONSTELLATION-1 (CSA)	2013	Canada	SAR, C-band, quad-polar	3-100m	20-500km
SAC-F (CONAE)	2014	Argentina	VSWIR, 5 bands	10m (5 pan)	60-117km
SAOCOM-2A (CONAE)	2014	Argentina	SAR, L-band	10-100m	40-320km
COMS-2	2014	Japan	VNIR, 8 bands	236 x 360m	1440km
GCOM-C1(JAXA)	2014	Japan/USA	VTIR, 35 bands	250-1000m	1150-1400km
Sentinel-2B (ESA/EC)	2014	EU	VSWIR, 13 bands	10 (VNIR) and 20-60m(higher)	290km
RISAT-L(ISRO)	2014	India	SAR, L-ban		
RADARSAT CONSTELLATION-3 (CSA)	2014	Canada	SAR, C-band, quad-polar	3-100m	20-500km
COES-S(NOAA)	2014	USA	VTIR, 26 bands	0.5km in the visible, 1km NIR-SWIR, 2km	Full Earth disc imaged

				TIR	
FY-3F(NRSCC/CMA)	2014	China	VSWIR, 20 bands & VTIR, 10 bands	250-1000m & 1.1km	2800km
Electro-L N3 (Roshydromet/ Roscosmos)	2014	Russia	VIR, 10 bands	1km visible, 4km IR, daily	Full Earth disc imaged
SAO-2B (CONAE)	2015	Argentina	SAR, L-bands	10-100m	40-320km
ICESat-2(NASA)	2016	USA	LiDAR	70m footprint, 183 days	Footprint centers 170m apart
RADARSAR CONSTELLATIOn-2 (CSA)	2015	Canada	SAR,C-band, quad-polar	3-100m	20-500km
GOES-R (NOAA)	2015	USA	VTIR, 26 bands	0.5km in the visible, 1km NIR-SWIRm 2km TIR	Full Earth disc imaged
Sentinel-3B (ESA/EC)	2015	EU	VSWIR, 21 bands	300m	750-1675km
MetOp-B (EUMETSAT)	2015	EU	VTIR, 4-6 bands	1.1km, bi-daily	3000km
FY-4 O/B (NRSCC/CMA)	2015	China	VTIR, 12 bands	1km visible, 2 km 1IR, 4km TIR, daily	Full Earth disc imaged
FY-4 O/C (NRSCC/CMA)	2015	China	VTIR, 12 bands	1km visible, 2 km IR< 4km TIR, daily	Full Earth disc imaged
HypsIRI (NASA)	2015	USA	VTIR, 210 bands & 5 bands (TIR)	19m (VSWIR), 90m (TIR), 9-30 days	90km(SWIR) & 400km (TIR)
DESDynI	2015	USA	LiDAR & InSAR, L-band, quad-polar	25m LiDAR footprint, SAR resolution, variable, 8	>340km

				days	
NPOESS-2(NOAA)	2016	USA	VTIR, 22 bands	400m-1.6km	3000km
FY-3G (NRSCC/CMA)	2016	China	VSWIR, 20 bands & VTIR, 10 bands	250-1000m, 1.1km	2800km
BIOMASS (ESA)	2016	EU	InSAR, P-band, quad-polar	50m, 27 days	102km

Table AI.2. Current and Recent Hyperspectral Sensors and Data Providers (Fagan & DeFries, 2009)

Satellite Sensors	**Manufacturer**	**Number of Bands**	**Spectral Range**
FTHSI on MightySat II	Air Force Research Lab	256	0.25 to 1.05 μm
Hyperion on EO-1	NASA Goddard Space Flight Center	220	0.4 to 2.5 μm
Airborne Sensors	**Manufacturer**	**Number of Bands**	**Spectral Range**
AVIRIS (Airborne Visible Infrared Imaging Spectrometer)	NASA Jet Propulsion Lab	224	0.4 to 2.5 μm
HYDICE (Hyperspectral Digital Imagery Collection Experiment)	Naval Research Lab	210	0.4 to 2.5 μm
PROBE-1	Earth Search Sciences Inc	128	0.4 to 2.5 μm
CASI (Compact Airborne Spectrographic Imager	ITRES Research Limited	up to 228	0.4 to 1.0 μm
HyMap	Integrated Spectronics	100-200	Visible to thermal infrared
EPS-H (Environmental Protection System)	GER Corporation	VIS/NIR (76), SWIRI (32), SWIR2 (32), TIR (12)	VIS/NIR (0.43 to 1.05 μm), SWIR1 (1.5 to 1.8 μm), SWIR2 (2.0 to 2.5 μm) and TIR (8.0 to 12.0 μm)
DAIS 7915 (Digital Airborne Imaging Spectrometer)	GER Corporation	VIS/NIR (32), SWIRI (8), SWIR2 (32), MIR(1), TIR (6)	VIS/NIR (0.43 to 1.05 μm), SWIR1 (1.5 to 1.8 μm), SWIR2 (2.0 to 2.5 μm), MIR (3.0 to 5.0 μm) and TIR (8.7 to 12.3 μm)

DAIS 21115 (Digital Airborne Imaging Spectrometer)	GER Corporation	VIS/NIR (76), SWIRI (64), SWIR2 (64), MIR(1), TIR (6)	VIS/NIR (0.43 to 1.05 µm), SWIR1 (1.5 to 1.8 µm), SWIR2 (2.0 to 2.5 µm), MIR (3.0 to 5.0 µm) and TIR (8.0 to 12.0 µm)
AISA (Airborne Imaging Spectrometer)	Spectral Imaging	up to 288	0.43 to 1.0 µm

Appendix II
Global AGB Earth Observation Projects

Table AII.1. A summary of the current global AGB Earth Observation projects (Viergever, 2008)

Project	Aim(s)
FLUXNET	-It promotes the synthesis and analysis of long-term carbon, water and energy flux data acquired globally by various regional flux networks (Baldocchi et al., 2001) -It validates the estimation of the net primary productivity, evaporation and energy absorption based on observations by NASA's EOS/Terra satellite (Baldocchi et al., 2001)
Global Carbon Project (GCP)	-It develops comprehensive understanding, relevant to policy, of the natural and human elements of the global carbon cycle and their interactions and feedbacks. -An internationally consistent framework for the coordination and integration of research of the carbon-climate-human system is provided on regional and global scales (Plummer et al., 2006).

Integrated Global Carbon Observation (IGCO)	-It develops close collaboration with the international carbon cycle research community and provide long-term observations to improve understanding of the global carbon cycle -It monitors and assesses the effectiveness of carbon sequestration and emission reduction activities on global atmospheric CO2 levels (Ciais et al., 2007).
Global Rain Forest and Global Boreal Forest Mapping project (GRFM/GBFM)	-It produces image mosaics from spatially and temporally contiguous L-band SAR data and develope operational forest monitoring technique for tropical and boreal forests (Rosenqvist et al., 2000). -The GRFM project is divided into geographical regions: South-East Asia, Australia, South and Central America and Equatorial Africa while the GBFM is divided into Boreal North America, Siberia and Europe.
ESA TESEO initiative	-It explores the potential of EO to support the implementation of the Kyoto Protocol within the UNFCCC.
Kyoto Inventory	-It builds on the TESEO-CARBON project with the remit to develop an operational service to support national bodies in charge of reporting for the Kyoto Protocol or for trading resulting from the Protocol during the first commitment period 2008-2012.

GLOBCARBON	-It creates global terrestrial vegetation for Dynamic Global Vegetation Models and improves the accuracy of climate change forecasting (Plummer et al.,2006).
GLOBCOLOUR	-It develops calibrated global oceanic products for a period of 10 years in support of ocean carbon-cycle research.
ALOS Kyoto & Carbon Initiative	-It continues the GRFM/GBFM project using ALOS Earth Observation data. -It defines and optimises provision of data products and validated thematic information derived from in sity and Earth Observation data required by international environmental conventions such as UNFCCC, carbon cycle scientists and conservation program (CCCs) (Rosenqvist et al., 2007).
Global Observation for Forest and Land Cover Dynamics (GOFC-GOLD)	-It provides ongoing Earth Observation based data and in-situ observation of forest and other vegetation cover -It provides regional and global datasets containing information on forest cover -It promotes globally consistent data processing and interpretation methods -It promotes international networks for data access, data sharing and international collaboration

Table AII.2. Research projects from different region for carbon accounting purpose (Viergever, 2008)

	Project	Aims
Africa	CARBOAFRICA	-It contributes to the enhancement of an Earth observations system, strengthening the capacity of Europe to understand global change process.
		-It promotes the integration of the environmental dimension in the social and economic context, supporting Sub-Saharan African countries on the path of a sustainable development.
Amazonia	Carbon Cycle Research-LBA The Large Scale Biosphere-Atmosphere Experiment in Amazonia (LBA)	-It creates the new knowledge needed to understand the climatological, ecological, biogeochemical, and hydrological functioning of Amazonia, the impact of land use change on these functions, and the interactions between Amazonia and the Earth system.
	Amazon Forest Inventory Network (RAINFOR)	-It monitors the biomass and dynamics of Amazonian forests
		-RAINFOR was established as part of CARBONSINK, the European contribution to the large-scale biosphere-atmosphere experiment in Amazonia (LBA).

Australia	Australian Blueprint for terrestrial carbon research	-It brings together all of the major Australian researchers/institutions in terrestrial atmospheric carbon cycle research work towards a more focused, integrative programme at the national level.
	National Carbon Accounting System	-It tracks sources and sinks of greenhouse gases from Australian land based systems. The system underpins National Greenhouse Gas Inventory reporting, and provides a basis for emissions projections to assess progress towards meeting Australia's emissions target.
	Australia CSIRO Biosphere Working Group Science Plan	-The Biosphere Working Group (BWG) brings together a multi-disciplinary team of scientists from several different CSIRO Divisions. Its focus is the interaction between the terrestrial biosphere and the atmosphere, particularly the role of the biosphere in the cycles of greenhouse gases (carbon dioxide, methane, nitrous oxide and others).
Canada	BIOCAP	-Capturing Canada’s Green Advantage by building research partnerships to encourage productive, competitive and sustainable methods for using our country’s biological capital to create clean, sustainable forms of energy, fight climate change and encourage rural

		economic development.
China	Study on Carbon Budget for Ecosystems of China	-Study on Carbon Budget for Ecosystems of China: Aspects and Progress, Institute of Atmospheric Physics, Chinese Academy of Sciences presented at the 20th SC-IGBP Meeting, Feb. 19~23, 2005, Beijing.
	Integrated Assessment of the European and North Atlantic Carbon Balance (2009)	-Key results, policy implications for post 2012 and research needs. A recent publication by the European Commission provides a comprehensive assessment of the European and North Atlantic carbon balance based on results of two integrated research activities under the 6th Framework Programme for Research: CARBOEUROPE and CARBOOCEAN. The report highlights key scientific findings, their implication for policy making and future research needs, unfolding some of the complex and emerging scientific and policy issues associated with climate change and the carbon cycle.

	Integrated Carbon Observation System (2008-2011)	-The project aims are: 1. To provide the long-term observations required to understand the present state and predict future behavior of the global carbon cycle and greenhouse gas emissions. 2. To monitor and assess the effectiveness of carbon sequestration and/or greenhouse gases emission reduction activities on global atmospheric composition levels, including attribution of sources and sinks by region and sector.
	CarboEurope Integrated project	-To advance our understanding in a multidisciplinary and integrated way, 61 research centres from 17 European countries have joined forces for a 5-year EU-funded research project started in January 2004.CarboEurope-IP addresses basic scientific questions of high political relevance.
		-The overarching aim of the CarboEurope-IP is to understand and quantify the present terrestrial carbon balance of Europe and the associated uncertainty at local, regional and continental scale.

	CarboEurope - Greenhouse Gas Budgets	-It aims to provide a synthesis based on current research results of the European greenhouse gases budget, including both human induced and biospheric sources and sinks and recommendations for a multi-disciplinary integration in order to provide the scientific foundation for a full carbon and, even broader, full greenhouse gas accounting system by 2010.
	Geoland: Carbon Observatory	-The integrated GMES project on land cover and vegetation aims to develop and demonstrate a range of reliable, affordable and cost efficient European geo-information services, supporting the implementation of European directives and their national implementation, as well as European and International policies.
	CARBO-North	-It addresses the topic of Regional Carbon and Greenhouse Budgets and aims at quantifying the carbon budget in Northern Russia across temporal and spatial scales.
	Greenhouse Gas Management of the European Land Systems	-The GHG-Europe project aims to improve our understanding and capacity for predicting the European terrestrial carbon and greenhouse gas budget.
India	Terrestrial Carbon Budget of India	-Regional carbon budgets: From Methodologies to Quantification, GCP Workshop 2004.

Japan	ALOS Kyoto-Carbon Initiative	-The ALOS Kyoto & Carbon Initiative is an international collaborative project led by JAXA Earth Observation Research Center (EORC). It forms the continuation of JAXA's on-going JERS-1 SAR Global Rain Forest and Global Boreal Forest Mapping project (GRFM/GBFM) into the era of the Advanced Land Observation Satellite (ALOS).
Mexico	The Programa Mexicano del Carbono (PMC)	-It aims to coordinate scientific activities related to the study of the carbon cycle in Mexico, serve as the Mexican scientific counterpart to similar programs in other countries, develop and encourage scientific research concerned with the carbon cycle in Mexico, and systematize scientific data about carbon.
New Zealand	Research on Greenhouse Gases and Carbon Sinks	-Science underpinning New Zealand's ability to significantly reduce its greenhouse gas emissions, move towards a permanent downward trend for total emissions, adapt to the effects of climate change, and manage risks and opportunities arising from climate change impacts.
Russia and Northern Eurasia	Northern Eurasia Earth Science Partnership Initiative, or NEESPI	-It is a currently active, yet strategically evolving program of internationally-supported Earth systems science research, which has as its foci issues in northern

		Eurasia that are relevant to regional and Global scientific and decision-making communities.
Southeast Asia	The CARBOPEAT project	-It is funded by the European Union as a Specific Support Action under Framework Programme 6. Utilizing and synergizing results from 3 INCO research projects, CARBOPEAT promotes enhanced understanding and awareness of carbon-climate-human interactions in tropical peatlands, focusing on vulnerabilities of and risks to their carbon pools and mitigation to reduce greenhouse gas (GHG) emissions, through 'wise use' of natural resources.
United Kingdom	Land Use Change and Forestry Sector of the Greenhouse Gas Inventory	-It is a source and archive of data and calculations related to the Land Use Change and Forestry Sector of the Greenhouse Gas Inventory for the UK. Estimates of future Removals and Emissions of carbon dioxide by Land Use Change and Forestry are also available.
	Quantifying and Understanding the Earth System	-The purpose of QUEST's programme is to deliver a step-change improvement in scientists' ability to predict environmental change, to assess the implications for the sustainable use of resources, to seek action-oriented research outputs, and to

		inform decision-making.
United States	State of the Carbon Cycle Report (SOCCR)	-It was first developed by the Carbon Cycle Interagency Working Group (CCIWG) of the U.S. Climate Change Science Program in consultation with its Carbon Cycle Science Steering Group. This is the first State of the Carbon Cycle Report and talks about the North American Carbon Budget and the Implications for the Global Carbon Cycle.
	Carbon Cycle Science Program – An Interagency Partnership	-It supports coordination of the research among the interagency partners aimed at the understanding of carbon sources and sinks of North America and adjacent oceans.
	Carbon Cycle Greenhouse Gases Group (CCGG)	-It makes ongoing discrete measurements from land and sea surface sites and aircraft, and continuous measurements from baseline observatories and tall towers. These measurements document the spatial and temporal distributions of carbon-cycle gases and provide essential constraints to our understanding of the global carbon cycle.

	China Carbon Consortium (USCCC)	-It is a collaborative consortium between American and Chinese institutions interested in studying the role of managed ecosystems in the global carbon and water cycles.
	CQUEST - Carbon Query and Evaluation Support Tools	-It provides access to geographic data from NASA Ames Research Center, Ecosystem Science and Technology Branch for carbon sequestration predictions throughout the United States.
	Repeat hydrography in support to CLIVAR and C programs	-It provides background on the scientific rationale and scope of the integrated approach to a global observational program for carbon, hydrographic and tracer measurements.
	Carbon Cycle Research Program (CCSP)	-It is an interagency partnership that draws on the expertise and ongoing research in seven agencies, with the objective of developing a whole-system predictive capability for the global carbon system.
	US-Strategic Plan for Climate Change Science Program	-It is the first comprehensive update of a national plan for climate and global change research since the original U.S. Global Change Research Program strategy was issued at the inception of the program in 1989.
	US-DOE Carbon sequestration. Technology	-It is the 2003 vision of how to proceed in the development of carbon sequestration

	roadmap and program plan	technology
	Carbon Sequestration	-It is the technology Roadmap and Program Plan 2005. Developing the Technology Base and Infrastructure to Enable Sequestration as a Greenhouse Gas Mitigation Option. May 2005.
	A Large-Scale CO2 Observing Plan: In Situ Oceans and Atmosphere (LSCOP)	-A contribution to the implementation of the US Carbon Cycle Science Plan (2002). Authors: Observation Working Group.
	The North American Carbon Program	-A report of the NACP Committee of the US Interagency Carbon Cycle Science Program.

References

ABDALATI, W.Z, WALLY, H.J., BINDSCHADLER, R. (2010). The ICESat-2 laser altimetry mission. *Proceedings of the IEEE*, 98 (5), 735-751.

ABOAL, J.R., AREVALO, J.R. & FERNANDEZ, A. (2005). Allometric relationships of different tree species and stand AGB in the Gomera laurel forest (Canary Islands). Flora-Morphology, Distribution. *Functional Ecology of Plants*, 200(3), 264-274.

ADIO, A.F., OJO, A.R. & ASINWA, I.O. (2010). Climate Change: Forestry, A Step In The Right Direction. I*nternational Conference on Environmental Engineering and Applications (ICEEA 2010)*, 68-71.

AHOKAS, E., YU, X., OKSANEN, X, HYYPPÄ, J., KAARTINEN, H. & HYYPPÄ, H. (2005). Optimization of scanning angle for countrywide laser scanning, International Archives of Photogrammetry. *Remote Sensing and Spatial Information Sciences*, 36, 115-119.

ALLOUIS, T., DURRIEU, S., CUESTA, J., CHAZETTE, P., FLAMANT, P.H., COUTERON, P. (2010). Assessment of tree and crown heights of a maritime pine forest at plot level using a fullwaveform UltraViolet Lidar prototype. *IEEE International Geoscience and Remote Sensing Symposium*, 1382-1385.

AMMANN, C., JOOS., F., SCHIMEL, D. S., BLIESNER, B. & TOMAS, R. (2007). Solar influence on climate during the past millennium: Results from transient simulations with the NCAR Climate System Model. *Proceedings of the National Academy of Sciences of The United States of America*, 104(10), 3713-3718.

ANDERSEN, H.E., REUTEBUCH, S.E. & MCGAUHEY, R.J. (2006). A rigorous assessment of tree height measurements obtained using airborne lidar and conventional field methods. *Canadian Journal of Remote Sensing*, 32(5), 355-366.

ANDERSSON, K., EVANS, T. P. & RICHARDS, K.R. (2009). National forest carbon inventories: Policy needs and assessment capacity. *Climatic Change* 93(1 - 2), 69 - 101.

ARAUJO, T.M., HIGUCHI. N. & CARVALHO, J.A. (1999). Comparison of formulae for biomass content determination in a tropical rain forest site in the state of Para, Brazil. *Forest Ecology and Management*, 117(1-3), 43-52.

ARCHARD, F. R., DEFRIES, EVA, H., HANSEN, M., MAYAUX, P and STIBIG, H. J. (2007). Pan-tropical monitoring of deforestation. *Environmental Research Letters*, 2(4),045022.

AREVALO, C.B.M., VOLK, T.A., BEVILACQUA, E. & ABRAHAMSON, L. (2007). Development and validation of aboveground biomass estimation for four Salix clones in central New York. *Biomass and Bioenergy*, 31(1), 1-12.

ARKLE, P. & EDWARDS, C. (1996). Age Distribution of Native Scots Pine Trees in Glen Affric. Foresty Commission, Contact Report SILV.

ASHMOLE, P. (2006). The lost mountain woodland of Scotland and its restoration, Scottish *Forestry*, 60(1), 9-22.

ASNER, G.P. (1998). Biophysical and Biochemical Sources of Variablity in canopy reflectance. *Remote Sensing of Environment,* 64, 234-253.

ASNER, G.P., & VITOUSEK, P.M. (2005). Remote analysis of biological invasion and biogeochemical change. *Proceedings of the National Academy of Sciences*, 102, 4383- 4386.

ATTEMA, E.P.W., & ULABY, F.T. (1978). Vegetation Modeled as a Water Cloud. *Radio Science*, 13, 357-364.

AVERIS, A.B.G. (1994). Vegetation Survey of Glen Affric, Inverness District, Scotland.

BAKER, J.R., MITCHELL, P.L. & CORDEY, R.A. (1994). Relationships between physical characteristics and polarimetric radar backscatter for corsican pine stands in Thetford Forest, U.K. *International Journal of Remote Sensing*, 15, 2827–2849.

BALDOCHI, D., FALGE, E., GU, L., OLSON, R., HOLLINGER, D., RUNNING, S., ANTHONI, P., BERNHOFER, C., DAVIS, K., EVANS, R., FUENTES, J., GOLSTEIN, A., KATUL, G., LAW, B., LEE, X., MALHI, Y., MEYERS, T., MUNGER.W., OECHEI, W., PAW, K.T., PILEGAARD, K., SCHMID, H.P.., VALENTINI, R., VERMA, S., VESALA, T., WILSON, K., & WOFSY, S. (2001). FLUXNET: A new tool to study the temporal and spatial variability of ecosystem-scale carbon-dioxide, water vapor, and energy flux densities. *Bulletin of the American Meterological Society*, 82(11), 2415- 2434.

BALTSAVIAS, E.P. (1999a). A comparison between photogrammetry and laser scanning. *ISPRS. Journal of Photogrammetry & Remote Sensing*, 54, 83-94.

BALTSAVIAS, E.P. (1999b). Airborne laser scanning: basic relations and formulas. *ISPRS Journal of Photogrammetry & Remote Sensing*, 54, 199-214.

BALTSAVIAS, E.P. (1999c). Airborne laser scanning: existing systems and firms and other resources. *ISPRS Journal of Photogrammetry and Remote Sensing*, 54, 1 64-198.

BARAKAT, R. (1963). Theory of the coherency matrix for light of arbitrary spectral bandwidth. *The Journal of the Optical Society of America*, 53(3), 317-322.

BARNSLEY, J., LEWIS, P., O'DWYER, S., DISNEY, M., HOBSON, P., CUTTER, M. & LOBB, D. (2000). On the potential of CHRIS-PROBA for estimating vegetation canopy properties from space. *Remote Sensing Reviews*, 19, 171-189.

BEAUDOIN, A., LE TOAN, T., GOZE, S., NERZY, E. & LOPES, A. (1994). Retrieval of forest biomass from SAR data. *International Journal of Remote Sensing*, 15, 414.

BECKER, F. & LI, Z. (1995). Surface temperature and emissivity at various scales: Definition, measurement and related problems. *Remote Sensing Reviews*, 12, 225-253.

BENESTAD, R.E. & SCHMIDT, G. A. (2009). Solar trends and global warming, Journal of Geophysical Research, 114(14). Available online: http://adsabs.harvard.edu/abs/2009JGRD..11414101B

BICHERON, P., DEFOURNY, P.,BROCKMANN, C., SCHOUTEN, L., VANCUTSEM, C., HUC, M., BONTEMPS, S., LEROY, M., ACHARD, F., HEROLD. M., RANERA, F., & ARINO, O. (2008). GLOBCOVER Products Description and Validation Report. MEDIAS-France, ftp://uranus.esrin.esa.int/pub/globcover_v2/global/ BIOMASS Report for Assessment, European Space Agency, November 2008.

BLACKBURN, G.A. (1999). Relationships between spectral reflectance and pigment concentrations in stacks of deciduous broadleaves. *Remote Sensing of Environment*, 70(2), 224-237.

BLAIR, J.B., & HOFTON, M.A. (1999). Modeling laser altimeter return waveforms over complex vegetation using high-resolution elevation data. *Geophysical Research Letters*, 26(16), 2509-2512.

BOERNER, W.M. (1990). Introduction to radar polarimetry with assessments of the historical development and of the current state-of- the-art, *Proceedings of International Workshop on Radar Polarimetry*, 90.

BOERNER, W.M., MOTT, H., LUNEBURG, E., LIVINGSTON, C., BRISCO, B., BROWN, R.J. & PATERSON, J.S. (1998). Polarimetry in radar remote sensing: Basic and applied concepts, 2, 3rd. edition, John Wiley & Sons, New York.

BOSSARD, M., FERANEC, J. & OTAHEL, J. (2000). CORINE land cover technical guide—Addendum 2000, Eur. Environ. Agency, Copenhagen, Denmark, Tech. Rep. 40.

BOURDREAU, J., NELSON,R.F., MARGOLIS, A., BEAUDOIN, L., GUINDON & KIMES, Quebec. *Remote Sensing of Environment*, 112(10), 3876-3890.

BRACK, C. (1999). Merchantable height of a single tree. Available online: http://sres-associated.anu.edu.au/mensuration/merchhgt.htm#bolehgt

BRANDTBERG, T., WARNER, T.A., LANDENBERGER, R.E. & MCGRAW, J.B. (2003). Detection and analysis of individual leaf-off tree crowns in small footprint, high sampling density lidar data from the eastern deciduous forest in North America. *Remote Sensing of Environment,* 84, 290-303.

BROVKIN, V., SITCH, S., VON BLOH, W., CLAUSSEN, M., BAUER, E. & CRAMER, W. (2004). Role of land cover changes for atmospheric CO2 increase and climate change during the last 150 years. *Global Change Biology*, 10, 1253-1266.

BROWN , I. F., MARTINELL, L. A., THOMAS, W. W., MOREIRAC, M. Z., CID FERREIRAE, C. A. & REYNALDO, A. V. (1995). Uncertainty in the biomass of Amazonian forests: An example from Rondonia, Brazil, *Forest Ecology and Management*, 75.

BROWN, R.J. & PATERSON, J.S. (1998). Polarimetry in radar remote sensing: Basic and applied concepts, 2, 3rd. edition, *John Wiley & Sons*, New York.

BROWN, S. (1997). Estimating Biomass and Biomass Change of Tropical Forests: a Primer (FAO Forestry Paper-134), *FAO, United Nations*, Rome.

BROWN, S. (2002). Measuring carbon in forests: Current status and future challenges. *Environmental Pollution*, 116(3), 3563.

BROWN, S. BROWN, I.F., MARTINELL, L.A., THOMAS, W.W., MOREIRAC, M.Z., CID FERREIRAE, C.A. & REYNALDO, A.V. (1995). Uncertainty in the biomass of Amazonian forests: An example from Rondonia Brazil, *Forest Ecology and Management*, 75.

CAICOYA, A.T., KUGLER, F., PAPATHANASSIOU, K., BIBER, P. & PRETZSCH, H. (2010). Biomass estimation as a function of vertical forest structure and forest height - Potential and limitations for Radar Remote Sensing, *8th European Conference on Synthetic Aperture Radar (EUSAR)*, 1 - 4.

CALISKAN, N., JADRAQUE, E., THAM, Y. & MUNEER, T. (2011). Evaluation of the accuracy of mathematical models through use of multiple metrics. *Sustainable Cities and Society* 1, 63-66.

CALLE, F., Groot, P., Hemstock, S. L. & Woods, J. (2007). The Biomass Assessment Handbook, Earthscan Publishing.

CANNELL, M.G.R. & DEWAR, R.C. (1995). The carbon sink provided by plantation forests and their products in Britain. *Forestry*, 68, 35–48.

CANNELL, M.G.R., MILNE, R., HARGREAVES, K.J., BROWN, T.A.W., CRUIKSHANK, M.M., BRADLEY, R.I., SPENCER, T., HOPE, D., BILLET, M.F., ADGER, W.N. & CARTER, G.A. (1998). Reflectance bands and indices for remote estimation of photosynthesis and stomatal conductance in pine canopies. *Remote Sensing of Environment*, 63, 61-72.

CASSELLS, G.F., WOODHOUSE, I.H., MITCHARD, E.T.A. & TEMBO, M.D. (2009). The use of ALOS PALSAR for supporting sustainable forest use in southern Africa: A case study in Malawi. *IEEE International Geoscience and Remote Sensing Symposium 2009*,2,26-209.

CCC (2008). Independent advisors to the UK Government on tackling and preparing for climate change. Available online: http://www.theccc.org.uk/about-the-ccc/climate-change-act

CHAVE, J. (2004). Error propagation and scaling for tropical forest biomass estimates. *Philisophical Transactions*, The Royal Society London, 359, 409-420.

CHAVE, J., CONDIT, R., SALOMON, A., HERNANDEZ, A., LAO, S. & PEREZ, R. (2004). Error Propagation and Scaling for Tropical Forest Biomass Estimates. *Philosophical Transactions*: Biological Sciences, 259 (1443), 409-420.

CHEN, G., HAY, G.J. & ZHOU, Y.L. (2010). Estimation of forest height, biomass and volume using support vector regression and segmentation from lidar transects and Quickbird imagery. *18th International Conference on Geoinformatics*,1-4.

CHEN, J., FALK, M., EUSKIRCHEN, E., PAW-U, K.T., SUCHANEK, T.H., USTIN, S.L., BOND, B.J., BROSOFSKE, K.D., PHILIPS, N. & RUNCHENG, B-I (2002). Biophysical controls of carbon flows in three successional Douglas-fir stands based on eddy-covariance measurements. *Tree Physiology*, 22, 169-177.

CHEN, J.M., LEBLANC, S.G., MILLER, J.R., FREEMANTLE, J., LOECHEL, S.E., WALTHALL, C.L., INNANEN, K.A. & WHITE, H.P. (1999). Compact airborne spectrographic imager (CASI) used for mapping biophysical parameters of boreal forests. *Journal of Geophysical Research*, 104, 927-945.

CHEN, X., VIERLING, L., ROWELL, E., and DEFELICE, T. (2004). Using lidar and effective LAI data to evaluate IKONOS and Landsat 7 ETM+ vegetation cover estimates in a ponderosa pine forest. *Remote Sensing of Environment*, 91, 14-26.

CIAIS, P., MOORE, B., STEFFEN, W., HOOD, M., QUEGAN, S., CIHLAR, J., RAUPACH, M., RASOOL, I., DONEY, S., HEINZE, C.,SABINE, C., HIBBARD, K., SCHULZE, D., HEIMANN, M., CHÉDIN, A., MONFRAY, P., WATSON, A.,LEQUÉRÉ, C., TANS, P., DOLMAN, H., VALENTINI, R., ARINO, O., TOWNSHEND, J., SEUFERT, G., FIELD, C., IGRASHI, T., GOODALE, C., NOBRE, A., INOUE, G., CRISP, D., BALDOCCHI, D.,

TSCHIRLEY, J., DENNING, S., CRAMER, W., FRANCEY, R. & WICKLAND, D. (2004). Integrated Global Carbon Observation Theme: A Strategy to Realize a Coordinated System of Integrated Global Carbon Cycle Observations,1-61. Available online: http://www.fao.org/gtos/doc/ECVs/T09/ECV-T9-landcover-ref24-IGCO-carbontheme.pdf

CLEVERS, J.G.P.W. (1999). The use of imaging spectrometry for agricultural applications. *ISPRS Journal Photogrammetry Remote Sensing*, 54, 299-304.

CLEWLEY, D., LUCAS, R.M., MOGHADDAM, M., BUNTING, P., DWYER, J.& CARREIRAS, J. (2010). Forest parameter retrieval from SAR data using an estimation algorithm applied to regrowing forest stands in Queensland, Australia. *IEEE Journal of Geoscience and Remote Sensing Symposium (IGARSS)*, 1238-1241.

CLOUDE, S.R. (2008). Multifrequency 3-D Imaging of Tropical Forest using Polarization Coherence Tomography. *7th European Conference on Synthetic Aperture Radar (EUSAR)*, 1-4.

CLOUDE, S. R. (2010). Forest Vertical Structure from P/L band Spaceborne POLInSAR. *8th European Conference on Synthetic Aperture Radar (EUSAR)*, 1-4.

CLOUDE, S. R. (2011). POLInSAR: From SIR-C to Tandem-X. *IEEE International Geoscience and Remote Sensing Symposium*, 2570-2573.

CLOUDE, S. R, PAPATHANASSIAO, K.P., WOODHOUSE, I, HOPE, J., SUAREZ, J., OSBORNE, P.E. & WRIGHT, G. (2001). The Glen Affric radar project: Forest mapping using polarimetric interfererometry. *Proceedings of IEEE International Geoscience and Remote Sensing Symposium*, 4(1), 1642-1644.

CLOUDE, S.R. and POTTIER, E. (1996). A review of target decomposition theorems in radar polarimetry. *lEEE Transactions of Geoscience and Remote Sensing*, 34, 498-518.

CLOUDE, S.R., PAPATHANASSIOU, K.P., WOODHOUSE, I., HOPE, J., SUAREZ J., MINGUEZ, J.C., OSBORNE, P. & WRIGHT, G. (2001). The Glen-Affric Project: Forest Mapping using Polarimetric Radar Interferometry. *IEEE International Geoscience and Remote Sensing Symposium*, 4, 1642-1644.

CLOUDE, S.R.,VIERGEVER, K., WOODHOUSE, I.H., SUAREZ, J. (2008). Mapping Scotland with PALSAR: An Assessment of the Importance of L-Band Polarimetry. *Proceedings of 2nd ALOS PI Workshop*, Rhodes, Greece.

CLOUDE, S. R., WOODHOUSE, L. H., HOPE, J., MINGUEZ, J. C. S., OSBORNE, P., & WRITE, G. (2001). The Glen Affric Project: forest mapping using dual baseline polarimetric radar interferometry. *Proceedings of the Third*

International Symposium on Retrieval of Bio- and Geophysical Parameters from SAR Data for Land Applications, 11-14 September, Sheffield, UK.

COLE, T.G. & EWEL, J.J. (2006). Allometric equations for four valuable tropical tree species. *Forest Ecology and Management*, 229(1-3), 351-360.

COOK, B.D., SUN, G., RANSON, K.J., MONTESANO, P.M., LUTHCKE, S.B. & BLAIR, J.B. (2009). Accuracy of DESDynI Biomass Estimates using Lidar and Data Fusion Methods. American Geophysical Union. Available Online : http://adsabs.harvard.edu/abs/2009AGUFM.B31A0318C

COTTON, N. & ETTL, G.J. (2001). Estimating populations of whitebark pine in Mount Rainier National Park, Washington, using aerial photography. *Northwest Science*, 75, 397-406.

CUNIA, T. (1986a). Error of forest inventory estimates: its main components. E.H. Wharton and T. Cunia (ed.), Estimating tree biomass regressions and their error. USDA, Northeaster Forest Experimental Station, Broomall, Pennsylvania.

CUNIA, T. (1986b). On the error of forest inventory estimates: stratified sampling and double sampling for stratification. E. H. Wharton and T. Cunia, Estimating tree biomass regression and their error. USDA, Northeastern Forest Experimental Station, Bromall, Pennsylvania.

DALPONTE, M., COOPS, N.C., BRUZZONE, L. & GIANELLE, D. (2009). Analysis on the Use of Multiple Returns LiDAR Data for the Estimation of Tree Stems Volume. *IEEE Journal of Selected Topics in Applied Earth Observations and Remote Sensing*, 2(4), 310-318.

DAVIES, A.L. (1999). High spatial resolution holocene vegetation and land-use history in west Glen Affric and Kintail, Northern Scotland., PhD Thesis, University of Stirling.

DAWSON, B. & SPANNAGLE, M. (2009). The Complete Guide to Climate Change, Routledge.

DE GIER, A. (1989). Woody biomass for fuel: estimating the supply in natural woodlands and shrublands. Doctorate dissertation Thesis, Albert Ludwigs University Freiburg i Br., Germany, 186.

DE GIER, A. (1999). Woody biomass assessment in woodlands and shrublands, Off-forest tree resources of Africa, Arusha, Tanzania.

DE GIER, A. (2003). A new approach to woody biomass assessment in woody biomass assessment in woodlands and shrublands, P. Roy (Ed), *Geoinformatics for Tropical Ecosystems, India*, 161-198.

DEFRIES, R., (2008). Terrestrial vegetation in the coupled human-earth system: Contributions of remote sensing. *Annual Review of Environment and Resources*, 33, 369-390.

DEFRIES, R., ACHARD, F., BROWN, S., HEROLD, M., MURDIYARSO, D., SCHLAMADINGER, B., SOUZA, C. (2007). Earth observations for estimating greenhouse gas emissions from deforestation in developing countries. *Environmental Science & Policy*, 10, 385-394.

DEFRIES, R.S., HOUGHTON, R.A., HANSEN, M.C., FIELD, C.B., SKOLE, D. & TOWNSHEND, J. (2002). Carbon emissions from tropical deforestation and regrowth based on satellite observations for the 1980s and 1990s. *Proceedings of the National Academy of Sciences of the United States of America*, 99(22), 14256-14261.

DEGRAFF, M-A., SIX, J., HARRIS, D., BLUM, H. & Van Kessel, C. (2004). Decomposition of soil and plant carbon from pasture systems after 9 years of exposure to elevated CO2: impact on C cycling and modeling. *Global Change Biology*, 10, 1922-1935.

DIEDERSHAGEN, O., KOCH, B. & WEINACKER, H. (2003). Automatic Estimation of Forest Inventory Parameters Based on Lidar, Multi-spectral and fogis data. Optical 3-D Measurement Techniques. *ETH Höngerberg. Conference Proceedings*, 2, 259 – 268.

DIMITRIS, Z., PETTERI, M., RAISA, M., MAURIZIO, M. (2005). Biomass and stem volume equations for tree species in Europe. *Silva Fennica Monographs*, 4, 63.

DOBSON, M.C., ULABY, F.T., LETOAN, T., BEAUDOIN, A., KASISCHKE, E.S. & CHRISTENSEN, N. (1992). Dependence of radar backscatter on conifer forest biomass. *IEEE Transactions of Geoscience and Remote Sensing*, 30, 412-415.

DONG, Y., FORSTER, B.C. AND TICEHURST,C. (1998). A new decomposition of radar polarization signatures. *IEEE Transactions on Geoscience and Remote Sensing*, 36, 933-939.

DRAKE, J.B., DUBAYAH, R.O. CLARK, D.B., KNOX, R.G., BLAIR, J.B., HOFTON, M.A., CHAZDON, R.L (2002a). Estimation of tropical forest strucutral characteristics using large-footprint lidar. *Remote Sensing of Environment,* 79(2-3), 305-219.

DRAKE, J.B., DUBAYAH, R.O., KNOX, R.G., CLARK, D.B. & BLAIR, J.B. (2002b). Sensitivity of large-footprint lidar to canopy structure and biomass in a neotropical rainforest. *Remote Sensing of Environment*, 81(2-3), 378-392.

DRAKE, J.B., KNOX, R.G., DUBAYAH, R.O., CLARK, D.B., CONDIT, R, BLAIR, J.B. & HOFTON, M. (2003). Above-ground biomass estimation in closed canopy Neotropical forests using lidar remote sensing: factors affecting the generality of relationships. *Global Ecology & Biogeography*, 12, 147-159.

DRAPER, N. & SMITH, H. (1998). Applied regression analysis. New York: Wiley.

DUBAYAH, R.O. & DRAKE, J.B. (2000). LiDAR remote sensing for forestry. *Journal of Forestry*, 98, 44–46.

EEA (2011). The 2020 outlook. Available online: http://www.eea.europa.eu/soer/countries/uk/soertopic_view?topic=climate%20change

ELVIDGE, C.D. & CHEN, Z. (1995). Comparison of broad-band and narrow-band red and near-infrared vegetation indices. *Remote Sensing of Environment*, 54, 38-48.

ENGLUND, S.R, O'BRIEN, J.J., CLARK, D.B. (2000). Evaluation of digital and Wlm hemispherical photography and spherical densiometry for measuring forest light environments, *Canadian Journal For Remote Sensing*, 30, 1999– 2005.

ERLYKIN, A.D., SLOAN, T. & WOLFENDALE (2009). Solar Activity and the Mean Global Temperature. Available online: http://arxiv.org/PS_cache/arxiv/pdf/0901/0901.0515v1.pdf

ESA Future Earth Explorer Missions. Available online: http://www.esa.int/esaLP/ESADQ0UHN6D_LPfuturemis_0.html, 17 August 2011

FAGAN, M. & DEFRIES, R. (2009). Measurement and Monitoring of the World's Forests: A Review and Summary of Remote Sensing Technical Capability 2009-2015, RFF Report. Available online: http://www.rff.org/rff/documents/rff-rpt-measurement%20and%20monitoring_final.pdf

FAO (FOOD AND AGRICULTURE ORGANIZATION) (1948). Forest Resources of the World. Unasylva, 2(4), 1-22.

FAO (FOOD AND AGRICULTURE ORGANIZATION) (1997). The state of world's forest. Rome , Italy.

FAO (FOOD AND AGRICULTURE ORGANIZATION) (2004). Global forest resources and assessment update 2005. Terms and definition, Rome. Available online: http://www.fao.org/docrep/007/ae156e/ae156e00.htm

FAO (FOOD AND AGRICULTURE ORGANIZATION) (2006). Global forest resources assessment. FAO (Food and Agriculture Organization) Forestry Paper 147. Rome: Rome Food and Agriculture Organization of the United Nations.

FAO (FOOD AND AGRICULTURE ORGANIZATION) (2008). Terrestrial Essential Climate Variables for Climate Change Asesment, Mitigation and Adaptation [GTOS 52] Available online: http://www.fao.org/gtos/doc/pub52.pdf

FAO (FOOD AND AGRICULTURE ORGANIZATION) (2010). Global Forest Resources Assessment 2010: Main Report, FAO Forestry Paper163. Available online: http://www.fao.org/docrep/013/i1757e/i1757e.pdf

FERRAZOLLI, P & GUERRIERO, L. (1995). Radar sensitivity to tree geometry and woody volume: a model analysis, IEEE Transactions on Geoscience and Remote Sensing, 33(2), 360-371.

FILELLA, I.P., JOSEP, U., LAURA, L. & MARC, E. (2004). Reflectance assessment of seasonal and annual changes in biomass and CO2 uptake of a Mediterranean shrubland submitted to experimental warming and drought. Remote Sensing of Environment, 90(3), 308-318.

FOREST ENTERPRISE (1997). Glen Affric Caledonian Forest Reserve Endangered Habitat Management Plan. Unpublised document, Forest Enterprise, Fort Augustus.

FORESTRY COMMISSION (2002a). Forestry statistics 2002. A compendium of statistics about woodland, forestry and primary wood processing in the United Kingdom. Available online: http://www.forestry.gov.uk/website/pdf.nsf/pdf/forestrystatistics2002.pdf/$FILE/forestrystatistics2002.pdf

FORESTRY COMMISSION (2002b). Forestry facts and figures 2002: a summary of statistics about woodland and forestry in Great Britain. Available online: http://www.forestry.gov.uk/website/pdf.nsf/pdf/fff2002.pdf/$FILE/fff2002.pdf

FORESTRY COMMISSION (2002c). National inventory of woodlands and trees. Available online: http://www.forestry.gov.uk/forestry/HCOU-54PG9U

FORESTRY COMMISSION (2008). Improving the ecological content of forest plans: A case study from Glen Affric.

FOUKAL, P., FROHLICH, C., SPRUIT, H. & WIGLEY, T. M.L. (2006). Variations in the solar luminosity and their effect on the Earth's climate, Nature, 443(14), 161-166. Available online: http://www.mpa-garching.mpg.de/mpa/publications/preprints/pp2006/MPA2001.pdf

FRANK ROSILLO-CALLE, PETER DE GROOT, SARAH L. HEMSTOCK & WOODS, J. (2007). The Biomass Assessment Handbook, London, Earthscan.

FREEMAN. A. & DURDEN S. L. (1998). A three component model for polarimetric SAR data. *IEEE Transactions on Geoscience and Remote Sensing*, 36, 963-973.

FREER-SMITH, P.H., BROADMEADOW, M.S.J. & LYNCH, J.M. (2008). Forestry and climate change. *Forest Research*, Crownwell Press.

FROCLICH, C. & LEAN, J. (1998). The Sun's total irradiance: Cycles, trends and related climate change uncertainties since 1976. *Geophysical Research Letters*, 25(23), 4377- 4380,1998. Available online: http://ieg.or.kr/abstractII/G0102523037.PDF

FURBY, S. L., WALLACE, J. F. & CACCETTA, P. A. (2007). Monitoring sparse perennial vegetation cover over Australia using sequences of Landsat imagery. *International Society for Environmental Information Sciences*, 5, 585-590.

GANG, C., HAY, G.J.& ZHOU, Y.. (2010). Estimation of forest height, biomass and volume using support vector regression and segmentation from lidar

transects and Quickbird imagery. *International Conference on Geoinformatics*, 1-4.

GARCIA-MARTIN, A., PEREZ-CABELLO, F., DE LA RIVA FERNANDEZ, J. & LLOVERIA, R.M. (2008). Estimation of Crown Biomass of Pinus spp. From Landsat TM and Its Effect on Burn Severity in a Spanish Fire Scar. *IEEE Journal of Selected Topics in Applied Earth Observations and Remote Sensing*, 1(4), 254-265.

GARG, A., MITHAL, V., CHAMBER, Y., BRUGERE, I., CHAUDHARI, V., DUNHAM, M., KRISHNA, V., KRISHNAMURTHY, S., VANGALA, S., BORIAH, S., STEINBACH, M., KUMAR, V., CHO, A., STANLEY, JD., ABRAHAM, T., CASTILLA-RUBIO, J.C.., POTTER, C. & KLOOSTER, S. (2011). Gopher: Global observation of Planetary Health and Ecosystem Resources, *IEEE International Geoscience and Remote Sensing Symposium*, 1449-1452.

GAVEAU, D.A. & HILL, R.S. (2003). Quantifying canopy height underestimation by laser pulse penetration in small-footprint airborne laser scanner data. *Canadian Journal of Remote Sensing,* 29, 650-657.

GCOS (Global Climate Observing System) (2003), The second report on Adequacy of Global Observation Systems for Climate in Support of the UNFCCC, Global Climate Observing System, Report GCOS, 82. Available online : http://www.wmo.int/pages/prog/gcos/Publications/gcos-82_2AR_ExecSum.pdf

GIBBS. H. K., BROWN, S., NILES, J.O. & FOLEY, J. A. (2007). Monitoring and estimating tropical forest carbon stocks: Making REDD a reality. *Environmental Research Letter*, 2(4), 045023.

Global Climate Observing System (GCOS) (2003), The second report on Adequacy of Global Observation Systems for Climate in Support of the UNFCCC, Global Climate Observing System, Report GCOS, 82. Available online : http://www.wmo.int/pages/prog/gcos/Publications/gcos-82_2AR_ExecSum.pdf

GOETZ, S & DUBAYAH, R. (2011). Advances in remote sensing technology and implications for measuring and monitoring forest carbon stocks and change. *Carbon Management*, 2(3), 231-244.

GOODENOUGH, D.G., CHEN, H., DYK, A., HAN, T. & LI, J.Y. (2005b). Multisensor Data Fusion For Aboveground Carbon Estimation, *Proc. XXVIIIth General Assembly of the International Union of Radio Science (URSI)*, New Delhi, India, vol. CD, 1-4.

GOODENOUGH, D.G., CHEN, H., DYK, A., HAN, T., MCDONALD, S., MURDOCH, M., NIEMANN, K.O., PEARLMAN, J., STAENZ, K. & WEST, C. (2003). Forest information products from AVIRIS and Hyperion. *Proceedings of 12th*

JPL Airborne Earth Science Workshop, Pasadena, California, USA, Vol. JPL Pub. 04-6, 83-89.

GOODENOUGH, D.G., DYK, A., NIEMANN, K.O., PEARLMAN, J., CHEN, H., HAN, T., MURDOCH, M. & WEST, C. (2003). Processing Hyperion and ALI for Forest Classification. *IEEE Transactions on Geoscience and Remote Sensing*, 41, 1321-1331.

GOODENOUGH, D.G., HAN, T., DYK, A., GOUR, J. & LI, J.Y. (2005c). Mapping Forest Biomass with AVIRIS and Evaluating SNR Impact on Biomass Prediction, Natural Resources Canada.

GOODENOUGH, D.G., NIEMANN, K.O., DYK, A., HOBART, G., GORDON, P., LOISEL, M.& CHEN, H. (2008). Comparison of AVIRIS and AISA airborne hyperspectral sensing for above-ground forest carbon mapping. *IEEE International Geoscience and Remote Sensing (IGARSS)*, 129-132.

GOODENOUGH, D.G., PEARLMAN, J., CHEN, H., DYK, A., HAN, T., LI, J.Y., MILLER, J., & NIEMANN, K.O. (2004). Forest Information from Hyperspectral Sensing. *IEEE International Geoscience and Remote Sensing (IGARSS)*, Anchorage, Alaska, 4, 2585-2589.

GRACE, J., 2004. Understanding and managing the global carbon cycle. *Journal of Ecology*, 92, 189-202.

GULLISON, R.E., FRUMHOFF, P.C., CANADELL, J.G., FIELD, C.B., NEPSTAD, D.C., HAYHOE, K., AVISSAR, R., CURRAN, L.M., FRIEDLINGSTEIN, P., JONES, C.D. & NOBRE, C. (2007). Tropical forests and climate policy. *Science*, 316(5827), 985–986.

GUO, Z., NI, W. & SUN, G. (2010). Forest biomass estimation in northeastern China using ALOS PALSAR data combined radiative transfer model. *IEEE International Geoscience and Remote Sensing Symposium 2010*,1497-1500.

GUO, Z., SUN, G., RANSON, K.J., Ni, W. & Qin, W. (2008). The Potential of Combined Lidar and SAR data in Retrieving Forest Parameters Using Model Analysis. *IEEE International Geoscience and Remote Sensing Symposium* 2008, 542-545.

HADDOW, K.A., KING, D.J., POULIOT, D.A., PITT, D.G. & BELL, F.W. (2000). Early regeneration conifer identification and competition cover assessment using airborne digital camera imagery. *The Forestry Chronicle*,76, 915-928.

HAIGH, J. D. (2003). The effects of solar variability on the Earth's climate, Philosophical Transactions – Royal Society, Mathematical, Physical and Engineering Sciences, 361 (1802), 95-111. Available online: http://cat.inist.fr/?aModele=afficheN&cpsidt=14604941

HALL, R.J., SKAKUN, R.S., BEAUDOIN, A., WULDER, M.A., ARSENAULT, E.J., BERNIER, P.Y., GUINDON, L., LUTHER, J.E. & GILLIS, M.D. (2010).

Approaches for forest biomass estimation and mapping in Canada, *IEEE International Geoscience and Remote Sensing Symposium (IGARSS)*, 1988-1991.

HANSEN, M.C., ROY, D.P., LINDQUIST, E., ADUSEI, B., JUSTICE, C.O., & ALSTATT, A. (2008). A method for integrating MODIS and Landsat data for systematic monitoring of forest cover and change in the Congo Basin, *Remote Sensing of Environment*, 112(5), 2495-2513.

HANSEN, P.M.S. (2003). Reflectance measurement of canopy biomass and nitrogen status in wheat crops using normalized difference vegetation indices and partial least squares regression. *Remote Sensing of Environment*, 86(4), 542-553.

HARRELL, P. A., KASISCHKE, E. S., BOURGEAU-CHAVEZ, L. L., HANEY, E., AND CHRISTENSEN, N. L. (1997). Comparison of approaches to estimate of aboveground biomass in southern pine forests using SIR-C data. *Remote Sensing of Environment*, 59, 223-233.

HAVEMANN, T. (2009). Measuring and monitoring Terrestrial Carbon. Available online: http://www.terrestrialcarbon.org/site/DefaultSite/filesystem/documents/MM%20Report%20090922.pdf

HE, Q.,CAO, C., CHEN, E., LING, F. & ZHANG H. (2009). Relationship between SAR and biomass derived from LIDAR in mountainous areas. *Second Asian-Pacific Conference on Synthetic Aperture Radar 2009*, 136-139.

HE, Y.G., XULIN &WILMSHURST, J. (2006). Studying mixed grassland ecosystmens I: suitable hyperspectral vegetation indices. Canadian Journal of Remote Sensing, 32(2), 98-107.

HELIERE, F., LIN, C.C., FOIS, F., DAVIDSON, M., THOMPSON, A. & BENSI, P. & ESTEC, N. (2009). BIOMASS: A P-band SAR earth explorer core mission candidate. *IEEE Radar Conference*, 1-6.

HELMER, E.H., LEFSKY,M.A. (2009). Biomass accumulation rates of Amazonian secondary forest and biomass of old-growth forests from Landsat time series and the Geoscience laser Altimeter System. *Journal of Applied Remote Sensing*, 3(1), 033505.

HESE, S. LUCHT, W., SCHMULLIUS, C. BARNSLEY, M., DUBAYAH, R., KNORR, D., NEUMANN, K., RIEDEL, T. & SHROTER, K. (2005). Global biomass mapping for an improved understanding of the CO2 balance- the Earth observation mission Carbon-3D. *Remote Sensing of Environment*, 94, 94-104.

HIKOSAKA, K., KINUGASA, T., OIKAWA, S., ONODA, Y & HIROSE, T. (2010). Effects of elevated CO2 concentration on seed production in C3 annual plants. *Journal of Experimental Botany*, 62 (4), 1523-1530.

HILL, M.J., TICEHURST, C.J., JONG-SEN LEE, GRUNES, M.R., DONALD, G.E. & HENRY, D. (2005). Integration of optical and radar classifications for mapping

pasture type in Western Australia. *IEEE Transactions on Geoscience and Remote Sensing*, 43(7), 1665-1681.

HOLMGREN, M., & PERSSON, A. (2004). Identifying species of individual trees using airborne laser scanner. *Remote Sensing of Environment*, 90(4), 415-423. Available online: http://www.gisdevelopment.net/application/environment/ffm/mi08_324.htm

HOLOPAINEN, M., HAAPANEN, R., KARJALAINEN, M., VASTARANTA, M., HYYPPÄ, J., YU, X., TUOMINEN, S. & HYYPPÄ, H. (2010). Comparing accuracy of airborne laser scanning and TerraSAR-X radar images in the estimation of plot-level forest variables. *MDPI Remote Sensing Journal*, 2, 432-445.

HOMER, C., DEWITZ, J.,FRY, J., COAN, M.,HOSSAIN, N., LARSON, C., HEROLD, N.,MCKERROW, A., VANDRIEL, J. & WICKHAM, J. (2007). Completion of the 2001 national land cover database for the conterminous United States. *Photogrammetric Eng. Remote Sensing.,* 73 (4), 337–341.

HOUGHTON, J. T. & Y. DING (2001). Climate Change 2001: The Scientific Basis, Cambridge University Press, Cambridge.

HOUGHTON, R. A., LAWRENCE, K. T., HACKLER, J. L. & BROWN, S. (2001). The spatial distribution of forest biomass in the Brazillian Amazon: a comparison estimates. *Global Change Biology*, 7(7), 731-746.

HOUGHTON, R.A. (2005). Aboveground forest biomass and the global carbon balance. *Global Change Biology*, 11(6), 945-958.

HUANG, K., PANG, Y., SHU, Q. & FU, T. (2010). Regional aboveground forest biomass estimation using airborne and spaceborne LiDAR fusion with optical data in the Southwest of China. *18th International Conference on Geoinformatics*, 2010, 1-6.

HUSCH, B., BEERS, T.W. and KERSHAW, J.A.J. (2003). Forest Mensuration, 4th edition., Hoboken, New Jersey, John Wiley & Sons.

HUSCH, B., MILLER, C. & BEERS, T. (1972). Forest mensuration. 2th ed. Ronald Press Company, New York.

HUSSIN., Y.A. , REICH, R.M. & HOFFER, R.M. (1991). Estimating slash pine biomass using radar backscatter. *IEEE Transactions of Geoscience and Remote Sensing*, 29(3). 427-431.

HYYPPÄ, J. & INKINEN, M. (1999). Detecting and estimating attributes for single trees using laser scanner. *Photogrammetric Journal of Finland*, 16, 27-42.

HYYPPÄ, J., SCHARDT, M., HAGGRÉN, H., KOCH, B., LOHR, U. SCHERRER, H.U., PAANANEN, R., LUUKKONEN, H., ZIEGLER, M., HYYPPÄ, H., PYYSALO, U., FRIEDLÄNDER, H., UUTTERA, J., WAGNER, S., INKINEN, M., WIMMER, A., KUKKO, A., AHOKAS, A. AND KARJALAINEN, M.

(2001). HIGH-SCAN: The first European-wide attempt to derive single-tree information from laser scanner data. *The Photogrammetric Journal of Finland*, 18, 43-53.

IGCOS (2004). Integrated Global Carbon Observation Theme: A strategy to realise a coordinated system of Integrated Global Carbon Cycle Observations. IGOS 2004, Integrated Global Carbon Observation System, Implementation Plan, Draft 1.0. Available online: http://www.fao.org/gtos/doc/ECVs/ECV-T12-biomass-ref02-IGCO- implementation.pdf

IIASA (INTERNATIONAL INSTITUTE FOR APPLIED SYSTENS ANALYSIS) (2009). GeoWiki Project: Help Improve Global Land Cover. *International Institute for applied Systems Analysis*. http://geo-wiki.org/

IMHOFF, M.L. (1995a). A theoretical analysis of the effect of forest structure on synthetic aperture radar backscatter and the remote sensing of biomass. *IEEE Transactions on Geoscience and Remote Sensing*, 33(2), 341-352.

IMHOFF, M.L. (1995b). Radar backscatter and biomass saturation: ramifications for global biomass inventory. *IEEE Transactions Geoscience and Remote Sensing Symposium*, 33(2), 511-518.

INFOTERRA (2009). TerraSAR-X Services -Image Product Guide, available online: http://www.infoterra.de/asset/cms/file/20091208_tsxx-itd-ma-0009_tsx-productguide_i1.00.pdf

INFOTERRA (2001). Inversion of a lidar waveform model for forest biophysical parameter estimation. *IEEE Geoscience and Remote Sensing Letters*, 3(1), 49-53. Available online: http://www.infoterra.de/terrasar-x-satellite

IPCC (2007). Climate Change 2007: Climate Impacts, adaptation and vulnerability: summary of policymakers, working group, contribution to the Intergovernmental Panel on Climate Change Fourth Assessment Report.

JACQUEMOUD, S. & USTIN, S.L. (2003). Application of radiative transfer models to moisture content estimation and burned land mapping. *Proc. 4th International Workshop on Remote Sensing and GIS Applications to Forest Fire Management*, Ghent, Belgium, 3-12.

JÄGER, M., NEUMANN, M., GUILLASO, S. & REIGBER, A. (2007). A self-initializing PolInSAR classifier using interferometric phase differences. *IEEE Transactions of Geoscience and Remote Sensing*, 45(11), 3503–3518.

JENKINS, J.C., CHOJNACKY, D.C., HEATH, L.S. & BIRDSEY, R.A. (2003). National-scale biomass estimators for United States Tree Species. *Forest Science*, 49, 12-35.

JENSEN, J.R. (2007). Remote Sensing of the Environment: An Earth Resource Perspective, 2nd Edition. Upper Saddle River, Nj: Prentice Hall.

JONFORSEN, S.G., FOLKESSON, K., HALLBERG, B., ULANDER, L.M.H. (2007). Effects of Forest Biomass and Stand Consolidation on P-Band Backscatter. *IEEE Geoscience and Remote Sensing Letters*, 4, 669-673.

KASILINGAM, D. CHEN, H., SHULER, D. L. & LEE, J. S. (2000). Ocean surface slope spectra from polarimetric SAR images of the ocean surface. *Proceedings of International Geoscience and Remote Sensing Symposium 2000*, 1110-1112.

KASISCHKE, E.S. (1992). Monitoring changes in aboveground biomass in loblolly pine forests using multi-channel synthetic aperture radar data. PhD dissertation, The University of Michigan.

KASISCHKE, E.S., BOURGEAU-CHAVEZ, L.L., CHRISTENSEN, N.L., JR. & HANEY, E. (1994). Observation on the sensitivity of ERS-1 SAR image intensity to changes in above-ground biomass in young loblolly pine forests. *International Journal of Remote Sensing*, 15, 3-16.

KASISCHKE E.S. & CHRISTENSEN N.L.J. (1990). Connecting forest ecosustem and microwave backscatter models. *International Journal of Remote Sensing*, 11(7), 1277-1298.

KASISCHKE, E.S., CHRISTENSEN, N.L.J., JR., BOURGEAU-CHAVEZ, L.L. (1995). Correlating radar backscatter with components of biomass in loblolly pine forests. *IEEE Transactions Geoscience and Remote Sensing Symposium*, 33(3), 643-659.

KASISCHKE, E.S., MELACK, J. M. & CRAIG DOBSON, M. (1997). The use if imaging radars for ecological applications - A review. *Remote Sensing of Environment*, 59(2), 141-156.

KATSCH, C. & STOCKER, M. (2000). Automatic determination of stand heights from aerial photography using digital photogrammetric systems. Allgemeine Forst und Jagdzeitung, 171, 74-80.

KELLNDORFER, J.M., DOBSON, C., VONA, J & CLUTTER, M (2003). Toward precision forestry: Plot-level parameter retrieval for Slash Pine plantations with JPL AIRSAR. *IEEE Transactions on Geoscience and Remote Sensing*, 41(7), 1571-1582.

KELLNDORFER, J.M., PIERCE, L.E., DOBSON, M.C. & ULABY, F.C. (1998). Toward consistent regional-to-global-scale vegetation characterization using orbital SAR systems. *IEEE Transactions on Geoscience and Remote Sensing*, 36(5), 1396-1411.

KELLNDORFER, J.M., WALKER, W., PIERCE, L., DOBSON, C., FITES, J.A., HUNSAKER, C.,VONA, J. & CLUTTER, M. (2004). Vegetation height estimation from shuttle radar topography mission and national elevation datasets. *Remote Sensing of Environment*, 93(3), 339–358.

KEMPENEERS, P., SEDANO, F., SEEBACH, L., STROBL, P. & SAN-MIGUEL-AYANZ, J. (2011). Data fusion of different spatial resolution remote sensing

images applied to forest-type mapping. *IEEE Transactions on Geoscience and Remote Sensing*, 99, 1-10.

KETTERINGS, Q. M., COE, R., VAN NOORDWIJK, M., AMBAGAU, Y. & PALM, C. A. (2001). Reducing uncertainty in the use of allometric biomass equations for predicting above-ground tree biomass in mixed secondary forests. *Forest Ecology and Management*, 146 (1-3), 199-209.

KINI, A. & S. C. POPESCU S. C. (2004). TreeVaW: a versatile tool for analyzing forest canopy LIDAR data: A preview with an eye towards future. ASPRS 2004 Fall Conference, Kansas City , Missouri.

KOHL, M. & HUSSENDORFER, E. (2000). Conversion of forests: approaches for describing the potential extension of regeneration by means of remote sensing and GIS. Allgemeine Forst und Jagdzeitung, 171, 102-109.

KOKALY, R.F., DESPAIN, D.G., CLARK, R.N., LIVO, K.E. (2003). Mapping vegetation in Yellowstone National Park using spectral feature analysis of AVIRIS data. *Remote Sensing Environment*, 84, 437-456.

KONSTINSKI, A.B. & BOERNER, W.M. (1986). On foundations of radar polarimetry. *IEEE Transaction on Antennas and Propagation*, 34, 1395-1404.

KRAENZEL, M., CASTILLO, A.,MOORE, T & POTVIN, C. (2003). Carbon storage of harvest-age teak (Tectona grandis) plantations, Panama. *Forest Ecology and Management*, 146 (1-3), 213-225.

KRAUS, K. & MIKHAIL (1972). Linear least squares interpolation. *Photogrammetric Engineering*, 38, 1016 – 1029.

KRAUS, K. & PFEIFER, N. (1998). Determination of terrain models in wooded areas with airborne laser scanner data. *ISPRS Journal of Photogrammetry & Remote Sensing*, 53, 193-203.

KRIEGER, G., HAJNSEK, I., PAPATHANASSIOU, K., EINEDER, M., YOUNIS, M., DE ZAN, F., LOPEZ-DEKKER, P., HUBER, S., WERNER, M., PRATS, P., FIEDLER, H., FREEMAN, A., ROSEN, P., HENSLEY, S., JOHNSON, W., VEILLEUX, L., GRAFMUELLER, B., WERNINGHAUS, R., BAMLER, R & MOREIRA, A. (2010). TanDEM-L: A mission for monitoring Earth system dynamics with high resolution SAR interferometry. *EUSAR 2010*, 506-509.

KUGLER, F., CAYCOYA, A.T., HAJNSEK, I & PAPATHANASSIOU, K. (2011). Forest Characterisation by Means of TerraSAR-X and TanDEM-X Polarimetric Interferometric Data. *Polinsar 2011*, Frascati, Italy.

KUMAR, L., SCHMIDT, K.S., DURY, S., SKIDMORE, A.K. (2001). Review of hyperspectral remote sensing and vegetation, Science In: Van Der Meer FD, De Jong S.M. (eds) Imaging Spectrometry: basic principles and prospective applications. Kluwer, Dordrecht, The Netherlands.

KUPLICH, T.M., CURRAN, P.J., ATKINSON, P.M. (2003). Relating SAR image texture and backscatter to tropical forest biomass. *IEEE International Geoscience and Remote Sensing Symposium*, 4, 2872-2874.

KWOUN, O.-I. CUDDY, D. KON LEUNG CALLAHAN, P. CRICHTON, D. MATTMANN, C.A. FREEBORN, D. (2010). A Science Data System approach for the DESDynI mission. *IEEE Radar Conference 2010*, 1265-1269.

LACLAU, P. (2003). Biomass and carbon sequestration of ponderosa pine plantations and native cypress forests in northwest Patagonia. *Forest Ecology and Management*, 180(1-3), 317- 333.

LAW, B.E., CAMPBELL, J.L., SUN, O., VAN INGEN, C. & VERMA, S. (2008).Terrestrial Carbon Observations: Protocols for Forest Sampling and Data Submission. FAO, GTOS Publication Series, 52, Rome, 79.

LE TOAN, T., BEAUDOIN, A., RIOM, J. & GUYON, D. (1992). Relating forest biomass to SAR data. *IEEE Transactions of Geoscience and Remote Sensing*, 30(2), 403-411.

LE TOAN, T., QUEGAN, S., WOODWARD, I., LOMAS, M. DELBART, N & PICARD, G. (2004). Relating radar remote sensing of biomass to modeling of forest carbon budgets. *Climate Change*, 67, 379-402.

LEAN, J.L. & RIND, D. H. (1999). Evaluating sun-climate relationships since the Little Ice Age. *Journal of Atmospheric and Solar-Terrestrial Physics*, 61(1), 25-36.

LEAN, J.L. & RIND, D. H. (2008). How natural antropogenic influences alter global and regional surface temperature: 1889 to 2006. *Geophysical Research Letters*, 35, 1-6. Available online: http://pubs.giss.nasa.gov/docs/2008/2008_Lean_Rind.pdf

LECKIE, D. G. & RANSON, K. J. (1998). Forestry applications using imaging radar. *Principles and Applications of Imaging Radar*, 2, 435-509.

LEE J. S. & POTTIER, E. (2009). Polarimetric Radar Imaging: From Basic to Applications, Taylor & Francis Group, 336.

LEE, J. S., SCHULER, D. L. & AINSWORTH, T. L. (2000). Polarimetric SAR data compensation for terrain azimuth slope variation. *IEEE Transactions on Geoscience and Remote Sensing, 38 (5)*, 2153-2163.

LEE, J. S., SCHULER, D. L., AINSWORTH, T. L., KROGAGER, E., KASILINGAM, D. & BOERNER, W.M. (2002). On the estimation of radar orientation shifts induced by terrain slopes. *IEEE Transactions on Geoscience and Remote Sensing*, 40 (1), 30-41.

LEE, J.S., CLOUDE, S.R., PAPATHANASSIOU, K.P., GRUNES, M.R. & WOODHOUSE, I.H. (2003). Speckle filtering & coherence estimation of polarimetric SAR interferometry data for forest application. *IEEE Transactions of Geoscience and Remote Sensing*, 41(10), 2254–2263.

LEFSKY, M.A., COHEN, W.B., ACKER, S.A., PARKER, G.G., SPIES, T.A., & Harding, D. (1999). Lidar remote sensing of the canopy structure and biophysical properties of Douglas-fir western hemlock forests. *Remote Sensing of Environment*, (70), 339-361.

LEFSKY, M.A., COHEN, W.B., HARDING, D.J., PARKER, G.G., ACKER, S.A. & GOWER, S.T. (2002). Lidar remote sensing of above-ground biomass in three biomes. *Global Ecology and Biogeography*, 11(5), 393-399.

LEMMON, P.E. (1956). A spherical densiometer for estimating forest overstory density. *For Sci* 2(4),314–320.

LETOAN, T., BEAUDOIN, A, RIOM, J. & GUYON, D. (1992). Relating forest biomass to SAR data. *IEEE Transactions of Geoscience and Remote Sensing*, 30, 403-411.

LI, J.Y., GOODENOUGH, D.G. & DYK, A. (2005). Mapping Relative Water Content in Douglas-Fir with AVIRIS and a Canopy Model. *IEEE International Geoscience and Remote Sensing Symposium*, Seoul, Korea, 5, 3572-3574.

LI, M., QU, J.J. & XIANJUN H. (2009). Estimating aboveground biomass for different forest types based on Landsat TM measurements. *17th International Conference on Geoinformatics*, 1-6.

LIM, K.S. & TREITZ, P.M. (2004). Estimation of above ground forest biomass from airborne discrete return laser scanner data using canopy-based quantile estimators. *Scandinavian Journal of Forest Research*, 19, 558-570.

LIM, K.S., TREITZ, P.M., WULDER, M., ST-ONGE, B. & FLOOD, M. (2003). LiDAR remote sensing of forest structure. *Progress in Physical Geography*, 27, 88−106.

LIM, K.S.; TREITZ, P.M.; BALDWIN, K.; MORRISON, I. & GREEN, J. (2003). Lidar remote sensing of biophysical properties of tolerant northern hardwood forests. *Canadian Journal of Remote Sensing*, 29, 658-678.

LINDQUIST, E.J., HANSEN, M.C., ROY, D.P. & JUSTICE, C.O. (2008). The suitability of decadal image data sets for mapping tropical forest cover change in the Democratic Republic of Congo: Implications for the global land survey. *International Journal of Remote Sensing*, 29(24), 7269-7275.

LOCKWOOD, M. & FROHLICH, C. (2008). Recent oppositely directed trends in solar climate forcings and the global mean surface air temperature: Different reconstructions of the total solar irradiance variation and dependence on response time scale. *Proceedings of the Royal Society*, 464 (2094), 1367-1385.

LOKEWOOD, M. (2008). Recent changes in solar outputs and the global mean surface temperature : Analysis of contributions to global mean air surface temperature rise. *Proceedings of the Royal Society*, 464(2094), 1381-1404.

LOPEZ-SANCHEZ, J.M., BALLESTER-BERMAN, J.D. & HAJNSEK, I. (2011). First results of rice monitoring practices in spain by means of time series of TerraSAR-X dual-Pol images. *IEEE J. Sel. Topics Appl. Earth Observ.Remote Sens. (JSTARS)*, 4(2), 412–422.

LOSI, C.J., SICCAMA, T.G., CONDIT, R. & MORALES, J. E. (2003). Analysis of alternative methods for estimating carbon stock in young tropical plantations. *Forest Ecology and Management*, 184(1-3), 355-368.

LUCAS, R., ARMSTON, J., FAIRFAX, R., FENSHAM, R., ACCAD, A., CARREIRAS, J., KELLEY, J., BUNTING, P., CLEWLEY, D., BRAY, S., METCALFE, D., DWYER, J., BOWEN, M., EYRE, T., LAIDLAW, M. & SHIMADA, M. (2010). An Evaluation of the ALOS PALSAR L- Band Backscatter- Above Ground Biomass Relationship Queensland, Australia: Impacts of Surface Moisture Condition and Vegetation Structure. *IEEE Journal of Selected Topics in Applied Earth Observations and Remote Sensing*, 3(4), 576-593.

LUCAS, R.M. & ARMSTON, J.D. (2007). ALOS PALSAR for characterizing wooded savannas in Northern Australia. *IEEE International Geoscience and Remote Sensing Symposium 2007*,3610-3613.

LUCAS, R.M., ARMSTON, J., CARREIRAS, J., NUGROHO, N., CLEWLEY, D. & DE GRANDI, F. (2010). Advances in the integration of ALOS PALSAR and Landsat sensor data for forest characterisation, mapping and monitoring. *IEEE International Geoscience and Remote Sensing Symposium*, 1851-1854.

LUMSDON, P., CLOUDE, S.R., WRIGHT, G. (2005). Polarimetric Classification of Land Cover for the Glen Affric Radar Project. *IEE Proceedings Radar,Sonar and Navigation*, 152, 404-412.

LUMSDON, P., MERCER, B. & ZHANG, Q.P. (2008). Digital Elevation Estimation of Seminatural Forests Using Polarimetric Interferometric SAR. *Proceedings of 2nd ALOS-PI Workshop*, Rhodes.

MACRAE, F. (1980). The native pinewoods of Glen Affric. *Aboriculture Journal*,4, 1-10.

MAITRE, H. (2008). Processing of Synthetic Aperture Radar Images, John Wiley & Sons, Inc, USA, 12.

MAJER, C.A., ALBAUGH, T.J., ALLEN, H.L., & DOUGHERTY, P.M. (2004). Respiratory carbon use and carbon storage in mid-rotation loblolly pine (Pinus taeda L.) plantations: the effect of site resources on the stand carbon balance. *Global Change Biology*,10, 1335-1350.

MANIATIS, D., SAINT-ANDRE L, TEMMERMAN M, MALHI Y. & BEECKMAN H. (2011). The potential of using xylarium wood samples for wood density

calculations: a comparison of approaches for volume measurement and preliminary ecological results. *iForest 4*, 150-159.

MAST, J.N., VEBLEN, T.T. & HODGSON, M.E. (1997). Tree invasion within a pine/grassland ecotone: An approach with historic aerial photography and GIS modelling. *Forest Ecology and Management*, 93, 181-194.

MAYAUX, P., HOLMGREN, P., ACHARD, F., EVA, H., STIBIG, H. & BRANTHOMME, A. (2005). Tropical forest cover change in the 1990s and options for future monitoring. *Philosophical Transactions of the Royal Society B-Biological Sciences*, 360(1454), 373-384.

MCCATHY, J. J. & CANZIANI, O.F. et al. (2001). Climate Change 2001: Impacts, adaptation, and vulnerability. Cambridge University Press, Cambridge.

MCDONALD, K.C. (1991). Modeling microwave backscatter from canopies. PhD. Dissertation. University of Michigan.

MCGAUGHEY, R. J. & CARSON, W.W. (2003). Fusing LIDAR data, photographs, and other data using 2D and 3D visualization techniques, Applications and Visualization – Making the Connection, October 28-30, 2003; Charleston, South Carolina: Bethesda, MD: *American Society for Photogrammetry and Remote Sensing*. 16-24.

MCNEILL, S.J., PAIRMAN, D., BELLISS, S.E., DALLEY, D. & DYNES, R. (2010). Robust estimation of pasture biomass using dual-polarisation TerrASAR-X imagery. *IEEE International Geoscience and Remote Sensing Symposium* , 3094-3097.

MEANS, J.E., ACKER, S.A., BRANDON, J.F., RENSLOW, M., EMERSON, L., HENDRIX, C.J. (2000). Predicting forest stand characteristics with airborne scanning lidar. *Photogrammetric Engineering and Remote Sensing,* 66, 1367−1371.

MEANS, J.E., ACKER, S.A., HARDING, D.J., BLAIR, J.B., LEFSKY, M.A., COHEN, W.B., HARMON, M.E. & MCKEE, W.A. (1999). Use of large-footprint scanning airborne lidar to estimate forest stand characteristics in the Western Cascades of Oregon. *Remote Sensing of Environment*, 67(3), 298-308.

METTE, T., PAPATHANASSIOU, K.P., HAJNSEK, I. & ZIMMERMANN, R. (2002). Forest Biomass Estimation using Polarimetric SAR Interferometry. *IEEE International Geoscience and Remote Sensing Symposium*, Toronto, Canada.

METZ, B. & DAVIDSON, O.(2001). Climate Change 2001: Mitigation. Cambridge University Press, Cambridge.

MIDDLETON, N. (1999). The Global Casino: An Introduction to Environmental Issues, Second Edition, London, Arnold.

MILLER, J.R., WU, J.Y., BOYER, M.G., BELANGAR, M & HARE, E. W. (1991). Seasonal patterns in leaf reflectance red-edge characteristics. *International Journal of Remote Sensing*, 12, 1509-1523.

MIRIK, M., NORLAND, J.E., CRABTREE, R.L. & BIONDINI, M.E. (2005). Hyperspectral one-meter-resolution remote sensing in yellowstone national park, wyoming I, Forage nutritional values. *Rangeland & Ecology Management*, 58(5), 452-458.

MITCHARD, E.T.A., SAATCHI, S.S. WOODHOUSE, I.H., NANGENDO, G., RIBEIRO, N.S., WILLIAMS, M., RYAN, C.M., LEWIS, S.L., FELDPAUSH, T.R., & MEIR, P. (2009). Using satellite radar backscatter to predict above-ground woody biomass: A consistent relationship across four different African landscapes. *Geophysical Research Letters*, 36, L23401.

MOGHADDAM, M. & SAATCHI, S. (1995). Analysis of scattering mechanisms in SAR imagery over boreal forest: results from BOREAS' 93. *IEEE Transactions on Geoscience and Remote Sensing*, 33(5), 1290-1296.

MOGHADDAM, M., DUNGAN, J.L. & ACKER, S. (2002). Forest variable estimation from fusion of SAR and multispectral optical data. *IEEE Transactions on Geoscience and Remote Sensing*, 40(10), 2176-2187.

MONTAGNINI, F & PORRAS, C. (1998). Evaluating the role of plantation as carbon sinks: an example of an integrative approach from the humid tropics. *Environmental Management*, 22, 459-470.

MONTAGU, K.D., DUTTMER, K., BARTON, C.V.M. & COWIE, A.L. (2005). Developing general allometric relationships for regional estimates of carbon sequestration - an example using Eucalyptus pilularis from seven contrasting sites. *Forest Ecology and Management*, 204(1), 115-129.

MONTGOMERY, D.,& PECK, E. (1992). Introduction to linear regression analysis. New York: Wiley.

MORSDORF, F. (2006). LIDAR Remote Sensing for Estimation of Biophysical Vegetation Parameters, Ph.D. Thesis, University of Zurich, 12.

MORSDORF, F. NICHOL, C., MALTHUS, T & WOODHOUSE, I. (2009). Assessing forest structural and physiological information content of multi-spectral LiDAR waveforms by radiative transfer modelling. *Remote Sensing of Environment*, 113(10), 2152-2163.

MORSDORF, F., MEIER, E., KÖTZ, B., ITTEN, K.I., DOBBERTIN, M., ALLGÖWER, B. (2004). LIDAR-based geometric reconstruction of boreal type forest stands at single tree level for forest and wildland fire management. *Remote Sensing of Environment*, 3(92), 353-362.

MRV (Measurement, Reporting & Verification) (2011). Measurement, Reporting & Verification Framework Document: With reference to safeguards information

and monitoring of PAMS. Available online: http://vietnam-redd.org/Upload/CMS/Content/SWG.MRV/MRV%20Framework%20Document_V1_Draft2.pdf

MUTANGA, O.S. & SKIDMORE, K. (2004). Hyperspectral band depth analysis for a better estimation of grass biomass (Cenchrus ciliaris) measured under controlled laboratory conditions. *International Journal of Applied Earth Observation and Geoinformation*, 5(2), 87-96.

NAESSAT, E. & OKLAND, T. (2002). Estimating tree height and tree crown properties using airborne scanning laser in a boreal nature reserve. Remote Sensing of Environment, 79, 105-115.

NAESSAT, E. (2002). Predicting forest stand characteristics with airborne scanning laser using a practical two-stage procedure and field data. *Remote Sensing of Environment*, 80 (1), 88-99.

NAKASHIZUKA, T., KATSUKA, T. & TANAKA, H. (1995). Forest canopy structure analyzed by using aerial photographs. *Ecological Research*, 10, 13-18.

NEEFF, T., DUTRA, L.V., DOS SANTOS, J.R., FREITAS, C.D. & ARAUJO, L.S. (2005). Tropical forest measurement by interferometric height modeling and P‐band radar backscatter. *Forest Science* 51(6), 585‐594.

NELSON, R., KRABILL, W. & MACLEAN, G. (1984). Determining forest canopy characteristics using airborne laser data. *Remote Sensing of Environment*, 15, 201−212.

NELSON, R., KRABILL, W. & TONELLI, J. (1988). Estimating forest biomass and volume using airborne laser data. *Remote Sensing of Environment*, 24, 247−267.

NELSON, R., SHORT, A. & VALENTI, M. (2004). Measuring biomass and carbon in Delaware using an airborne profiling lidar. *Scandinavian Journal of Forest Research*, 19, 500−511.

NIGHTINGALE, J.M., PHINN, S.R., & HELD, A.A. (2004). Ecosystem process models at multiple scales for mapping tropical forest productivity. *Progress in Physical Geography,* 28(2), 241-281.

NIX, S. (1997). D.B.H. (Diameter Breast Height). Available online: http://forestry.about.com/cs/glossary/g/dbh.htm

NOVO, D.M., E. & DA SILVA, M.L.S. (1995). Combined analysis of SAR C and TM/Landsat data in the assessment of aquatic vegetation changes in the Tucurui reservoir, Para State, Brazilian Amazon. *IEEE International Geoscience and Remote Sensing Symposium*, 1242-1245.

OGILVY, T. (2004). Regeneration ecology of broadleaved trees in Caledonian Forest, PhD Thesis, The University of Edinburgh.

OLANDER, L.P., GIBBS, H. K., STEININGER, M., SWENSON, J.J. & MURRAY, B.C., (2008). Reference scenarios for deforestation and forest degradation in support of REDD: A review of data and methods. *Environmental Research Letters*, 3(2): 025011.

OLIVER, C.J. & QUEGAN, S. (1998). Understanding Synthetic Aperture Radar Images. New York: Artech House.

ONGE, B.S., HU, Y. & VEGA, C. (2008). Mapping the height and above-ground biomass of a mixed forest using lidar and stereo ikonos images. *International Journal of Remote Sensing*, 29(5), 1277-1294.

OSBORNE, S.L., SCHEPERS, J.S., FRANCIS, D.D & SCHLEMMER, M.R. (2002). Use of spectral radiance to estimate in-season biomass and grain yield in nitrogen- and water- stressed corn. *Crop Science*, 42 (1-2), 165-175.

OVERMAN, J.P.M, WITTE, H.J.L. & SALDARRIAGGE, J.G. (1994). Evaluation of regression models for above-ground biomass determination in Amazon rainforest. *Journal of Tropical Ecology*, 10, 207-218.

PAIRMAN, D., MCNEILL, S., BELLISS, S., DALLEY, D. & DYNES, R. (2008). Pasture monitoring from polarimetric TerraSAR-X Data. *IEEE International Geoscience and Remote Sensing Symposium*, 820-823.

PAPATHANASSIOU, K. & CLOUDE, S.R. (2001) Single-baseline polarimetric SAR interferometry. *IEEE Transactions of Geoscience and Remote Sensing*, 39(11), 2352–2363.

PAPATHANASSIOU, K., KUGLER, F., KIM, J.S., HAJNSEK, I., PARRELLA, G. & KRIEGER, G. (2011). Exploring the Potential Pol-InSAR Techniques at X-Band: First Results & Experiments from TanDEM-X, *Polinsar 2011*, Frascati, Italy.

PATENAUDE, G., MILNE, R. & DAWSON, T.P. (2005). Synthesis of remote sensing approaches for forest carbon estimation: Reporting to the Kyoto Protocol. *Environmental Science and Policy*, 8(2), 161-178.

PEKKARINEN, A., REITHMAIER, L. & STROBL, P. (2009). Pan-European forest/nonforest mapping with Landsat ETM+ and CORINE land Cover 2000 data. *Journal of Photogrammetric and Remote Sensing*, 64(2), 171–183.

PERRING, F.H. & WALTERS, S.M. (1962). Atlas of the British Flora. Thomas Nelson & Sons, London.

PETZOLD, B. P. R and STOSSEL, W. (1999). Laser scanning - surveying and mapping agencies are using a new technique for the derivation of digital terrain models. *Journal of Photogrammetric and Remote Sensing,* 54, 95-104.

PITT, D.G., RUNESSON, U., BELT, F.W. (2000). Application of large- and medium-scale aerial photographs to forest vegetation management: A case study. *Forestry Chronicle*, 76, 903-913.

PLUMMER, S., ARINO, O., SIMON, M. & STEFFEN, W. (2006). Establishing a Earth Observation product service for the terrestrial carbon community: The GlobCarbon Initiative. *Mitigation and Adoption Strategies for Global Change*, 11, 97-111.

POPESCU, S.C., WYNNE, R.H. & SCRIVANI, J.A. (2004). Fusion of small-footprint lidar and multispectral data to estimate plot-level volume and biomass in deciduous pine forests in Virginia, USA. *Forest Science*, 50(4), 551-565.

PORDER, S., ASNER, G.P. & VITOUSEK, P.M. (2005). Ground-based and remotely sensed nutrient availability across a tropical landscape, *Proceedings of the National Academy of Sciences*, 102, 10909-10912.

POTTIER, E., SCHULER, D.L., LEE, J. S. & AINSWORTH, T.L. (1999). Estimation of the terrain surface azimuth/range slopes using polarimetric decomposition of POLSAR data. *Proceedings of International Geoscience and Remote Sensing Symposium*, 2212-2214.

PRAKS, J. KUGLER, F., PAPATHANASSIOU, K. & HALLIKAINEN, M. (2007). Forest height estimates for boreal forest using L- and X-band POLInSAR and HUTSCAT scatterometer. *POLINSAR 2007*.

PRICE, J.C. (1992). Variability of high resolution crop reflectance spectra. *International Journal of Remote Sensing*, 14, 2593-2610.

PRICE, M.F. & BUTT, N. (2000). Forests in sustainable mountain development: a state of knowledge report for CAB International, Wallingford.

PYATT, D.G. (1995). Notes on site factors at Affric, Fort Augustus Forest District. *Unpublished report*, Forest Research, Roslin.

PYATT, D.G., RAY, D. & FLETCHER, J. (2001). Ecological Site Classification for forestry in Great Britain. *Forestry Commission Bulletin 124*. Forestry Commission, Edinburgh.

RAMANKUTTY, N., GIBBS, H.K., ACHARD, F., DEFRIES, R., FOLEY, J.A. & HOUGHTON, R.A. (2007). Challenges to estimating carbon emissions from tropical deforestation. *Global Change Biology*, 13, 51–66.

RANSON, K. J. & SUN, G. (1994). Mapping biomass of a northern forest using multifrequency SAR data. *IEEE Transactions on Geoscience and Remote Sensing*, 32(2), 388-396.

RAUSTE, Y., LONNQVIST, A., MOLINIER, M., AHOLA, H. & HAME, T. (2007). ALOS PALSAR data in boreal forest monitoring and biomass mapping. *Proceedings of 1st Joint PI Symposium of ALOS Data Nodes*, Kyoto, Japan.

REDD (2009). The history of REDD policy, Carbon Planet White Paper. Available online:http://unfccc.int/files/methods_science/redd/application/pdf/the_history_of_redd_carbon_planet.pdf

RENSLOW, M.S., GREEFIELD, P. & GUAY, T. (2000). Evaluation of Multi-Return LIDAR for Forestry Applications. Report prepared for The Inventory and Monitoring Steering Committee of the USDA Forest Service. US Department of Agriculture Forest Service – *Engineering. Remote Sensing Applications Center*, November .

RIANO, D., VAUGHAN, P., CHUVIECO, E., ZARCO-TEJADA, P.J., & USTIN, S.L. (2005). Estimation of fuel moisture content by inversion of radiative transfer models to simulate equivalent water thickness and dry matter content: analysis at leaf and canopy level. *IEEE Transactions on Geoscience and Remote Sensing*, 43, 819-825.

RIGNOT, E., WAY, J., WILLIAMS, C., VIERECK, L. (1994). Radar estimates of aboveground biomass in boreal forests of interior Alaska. *IEEE Transactions Geoscience and Remote Sensing Symposium*, 32(5), 1117-1124.

RODWELL, J. S. (1991). British Plant Communities. I, Woodlands and Shrub. Cambridge University Press, Cambridge.

ROSENQVIST, A., SHIMADA, M. & MILNE, A.K. (2007). The ALOS Kyoto & Carbon Initiative. *IEEE International Geoscience and Remote Sensing Symposium*, 3614-3617.

ROSENQVIST, A., SHIMADA, M., CHAPMAN, B., FREEMAN, A., DE GRANDI, G., SAATCHI, S. & RAUSTE, Y. (2000). The Global Rain Forest Mapping project - review. *International Journal of Remote Sensing*, 21(6-7), 1375-1387.

ROSENQVIST, A., SHIMADA, M., ITO, N., & WATANABE, M. (2007). ALOS PALSAR: A pathfinder mission for global-scale monitoring of the environment. *IEEE Transactions on Geoscience and Remote Sensing*, 45(11), 3307-3316.

ROSSO, P.H., USTIN, S.L.& HASTINGS, A. (2005). Mapping marshland vegetation of San Francisco Bay, California using hyperspectral data. *International Journal of Remote Sensing*, 26, 5169-5191.

SAINT-ANDRE, L. (2005). Age-related equations for above and below ground biomass of a Eucalyptus hybrid in Congo. *Forest Ecology and Management*, 205(1-3),199-214.

SAMALCA, I.K. (2007). Estimation of Forest Biomass and its Error: A case in Kalimantan, Indonesia, Master of Science, University of Southampton.

SANCHEZ-AZOFEIFA, G.A., CASTRO-ESAU, K.L., KURZ, W.A. & JOYCE, A. (2009). Monitoring carbon stocks in the tropics and the remote sensing operational limitations: From local to regional projects. *Ecological Application*, 480-494.

SARMIENTO, G., PINILLOS, M. & GARAY, I. (2005). Biomass variability in tropical american lowland rainforests. *Ecotropicos*, 18(1), 1-20.

SAUER, S., KUGLER, F., SEUNG-KUK LEE & PAPATHANASSIOU, K. (2010). Polarimetric decomposition for forest biomass retrieval. *IEEE International Geoscience and Remote Sensing Symposium (IGARSS)*, 4780-4783.

SCAFETTA, N. (2006). Phenomenological solar signature in 400 years of reconstructed Northern Hemisphere temperature control, Geophysical Research Letters. Available online: http://www.acrim.com/Reference%20Files/Sun%20&%20Global%20Warming_GRL_2006.pdf

SCHOENE, D. & NETTO, M. (2005). The Kyoto Protocol: What does it mean for forests and forestry? *Unasylva* 222, 56(3), Forests, Climate and Kyoto.

SCHREUDER, H., GREGOIRE, T. & WOOD, G. (1993). Sampling methods for multiresource forest inventory. Wiley, New York.

SCHULER, D.L., LEE, J. S. & DE GRANDI, G. (1996). Measurement of topography using polarimetric SAR images. *IEEE Transactions on Geoscience and Remote Sensing*, (5), 1266-1277.

SEGURA, M & KANNINEN, M. (2005). Allometric models for tree volume and total AGB in a tropical humid forest in Costa Rica. *Biotropica*, 37(1), 2-8.

SHAW, H. & TIPPING, R. (2003). Allt an laghair, East Glen Affric: Recent woodland history from pollen analysis. In : The quaternary of Glen Affric and Kintail, University of Stirling, 105-110.

SMITH, R.J. (1993). Logarithmic transformation bias in allometry. American Journal of Physical *Antrhopology*, 90(2), 215-228.

SMOUT, T.C. (2003). 'To stand in them is to feel the past': pinewoods and birchwoods Wildtrack Publishing, 32-36.

SOLANKI, S. K. & KRIVOVA. N.A. (2003). Can solar variability explain global warming since 1970? Journal of Geophyiscal Research, 108(A5), 1-8. Available online: http://www.mps.mpg.de/homes/natalie/PAPERS/warming.pdf

SOLANKI, S.K., USOSKIN, I.G., KROMER, B., SCHUSSLER, M. & BEER, J. (2004). Unusual activity of the Sun during recent decades compared to the previous 11,000 years, Letters to nature, 431, 1084-1087. Available online: http://cc.oulu.fi/~usoskin/personal/nature02995.pdf

SOLOMON, S., PLATTNER, G.K., KNUTTI, R. & FRIEDLINGSTEIN, P. (2009). "Irreversible climate change due to carbon dioxide emissions. *Proceedings of the National Academy of Sciences*, 106(6), 1704-1709.

STERN, N.H. (2006). Reducing US Greenhouse Gas Emissions: How much at what costs?, McKinsey & Company Report.

STEVEN, H.M. & CARLISLE, A. (1959). The Native Pinewoods of Scotland. Oliver & Boyd, Edinburgh.

STOTT, P. A., JONES, G. S. & MITCHELL, J. F. B. (2003). Do models underestimate the solar contribution to recent climate change? *Journal of Climate*, 16, 4079-4093. Available online: http://climate.envsci.rutgers.edu/pdf/StottEtAl.pdf

SUAREZ, J.C., ONTIVEROS, C., SMITH, S & SNAPE, S (2005). Use of airborne LiDAR and aerial photograph in the estimation of individual tree heights in forestry. *Computers and Geosciences*, 31(2), 253-262.

SUBAK, S. (1999). National inventories of terrestrial carbon sources and sinks: the UK experience. *Climatic Change,* 42, 505–530.

SUN, G. (1990). Radar backscattering modelling of coniferous forest canopies. PhD Dissertation, The University of California.

SUN, G., RANSON, K., MASEK, J., FU, A. & WANG, D. (2007). Predicting tree height and biomass from GLAS data, 10th International Symposium on Physical Measurements and Signatures in Remote Sensing, Davos, Switzerland.

SWANSON, A., ABELSON, L., MANNING, T. & NEWHART, L. (2009). Remote sensing assessment of forest carbon content, Northrop Grumman Aerospace Systems, Northrop Grummond Corporation, Washington, D.C.

TAKESHI, M., MASANOBU, S., OSAMU, I.,MASAE, I., SUZUKI, I. & SATOSHI, N. (2001). Relationships between PALSAR backscattering data and forest above ground biomass in Japan. *IEEE International Geoscience and Remote Sensing Symposium*, 3518 - 3521.

TAN, C.P. MARINO, A.,WOODHOUSE, I.H., CLOUDE, S.R., SUAREZ, J. & EDWARDS, C. (2011a). The Potential of TERRASAR-X in Assessing Forest Above-Ground Biomass in Scotland. *POLINSAR 2011*, ESA ESRIN, Frascati, 24 - 28 January 2011.

TAN, C.P. MARINO, A.,WOODHOUSE, I.H., CLOUDE, S.R., SUAREZ, J. & EDWARDS, C. (2011b). A Comparison Study of Biomass Estimation Using ALOS PALSAR and LiDAR data. *POLINSAR 2011*, ESA ESRIN, Frascati, 24 - 28 January 2011.

TAN, C.P. MARINO, A.,WOODHOUSE, I.H., CLOUDE, S.R., SUAREZ, J. & EDWARDS, C. (2011c). See The Forests With Different Eyes, IEEE International Geoscience and Remote Sensing Symposium, 1405-1408.

TAN, C.P. MARINO, A.,WOODHOUSE, I.H., CLOUDE, S.R., SUAREZ, J. & EDWARDS, C., PERKS, M. (2011d). Potential Use of ALOS PALSAR and LiDAR for Aboveground Biomass Estimation in Glen Affric. *Journal of Plant Ecology and Diversity* (In Review).

TAN, C.P. WOODHOUSE, I.H., SUAREZ, J., EDWARDS, C. & PERKS, M. (2010). The Use of LIDAR Technology For Sustainable Forest Management in Glen Affric. *European Association of Remote Sensing Laboratories*, 365-370.

TAN, C.P., MARINO, A., WOODHOUSE, I.H., CLOUDE, S.R., SUAREZ, J. & EDWARDS, C. (2011). See the forests with different eyes. *IEEE International Geoscience and Remote Sensing Symposium*, 1405 - 1408.

TARR, A.B., MOORE, K.J. & DIXON, P.M., (2005). Spectral reflectance as a covariate for estimating pasture productivity and composition. *Crop Science*, 45(3), 996-1003.

TEMS (TERRESTRIAL ECOSYSTEMS MONITORING SITES) Available online: www.fao.org/gtos/tems/variable_list.jsp.

THENKABAIL, P.S., ENCLONA, E.A., ASHTON, M.S, LEGG, C., MINKO , J.D.D. (2004). Hyperion, IKONOS, ALI and ETM+ sensors in the study of African rainforests, *Remote Sensing of Environment*, 90, 23-43.

THENKABAIL, P.S., NOLTE, C. & LYON, J.G. (2000). Remote sensing and GIS modeling for selection of benchmark research area in the inland valley agroecosystems of West and Central Africa. *Photogrammetric Engineering and Remote Sensing. Africa Applications Special Issue*, 66(6), 755-768.

TICEHURST, C., HELD, A. & PHINN, S. (2004). Integrating JERS-1 imaging radar and elevation models for mapping tropical vegetation communities in Far North Queensland, Australia. *Photogrammetric Engineering and Remote Sensing*, 70(11), 1259-1266.

TREUHAFT, R.N. & SIQUEIRA, P.R. (2000). The Vertical Structure of Vegetated Land Surfaces from Interferometric and Polarimetric Radar. *Radio Science*, 35(1), 141-177.

TREUHAFT, R.N., LAW, B.E. & ASNER, G.P. (2004). Forest attributes from radar interferometric structure and its fusion with optical remote sensing. *Bioscience*, 54, No. 6, 561-571.

ULABY, F. T., SARABANDI, K., MCDONALD, K.C., WHITT, M. & DOBSON, M.C. (1990). Michigan Microwave Canopy Scattering Model (MIMICS). *International Journal of Remote Sensing*, 11, 1223-1253.

ULABY, F., MOORE, R.K., FUNG, A.K. (1986). Microwave Remote Sensing. Active and Passive, 3, Artech House.

ULANDER, LARS M.H., SANDBERG, GUSTAF, SOJA, MACIEJ J. (2011). Biomass retrieval algorithm based on P-band biosar experiments of boreal forest. *IEEE International Geoscience and Remote Sensing Symposium*, 4245-4248.

UNFCCC (2011). Fact sheet: The Kyoto Protocol. Available online: http://unfccc.int/files/press/backgrounders/application/pdf/fact_sheet_the_kyoto_protocol.pdf

UNFCCC (United Nations Framework Convention on Climate Change) (2001). COP-7: The Marrakech Accords. Bonn, Germany.

UNOOSA (United Nations Office for Outer Space Affairs). 2009. General Assembly Resolution 41/65: Principles Relating to Remote Sensing of the Earth from Outer Space. United Nations Office for Outer Space Affairs. Available online: http://www.oosa.unvienna.org/oosa/en/SpaceLaw/gares/html/gares_41_0065.html

USOSKIN, I. G., SCHUSSLER, M., SOLANKI, S. K. & MURSULA, K. (). Solar activity over the last 1150 years: Does it correlate with climate? Available online; http://www.mps.mpg.de/dokumente/publikationen/solanki/c153.pdf

USTIN, S. L. E. (2004). Remote sensing for natural resource management and environmental monitoring, Hoboken etc., Wiley & Sons.

USTIN, S.L., ROBERTS, D.A., GAMON, J.A., ASNER, G.P. & GREEN, R.O. (2004). Using imaging spectroscopy to study ecosystem processes and properties, *BioScience*, 54, 523-534.

VAN ZYL, J.J. (1989). Unsupervised classification of scattering behavior using radar polarimetry data, *IEEE Transactions of Geoscience and Remote Sensing*, 27, 36-45, 1989.

VAN ZYL, J.J., ARII, M. & KIM, Y. (2011). Model-based decomposition of polarimetric SAR covariance matrices constrained for nonnegative eigenvalues,49(9), 3452-3459.

VAZIRABAD Y., KARSLIOGLU, M.O. (2010). Airborne laser scanning data for single tree characteristics detection. *ISPRS Journal of Photogrammetry and Remote Sensing, Istanbul Workshop*, Modelling of Optical Airborne and Space Borne Sensors, WGI/4. Istanbul, Turkey.

VIERGEVER, K.M. (2008). Establishing the sensitivity of Synthetic Aperture Radar to above-ground biomass in wooded savannas, PhD Thesis, The University of Edinburgh.

VIERGEVER, K.M., WOODHOUSE, I.H., MARINO, A., BROLLY, M., STUART, N. (2009). Backscatter and interferometry for estimating above-ground biomass of sparse woodland: A case study in Belize. *IEEE International Geoscience and Remote Sensing Symposium*, 3, 1047-1050.

VIERGEVER, K.M., WOODHOUSE, I.H. & STUART, N. (2007). Backscatter and interferometry for estimating above- ground biomass intropical savanna woodland. *IEEE International Geoscience and Remote Sensing Symposium*, 2346-2349.

WALKER, W.S., KELLNDORFER, J.M & PIERCE, L. (2007). Quality assessment of SRTM C and X band interferometric data: Implications for the retrieval of vegetation canopy height. *Remote Sensing of Environment*, 106, 428-448.

WALLENTIN, G., Spatial Biases in LiDAR-Based Tree Delineation, Map India, Greater Noida, 6.

WANG, Y., DAVIES, F.W. & MELACK, J.M. (1995). The effects of changes on forest biomass on radar backscatter from tree canopies. *International Journal of Remote Sensing*, 16(3), 503-513.

WAPLE, A. M. (1999). The sun-climate relationship in recent centuries: a review. *Progress in Physical Geography*, 23(3), 309-328.

WARING, R H & RUNNING, S W (1998). Forest Ecosystems: Analysis at Multiple Scales, 2nd edition, Academic Press, San Diego, CA.

WIELD, M. (2001). Glen Affric: a case study for biodiversity. *The Horticulturist Spring*: 6-8.

WILLIAMS, M.L., SILMAN, M., SAATCHI, S., HENSLEY, S., SANFORD, M., YOHANNAN, A., KOFMAN, B., REIS, J. & KAMPES, B. (2010). Analysis of geosar dual-band InSAR data for peruvian forest. *IEEE International Geoscience and Remote Sensing Symposium*, 1398-1401.

WILLIAMS, M.L., MILNE, T., TAPLEY, I., REIS, J.J., SANFORD, M., KOFMAN, B. & HENSLEY, S. (2009). Tropical forest biomass recovery using GeoSAR observations. *IEEE International Geoscience and Remote Sensing Symposium*, 4, 173-176

WOLFF, H. & TIPPING, R. (1999). Recent vegetation change within the pinewoods of east Glen Affric for their conservation management. University of Stirling.

WOODHOUSE, I.H. (2006). Predicting backscatter-biomass and height-biomass trends using a macroecology model. *IEEE Transactions on Geoscience and Remote Sensing*, 44(4), 871-877.

WOODHOUSE, I.H., CLOUDE, S., PAPATHANASSIOU, K., HOPE, J., SUAREZ, J., OSBORNE, P. & WRIGHT, G. (2002). Polarimetric interferometry in the Glen Affric project: results & conclusions. *IEEE International Geoscience and Remote Sensing Symposium*, 2, 820-822.

WU, S. T. (1987). Potential application of multipolarization SAR for pine-plantation biomass estimation. *IEEE Transactions on Geoscience and Remote Sensing*, 25, 403-409.

XIAN, G., HOMER, C. & FRY, J. (2009). Updating the 2001 national land cover database land cover classification to 2006 by using Landsat imagery change detection methods. *Remote Sensing of Environment*, 113 (6), 1133–1147.

XIE, P., He B. & XING, M. (2011). Estimation above-ground biomass of wetland bulrush in Qaidam Basin, China, combining regression model with vegetation index. *19th International Conference on Geoinformatics*, 1-4.

XU, X.O., MARINO, A. & LEI LI (2011). Biomass related parameter retrieving from quad-pol images based on Freeman-Durden decomposition. *IEEE International Geoscience and Remote Sensing Symposium (IGARSS)*, 405-408.

YAMAGUCHI, Y. MORIYAMA, T. ISHIDO, M., AND YAMADA, H. (2005). Four component scattering model for polarimetric SAR image decomposition. *IEEE Transactions on Geoscience and Remote Sensing*, 43(9), 1699-1706.

YAMAGUCHI, Y., YAJIMA, Y & YAMADA, H. (2006). A four-component decompostion of POLSAR Images Based on the coherency matrix. *IEEE Transactions of Geoscience and Remote Sensing*, 3(3), 292-296.

YING, G., LI, Z.Y., CHEN, E. & HE, Q.S. (2011). Estimation of forest biomass using Support Vector machines from comprehensive remote sensing data. *International Conference on Remote Sensing, Environment and Transportation Engineering (RSETE)*, 2146-2150.

YU, X., HYYPPÄ, J., VASTARANTA, M., HOLOPAINEN, M., & VIITALA, R. (2011). Predicting individual tree attributes from airborne laser point clouds based on the random forests technique. *ISPRS Journal of Photogrammetry and Remote Sensing*, 66, 28-37.

ZARCO-TEJADA, P.J., MILLER, J.R., HARRON, J., HU, B., NOLAND, T.L., GOEL, N., MOHAMMED, G.H. & SAMPSON, P. (2004). Needle chlorophyll content estimation through model inversion using hyperspectral data from boreal conifer forest canopies. *Remote Sensing of Environment*, 89, 189-199.

ZHANG, Z., YONG WANG, GUOQING SUN, WENJIAN NI, WENLI HUANG & LIXIN ZHANG (2011). Biomass retrieval based on polarimetric target decomposition. *IEEE International Geoscience and Remote Sensing Symposium (IGARSS)*, 1942-1945.

ZHENG, L., TONG, Q., ZHANG, B. LI, X & LIU, J. (2001). Urban sensing by hyperspectral data. *22nd Asian Conference on Remote Sensing*, Singapore.

ZIANIS, D., MUUKKONEN, P., MAKIPAA, R. and MENCUNCCINI, M. (2005). Biomass and stem volume equations for tree species in Europe. *Silva Fennica*, 4, 63.

List of Publications

List of Publications during the PhD

Tan, C.P. (2009). The Use of Remote Sensing For Sustainable Forest Management in Glen Affric, Scotland, *The University of Edinburgh Postgraduate Research Conference 2009*, Edinburgh, 24-25 March 2009.

Tan, C.P. (2010). How Green is Glen Affric? *The University of Edinburgh Postgraduate Research Conference 2010*, Edinburgh, 23-24 March 2010 – **RUNNER UP FOR POSTER PRESENTATION AWARD.**

Tan, C.P., Woodhouse, I.H., Patenaude, G., Cloude, S.R., Suarez, J., Edwards, C. & Perks, M. (2010). Investigation of Radar Backscatter Responses to Carbon for Glen Affric Radar Project, *Remote Sensing and Photogrammetry Society Conference: Remote Sensing and Carbon Cycle*, Burlington House, London, 05 May 2010 – **BEST POSTER PRESENTATION AWARD.**

Tan, C.P., Woodhouse, I.H., Suarez, J., Edwards, C. & Perks, M. (2010). The Use of LIDAR Technology For Sustainable Forest Management in Glen Affric, *European Association of Remote Sensing Laboratories*, Paris, 365-370, 31 May – 03 June 2010.

Tan, C.P., Woodhouse, I.H., Patenaude, G., Cloude, S.R., Suarez, J., Edwards, C. & Perks, M. (2010). The Use of Remote Sensing for Sustainable Forest Management in Glen Affric, *18th Commonwealth Forestry Conference*, Edinburgh, 28 June - 2 July 2010.

Tan, C.P., Marino, A., Woodhouse, I.H., Cloude, S.R., Suarez, J. & Edwards, C. (2011). The Potential of TERRASAR-X in Assessing Forest Above-Ground Biomass in Scotland, *POLINSAR 2011*, ESA ESRIN, Frascati, 24 - 28 January 2011.

Tan, C.P., Marino, A., Woodhouse, I.H., Cloude, S.R., Suarez, J. & Edwards, C. (2011). A Comparison Study of Biomass Estimation Using ALOS PALSAR and LiDAR data, *POLINSAR 2011*, ESA ESRIN, Frascati, 24 - 28 January 2011.

Tan, C.P., Marino, A., Woodhouse, I.H., Cloude, S.R., Suarez, J. & Edwards, C. (2011). See The Forests With Different Eyes, *IEEE International Geoscience and Remote Sensing Symposium*, Vancouver, Canada, 1405-1408, 24-29 July 2011.

Tan, C.P., Marino, A., Woodhouse, I.H., Suarez, J., Edwards, C. & Perks, M. (In Review). Potential Use of ALOS PALSAR and LiDAR for Aboveground Biomass Estimation in Glen Affric, *Journal of Plant Ecology and Diversity*.